

**Doctoral Dissertation**  
**博士論文**

**Problems of Thermalization in Closed and  
Open Quantum Many-Body Systems**

(孤立および開放量子多体系における熱平衡化に関する問題)

*A Dissertation Submitted for  
the Degree of Doctor of Philosophy*

*December 2019*  
令和元年12月博士(理学)申請

*Department of Physics, Graduate School of Science,*

*The University of Tokyo*  
東京大学 理学系研究科 物理学専攻

**Ryusuke Hamazaki**  
**濱崎立資**

# Abstract

In this Thesis, we investigate problems of thermalization in closed (or isolated) and open quantum many-body systems, which are deeply tied to the foundations of quantum statistical mechanics. Such studies have attracted growing interest thanks to recent experimental realizations of controllable quantum many-body systems, *e.g.*, cold atoms and ions.

We firstly discuss thermalization in closed quantum many-body systems. The eigenstate thermalization hypothesis (ETH) has been proposed as a sufficient condition for a system to be described by the microcanonical ensemble after a long-time dynamics. The ETH is expected to hold true for generic systems except for some systems such as many-body localized (MBL) systems with strong disorder. On the other hand, the reason why the ETH generically holds true has not yet been fully understood. We here rigorously show that the typicality argument, which has long been thought to justify the ETH, does not hold true for a realistic setup with few-body properties of observables and Hamiltonians.

We secondly discuss thermalization in open quantum many-body systems. State-of-the-art experiments (*e.g.*, experiments under continuous measurement) have now enabled us to control dissipation, which may enrich properties of closed systems. As one of the fundamental problems of thermalization in open quantum systems, we study the MBL in non-Hermitian systems, which are relevant for continuously measured systems. We show that the transition between delocalized (ETH) and MBL phases occurs even for non-Hermitian many-body Hamiltonians and affects spectral and dynamical properties. In particular, we find that a novel real-complex transition occurs upon MBL and affects the dynamical stability in non-Hermitian interacting systems with asymmetric hopping.

Just as delocalized phases in closed systems are characterized by Hermitian random matrices, those in open quantum systems are characterized by non-Hermitian random matrices. On the other hand, in contrast with the Hermitian cases, the universality in non-Hermitian random matrices and its relation to symmetries are not well understood. In Hermitian random matrices, there are three universality classes of local spectral statistics dependent on time-reversal symmetry (TRS). However, TRS is known not to alter universality in non-Hermitian random matrices. We here show that three different universal level-spacing distributions appear even for non-Hermitian random matrices when we consider transposition symmetry instead of TRS. This result serves as a basis for characterizing nonintegrability and delocalization in open quantum systems with symmetry.

# Contents

<b>Abstract</b>	<b>ii</b>
<b>1 Introduction</b>	<b>4</b>
1.1 Problems of thermalization: foundations of quantum statistical mechanics . . . . .	4
1.1.1 Thermalization in closed quantum systems . . . . .	4
1.1.2 Thermalization in open quantum systems . . . . .	6
1.2 Experiments of artificial quantum many-body systems . . . . .	8
1.2.1 Experiments of thermalization in closed systems . . . . .	8
1.2.2 Experiments of thermalization in open systems . . . . .	12
1.3 Organization of this thesis . . . . .	14
<b>2 Review: thermalization, universality, and localization in closed quantum many-body systems</b>	<b>17</b>
2.1 Long-time dynamics and eigenstate thermalization hypothesis . . .	17
2.1.1 Relaxation to thermal equilibrium . . . . .	17
2.1.2 Eigenstate thermalization hypothesis (ETH) . . . . .	20
2.1.3 Other possible definitions of the ETH . . . . .	22
2.2 Nonintegrability and Universality of random matrices . . . . .	24
2.2.1 Nonintegrability, the ETH and random matrices . . . . .	24
2.2.2 Numerical results . . . . .	27
2.2.3 Analytical results . . . . .	30
2.3 Many-body localization (MBL) and non-thermalization . . . . .	32
2.3.1 Many-body localization and its phenomenology . . . . .	32
2.3.2 Characterizing the MBL transition . . . . .	36
2.3.3 Other systems where thermalization is absent . . . . .	39
2.4 Relaxation dynamics in closed quantum many-body systems . . . .	42

<b>3</b>	<b>Atypicality of most few-body observables</b>	<b>44</b>
3.1	Motivation . . . . .	44
3.2	Review on the typicality argument . . . . .	45
3.3	Atypicality of most few-body observables . . . . .	48
3.3.1	Setup . . . . .	48
3.3.2	Proof of atypicality of most few-body observables . . . . .	51
3.4	Typicality of most $N$ -body observables . . . . .	55
3.5	Extension of the setup with locality . . . . .	56
3.6	Discussions . . . . .	59
<b>4</b>	<b>Review: theory of open quantum systems</b>	<b>61</b>
4.1	Repeatedly or continuously measured open quantum systems . . .	62
4.1.1	Repeatedly measured quantum systems . . . . .	62
4.1.2	Continuously measured quantum systems . . . . .	64
4.2	Non-Hermitian systems . . . . .	66
4.2.1	Basic aspects of non-Hermitian matrices . . . . .	66
4.2.2	Non-Hermitian quantum dynamics . . . . .	69
4.2.3	Other non-Hermitian systems . . . . .	69
4.3	Previous studies on thermalization of open quantum many-body systems . . . . .	70
4.3.1	Thermalization under the Lindblad equations . . . . .	70
4.3.2	Decay of the many-body localization under the Lindblad dynamics . . . . .	71
4.3.3	Thermalization dynamics without ensemble averaging . . .	72
<b>5</b>	<b>Non-Hermitian many-body localization</b>	<b>74</b>
5.1	Motivation . . . . .	74
5.2	Brief review of the Hatano-Nelson model . . . . .	75
5.3	Real-complex phase transition in an interacting model with asym- metric hopping . . . . .	79
5.3.1	Fraction of complex energy eigenvalues . . . . .	80
5.3.2	Transition of dynamical stability . . . . .	80
5.4	Non-Hermitian many-body localization . . . . .	83
5.5	Relation between two transition points . . . . .	86
5.6	A gain-and-loss model . . . . .	88
5.7	Discussions . . . . .	89

<b>6</b>	<b>The threefold way in non-Hermitian random matrices</b>	<b>92</b>
6.1	Motivation . . . . .	92
6.2	Review on Ginibre’s symmetry classes . . . . .	93
6.2.1	Definition . . . . .	93
6.2.2	Spectral properties . . . . .	97
6.3	Review on non-Hermitian symmetry classes . . . . .	98
6.3.1	Overview . . . . .	98
6.3.2	Detailed classification . . . . .	99
6.4	New threefold way in non-Hermitian random matrices and univer- sality of level-spacing distributions . . . . .	105
6.5	Analysis for small matrices . . . . .	109
6.5.1	Detailed analysis . . . . .	113
6.6	Universality in dissipative many-body systems . . . . .	115
6.6.1	Non-Hermitian many-body systems . . . . .	116
6.6.2	Lindblad many-body dynamics . . . . .	118
6.7	Discussions . . . . .	120
<b>7</b>	<b>Conclusions and Outlook</b>	<b>122</b>
<b>A</b>	<b>Details of Chapter 5</b>	<b>125</b>
A.1	Results for other models and parameters . . . . .	125
A.1.1	Real-complex transition for stronger non-Hermiticity $g$ . . .	125
A.1.2	Real-complex transition as a function of non-Hermiticity $g$ .	127
A.1.3	Case with quarter-filling . . . . .	127
A.1.4	Real-complex transition for the Bose-Hubbard model with asymmetric hopping . . . . .	129
A.2	Other probes to characterize the transitions . . . . .	130
A.2.1	Maximum imaginary values . . . . .	130
A.2.2	Entanglement and eigenstate stability as functions of the size of the system . . . . .	131
A.2.3	Standard deviation of entanglement . . . . .	132
A.3	Similarity transformation of the Hamiltonian with interaction and asymmetric hopping . . . . .	132
<b>B</b>	<b>Details of the level-spacing distributions for small matrices in Chapter 6</b>	<b>137</b>
B.1	Probability distribution of $ X_f ^2$ . . . . .	137
B.1.1	Level-spacing distribution for $H_{\text{small}}$ . . . . .	139

B.2 Simpler forms . . . . .	140
<b>Acknowledgements</b>	<b>140</b>

# List of Publications

This Thesis is based on the following publications.

1. *The Threefold Way in Non-Hermitian Random Matrices*  
Ryusuke Hamazaki, Kohei Kawabata, Naoto Kura and Masahito Ueda,  
arXiv:1904.13082 (2019).
2. *Non-Hermitian Many-Body Localization*  
Ryusuke Hamazaki, Kohei Kawabata and Masahito Ueda,  
Phys. Rev. Lett. **123**, 090603 (2019).
3. *Atypicality of Most Few-Body Observables*  
Ryusuke Hamazaki and Masahito Ueda,  
Phys. Rev. Lett. **120**, 080603 (2018).

The following publications are related but are not claimed in this Thesis.

1. *Nonequilibrium many-body stationary states stabilized by indirect-measurement feedback control*  
Ryusuke Hamazaki, Snir Gazit, Ehud Altman and Marin Bukov,  
in preparation.
2. *Error bounds for constrained dynamics in gapped quantum systems: Rigorous results and generalizations*  
Zongping Gong, Nobuyuki Yoshioka, Naoyuki Shibata, and Ryusuke Hamazaki,  
arXiv:2001.03421 (2020).
3. *Universal Error Bounds for Constrained Quantum Dynamics*  
Zongping Gong, Nobuyuki Yoshioka, Naoyuki Shibata, and Ryusuke Hamazaki,  
arXiv:2001.03419 (2020).
4. *Magnetic solitons in a spin-1 Bose-Einstein condensate*  
Xiao Chai, Di Lao, Kazuya Fujimoto, Ryusuke Hamazaki, Masahito Ueda,  
and Chandra Raman,  
arXiv:1912.06672 (2019).
5. *Family-Vicsek Scaling of a Roughness Growth in a Strongly Interacting Bose Gas*  
Kazuya Fujimoto, Ryusuke Hamazaki, and Yuki Kawaguchi,  
arXiv:1911.10707 (2019).

6. *Operator Noncommutativity and Irreversibility in Quantum Chaos*  
**Ryusuke Hamazaki**, Kazuya Fujimoto and Masahito Ueda,  
arXiv:1807.02360 (2018).
7. *Constructing neural stationary states for open quantum many-body systems*  
Nobuyuki Yoshioka and **Ryusuke Hamazaki**,  
Phys. Rev. B **99**, 214306 (2019).  
[Featured on Viewpoint in Physics, Selected as Editor's Suggestion.]
8. *Flemish Strings of Magnetic Solitons and a Non-Thermal Fixed Point in a One-Dimensional Antiferromagnetic Spin-1 Bose Gas*  
Kazuya Fujimoto, **Ryusuke Hamazaki** and Masahito Ueda,  
Phys. Rev. Lett. **122**, 173001 (2019).
9. *Random-matrix behavior of quantum nonintegrable many-body systems with Dyson's three symmetries*  
**Ryusuke Hamazaki** and Masahito Ueda,  
Phys. Rev. E **99**, 042116 (2019).
10. *Unconventional Universality Class of One-Dimensional Isolated Coarsening Dynamics in a Spinor Bose Gas*  
Kazuya Fujimoto, **Ryusuke Hamazaki** and Masahito Ueda,  
Phys. Rev. Lett. **120**, 073002 (2018).
11. *Discrete Time-Crystalline Order in Cavity and Circuit QED Systems*  
Zongping Gong, **Ryusuke Hamazaki** and Masahito Ueda,  
Phys. Rev. Lett. **120**, 040404 (2018).
12. *Generalized Gibbs ensemble in a nonintegrable system with an extensive number of local symmetries*  
**Ryusuke Hamazaki**, Tatsuhiko N. Ikeda and Masahito Ueda,  
Phys. Rev. E **93**, 032116 (2016).

## Abbreviations

1D/2D/3D	one/two/three dimension
BGS	Bohigas-Giannoni-Schmit
dim	dimension
DM	Dzyaloshinskii-Moriya
DTC	discrete time-crystalline
ETH	eigenstate thermalization hypothesis
GGE	generalized Gibbs ensemble
GinOE/GinUE/GinSE	Ginibre's orthogonal/unitary/symplectic ensemble
GOE/GUE/GSE	Gaussian orthogonal/unitary/symplectic ensemble
MBL	many-body localization/localized
OTOC	out-of-time-ordered correlator
pH	pseudo Hermiticity
Re/Im	real/imaginary
RMT	random matrix theory
SFF	spectral form factor
TRS/PHS/CS/SLS	time-reversal/particle-hole/chiral/sublattice symmetry

### (The followings are used as subscripts)

A/S	ancilla/system
con	continuum
eff	effective
erfc	complementary error function
F	field
Gin	Ginibre
I	Ising
jpdf	joint probability distribution function
KI	kicked Ising
loc	local
mic	microcanonical
NH	non-Hermitian
op	operator
Po	Poisson
sam	sample
Th	thermodynamic
tot	total

# Chapter 1

## Introduction

### 1.1 Problems of thermalization: foundations of quantum statistical mechanics

#### 1.1.1 Thermalization in closed quantum systems

Many of the natural phenomena that we see in everyday life appear at the macroscopic level by forming solids, liquids or gases. Statistical mechanics provides a framework to understand such collective phenomena from the perspective of microscopic theories, such as quantum mechanics. Indeed, equilibrium statistical mechanics originally developed by Boltzmann is now indispensable for understanding various fields of science, including chemistry and neural networks, not to mention physics. It allows us to calculate thermodynamic variables and their fluctuations using microscopic Hamiltonians [1] without explicitly solving complicated dynamics.

Equilibrium statistical mechanics asserts that observables at thermal equilibrium can be computed by the microcanonical ensemble  $\hat{\rho}_{\text{mic}}$ :

$$\hat{\rho}_{\text{mic}}(E) := \frac{1}{\dim[\mathcal{H}_{E,\Delta E}]} \hat{\mathcal{P}}_{E,\Delta E}, \quad (1.1)$$

where  $\mathcal{H}_{E,\Delta E}$  denotes the Hilbert space spanned by eigenstates in the microcanonical energy shell with mean  $E$  and width  $2\Delta E$ , and  $\hat{\mathcal{P}}_{E,\Delta E}$  is the projection operator onto the energy shell given as

$$\hat{\mathcal{P}}_{E,\Delta E} := \sum_{|E_\alpha\rangle \in \mathcal{H}_{E,\Delta E}} |E_\alpha\rangle \langle E_\alpha| \quad (1.2)$$

with the eigenstates  $|E_\alpha\rangle$  of the Hamiltonian. Then, the expectation value of an

operator  $\hat{O}$  at thermal equilibrium is given by  $\text{Tr}[\hat{O}\hat{\rho}_{\text{mic}}]$ .

Despite the success of equilibrium statistical mechanics, the reason why the microcanonical ensemble correctly describes equilibrium states has not yet been justified in terms of microscopic dynamical laws. One of the most fundamental questions related to this issue is how initially nonequilibrium quantum systems relax to states described by the microcanonical ensemble only by unitary time evolution, *i.e.*, the problem of thermalization in closed quantum systems.

The problem of thermalization in closed quantum systems was first tackled by von Neumann in 1929 [2], just three years after the Schrödinger equation had been proposed. Von Neumann raised the following important questions:

1. How should we characterize thermal equilibrium in terms of the microscopic theory? What is the meaning that "thermal equilibrium is described by the microcanonical ensemble?"
2. What is the condition for any initial states to relax to states described by the microcanonical ensemble only by unitary time evolution?
3. Finally, why should the condition obtained above hold true for macroscopic quantum systems?

He attempted to answer these questions only by using quantum mechanics, but unfortunately, his answers were forgotten for a long time [3] owing to misunderstanding of the results [4, 5, 6]. It is only after around this decade that his answers have been recognized and developed in a modern way along with a support of experiments of almost closed quantum systems using, *e.g.*, cold atomic systems; see the next section.

The answer to the first question is that we should consider some set  $\mathcal{S}$  of observables to judge whether the state  $\hat{\rho}$  is in thermal equilibrium or not. Namely, if

$$\text{Tr}[\hat{\rho}\hat{O}] \simeq \text{Tr}[\hat{\rho}_{\text{mic}}\hat{O}] \quad (1.3)$$

for all  $\hat{O} \in \mathcal{S}$  (" $\simeq$ " means that the equality holds true up to subextensive corrections),  $\hat{\rho}$  is in thermal equilibrium; otherwise  $\hat{\rho}$  is out of equilibrium. This definition of thermal equilibrium depends on  $\mathcal{S}$ . We often take  $\mathcal{S}$  to be a set of local observables or macroscopic observables, which define the so-called "microscopic thermal equilibrium [7, 8, 9, 10]" or "macroscopic thermal equilibrium [2, 11, 3, 9, 12, 10]." In any case, the important thing to note is that thermal equilibrium is defined through experimentally relevant quantities rather than

density matrices themselves. We note that almost all pure states belong to thermal equilibrium [7, 8, 13] for local or macroscopic observables; if we take a random pure state  $|\psi\rangle \in \mathcal{H}_{E,\Delta E}$  over the Haar measure,  $\hat{\rho} = |\psi\rangle\langle\psi|$  satisfies Eq. (1.3) with unit probability in the thermodynamic limit.

Von Neumann's answer to the second question has now been refined and known as the (strong) eigenstate thermalization hypothesis (ETH) [14, 15, 16, 17, 18]. The ETH essentially states that all eigenstates  $|E_\alpha\rangle \in \mathcal{H}_{E,\Delta E}$  of the Hamiltonian are thermal:

$$\langle E_\alpha|\hat{\mathcal{O}}|E_\alpha\rangle \simeq \text{Tr}[\hat{\rho}_{\text{mic}}\hat{\mathcal{O}}], \quad (1.4)$$

$$\langle E_\alpha|\hat{\mathcal{O}}|E_\beta\rangle \simeq 0 \quad (\text{for } \alpha \neq \beta) \quad (1.5)$$

up to subextensive corrections for all  $\hat{\mathcal{O}} \in \mathcal{S}$ ; other possible definitions are reviewed in Chapter 2. The ETH provides a sufficient condition for any initial state to relax to thermal equilibrium characterized by  $\mathcal{S}$ . Many numerical simulations suggest that the ETH is actually a mechanism to explain thermalization in a wide class of closed quantum many-body systems [18, 19, 20, 21, 22, 23, 24, 25, 26, 27, 28, 29]. On the other hand, rigorously proving the ETH in specific quantum systems is a formidable task.

Instead of a rigorous proof, von Neumann argued why the obtained condition, which is essentially the ETH, holds true for generic systems, as the answer to the third question above. We here call it a typicality argument [30, 31]. This argument essentially conjectures that energy eigenstates behave as if they were pseudo-random vectors against observables in the microcanonical energy shell [2, 30]; the precise definition is reviewed in Chapter 3. If the typicality argument is correct, we can justify the ETH.

An overview described here will be detailed in Chapters 2 and 3. There we will also review important related concepts, such as random matrix theory and many-body localization.

### 1.1.2 Thermalization in open quantum systems

While the entire universe is expected to be isolated and follow unitary time evolutions, most physical systems are not regarded as being isolated. Such open quantum systems are described by non-unitary time evolutions and there are many distinct properties for their dynamics and stationary states. For example, an external bath often makes the system thermalized at the same temperature by exchanging energies and particles. On the other hand, for ultracold atomic

systems, particle loss usually leads to the vacuum stationary states. More interestingly, stationary states of many open systems may be genuinely nonequilibrium for certain cases. Thus, study of dynamics and stationary states in open quantum many-body systems may unveil nonequilibrium statistical mechanics, which has yet to be understood. We will call this problem thermalization in open quantum systems, where we consider the approach not only to thermal equilibrium but also to other possible nonequilibrium stationary states.

Various microscopic equations of motion are proposed to describe open quantum systems, depending on the relation between the system and bath [32]. The best known example is the Lindblad master equation, which is obtained by tracing out the bath degrees of freedom with several assumptions (*e.g.*, the Markov property and the weak system-bath coupling):

$$\frac{d\hat{\rho}}{dt} = \mathcal{L}[\hat{\rho}] = -i(\hat{H}_{\text{NH}}\hat{\rho} - \hat{\rho}\hat{H}_{\text{NH}}^\dagger) + \sum_m \gamma_m \hat{L}_m \hat{\rho} \hat{L}_m^\dagger. \quad (1.6)$$

Here  $\hat{H}_{\text{NH}} = \hat{H} - (i/2) \sum_m \gamma_m \hat{L}_m^\dagger \hat{L}_m$  is an effective non-Hermitian Hamiltonian, where  $\hat{H}$  is the system's Hamiltonian and  $\hat{L}_m$  is a so-called jump operator with strength  $\gamma_m$ .

In some non-unitary processes represented by the dynamics under continuous quantum measurement, we can trace each stochastic trajectory under measurement backaction by keeping track of every measurement outcome. The dynamics of such trajectories, called quantum trajectories, is described by (I) continuous non-Hermitian dynamics with  $\hat{H}_{\text{NH}}$ , and (II) a sudden stochastic change of the state (called a quantum jump) characterized by  $\hat{L}_m$ . If we take an average over all quantum jumps (*i.e.*, measurement outcomes), the averaged state obeys the Lindblad master equation given in Eq. (1.6).

Such quantum trajectories, which are, in fact, accessible in experiments [33, 34, 35, 36, 37], uncover richer physics which is not obtained in the conventional Lindblad master equation. For example, we can access to rare quantum trajectories in which the number of quantum jumps is away from the average. For quantum trajectories with few numbers of quantum jumps, the dynamics is almost characterized by non-Hermitian time evolution  $\hat{H}_{\text{NH}}$ . Such non-Hermitian dynamics has been intensively studied recently, and known to exhibit interesting properties such as real-complex transitions of eigenvalues [38, 39].

The overview described here is later detailed in Chapters 2 and 3. We will review the formulations and recent advancement of thermalization in open quantum many-body systems and recent developments in non-Hermitian systems.

## 1.2 Experiments of artificial quantum many-body systems

Thermalization dynamics of many-body systems which we saw in the previous section has now been observed experimentally using artificially controlled quantum many-body systems. The idea of such artificial quantum systems was first proposed by Feynman with the following quote [40]:

*“... nature isn’t classical, dammit, and if you want to make a simulation of nature, you’d better make it quantum mechanical, and by golly it’s a wonderful problem, because it doesn’t look so easy.”*

In other words, since quantum many-body systems have large complexity and it is quite hard to simulate them with a classical computer, it is better to make quantum devices that can simulate them. While Feynman’s idea encourages many researchers to create quantum computers [40], here we mainly focus on analogue quantum simulators, which imitate various models and Hamiltonians in a highly controllable way. Indeed, state-of-the-art technologies enable us to simulate quantum models with ultracold atoms, ions, nitrogen-vacancy centers in diamonds, superconducting qubits to name but a few [41, 42]. These quantum simulators have succeeded in verifying the theory on thermalization of many-body systems. Moreover, these artificial quantum many-body systems open up the research of novel dynamical phases of matter (such as discrete time crystals [43, 44]), which cannot be realized by the conventional condensed matter systems. Here, we review some of the experiments that have addressed the thermalization dynamics of quantum many-body systems.

### 1.2.1 Experiments of thermalization in closed systems

Thermalization via unitary time evolutions has often been experimentally verified using cold atomic systems [45, 46] or cold ion systems [47]. One advantage of these systems is that they are almost isolated from the surrounding environment because they are trapped in a high vacuum chamber.

Let us briefly review the basics of these quantum simulators. Neutral atoms are cooled down and trapped in a vacuum chamber using magnetic fields and optical dipole interactions [48, 49]. Their short-range interactions can be controlled by the Feshbach resonance, and even long-range interactions come into play by dipole-dipole interactions for Rydberg atoms [50]. Various lattice models with different

shapes and dimensions are realized using atoms loaded on an optical lattice [51]. Instead, recent experiments show that more flexible lattice configurations are possible with Rydberg atoms on microtraps created by optical tweezers [50].

Trapped ions are in balance owing to their Coulomb interactions. The phonon modes around this balance mediate the long-range interactions between distant pseudospins (internal degrees of freedom) [52]. The degree of power decay of long-range interactions can be tuned in a rather flexible way [53].

### **Relaxation to the thermal state**

Let us first discuss relaxation to thermal equilibrium. Although the approach to thermal equilibrium seems ubiquitous, it is not easy to confirm that this is caused only by unitary time evolutions. This task was first accomplished by Trotzky *et al.* with  $^{87}\text{Rb}$  ultracold atoms [45]. They loaded atoms on a one-dimensional optical lattice with on-site interactions, which models a 1D nonintegrable Bose-Hubbard model. Starting from an initial state in which each particle is isolated only on an even site, they suddenly lowered the height of the lattice potential. Then, the atoms spread with time and the expectation value of the atom number in odd sites grows from zero, oscillates, and eventually relaxes to the thermal value, *i.e.*, 0.5. They found that the experimentally observed relaxation is well described by the numerical simulation of time-dependent density matrix renormalization group, which assumes unitary time evolutions.

Another experimental demonstration of thermalization was done by Kaufman and coworkers [46] with only six  $^{87}\text{Rb}$  atoms on six lattice sites. Such a small system can be controlled with the digital micromirror device at a single-site level. They prepared two copies of a 1D six-site Bose-Hubbard model with a unit filling by evaporating the other particles. Starting from a Mott state, they lowered the lattice potential so that the particles may get entangled. After a certain time, they measured the local particle number, the purity, and the Renyi entanglement entropy. Note that the purity and the entanglement entropy can be measured by the interference between the system and its copy [54]. After a sufficiently long time, they found that the local particle number obeys the Boltzmann distribution and that the entanglement entropy becomes the thermal value, while the global purity is almost kept constant. They also confirmed that the reduced density matrix at a local site is almost equal to the thermal density matrix. These results are surprising because six sites are far from the macroscopic limit: thermalization in such a small system is expected to take place owing to the genuinely quantum

property of entanglement, which is also relevant to the ETH.

Relaxation to thermal equilibrium in closed quantum systems has also been observed in other systems. Thermalization of spins through the coupling with the phonon modes was observed by Clos *et al.* with trapped ions, where the combined system of spins and phonons is almost isolated [47]. As another example, Ref. [55] used a dipolar-interacting Rydberg spin system in 3D to discuss collective dynamics of spins. They found that temporal fluctuations during the relaxation to the thermal state can be well described by the truncated Wigner approximation. Finally, Neill *et al.* [56] observed thermalization using three superconducting qubits with periodic drivings, which describe approximated unitary dynamics at every period while the energy is not conserved. They found that the entanglement entropy restricted to one qubit after a certain time becomes thermal for an initial state whose classical counterpart ( $S \rightarrow \infty$ ) belongs to a chaotic region in the phase space.

### **Absence of thermalization and novel phases of matter**

While the relaxation to the thermal state seems natural for large systems, it is known that certain closed systems do not thermalize even in the thermodynamic limit. Such non-thermal characters are also applied to create novel dynamical phases of matter represented by the discrete time-crystalline order.

As detailed in Chapter 2, one of the most important examples is the many-body localized (MBL) system [57, 58], in which many-body eigenstates become localized in the Fock space owing to (most commonly) strong disorder. The system in the MBL phase breaks the ETH owing to emergent (quasi-)local conserved quantities.

A series of experiments on the MBL has been performed by using ultracold atoms by the group in Max Planck Institute. They first demonstrated the MBL for a 1D interacting system with a quasiperiodic potential, which serves as an effective disorder [59]. After that they succeeded in preparing identically coupled 1D chains with quasiperiodic potential [60], 2D systems with genuine disorder [61], and 2D systems with quasiperiodic potential [62]. While they found delocalization in the presence of the interaction in Ref. [60], they found the signature of the MBL in Refs. [61, 62]. They also studied the effect of periodic driving on the localization. Using a 1D interacting system with quasiperiodic potential, they found that localized and delocalized phases are separated as a function of the driving strength and frequency as well as the strength of the interaction and lattice potential [63]. We note that, another group in Harvard succeeded in probing the

logarithmic growth of entanglement using cold atoms [64].

Experiments of the MBL have also been done for other systems. In Ref. [65], they considered a system of trapped ions in one dimension with tunable long-range interactions and on-site potentials. Their system is described by a long-ranged Ising model with disorder. Starting from the Neel state  $|\uparrow\downarrow \cdots \uparrow\downarrow\rangle$ , where  $|\uparrow\rangle$  and  $|\downarrow\rangle$  are the eigenstates of  $\hat{\sigma}^z$  with an eigenvalue  $+1$  and  $-1$ , respectively, they observed relaxation dynamics of each spin. They found that thermalization of the magnetization observed in the weak-disorder cases ceases to hold in the strong-disorder cases, which indicates the MBL transition as a function of disorder. In Ref. [66], the authors investigated the difference between the MBL and the noninteracting Anderson localization using the time evolution of a measure of the correlation length. References [67, 68] study the MBL using the superconducting qubits. In Ref. [68], they considered a model with long-range interactions and demonstrated the breakdown of thermalization for strong disorder. In Ref. [67], they created the Bose-Hubbard model and found the level-spacing statistics and the inverse-participation ratio for the eigenstates, with which they identified delocalized and MBL phases. Finally, we also note that the nitrogen-vacancy centers in diamonds have been used to demonstrate slow thermalization (dubbed as "critical thermalization") owing to disorder, although it is not an exact MBL [69].

The absence of thermalization (or slow dynamics) enables us to create novel dynamical phases of matter, which are not realized in equilibrium. For example, the periodically driven (=Floquet) MBL [44] and the critical thermalization [43] are used to create discrete time crystals, which spontaneously break discrete time-translation symmetry. Note that periodic driving rapidly heats the system and destroys such a time-crystalline order unless the system belongs to the MBL or the slowly thermalizing phases.

The MBL is not the only mechanism for absence of thermalization in the long-time limit. Integrable systems are known to approach the so-called generalized Gibbs ensemble (GGE) [70], which takes account of initial information for local conserved quantities, instead of the standard canonical ensemble. Absence of thermalization owing to integrability has experimentally been observed in Refs. [71, 72, 73, 74], and the GGE has also been confirmed in Ref. [74]. Another important mechanism for the absence of thermalization is a quantum many-body scar. The experiment by Bernien *et al.* [75] used Rydberg atoms trapped by optical tweezers to simulate quantum many-body dynamics with strong next-neighbor interactions. They found that some initial states (such as the Neel states) exhibit

long-time oscillations even though the system is nonintegrable. This unexpected behavior has motivated theorists to come up with a new reason for the absence of thermalization, namely a quantum many-body scar [76], which is a non-thermal eigenstate embedded in thermal eigenstates.

We also note that some long-ranged interacting systems seem to exhibit peculiar relaxation. Reference [77] observed prethermalization [78, 79, 80] of the trapped ions modeled by long-ranged Ising model. They argue that the prethermalized state cannot be described by the GGE. In Ref. [81], the dynamics of transverse Ising model with  $r^{-6}$  interaction was reported with Rydberg atoms trapped by optical tweezers in 1D (with linear and zigzag configurations). While the relaxation dynamics was approximated by an effective Fokker-Planck equation, the stationary state is distinct from thermal value because the ETH is broken.

### Other relaxation dynamics

Experiments in closed quantum many-body systems are also important to understand properties of nonequilibrium dynamics. For example, the speed of information propagation is finite owing to the Lieb-Robinson bound, which is confirmed with cold atoms [82] and trapped ions [83, 53]. Trapped ions are also used to study dynamical phase transition after quench [84]. As another example, the scaling dynamics across the phase transition (the Kibble-Zurek mechanism [85, 86]) has been observed in various systems [87, 88, 89]. Scaling dynamics is also observed in the intermediate timescale [90, 91], which is called the non-thermal fixed point. Transport phenomena are directly observed with fermionic [92] and bosonic [93] atoms. Finally, the dynamics of the out-of-time-ordered correlators (OTOC), which probes how the quantum information scrambles in the system, has been observed with the NMR system [94] and the trapped ions [95].

### 1.2.2 Experiments of thermalization in open systems

While we have explained that almost closed quantum many-body systems have been realized, recent experiments also enable us to control dissipation and measurement with high precision. Here we review experiments which involve such non-unitary dynamics.

In some cold atomic systems, dissipation can be introduced by one-body losses [96, 97, 98], for which the jump operator  $\hat{L}_m$  can be written as an annihilation operator. For example, in Ref. [96], the authors created one-body

localized dissipation by shining an electron beam on an atomic Bose-Einstein condensate. Surprisingly, they found that the loss of atoms was suppressed for strong dissipation, which has been attributed to the quantum Zeno effect. The same group also found a non-equilibrium phase transition of the stationary state for a one-dimensional array of atoms with a local one-body dissipation [97]. Another group succeeded in demonstrating non-Hermitian dynamics using tunable one-body losses mediated by synthetic lattices [98].

We can also tune two-body losses of cold atoms [99] and molecules [100, 101]. For example, in Ref. [99], they considered a 3D  $^{174}\text{Yb}$  system, which is described by a Bose-Hubbard model with on-site two-body losses. Such two-body losses are realized by a single-photon photoassociation beam, which converts two atoms at doubly occupied sites into a molecular state that is immediately dissociated from the optical lattice. They found that the melting of the Mott insulator is delayed for strong dissipation, which is a manifestation of the continuous quantum Zeno effect.

Other kinds of measurement of cold atoms also lead to nontrivial consequences. For the setups in which jump operators can be regarded as the number operators, strong dissipation is found to lead to negative differential conductivity [102], suppression of tunneling owing to the quantum Zeno effect [103], and destruction of the MBL [104]. For example, in Ref. [104], the authors create such dissipation by photon scattering. They found that, while the MBL decays with the rate that depends on dissipation, the susceptibility of the rate against dissipation can be a signature for the MBL transition point in the absence of the dissipation.

We note that the real-time feedback control after measurement is also possible [105, 106, 107]. In Ref. [105], they considered a gas of Rydberg atoms in one dimension. After setting optical tweezers, they measured which tweezers trap Rydberg atoms. Then they removed those tweezers that do not trap atoms and moved the position of the remaining tweezers freely using an acousto-optic deflector. Such a fast feedback control (which takes less than 400 milliseconds) enables us to prepare various spatial patterns of initial states, which has been essential for performing subsequent experiments [75, 89].

While we have considered ultracold atoms, we note that dissipation plays an important role for other many-body systems. In Ref. [108], the authors experimentally studied the dissipative preparation of the Greenberger-Horne-Zeilinger state using the trapped ions. In Ref. [109], the authors created a 2D chaotic dissipative billiard with exciton-polaritons and investigate its spectral properties. Finally,

dissipation naturally comes into play in *e.g.*, superconducting qubits and cavity QED systems, where a dissipative phase transition is found [110].

### 1.3 Organization of this thesis

In this thesis, some problems of thermalization in closed and open quantum many-body systems are addressed. The following chapters are organized as follows; see Fig. 1.1.

In Chapter 2, the theoretical advancement of thermalization, universality, and localization in closed quantum many-body systems is reviewed. I first review the conditions for a closed quantum system to relax to a state described by a thermal ensemble, with an emphasis on the ETH. Then, I explain the relation between nonintegrability, the ETH and random matrices, which has developed along with the idea of quantum chaos. Some of the known examples for which thermalization is absent, especially the MBL, are discussed. Finally, I briefly comment on the universality of relaxation dynamics in closed quantum systems before complete thermalization.

In Chapter 3, the issue on the origin of the ETH is addressed, revisiting von Neumann's seminal work. He showed that the ETH is justified if we assume that transformation matrices between two eigenbases that diagonalize the observable and the Hamiltonian are randomly (or typically) distributed in the microcanonical energy shell. We rigorously show, however, that such an assumption of typicality does not hold true for most few-body observables and a few-body Hamiltonian, which are of importance for physically relevant setup. This means that we need a different scenario that does not rely on the typicality argument to justify the ETH. This chapter is based on the following reference [31]:

- *Atypicality of Most Few-Body Observables*, Ryusuke Hamazaki and Masahito Ueda, Phys. Rev. Lett. **120**, 080603 (2018).

In Chapter 4, I review the basic theory of open quantum systems, particularly focusing on repeatedly or continuously measured quantum systems. First, the dynamics of quantum trajectories and its relation to the Lindblad master equation in such systems are formulated. I next discuss properties of non-Hermitian systems, which can be regarded as the simplest case of quantum trajectories. Recent developments on thermalization of open quantum many-body dynamics are also briefly reviewed, such as the decay of the MBL in the Lindblad-equation formalism.

In Chapter 5, we discuss how the MBL, which is a distinct phase of closed systems, can appear in open many-body systems described by non-Hermitian systems. We show that non-Hermitian MBL occurs and suppresses the imaginary part of the many-body energy eigenspectrum for a system which possesses time-reversal symmetry. In particular, we find a novel real-complex phase transition of eigenvalues owing to the non-Hermitian MBL in an interacting model with asymmetric hopping and disorder. This transition alters the stability of thermalization dynamics in such open systems. We also show that non-Hermitian MBL still occurs in a system without time-reversal symmetry, while the real-complex transition does not exist. This chapter is based on the following reference [111]:

- *Non-Hermitian Many-Body Localization*, **Ryusuke Hamazaki**, Kohei Kawabata and Masahito Ueda, *Phys. Rev. Lett.* **123**, 090603 (2019).

In Chapter 6, motivated by the relationship between thermalization and random matrix theory in Hermitian systems, we formulate fundamental universality classes of non-Hermitian random matrices, which can be applied to nonintegrable open quantum many-body systems. While level-spacing distributions of Hermitian systems become distinct depending on time-reversal symmetry, only one universality class of level-spacing distributions was known for non-Hermitian random matrices, even if we consider time-reversal symmetry. We show that, by considering transposition symmetry which is different from time-reversal symmetry owing to non-Hermiticity, new universality classes of level-spacing distributions appear. This chapter is based on the following reference [112]:

- *The Threefold Way in Non-Hermitian Random Matrices*, **Ryusuke Hamazaki**, Kohei Kawabata, Naoto Kura and Masahito Ueda, *arXiv:1904.13082* (2019).

In Chapter 7, we conclude this Thesis and discuss some future problems.

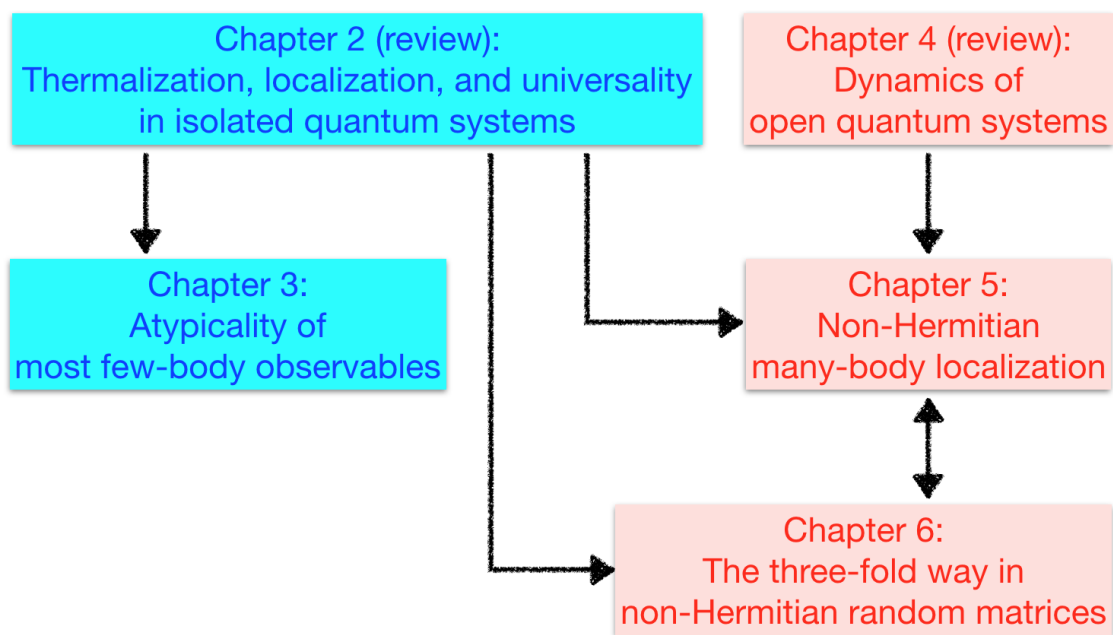


Figure 1.1: Relations between the chapters in the present thesis. Blue and red texts correspond to closed and open systems, respectively.

# Chapter 2

## Review: thermalization, universality, and localization in closed quantum many-body systems

In this Chapter, we review basic concepts on thermalization, universality, and localization in closed quantum many-body systems, particularly focusing on their theoretical perspectives.

### 2.1 Long-time dynamics and eigenstate thermalization hypothesis

#### 2.1.1 Relaxation to thermal equilibrium

Here we define the approach to thermal equilibrium in closed quantum systems. For that purpose, we note the following requirements and properties:

1. We naively expect that an initial state relaxes to some stationary state owing to time evolution in macroscopic systems and stays at that state for all times. On the other hand, closed quantum systems have the following recurrence properties [113, 114]: for an arbitrary small  $\epsilon > 0$  and an initial state  $|\psi(0)\rangle$ , an infinite sequence  $T_1, T_2, \dots$  exists such that

$$\| |\psi(T_i)\rangle - |\psi(0)\rangle \| < \epsilon \quad (T_i = T_1, \dots) \quad (2.1)$$

is satisfied. To keep in mind such atypical recurrence times, we require that the state be thermal for *almost all* (not all) times in the long run.

2. As mentioned in Chapter 1, a state is regarded as thermal when it has thermal expectation values for a set of observables of our interest; see Eq. (1.3). Thus, we require that the time evolution of the expectation values of such observables should become thermal in the long run.
3. Macroscopic systems relax to thermal states irrespective of initial conditions with the macroscopically same energy. Thus, we require that the relaxation to thermal states (in the above sense) should hold for any initial states that have certain energy.

In conclusion, we say that the system exhibits thermalization (at certain energy scale  $[E - \Delta E, E + \Delta E]$  and for a given set  $\mathcal{S}$ ) when the following condition holds: For any initial state satisfying  $|\langle \psi(0) | \hat{H} | \psi(0) \rangle - E| \leq \Delta E$  and all  $\hat{O} \in \mathcal{S}$ ,

$$\langle \psi(t) | \hat{O} | \psi(t) \rangle \simeq \text{Tr}[\hat{\rho}_{\text{mic}}(E) \hat{O}] \quad (2.2)$$

up to subextensive corrections, for almost all times  $t$  in the long-time limit. Here, " $\text{Tr}[\hat{\rho}_1 \hat{O}] \simeq \text{Tr}[\hat{\rho}_2 \hat{O}]$  up to subextensive corrections" means that

$$\frac{|\text{Tr}[\hat{\rho}_1 \hat{O}] - \text{Tr}[\hat{\rho}_2 \hat{O}]|}{\|\hat{O}\|_{\text{op}}} \rightarrow 0 \quad (2.3)$$

in the thermodynamic limit, where  $\|\hat{O}\|_{\text{op}}$  denotes the largest absolute value of eigenvalues of  $\hat{O}$ . Moreover, " $f(t) \simeq F$  almost all times in the long time limit" means that

$$\text{Prob}_{t \in [0, T]} [f(t) \simeq F] \rightarrow 1 \quad (2.4)$$

in the  $T \rightarrow \infty$  limit, where  $\text{Prob}_{t \in [0, T]}$  is the probability for which  $t$  is uniformly chosen from the interval  $[0, T]$ .

Let us investigate the condition (2.2) in more detail. Owing to the condition (2.4), we find that the stationary state should give the long-time average of  $\langle \psi(t) | \hat{O} | \psi(t) \rangle$  unless  $\langle \psi(t) | \hat{O} | \psi(t) \rangle$  exhibits singular behavior for exceptional  $t$ . Thus, the condition (2.2) can be decomposed into the following two steps:

- 1.

$$\langle \psi(t) | \hat{O} | \psi(t) \rangle \simeq \overline{\langle \psi(t) | \hat{O} | \psi(t) \rangle}, \quad (2.5)$$

for almost all times in the long-time limit, where

$$\overline{f(t)} = \lim_{T \rightarrow \infty} \frac{1}{T} \int_0^T f(t) dt \quad (2.6)$$

denotes the long-time average of  $f(t)$ .

2.

$$\overline{\langle \psi(t) | \hat{\mathcal{O}} | \psi(t) \rangle} \simeq \text{Tr}[\hat{\rho}_{\text{mic}}(E) \hat{\mathcal{O}}] \quad (2.7)$$

up to subextensive corrections.

The first condition is sometimes called the condition for equilibration.

To study the conditions above, we expand the state  $|\psi(t)\rangle$  with respect to the eigenstates  $|E_\alpha\rangle$  ( $\alpha = 1, \dots, D$ ) of  $\hat{H}$ , where  $D$  is the dimensionality of the Hilbert space. To simplify the notation, we define  $\mathcal{O}_{\alpha\beta} = \langle E_\alpha | \hat{\mathcal{O}} | E_\beta \rangle$  and  $c_\alpha = \langle E_\alpha | \psi(0) \rangle$ . Then, we obtain

$$\langle \psi(t) | \hat{\mathcal{O}} | \psi(t) \rangle = \sum_{\alpha\beta} c_\alpha^* c_\beta e^{i(E_\alpha - E_\beta)t} \mathcal{O}_{\alpha\beta}. \quad (2.8)$$

We now make two assumptions about energy eigenvalues. One is the non-degeneracy condition,

$$E_\alpha = E_\beta \Rightarrow \alpha = \beta, \quad (2.9)$$

and the other is the non-resonance condition,

$$E_\alpha - E_\beta = E_\gamma - E_\delta \neq 0 \Rightarrow \alpha = \gamma, \beta = \delta. \quad (2.10)$$

Note that these conditions are expected to be satisfied for nonintegrable systems which conserve only energy. We then find, using the non-degeneracy condition,

$$\overline{\langle \psi(t) | \hat{\mathcal{O}} | \psi(t) \rangle} = \sum_{\alpha} |c_\alpha|^2 \mathcal{O}_{\alpha\alpha} = \langle \hat{\mathcal{O}} \rangle_d, \quad (2.11)$$

where

$$\langle \hat{\mathcal{O}} \rangle_d := \text{Tr}[\hat{\rho}_d \hat{\mathcal{O}}] \quad (2.12)$$

with

$$\hat{\rho}_d = \sum_{\alpha} |c_\alpha|^2 |E_\alpha\rangle \langle E_\alpha|, \quad (2.13)$$

which is called the diagonal ensemble.

Let us consider the first condition for thermalization *i.e.*, Eq. (2.5) holds for almost all times. This condition is satisfied if the temporal fluctuation of  $\langle \psi(t) | \hat{\mathcal{O}} | \psi(t) \rangle$  around  $\langle \hat{\mathcal{O}} \rangle_d$  is sufficiently small, *i.e.*,

$$\Delta \mathcal{O}_T := \sqrt{(\langle \psi(t) | \hat{\mathcal{O}} | \psi(t) \rangle - \langle \hat{\mathcal{O}} \rangle_d)^2} \simeq 0 \quad (2.14)$$

up to subextensive corrections; *i.e.*,  $\Delta\mathcal{O}_T/|\|\hat{\mathcal{O}}\|_{\text{op}} \rightarrow 0$  in the thermodynamic limit. This is because Chebyshev's inequality leads to

$$\text{Prob}_{t \in [0, \infty)}[|\langle \hat{\mathcal{O}} \rangle_d - \langle \psi(t) | \hat{\mathcal{O}} | \psi(t) \rangle| > \epsilon] \leq \frac{\Delta\mathcal{O}_T^2}{\epsilon^2} \quad (2.15)$$

for any  $\epsilon$ . Then, using the non-resonance condition, we find the following condition:

$$\Delta\mathcal{O}_T = \sqrt{\sum_{\alpha \neq \beta} |c_\alpha|^2 |c_\beta|^2 |\mathcal{O}_{\alpha\beta}|^2} \simeq 0 \quad (2.16)$$

up to subextensive corrections. On the other hand, Eq. (2.7) becomes

$$\langle \hat{\mathcal{O}} \rangle_d = \sum_{\alpha} |c_\alpha|^2 \mathcal{O}_{\alpha\alpha} \simeq \text{Tr}[\hat{\rho}_{\text{mic}}(E) \hat{\mathcal{O}}] \quad (2.17)$$

up to subextensive corrections. Equations (2.16) and (2.17) constitute the conditions for thermalization represented by energy eigenvalues and eigenstates.

## 2.1.2 Eigenstate thermalization hypothesis (ETH)

The eigenstate thermalization hypothesis (ETH) provides a sufficient condition for thermalization. Indeed, Eqs. (2.16) and (2.17) hold true for any initial states with a sufficiently localized energy; the precise meaning is explained below. The ETH intuitively states that all energy eigenstates become thermal. Precisely speaking, we here define the ETH as a statement for matrix elements  $\mathcal{O}_{\alpha\beta}$  as follows: for all eigenstates  $|E_\alpha\rangle, |E_\beta\rangle \in \mathcal{H}_{E, \Delta E}$  and  $\hat{\mathcal{O}} \in \mathcal{S}$ , the matrix elements  $\mathcal{O}_{\alpha\beta}$  satisfy

$$\mathcal{O}_{\alpha\alpha} \simeq \text{Tr}[\hat{\rho}_{\text{mic}}(E) \hat{\mathcal{O}}], \quad (2.18)$$

$$\mathcal{O}_{\alpha\beta} \simeq 0 \quad (\alpha \neq \beta) \quad (2.19)$$

up to subextensive corrections.

Before proving the conditions for thermalization with the ETH, we impose one more assumption for the initial state. We demand that the initial state has a sufficiently localized energy around  $E$ , *i.e.*, the fraction of  $|c_\alpha|^2$  that is out of the energy shell is negligibly small in the thermodynamic limit:

$$\sum_{|E_\alpha\rangle \notin \mathcal{H}_{E, \Delta E}} |c_\alpha|^2 \rightarrow 0. \quad (2.20)$$

This is expected to be true for a typical quench setup in locally interacting many-

body systems [18]. Indeed, the standard deviation of the energy

$$\delta E := \sqrt{\sum_{\alpha} |c_{\alpha}|^2 (E - E_{\alpha})^2} \quad (2.21)$$

only scales as  $\delta E = O(V^{1/2})$  ( $V$  is the system size) for certain setups [18]. If  $|c_{\alpha}|$  is distributed without high-energy long tails, we expect that taking  $\Delta E = O(V^{1/2+a})$  for small  $a > 0$  is enough for Eq. (2.20) to be satisfied.

Now let us discuss Eqs. (2.16) and (2.17). Thanks to the assumption in Eq. (2.20), we have  $|\psi(0)\rangle \in \mathcal{H}_{E,\Delta E}$  to good approximation. Then, we find

$$\begin{aligned} \langle \hat{\mathcal{O}} \rangle_d &= \sum_{\alpha} |c_{\alpha}|^2 \mathcal{O}_{\alpha\alpha} \\ &\simeq \sum_{\alpha} |c_{\alpha}|^2 \text{Tr}[\hat{\rho}_{\text{mic}}(E) \hat{\mathcal{O}}] \\ &= \text{Tr}[\hat{\rho}_{\text{mic}}(E) \hat{\mathcal{O}}] \sum_{\alpha} |c_{\alpha}|^2 \\ &= \text{Tr}[\hat{\rho}_{\text{mic}}(E) \hat{\mathcal{O}}] \end{aligned} \quad (2.22)$$

using the ETH for diagonal matrix elements. We also find

$$\begin{aligned} \Delta \mathcal{O}_T &= \sqrt{\sum_{\alpha \neq \beta} |c_{\alpha}|^2 |c_{\beta}|^2 |\mathcal{O}_{\alpha\beta}|^2} \\ &\leq \sqrt{\max_{\alpha \neq \beta} |\mathcal{O}_{\alpha\beta}|^2 \sum_{\alpha \neq \beta} |c_{\alpha}|^2 |c_{\beta}|^2} \\ &\leq \sqrt{\max_{\alpha \neq \beta} |\mathcal{O}_{\alpha\beta}|^2} \simeq 0 \end{aligned} \quad (2.23)$$

up to subextensive corrections, using the ETH for off-diagonal matrix elements. Thus, the conditions for thermalization can be justified.

We note that the ETH is a sufficient but not a necessary condition for Eqs. (2.16) and (2.17) under additional conditions for initial states [115, 12]. For example, the so-called effective dimension about the initial state

$$d_{\text{eff}} := \frac{1}{\sum_{\alpha} |c_{\alpha}|^4} \quad (2.24)$$

is used to suppress the temporal fluctuation as

$$\begin{aligned}
\Delta \mathcal{O}_T^2 &= \sum_{\alpha \neq \beta} |c_\alpha|^2 |c_\beta|^2 |\mathcal{O}_{\alpha\beta}|^2 \\
&\leq \text{Tr} \left[ \hat{\rho}_d \hat{\mathcal{O}} \hat{\rho}_d \hat{\mathcal{O}} \right] \\
&= \text{Tr} \left[ \hat{\rho}_d \hat{\mathcal{O}} \left( \hat{\mathcal{O}} \hat{\rho}_d \right)^\dagger \right] \\
&\leq \sqrt{\text{Tr} \left[ \hat{\rho}_d \hat{\mathcal{O}} \left( \hat{\rho}_d \hat{\mathcal{O}} \right)^\dagger \right] \text{Tr} \left[ \left( \hat{\mathcal{O}} \hat{\rho}_d \right)^\dagger \hat{\mathcal{O}} \hat{\rho}_d \right]} \\
&= \text{Tr}[\hat{\rho}_d^2 \hat{\mathcal{O}}^2] \\
&\leq \|\hat{\mathcal{O}}\|_{\text{op}}^2 \text{Tr}[\hat{\rho}_d^2] \\
&= \frac{\|\hat{\mathcal{O}}\|_{\text{op}}^2}{d_{\text{eff}}}, \tag{2.25}
\end{aligned}$$

where we have used the Cauchy-Schwartz inequality and the inequality

$$\text{Tr}[\hat{A}\hat{B}] \leq \|\hat{A}\|_{\text{op}} \text{Tr}[\hat{B}] \tag{2.26}$$

for positive operators  $\hat{A}$  and  $\hat{B}$ . It is often the case that  $d_{\text{eff}}$  grows much larger than  $\|\hat{\mathcal{O}}\|_{\text{op}}^2$  with increasing the system size. In this case, temporal fluctuations vanish without assuming the ETH.

### 2.1.3 Other possible definitions of the ETH

The above definition of the ETH is directly relevant for thermalization in closed quantum systems. On the other hand, some literatures adopt different definitions of the ETH. While many of them are very close to the above definition, some of them are qualitatively different from it, which we explain below.

#### Srednicki's ansatz

We first discuss a conjecture proposed by Srednicki [116], which is actually stronger than the ETH defined above. We here call it Srednicki's conjecture, though it is often called the ETH in some literatures. Srednicki's conjecture states that matrix elements take the following form:

$$\mathcal{O}_{\alpha\beta} = \mathcal{A}(E)\delta_{\alpha\beta} + e^{-S_{\text{Th}}(E)/2} f(E, \omega) R_{\alpha\beta}. \tag{2.27}$$

Here,  $E = (E_\alpha + E_\beta)/2$ ,  $\omega = E_\alpha - E_\beta$ ,  $S_{\text{Th}}(E)$  denotes the thermodynamic entropy at energy  $E$ ,  $\mathcal{A}(E)$  and  $f(E, \omega)$  are smooth functions of their arguments, and

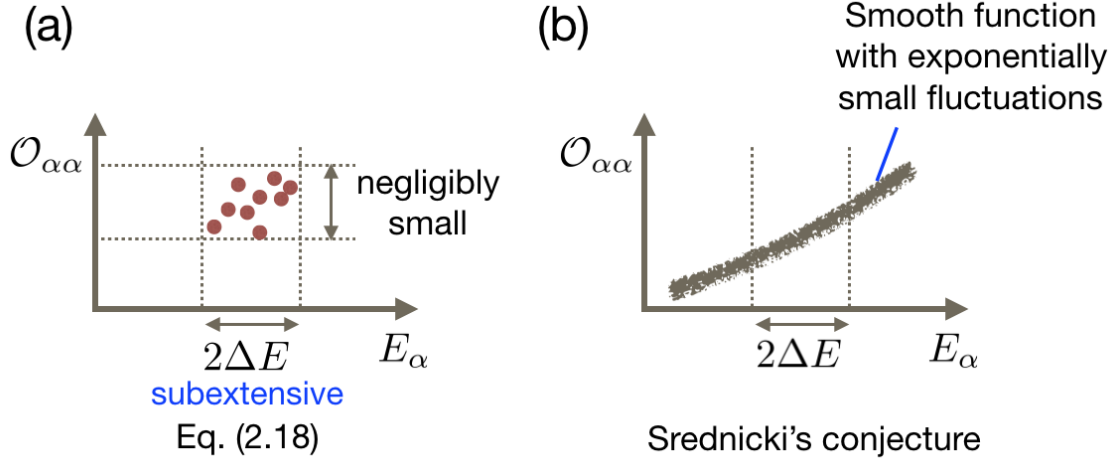


Figure 2.1: The difference between (a) Eq. (2.18) and (b) Srednicki's conjecture. The former only requires that the difference among diagonal matrix elements should be negligibly small for  $\Delta E$  with a subextensive width. The latter requires that the diagonal matrix elements be a smooth function with exponentially small fluctuations, which is stronger than Eq. (2.18).

$\delta_{\alpha\beta}$  is Kronecker's delta. Moreover,  $R_{\alpha\beta}$  is a normalized variable that fluctuates quasi-randomly depending on energy eigenstates; namely, the statistics of  $R_{\alpha\beta}$  are conjectured to be described by random matrices, as detailed in the next section.

The definition in Eqs. (2.18) and (2.19) is weaker than Srednicki's conjecture. For example, for diagonal matrix elements, the assumption in Eq. (2.18) does not require that the diagonal matrix elements be a smooth function with exponentially small fluctuations unlike Srednicki's conjecture; see Fig. 2.1. The former only requires that the difference among diagonal matrix elements should be negligibly small for  $\Delta E$  with a subextensive width.

Let us discuss the consequence of Srednicki's conjecture. First, the second term in Eq. (2.27) is usually exponentially small owing to the  $\exp(-S_{\text{Th}}(E)/2)$  factor; Note that  $S_{\text{Th}}(E)$  is an extensive quantity. Thus, we obtain

$$O_{\alpha\beta} \rightarrow \mathcal{A}(E)\delta_{\alpha\beta} \quad (2.28)$$

in the thermodynamic limit. Since  $\mathcal{A}(E)$  changes smoothly with  $E$ , this condition leads to the ETH in Eq. (2.18). Here, we find  $\mathcal{A}(E) \simeq \text{Tr}[\hat{\rho}_{\text{mic}}(E)\hat{O}]$ . In addition, Eq. (2.19) also holds true because the off-diagonal terms vanish.

Srednicki's conjecture is also relevant for the accuracy of the ETH and thermalization for finite systems. Indeed, since the second term in Eq. (2.27) vanishes exponentially, temporal fluctuations  $\Delta O_T$  are also known to vanish exponentially

with respect to the system size if we assume this conjecture. In addition, the accuracy of the microcanonical ensemble for small systems can be evaluated using this conjecture [117].

### Weak ETH

Another definition is often called the weak ETH, which states that the variance of diagonal matrix elements vanishes in the thermodynamic limit [118, 20]:

$$\frac{1}{\dim[\mathcal{H}_{E,\Delta E}]} \sum_{\alpha \in \mathcal{H}_{E,\Delta E}} \left( O_{\alpha\alpha} - \text{Tr} \left[ \hat{\rho}_{\text{mic}}(E) \hat{O} \right] \right)^2 \simeq 0 \quad (2.29)$$

up to subextensive corrections.

The weak ETH is not a sufficient condition for thermalization, unlike the ETH described above. Indeed, even if Eq. (2.29) holds true, there may exist an athermal eigenstate  $|E_\gamma\rangle$  satisfying  $O_{\gamma\gamma} \neq \text{Tr} \left[ \hat{\rho}_{\text{mic}}(E) \hat{O} \right]$ . Then, if we take an initial state as  $|\psi(0)\rangle = |E_\gamma\rangle$ , it trivially does not thermalize because Eq. (2.17) does not hold true.

The weak ETH can be rigorously justified for locally interacting many-body systems with translation invariance and cluster decomposition property [118]. Such systems include integrable systems, for which thermalization does not occur in general.

## 2.2 Nonintegrability and Universality of random matrices

In the previous section we define the ETH and discuss its consequence. Here, we review when and how this hypothesis holds true in quantum many-body systems. We especially discuss the relation between the ETH, nonintegrability, and random matrices, showing numerical and analytical results. The original argument by von Neumann, namely the typicality argument, will be reviewed in the next chapter.

### 2.2.1 Nonintegrability, the ETH and random matrices

The study about the relations among nonintegrability, the ETH, and random matrices, which is called quantum chaos theory, first developed from 1970's to 1990's especially for quantum systems that have well-defined semiclassical limits ( $\hbar \rightarrow 0$ ). One of the notable achievements is the Bohigas-Giannoni-Schmit (BGS)

conjecture [119], which states that local eigenvalue statistics of semiclassically chaotic (nonintegrable) systems are described by random-matrix theory (RMT). This is in contrast to semiclassically regular (integrable) systems, whose spectral statistics are conjectured to be the Poisson statistics [120]. For eigenstates, Berry proposed [121] that eigenstate statistics of semiclassically chaotic systems are delocalized in the phase space, consistent with RMT, whereas those of regular systems are localized. His proposal was applied to matrix elements [16], which led to the ETH and even Srednicki's conjecture in Eq. (2.27) for semiclassically chaotic systems.

The analogy between nonintegrable systems and RMT also turns out to be true for many-body systems without a well-defined semiclassical limit. In fact, roughly speaking, it is expected that local spectral statistics (represented by level-spacing statistics) are described by RMT and that Srednicki's conjecture including the ETH holds true in nonintegrable systems. Consequently, thermalization occurs in usual nonintegrable systems (while exceptions can be constructed [122]). We note that (non)integrability is not a trivial concept in quantum many-body systems, and that many definitions are proposed [123]. Here we define integrable systems as systems whose eigenstates are determined by a set of local conserved quantities. This definition includes systems that can be mapped to free particles [124, 125, 70, 126, 127, 128, 129, 74], systems solved by the Bethe ansatz [130, 131, 132, 133, 134, 135, 136, 137, 138], and fully many-body localized systems [139].

Let us briefly discuss how RMT is related to Srednicki's conjecture. For that purpose, we consider statistics of matrix elements of an observable  $\hat{O}$  with respect to eigenstates of a  $D \times D$  random matrix  $\hat{H}$ . By diagonalizing the observable as  $\hat{O} = \sum_i o_i |o_i\rangle \langle o_i|$ , we have

$$O_{\alpha\beta} = \sum_i o_i U_{\alpha i} U_{i\beta}, \quad (2.30)$$

where  $U_{\alpha i} = \langle E_\alpha | o_i \rangle$  denotes a transformation of the bases. When we assume that  $\hat{H}$  is drawn from the Gaussian unitary ensemble, *i.e.*, each element of  $\hat{H}$  is a complex variable that is independent and identically distributed, the matrix  $U$  can be regarded as a random matrix uniformly drawn from the unitary Haar

measure. This fact enables us to calculate the statistics of  $U$  as

$$\begin{aligned}
\overline{U_{\alpha i} U_{i \beta}} &= \frac{1}{D} \delta_{\alpha \beta}, \\
\overline{|U_{\alpha i}|^2 |U_{i \beta}|^2} &= \frac{1 + \delta_{\alpha \beta}}{D(D+1)}, \\
\overline{|U_{\alpha i}|^2 |U_{j \alpha}|^2} &= \frac{1 + \delta_{ij}}{D(D+1)}, \\
\overline{U_{\alpha i} U_{i \beta} U_{\beta j} U_{j \alpha}} &= -\frac{1}{D(D-1)(D+1)} \quad (\alpha \neq \beta, i \neq j),
\end{aligned} \tag{2.31}$$

where the overline denotes the ensemble average in this subsection. We then find that the average and variance of matrix elements become

$$\begin{aligned}
\overline{O_{\alpha \beta}} &= \frac{\delta_{\alpha \beta}}{D} \sum_i o_i, \\
\overline{O_{\alpha \alpha}^2} - \overline{O_{\alpha \alpha}}^2 &= \frac{1}{D+1} \left[ \frac{1}{D} \sum_i o_i^2 - \left( \frac{1}{D} \sum_i o_i \right)^2 \right], \\
\overline{|O_{\alpha \beta}|^2} &= \frac{D}{(D+1)(D-1)} \left[ \frac{1}{D} \sum_i o_i^2 - \left( \frac{1}{D} \sum_i o_i \right)^2 \right] \quad (\alpha \neq \beta).
\end{aligned} \tag{2.32}$$

Thus, for large  $D$ , matrix elements can be written as

$$O_{\alpha \beta} \sim \frac{\delta_{\alpha \beta}}{D} \sum_i o_i + \frac{1}{\sqrt{D}} \sqrt{\frac{1}{D} \sum_i o_i^2 - \left( \frac{1}{D} \sum_i o_i \right)^2} R_{\alpha \beta}, \tag{2.33}$$

where  $\overline{R_{\alpha \beta}} = 0$  and  $\overline{|R_{\alpha \beta}|^2} = 1$ . It can also be shown that the distribution of  $R_{\alpha \beta}$  becomes Gaussian for typical observables [140]. We note that the some statistics of  $R_{\alpha \beta}$  (such as the ratio of diagonal and off-diagonal matrix elements) depend on time-reversal symmetry of a random-matrix ensemble [141, 142, 140, 29].

The formula in Eq. (2.33) reminds us of Srednicki's conjecture in Eq. (2.27). In fact, the second fluctuating term of both equations vanish because of the factor proportional to the square root of the dimensionality of the Hilbert space ( $\sqrt{D}$  or  $e^{S_{\text{Th}}(E)/2}$ ), while the first term only contains diagonal elements. On the other hand, it is important to note that the RMT description of Srednicki's conjecture only holds within the very narrow energy shell. In Chapter 3, we show that the width of the energy shell should be exponentially small for the RMT to hold for few-body observables and Hamiltonians.

## 2.2.2 Numerical results

In this section, we review previous numerical results of the ETH, Srednicki's conjecture, and the universality described by RMT. The numerical simulation of the ETH was already demonstrated as early as in 1980's with semiclassically chaotic systems [143] and many-body spin chains [15].

One of the beautiful numerical simulations was done by Rigol, Dunjko, and Olshanii in 2008, which motivated subsequent studies. They clearly demonstrated that the ETH and thermalization hold true for nonintegrable systems, but they do not for integrable systems, using models with hardcore bosons. The ETH was then confirmed for various nonintegrable systems, *e.g.*, spinless [19] or spinful [21] fermionic systems, interacting spin systems [23], and Bose-Hubbard systems [20]. Some of them also addressed (a part of) Srednicki's conjecture [22, 24, 26, 141, 27, 142, 29, 28] and other similarities to RMT.

Let us discuss numerical results about the relation between RMT and nonintegrability in detail. In Ref. [29], it was numerically verified that nonintegrable systems exhibit universality of random-matrix ensemble whose symmetry class (called classes A, AI, or AII) corresponds to that of the system. Consider a spin chain with open boundary conditions that includes the Ising interaction, transverse and longitudinal fields, and the Dzyaloshinskii-Moriya (DM) interaction:

$$\begin{aligned}\hat{H} &= \hat{H}_I + \hat{H}_F + \hat{H}_{DM}, \\ \hat{H}_I &= - \sum_{i=1}^{N-1} J(1 + \epsilon_i) \hat{\sigma}_i^z \hat{\sigma}_{i+1}^z, \\ \hat{H}_F &= - \sum_{i=1}^N (h' \hat{\sigma}_i^x + h \hat{\sigma}_i^z), \\ \hat{H}_{DM} &= \sum_{i=1}^{N-1} \vec{D} \cdot (\vec{\sigma}_i \times \vec{\sigma}_{i+1}),\end{aligned}\tag{2.34}$$

where  $\vec{D} = D(\vec{e}_x + \vec{e}_z)/\sqrt{2}$ ,  $\epsilon_i$  is randomly chosen from the uniform distribution  $[-\epsilon, \epsilon]$  at each site to break the reflection symmetry of sites, and  $N$  is the number of the spins. We fix  $J = 1$  and  $h' = -2.1h$  in the following. While this model is integrable for  $h = D = 0$ , it becomes nonintegrable for other values of the parameters.

This model has different anti-unitary symmetries depending on parameters, which affect its local spectral statistics. In particular, the model respects complex

conjugate symmetry for  $D = 0$ , which means that  $[\hat{K}, \hat{H}] = 0$  with

$$\hat{K}\hat{\sigma}_i^x\hat{K}^{-1} = \hat{\sigma}_i^x, \hat{K}\hat{\sigma}_i^y\hat{K}^{-1} = -\hat{\sigma}_i^y, \hat{K}\hat{\sigma}_i^z\hat{K}^{-1} = \hat{\sigma}_i^z \quad (2.35)$$

for each  $i$ . Since  $\hat{K}^2 = 1$ , this model belongs to "class AI" in Dyson's classification [144]. On the other hand, for  $h = 0$ , the model respects another time-reversal symmetry

$$\hat{T}_0 := \left( \prod_{i=1}^N [i\hat{\sigma}_i^y] \right) \hat{K}, \quad (2.36)$$

which satisfies

$$\hat{T}_0\hat{\sigma}_i^x\hat{T}_0^{-1} = -\hat{\sigma}_i^x, \hat{T}_0\hat{\sigma}_i^y\hat{T}_0^{-1} = -\hat{\sigma}_i^y, \hat{T}_0\hat{\sigma}_i^z\hat{T}_0^{-1} = -\hat{\sigma}_i^z \quad (2.37)$$

and thus  $[\hat{T}_0, \hat{H}] = 0$ . Since  $\hat{T}_0 = (-1)^N$ , the model belongs to class AI for even  $N$  but class AII for odd  $N$ . Finally, for  $h \neq 0$  and  $D \neq 0$ , the model does not respect additional antiunitary symmetry and thus belongs to class A.

Figure 2.2 shows the level-spacing distribution  $P(s)$ , which is one of the prime indicators of local spectral statistics, for the models in Eq. (2.34) with different values of parameters and odd  $N$ . Here, the level spacing  $s$  is defined by  $s = \tilde{E}_{\alpha+1} - \tilde{E}_\alpha$  ( $E_0 \leq E_1 \leq \dots$ ), where  $\tilde{E}_\alpha$  is the unfolded eigenvalue (*i.e.*, the energy is normalized such that the density of states for  $\tilde{E}$  becomes constant [145]). In addition,  $P(s)$  is normalized such that

$$\int_0^\infty P(s)ds = \int_0^\infty sP(s)ds = 1. \quad (2.38)$$

For small  $D$  and  $h$ ,  $P(s)$  does not exhibit level repulsions characteristic of random-matrix universality, which means that the system is close to the integrable point ( $h = D = 0$ ). On the other hand, for sufficiently large  $h$  and  $D = 0$ , the level-spacing distribution obeys the universality of the Gaussian orthogonal ensemble (GOE) of random matrices, which is approximately given by

$$P_{\text{GOE}}(s) = \frac{\pi}{2} s e^{-\frac{\pi}{4}s^2}, \quad (2.39)$$

which corresponds to class AI. For sufficiently large  $D$  and  $h = 0$ ,  $P(s)$  obeys the universality of the Gaussian symplectic ensemble (GSE), which is approximately given by

$$P_{\text{GSE}}(s) = \frac{\delta(s)}{2} + \frac{4096}{729\pi^3} s^4 e^{-\frac{16}{9\pi}s^2}, \quad (2.40)$$

which corresponds to class AII (note that the delta peak at  $s = 0$  reflects the

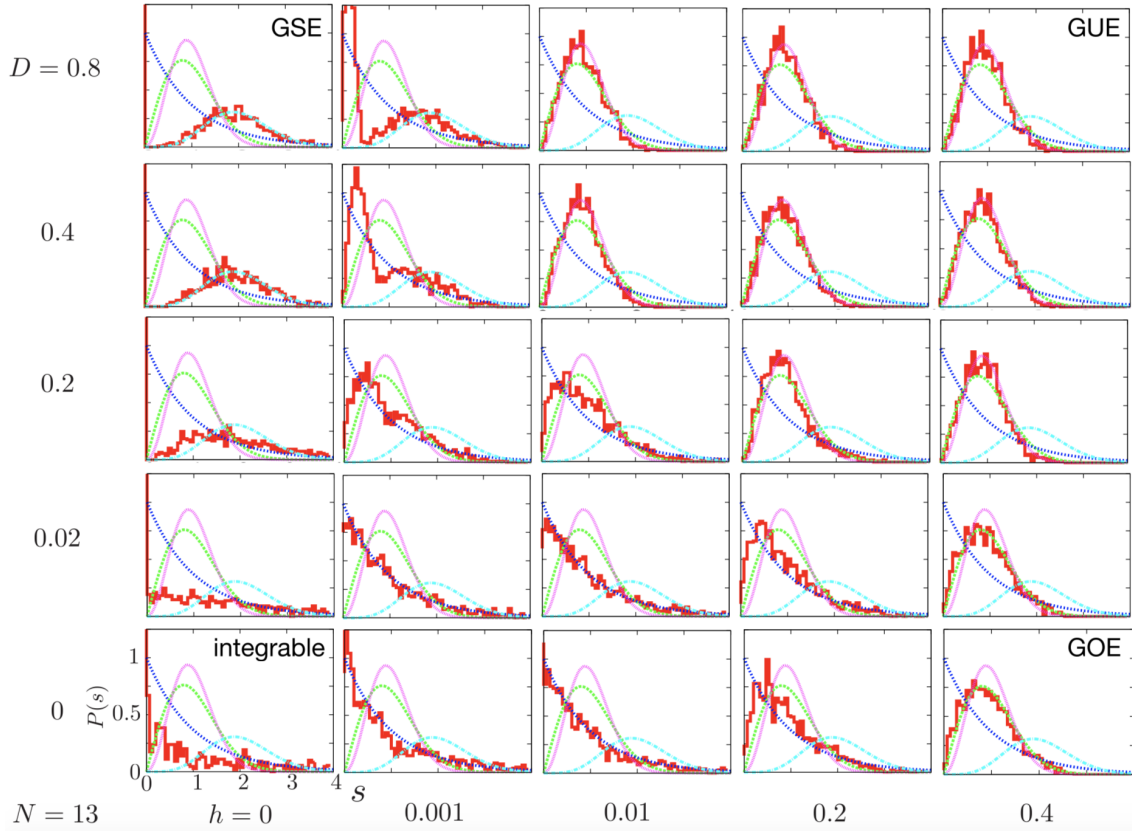


Figure 2.2: Level-spacing distributions  $P(s)$  for the models in Eq. (2.34) with different values of parameters and  $N = 13$ . For small  $D$  and  $h$ ,  $P(s)$  does not exhibit level repulsions, which demonstrates the closeness to the integrability. With increasing the parameters,  $P(s)$  shows the universality behavior described by random matrices (GUE: blue, GOE: green, or GSE: cyan), which reflects the nonintegrability of the system in classes A, AI, or AII, respectively. Reproduced from Fig. 3 of Ref. [29]. ©2019 American Physical Society.

presence of the Kramers degeneracies). Finally, for sufficiently large  $D$  and  $h$ ,  $P(s)$  obeys the universality of the Gaussian unitary ensemble (GUE), which is approximately given by

$$P_{\text{GUE}}(s) = \frac{32}{\pi^2} s^2 e^{-\frac{4}{\pi} s^2}, \quad (2.41)$$

which corresponds to class A. In the intermediate parameters, level-spacing distributions exhibit crossover between these universal distributions.

Reference [29] also investigated the statistical fluctuations of matrix elements  $O_{\alpha\beta}$ , *i.e.*, the  $R_{\alpha\beta}$  factor in Eq. (2.27). It was found that the statistics of  $R_{\alpha\beta}$  for nonintegrable systems depend on the symmetry of the Hamiltonian and the observable, and are described by the universality of random matrices. For example, the ratio of the standard deviations between diagonal and off-diagonal matrix elements becomes unity for class A, which is predicted by the GUE calculation; see Eq. (2.32). However, it becomes  $\sqrt{2}$  for the Hamiltonian in class AI and even observables under time-reversal transformation, which is predicted by the GOE calculation.

### 2.2.3 Analytical results

While we have explained that a vast amount of numerical results support the relation among nonintegrability, random matrices, and the ETH, its rigorous justification is very difficult and only few results exist. Up to now, there are no analytical proof of the ETH, Srednicki's conjecture, or the random-matrix universality of level-spacing distributions for any system.

On the other hand, several analytical results have been obtained for another local spectral statistics, *i.e.*, the spectral form factor (SFF), which is defined by the inverse Fourier transform of the two-point correlation function of the density of states, which is the function of energy. The SFF depends on a variable with the dimension of time, since the density of states depends on energy. For random matrices, the SFF  $K(\tau)$  ( $\tau$  is a rescaled time with respect to the inverse of the mean level spacing) is given by

$$K(\tau) = \tau \quad (2.42)$$

for GUE and

$$K(\tau) = 2\tau - \tau \ln(1 + 2\tau) = 2\tau - 2\tau^2 + 2\tau^3 - \dots \quad (2.43)$$

for GOE. The SFF of nonintegrable systems has numerically been known to ex-

hibit random-matrix universality that corresponds to the same symmetry class, consistent with the BGS conjecture [145].

The first step toward the proof of this conjecture for the SFF was made for semiclassically chaotic systems by Berry [146], who employed Gutzwiller's trace formula, which connects the quantum spectral property and classical periodic orbits. While he obtained only the leading term of the SFF with respect to  $\tau$ , subsequent works [147, 148] completed the full-order calculations for  $\tau$ , demonstrating the success of the BGS conjecture for the SFF in certain semiclassical systems (such as chaotic billiards).

Only recently has the SFF been investigated for many-body nonintegrable systems. In Ref. [149], the authors imitated Berry's method based on the periodic-orbit theory and derived the GOE universality of the SFF (up to the  $\tau^2$  term) semi-analytically. The same group also derived more rigorously the random-matrix universality of the GOE-type SFF (up to the leading order) in the following Floquet nonintegrable model [150]:

$$\begin{aligned}\hat{H}_{\text{KI}} &= \hat{H}_{\text{I}} + \sum_{m=-\infty}^{\infty} \delta(t - m) \hat{H}_{\text{K}}, \\ \hat{H}_{\text{I}} &= \sum_{j=1}^L \left\{ J \hat{\sigma}_j^z \hat{\sigma}_{j+1}^z + h_j \hat{\sigma}_j^z \right\}, \quad \hat{H}_{\text{K}} = b \sum_{j=1}^L \hat{\sigma}_j^x\end{aligned}\quad (2.44)$$

at some specific parameters (*e.g.*  $|J| = |b| = \pi/4$ ) with arbitrary on-site disorder  $h_j$ , utilizing the emergent spacetime duality of the model at these parameters. It was also investigated what happens when the parameters are away from the dual point [151].

Another type of nonintegrable models for which the SFF is analytically known is the random unitary circuits, where randomness ensures the chaotic behavior [152, 153, 154] while the systems keep locality and unitarity. In Ref. [155], the authors considered a one-dimensional circuit chain composed of  $L$  qudits (*i.e.* quantum spins with  $q$  states). Its dynamics is described by a Floquet operator  $W = W_2 W_1$ , where  $W_1 = U_1 \otimes U_2 \otimes \dots \otimes U_L$  generates independent random rotations at each site ( $U_j$  is given by  $q \times q$  random unitary matrices), and  $W_2$  couples neighboring sites  $j$  and  $j + 1$  by multiplying a random phase factor. Then, the SFF is exactly calculated in the  $q \rightarrow \infty$  limit, which turns out to obey the universality of the GUE. Similar results were obtained in another circuit model which conserves the local charge [156].

Note that these analytical techniques for many-body systems are also used

to justify some dynamical signatures of nonintegrable models. For example, the dynamics of bipartite entanglement entropy, which is expected to grow linearly before saturation for generic nonintegrable models, is analytically demonstrated for a spacetime-dual model [157] and random unitary circuits [158].

## 2.3 Many-body localization (MBL) and non-thermalization

While we have explained the scenario for thermalization in generic nonintegrable systems, some systems are known not to exhibit thermalization. As mentioned in the introduction, one of the most important examples is many-body localization (MBL), for which the ETH breaks down owing to (typically) strong disorder. Here, we review MBL and some other important concepts that challenge thermalization.

### 2.3.1 Many-body localization and its phenomenology

Many-body localization is often said to be an interacting version of the Anderson localization in noninteracting systems. Indeed, while the Anderson localization is a phenomenon in which energy eigenstates become localized in real space, eigenstates become localized in the Fock space for MBL. Such localization typically occurs owing to a strongly disordered potential; hopping of particles between neighboring sites is suppressed owing to a large potential difference. Consequently, the ETH is violated and thermalization does not occur in general.

Let us consider the prototypical example of the MBL, *i.e.*, the Heisenberg model with a disordered magnetic field in one dimension:

$$\hat{H} = \sum_{i=1}^L \hat{\mathbf{S}}_i \cdot \hat{\mathbf{S}}_{i+1} - h_i \hat{S}_i^z, \quad (2.45)$$

where  $\hat{\mathbf{S}}_i = (\hat{S}_i^x, \hat{S}_i^y, \hat{S}_i^z) = \hat{\sigma}_i/2$  and the periodic boundary condition is assumed. Here,  $h_i$  is uniformly and randomly chosen from the range  $[-h, h]$  depending on site  $i$ . The property of this model becomes completely different for small and large  $h$ . For small  $h$ , sufficiently highly excited states satisfy the ETH: this is in contrast with the Anderson localization, where arbitrary small disorder is enough to localize the system in one dimension. On the other hand, for  $3.6 \simeq h_c \leq h$ , all eigenstates are numerically found to become localized, which is called the "fully MBL [139]." This critical value defines the MBL transition.

We first discuss the phenomenology of the fully MBL phases. In such strongly

localized systems, we expect that there is no transport, which indicates that a set of local conserved quantities exists. Then, the Hamiltonian in Eq. (2.45) for large  $h$  can be diagonalized in the following form:

$$\hat{H} = E_0 + \sum_i h'_i \hat{\tau}_i^z + \sum_{ij} J'_{ij} \hat{\tau}_i^z \hat{\tau}_j^z + \sum_{n=3} \sum_{i_1 \dots i_n} K_{i_1 \dots i_n}^{(n)} \hat{\tau}_{i_1}^z \dots \hat{\tau}_{i_n}^z \quad (2.46)$$

with some constants  $E_0, h'_i, J'_{ij}, K_{i_1 \dots i_n}^{(n)}$ . Here,  $J'_{ij}$  and  $K_{i_1 \dots i_n}^{(n)}$  exponentially decrease with increasing  $|i - j|$  and  $|i_1 - i_n|$ . The new Pauli operators  $\hat{\tau}_i^\alpha$  ( $\alpha = x, y, z$ ) (called l-bits) are quasi-localized; they have a large overlap with  $\hat{\sigma}_i^\alpha$  and an exponentially small overlap with  $\hat{\sigma}_j^\alpha$  ( $|i - j| \gg 1$ ). Put differently,  $\hat{\tau}_i^\alpha$  can be obtained by a quasi-local unitary transformation of  $\hat{\sigma}_i^\alpha$  for sufficiently large disorder.

From the expression in Eq. (2.46), the energy eigenstates are known to be characterized by a set of quasi-localized conserved quantities as  $|E_\alpha\rangle = |\tau_1, \dots, \tau_N\rangle$ , where  $\tau_i = \pm 1$ . These conserved quantities lead to the breakdown of the RMT picture, such as the ETH [57] and Srednicki's conjecture [27]. In addition, the level-spacing distributions in the MBL phase obey the Poisson distribution

$$P_{\text{Po}}(s) = e^{-s}, \quad (2.47)$$

which reflects the fact that each neighboring eigenstate becomes uncorrelated owing to the conservation law. Another important feature is the area law of the entanglement entropy [159], as detailed in the next subsection.

These spectral properties of the MBL profoundly affect its dynamics. For example, the expectation values of local observables retain the information of initial values for a long time, as indicated by the breakdown of the ETH. As mentioned in the introduction, they are experimentally observed using *e.g.*, cold atoms [59, 61]. Disorder is also known to affect transport properties [160].

On the other hand, we need a more sophisticated probe to distinguish between the Anderson localization and MBL. One of the candidates is the half-chain entanglement entropy, which is defined as

$$S = -\text{Tr}[\hat{\rho}_{L/2} \ln \hat{\rho}_{L/2}], \quad (2.48)$$

where  $\hat{\rho}_{L/2} = \text{Tr}_{L/2}[\hat{\rho}]$  is the reduced density matrix for a state  $\hat{\rho}$ . After a quench starting from a product state, the state  $\hat{\rho}(t) = |\psi_t\rangle \langle \psi_t|$  gets entangled and  $S(t)$  starts to grow. If the system belongs to the delocalized (ETH) phase,  $S(t)$  typically linearly grows first and shows saturation to a thermal value [161]. If the system exhibits the Anderson localization,  $S(t)$  quickly becomes some constant [162]. Finally, if the system exhibits MBL,  $S(t)$  shows nontrivial logarithmic growth,

$S(t) \simeq \log t$  [162] (see Fig. 2.3). To intuitively understand this behavior for the MBL, we consider an initial product state in the basis of  $\hat{\tau}_j^z$  for simplicity:

$$|\psi_0\rangle = \prod_j (A_j |\tau_j = +1\rangle + B_j |\tau_j = -1\rangle), \quad (2.49)$$

where  $|A_j|^2 + |B_j|^2 = 1$  (although many works consider product states in the basis of the physical spins  $\hat{\sigma}_j^z$ ). Owing to the Hamiltonian in Eq. (2.46),  $|\psi_0\rangle$  acquires a phase. For the spin  $i$  to be entangled with the distant spin  $j$ , the phase owing to the interaction that connects these spins (e.g.,  $K_{i,\dots,j}^{(n)} \hat{\tau}_i^z \cdots \hat{\tau}_j^z$ ) should become large. Since the strength of such interactions decays exponentially, we need an exponentially long time to entangle distant spins. In turn, we have a logarithmic growth of entanglement as function of time.

Another dynamical probe with which we can distinguish the Anderson localization from MBL is an out-of-time-ordered correlator [163, 164, 165, 166], which is given by

$$C(t) = \langle [\hat{A}(t), \hat{B}]^\dagger [\hat{A}(t), \hat{B}] \rangle \quad (2.50)$$

for two local observables  $\hat{A}$  and  $\hat{B}$ . For example,  $C(t)$  is known to distinguish the way of information propagation of the system, which is linear, logarithmic and zero for the delocalized, MBL, and Anderson localized phases [167, 168, 169], respectively.

The absence of the ETH in many-body localized phases means that even highly excited states can possess quantum order, which is not allowed in thermal equilibrium, as mentioned in the introduction. For example, excited states can exhibit a phase transition within MBL phases, such as a transition between paramagnetic and spin-glass phases [170]. This is also the case for a Floquet system, where MBL prevents the system from heating. In a Floquet MBL system, another interesting phenomenon, *i.e.*, a discrete time-crystalline (DTC) phase appears. In a DTC-phase of a system which is periodically driven with a period  $T$ , the expectation value oscillates with the period  $nT$  ( $n = 2, 3, \dots$ ). It is known that the transition into a DTC phase is a consequence of the phase transition of the Floquet eigenstates that remain localized [171].

Since MBL is not easy to study analytically, many of the works aim to reveal its property with numerical simulations. Many numerical simulations rely on exact diagonalization [57, 162, 172, 139, 173], which gives complete information of the system but is limited to small system sizes. Another possible method is to use matrix-product states, which can simulate large systems as long as the state has

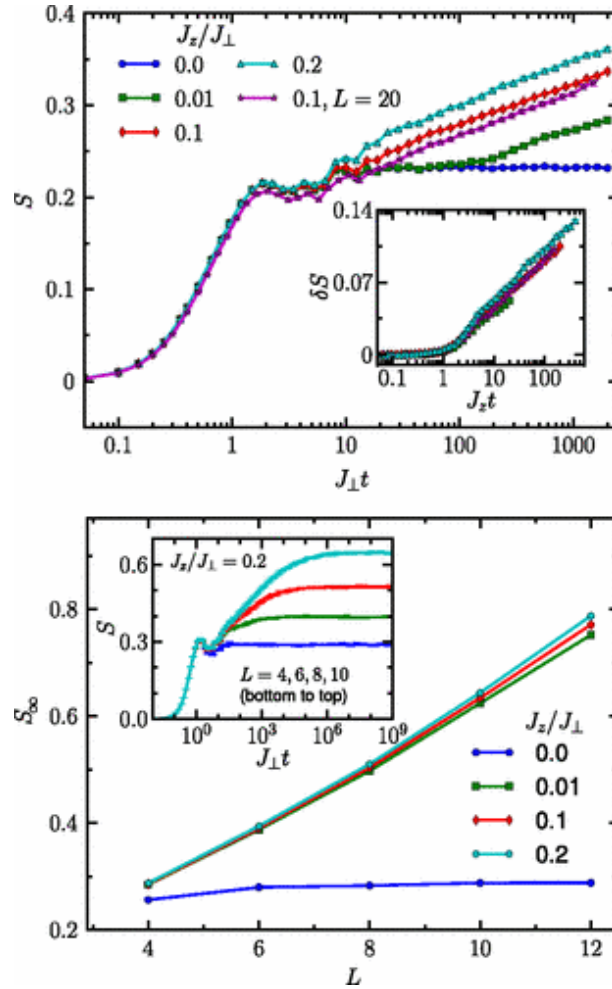


Figure 2.3: (Top) Half-chain entanglement entropy  $S(t)$  of a 1D XXZ spin system. The strength of the interaction is given by  $J_z/J_\perp$ , where  $J_z$  and  $J_\perp$  are coupling strengths of zz and xx (yy) components, respectively. For zero interaction (namely, in the case of the Anderson localization)  $S(t)$  is saturated quickly. On the other hand, for nonzero interactions (in the case of MBL)  $S(t)$  exhibits a logarithmic unbounded growth. Inset shows the same data with rescaled time, for which  $J_z = 0$  values are subtracted. (Bottom) Saturation values of the entanglement entropy. Reprinted figure with permission from Fig.1 of [Jens H. Bardarson, Frank Pollmann, and Joel E. Moore. Unbounded growth of entanglement in models of many-body localization. Phys. Rev. Lett., **109**:017202, Jul 2012 (Ref. [162])] Copyright 2012 by the American Physical Society.

low entanglement. Since energy eigenstates satisfy the area law of entanglement entropy and growth of entanglement is slow, matrix-product states are expected to be useful to simulate eigenstates and dynamics of MBL systems [174, 175]. We also note that state-of-the-art-techniques such as machine learning techniques are also utilized to identify MBL phases [176, 177].

While MBL is actively investigated for the above reasons, it is still under debate in what conditions the MBL phase exists [178]. In fact, the MBL is analytically proven only for the one-dimensional transverse Ising model with disorder on the basis of the picture of quasi-local conserved quantities discussed above [179, 180]. The existence of MBL in higher dimensions is more controversial. Semi-analytical arguments indicate that a small delocalized region, which exists owing to the fluctuation of disorder, is enough to delocalize the entire system in the thermodynamic limit for dimensions  $d \geq 2$  [181]. On the other hand, experimental [61] and numerical [182] studies of about  $10 \times 10$ -site lattice in two dimensions show the signature of MBL. Another ingredient that affects the existence of MBL is the symmetry of the system. Indeed, if the Hamiltonian respects a non-Abelian symmetry, the energy eigenstates cannot be MBL unless the system exhibits spontaneous symmetry breaking [183].

### 2.3.2 Characterizing the MBL transition

One of the most interesting challenges is to investigate the phase transition between delocalized and MBL phases. Indeed, such a transition is very different from the usual thermal or ground-state phase transitions, since the transition is defined by excited eigenstates. Reference [173] numerically investigated the transition point between delocalized and MBL phases by using several different measures such as the level-spacing distributions. Let us consider here the entanglement entropy of energy eigenstates. As shown in Fig. 2.4(top), the variance of the half-chain entanglement entropy  $\sigma_E$  is expected to have a peak near the critical point [170, 173] and exhibit a scaling behavior. Figure 2.4(middle) shows that the entanglement entropy  $S_E$  obeys the volume law (*i.e.*,  $S_E/L$  is almost constant for large  $L$ ) for delocalized phases and the area law (*i.e.*,  $S_E/L$  is decreasing as  $\propto L^{-1}$  for large  $L$ ) for localized phases; note that they considered a one-dimensional system. Moreover, Fig. 2.4(bottom) shows that  $S_E$  obeys a critical scaling as

$$\frac{S_E}{L} = f(L|h - h_c|^{\nu}), \quad (2.51)$$

where  $\nu$  is a critical exponent. Note that it is still a controversial problem to precisely evaluate  $\nu$  [184].

Another interesting criterion of the MBL transition was proposed in Ref. [185], which studied the distribution of matrix elements of a local observable between the eigenstates of the system. The authors of Ref. [185] consider the following measure:

$$\mathcal{G}(L) = \ln \frac{|V_{\alpha, \alpha+1}|}{E'_{\alpha+1} - E'_\alpha} \quad (2.52)$$

for some local observable  $\hat{V}$ , where  $E'_\alpha = E_\alpha + V_{\alpha\alpha}$ . This indicator measures the stability of energy eigenstate  $|E_\alpha\rangle$  of the original Hamiltonian  $\hat{H}$  against a local perturbation  $\hat{V}$ . Indeed, if we consider

$$\hat{H} + \hat{V} = \sum_{\alpha} E'_\alpha |E_\alpha\rangle \langle E_\alpha| + \sum_{\alpha \neq \beta} V_{\alpha\beta} |E_\alpha\rangle \langle E_\beta| \quad (2.53)$$

and use the first-order perturbation theory on the right-hand side, the perturbed eigenstates can be written as

$$|E_\alpha\rangle + \sum_{\beta(\neq\alpha)} \frac{V_{\beta\alpha}}{E'_\beta - E'_\alpha} |E_\beta\rangle + \dots \quad (2.54)$$

Thus, for the leading correction to be small, we require

$$\left| \frac{V_{\beta\alpha}}{E'_\beta - E'_\alpha} \right| \ll 1. \quad (2.55)$$

On the other hand, the perturbation breaks down (*i.e.*, eigenstates are unstable against the perturbation) when

$$\left| \frac{V_{\beta\alpha}}{E'_\beta - E'_\alpha} \right| \gg 1. \quad (2.56)$$

By taking the logarithm and setting  $\beta = \alpha + 1$ , we obtain the indicator in Eq. (2.52).

The crucial finding in Ref. [185] is that  $\mathcal{G}(L)$  considerably changes its behavior at the delocalized-MBL transition. Indeed, the authors found that  $\mathcal{G}(L) \sim \alpha L$  for the delocalized phase but  $\mathcal{G}(L) \sim -\beta L$  for the MBL phase ( $\alpha, \beta$  are some positive constants). At the transition point,  $\mathcal{G}(L)$  becomes independent of  $L$ . In other words, the eigenstates are unstable in the thermodynamic limit only for the delocalized phase.

The above behavior is understood as follows. For the delocalized (ETH) phase, matrix elements  $V_{\alpha, \alpha+1}$  are expected to be proportional to  $e^{-S_{\text{Th}}(E)/2}$  according to

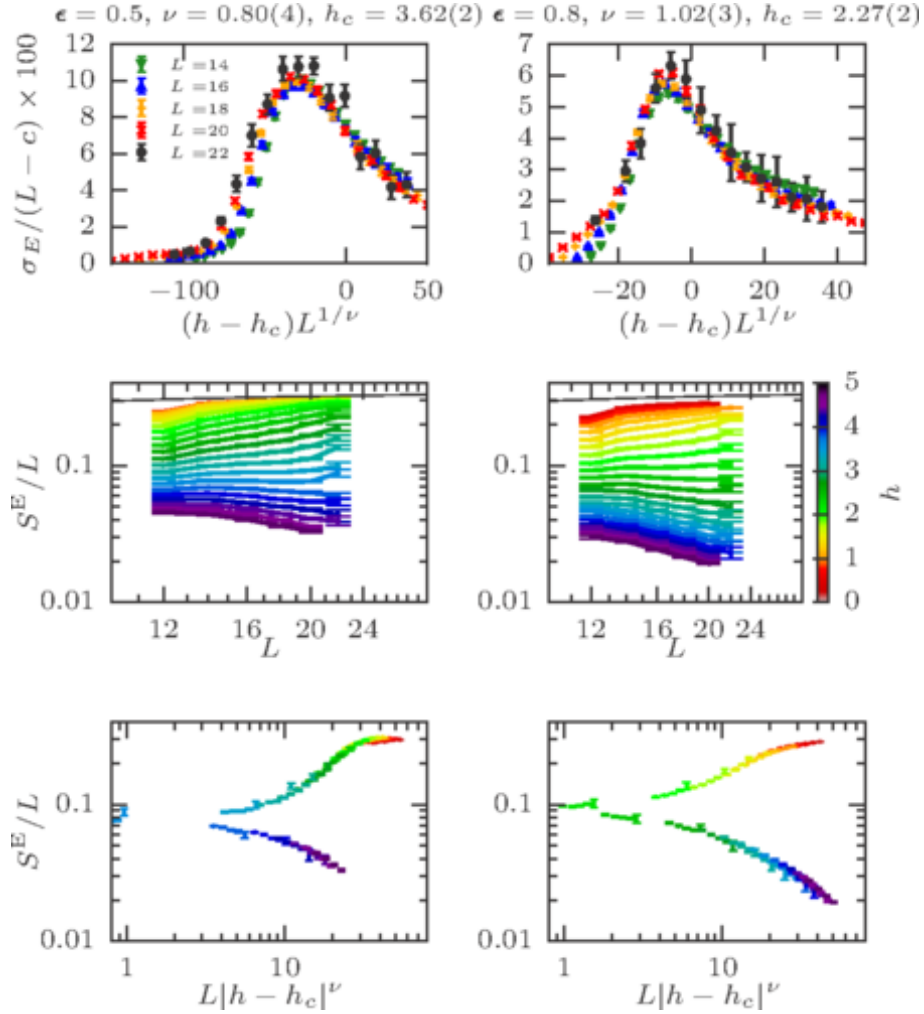


Figure 2.4: Transition between delocalized and MBL phases. The left and right columns show the results for different energy scales. (top) Rescaled standard deviation of the half-chain entanglement entropy for different system sizes. The scaling behavior is observed for appropriate  $\nu$  and  $h_c$ . (middle)  $L$ -dependence of the half-chain entanglement entropy  $S_E$  divided by  $L$  for different  $h$ . We find a crossover transition from the volume law to the area law with increasing  $h$ . (bottom) The critical scaling of  $S_E/L$ . We can see the data collapse for different  $h$  by using the same  $\nu$  and  $h_c$  as in the top figures. Reprinted figure with permission from Fig.3 of [David J. Luitz, Nicolas Laflorencie, and Fabien Alet. Many-body localization edge in the random-field heisenberg chain. Physical Review B, **91**:081103(R), Feb 2015 (Ref. [173])] Copyright 2015 by the American Physical Society.

Srednicki's conjecture in Eq. (2.27). On the other hand, the typical level spacing decreases as  $E'_{\alpha+1} - E'_\alpha \sim e^{-S_{\text{Th}}(E)}$ . Thus,  $\mathcal{G}(L) \sim \alpha L$  is expected for positive  $\alpha$ . For the MBL phase, however,  $V_{\alpha,\alpha+1}$  is far more suppressed because energy eigenstates  $|E_\alpha\rangle$  and  $|E_{\alpha+1}\rangle$  are characterized by different sets of quasi-local conserved quantities. The perturbation  $\hat{V}$  only acts on a local region and can little affect the quasi-local conserved quantities in the distance. Consequently,  $|E_{\alpha+1}\rangle$  and  $\hat{V}|E_\alpha\rangle$  have an exponentially small overlap, leading to  $\mathcal{G}(L) \sim -\beta L$  for positive  $\beta$ . Strictly speaking, there can be higher-order perturbation effects that alters the nature of the localization [180], but we neglect this for simplifying the discussion.

Phenomenologically, the critical phenomenon is understood by the growth of the delocalized (resonant) clusters. While they cannot grow enough to delocalize the entire system for the localized phase, they can encompass the entire system at and below the critical point. To describe this process, different renormalization-group methods are employed [186, 187, 188]. Such schemes predict the critical exponent  $\nu$  in large systems as well as the anomalous subdiffusive transport in the delocalized phase near criticality, namely the Griffiths phase [160].

### 2.3.3 Other systems where thermalization is absent

We here briefly review systems in which thermalization is absent even without localization.

#### Integrable systems

One of the important classes is integrable systems, whose importance on thermalization was known before the MBL. Let us consider semiclassical systems whose classical counterparts are integrable, *i.e.*, an extensive set of integrals of motion exists. In that case, the level-spacing distributions obey the Poisson distribution according to the Berry-Tabor conjecture [120] and the eigenstates do not obey RMT [121].

A similar result is expected to hold true for integrable quantum many-body systems. Here, we define integrable systems as those whose eigenstates are uniquely determined by an extensive number of local conserved quantities, although other definitions can also be made [123]. In particular, we focus on systems that are mapped to free particles [124, 125, 70, 126, 127, 128, 129, 74] or solved by the Bethe ansatz [130, 131, 132, 133, 134, 135, 136, 137, 138]. It is known that such integrable systems have the level-spacing distributions obeying the Poisson dis-

tribution, although a system that does not obey this principle has recently been found [189]. Moreover, the ETH and Srednicki's conjecture do not hold, and thus thermalization is absent [16, 18]. Instead, these systems is expected to relax to the so-called generalized Gibbs ensemble (GGE) [190, 191, 124, 70],

$$\hat{\rho}_{\text{GGE}} = \frac{e^{-\sum_m \lambda_m \hat{I}_m}}{\text{Tr}[e^{-\sum_m \lambda_m \hat{I}_m}]}, \quad (2.57)$$

where  $\hat{I}_m$  denote a set of conserved quantities that retain the initial information about the system in the course of time evolution. We note that the GGE appears owing to an extensive number of local conserved quantities and complete integrability is not necessarily needed [192].

Let us comment on the main difference between the clean integrable systems (free systems and Bethe-ansatz-solvable systems) and the (fully) MBL, both of which have integrable structures in that their eigenstates are uniquely determined by an extensive number of local conserved quantities. Firstly, while "local conserved quantities" denote an extensive sum of local operators (macroscopically conserved quantities) for the clean case, they are (quasi)locally conserved without taking the sum for the MBL. Secondly, while the clean integrable systems may not be robust under additional perturbations in the Hamiltonian parameters, MBL systems robustly exist for generic parameters if the disorder is strong.

## Quantum many-body scars

Another notable example without thermalization that have attracted much attention recently is a quantum many-body scar. A quantum scar was originally studied in semiclassical systems [193]; even when the classical limit is chaotic, there exist rare excited energy eigenstates that violate the RMT description, which reflects the unstable periodic orbits in classical chaotic systems.

Similarly, it has recently been found that non-thermal excited eigenstates can exist even in nonintegrable systems. These eigenstates are called quantum many-body scars and largely affect the dynamics for some specific initial states [75, 76]. One of the most important examples is the so-called PXP model, which effectively describes the blockade effect in Rydberg atoms [76, 194, 195, 196]:

$$\hat{H} = \hat{Q}_{i-1} \hat{\sigma}_i^x \hat{Q}_{i+1}, \quad (2.58)$$

where

$$\hat{Q}_i = \frac{1 - \hat{\sigma}_i^z}{2} = |\downarrow\rangle\langle\downarrow| \quad (2.59)$$

is the projection operator, and we consider the periodic boundary condition for simplicity. The dynamics of this model is constrained owing to the projections. Indeed, configurations including neighboring up states are not allowed. Then, the dimensionality of the Hilbert space essentially grows following the Fibonacci sequence. Importantly, the level-spacing distribution of this model obeys the Wigner-Dyson statistics, which indicates the nonintegrability of the system.

Reference [76] showed that the model in Eq. (2.58) hosts non-thermal rare eigenstates in the middle of the spectra, while most of the eigenstates obey the ETH. Owing to these non-thermal states, some initial state, such as the Neel state  $|\uparrow\downarrow\uparrow\downarrow \dots\rangle$ , exhibits an unusual long-time oscillation, while most of the initial states rapidly relax to thermal equilibrium. These eigenstates, called "quantum many-body scars," have been investigated in terms of the proximity of integrability [197], the forward-scattering approximation [194], and the semiclassical periodic orbits defined by the time-dependent variational principle [198]. It is also known exactly that these scar states can break the ETH in the thermodynamic limit [199]. Let us consider a matrix-product state

$$|\Phi_s\rangle \propto \sum_{\{\sigma\}=\uparrow,\downarrow} \text{Tr}[B^{\sigma_1} C^{\sigma_2} \dots B^{\sigma_{L-1}} C^{\sigma_L}] |\sigma_1 \dots \sigma_L\rangle \quad (2.60)$$

with

$$B^0 = \begin{pmatrix} 1 & 0 & 0 \\ 0 & 1 & 0 \end{pmatrix}, \quad B^1 = \sqrt{2} \begin{pmatrix} 0 & 0 & 0 \\ 1 & 0 & 1 \end{pmatrix}, \quad (2.61)$$

$$C^0 = \begin{pmatrix} 0 & -1 \\ 1 & 0 \\ 0 & 0 \end{pmatrix}, \quad C^1 = \sqrt{2} \begin{pmatrix} 1 & 0 \\ 0 & 0 \\ -1 & 0 \end{pmatrix}. \quad (2.62)$$

Note that the state in Eq. (2.60) satisfies  $\hat{H} |\Phi_s\rangle = 0$ . Thus,  $|\Phi_s\rangle = 0$  is an eigenstate of  $\hat{H}$  with  $E_\alpha = 0$ , which corresponds to the state at the infinite temperature. We can calculate that  $\langle\Phi_s|\hat{\sigma}_1^z|\Phi_s\rangle \neq \text{Tr}[\hat{\rho}_{T=\infty}\hat{\sigma}_1^z]$ , which means that  $|\Phi_s\rangle$  breaks the ETH.

Such non-thermal states embedded in the middle of the spectra of nonintegrable systems are actively investigated in several situations. Indeed, they are found to exist in systems including the Affleck-Kennedy-Lieb-Tasaki model [200, 201], Ising models with certain parameters of transverse and longitudinal fields [202],

a spin-ladder model [203], a spin-1 XY magnets [204], and "fractonic circuits [205]".

It is also known that the embedding can be done systematically [122, 206]. Reference [122] considered a Hamiltonian in the following form

$$\hat{H} = \sum_j \hat{P}_j \hat{h}_j \hat{P}_j + \hat{H}', \quad (2.63)$$

where  $\hat{P}_j$  is a local projector which eliminates the state in a set  $\mathcal{T}$  (*i.e.*,  $\hat{P}_j |\Phi\rangle = 0$  for  $|\Phi\rangle \in \mathcal{T}$ ) for any  $j$ ,  $\hat{h}_j$  is an arbitrary local operator and  $\hat{H}'$  is the Hamiltonian satisfying  $\hat{H}' |\Phi\rangle \in \mathcal{T}$  if  $|\Phi\rangle \in \mathcal{T}$ . Since  $\hat{h}_j$  can be arbitrarily complex,  $\hat{H}$  is in general nonintegrable. On the other hand,  $\hat{H}'$  determines eigenstates that are diagonalized in the  $\mathcal{T}$ -space regardless of  $\hat{h}_j$ , which means that the eigenstates in  $\mathcal{T}$  and the complement of  $\mathcal{T}$  are uncorrelated. This absence of the correlation leads to the breakdown of the ETH.

## 2.4 Relaxation dynamics in closed quantum many-body systems

We have mainly discussed long-time dynamics and relaxation to thermal states, which are understood by the ETH. On the other hand, there are a lot of universal phenomena before the complete relaxation, which are not explained by the ETH. Here we briefly discuss some recent topics on non-equilibrium dynamics of closed quantum many-body systems.

One interesting subject is dynamical chaos, probed by, *e.g.*, the out-of-time-ordered correlator (OTOC) defined in Eq. (2.50). To see the essence of the OTOC, let us consider a semiclassical system with one particle, which is described by canonical variables  $\hat{q}$  and  $\hat{p}$ . Then, with the semiclassical approximation,  $C(t)$  can be written as

$$C(t) = \langle [\hat{p}(t), \hat{q}]^\dagger [\hat{p}(t), \hat{q}] \rangle \rightarrow -\hbar^2 \left( \frac{\partial p_t}{\partial p} \right)^2 \sim e^{2\lambda t} \quad (2.64)$$

for a chaotic system. Here  $q$  and  $p$  are the corresponding classical variables,  $p_t$  is a momentum at time  $t$  obtained from the classical equation, and  $\lambda$  is the Lyapunov exponent, which characterizes classical chaos through its exponential sensitivity. Maldacena and coauthors [166] conjectured that  $\lambda$  obeys a nontrivial bound,  $\lambda \leq 2\pi k_B T / \hbar$  for a thermal state at temperature  $T$ . Such a bound is achieved by the Sachdev-Ye-Kitaev model, which consists of all-to-all Majorana many-body interactions and has a property analogous to that of some Black-

hole models [165, 164, 207, 208]. The OTOC is not only relevant to quantum chaos and the Black holes, but also related to quantum information [209, 153], characterization of static and dynamical phases of matter [167, 168, 169], and irreversibility [210].

Another important subject is whether or not the universality in nonequilibrium phenomena known in classical systems emerges in closed quantum many-body systems. For example, emergence of Kardar-Parisi-Zhang universality [211] or Edwards-Wilkinson universality [212] has been investigated in quantum many-body systems [213, 214, 215, 216, 217], inspired by fluctuation hydrodynamics [218, 219] and surface growth [220] in classical systems.

Another example of the universal phenomena appears in the coarsening dynamics of symmetry-broken domains, which shows a self-similar behavior during time evolution. To be more precise, the equal-time correlation function  $C(x = |i - j|, t) = \langle \hat{O}_i(t) \hat{O}_j(t) \rangle$  at time  $t$  obeys the scaling form

$$C(x, t) \propto f(x/L(t)), \quad (2.65)$$

where the growth of  $L(t)$  determines the universality of the coarsening dynamics. Though such scaling behavior is well known in dissipative classical systems [221], it has recently been known that closed quantum systems can obey this scaling law [222, 223, 224, 225, 216]. For instance,  $L(t) \propto t^{2/3}$ , namely binary liquid universality is obtained for the Ising-type domain in ferromagnetic spin-1 spinor gases in two dimensions [224], but  $L(t)$  is characterized by the exponential integral in one dimension [225]. A similar concept is a notion of the non-thermal fixed point, which states that certain initial states should be attracted to a long-lived nonequilibrium state and show the critical behavior there. Specifically, a non-thermal fixed point is expected to be diagnosed by the correlation function which behaves as  $C(x, t) = t^\gamma f(x/t^\beta)$  for some critical exponents  $\gamma$  and  $\beta$ . Originally proposed in Ref. [226], the non-thermal fixed points are actively investigated as a unifying mechanism for the scaling behavior in nonequilibrium systems.

# Chapter 3

## Atypicality of most few-body observables

### 3.1 Motivation

In the previous chapter, we have explained that the ETH is the most promising candidate to justify thermalization in closed quantum systems. While localization, integrability, and some other mechanisms (such as quantum many-body scars) can violate the ETH, it is still believed that the ETH holds true for generic few-body or local quantum many-body systems without such special reasons.

Interestingly, von Neumann already addressed analytically why the ETH seems to hold true for generic macroscopic systems in his paper in 1929 [2], relying on the "typicality argument". As detailed in the next section, the typicality argument essentially consists of two steps. First, we mathematically prove the typicality on the matrix elements; for almost all (*i.e.*, typical) unitary transformations of the bases between the Hamiltonian  $\hat{H}$  and observable  $\hat{O}$  over the uniform Haar measure, the maximum fluctuation of the matrix elements within the microcanonical energy shell becomes exponentially small. Secondly, we conjecture that the unitary transformation between physically relevant  $\hat{H}$  and  $\hat{O}$ , *i.e.*, few-body (or local) Hamiltonians and observables, is actually typical, *i.e.*, satisfies the above property on the maximum fluctuation, unless some special reason exists, such as integrability and localization. Note that while the first step is rigorous, the second step is a physical conjecture. The typicality argument is a sufficient condition for the ETH, since an exponentially small fluctuation of the matrix elements in the microcanonical shell implies the condition in Eqs. (2.18) and (2.19).

While the typicality argument has been a promising candidate to justify the

ETH for generic systems and followed by recent works [3, 30], whether this argument is really true for the experimentally relevant setups was not sufficiently discussed. In this chapter, we show that the typicality argument cannot be applied to the setup with most few-body observables and a few-body Hamiltonian, which is a natural setup for experiments. Indeed, the diagonal matrix elements for most few-body observables are shown not to behave typically if the width of the energy shell decreases at most polynomially as we increase the size of the system.

We first review the mathematical formulation of the typicality argument, following Ref. [30]. We then show our main results of the atypicality of most few-body observables, although near  $N$ -body observables can be consistent with the typicality argument, where  $N$  denotes the system size. We also prove atypicality in another setup with locality. Finally, we discuss the relation with previous related works and conclude the chapter with outlook.

## 3.2 Review on the typicality argument

We first review the rigorous formulation of the typicality argument on the basis of Ref. [30], which generalizes von Neumann's argument on macroscopic observables to arbitrary observables. We introduce the Hilbert space  $\mathcal{H}_{E,\Delta E}$  of an energy window with median  $E$  and width  $2\Delta E$ . The projection operator onto this Hilbert space is given by

$$\hat{\mathcal{P}}_{E,\Delta E} = \sum_{|E_\alpha - E| \leq \Delta E} |E_\alpha\rangle \langle E_\alpha|. \quad (3.1)$$

We consider the spectral decomposition of the observable  $\hat{O}$  projected onto  $\mathcal{H}_{E,\Delta E}$ :

$$\hat{\mathcal{P}}_{E,\Delta E} \hat{O} \hat{\mathcal{P}}_{E,\Delta E} = \sum_{i=1}^{d_{E,\Delta E}} a_i |a_i\rangle \langle a_i|, \quad (3.2)$$

where  $d_{E,\Delta E} = \dim[\mathcal{H}_{E,\Delta E}]$  denotes the dimensionality of the energy shell. The matrix elements of  $\hat{O}$  are then described by

$$O_{\alpha\beta} = \langle E_\alpha | \hat{\mathcal{P}}_{E,\Delta E} \hat{O} \hat{\mathcal{P}}_{E,\Delta E} | E_\beta \rangle = \sum_i a_i U_{\alpha i} U_{\beta i}^*, \quad (3.3)$$

where the basis transformation  $U_{\alpha i} = \langle E_\alpha | a_i \rangle$  constitutes a  $d_{E,\Delta E} \times d_{E,\Delta E}$  unitary matrix  $U$ .

Let us focus on the diagonal matrix elements in the following. If the fluctuation of such diagonal matrix elements within the energy shell vanishes in the

thermodynamic limit, then the ETH holds true in the energy shell (which is often taken as the microcanonical energy shell obeying  $\Delta E \propto \sqrt{N}$ , where  $N$  is the number of lattice sites). The magnitude of the fluctuation can be quantified by the comparison of

$$\max_{|E_\alpha - E|, |E_\beta - E| \leq \Delta E} |\mathcal{O}_{\alpha\alpha} - \mathcal{O}_{\beta\beta}| \quad (3.4)$$

and  $\|\hat{\mathcal{O}}\|_{\text{op}}$ , where  $\|\cdot\|_{\text{op}}$  denotes an operator norm. Let us denote  $\mathcal{U}_{\{a_i\}, \eta}$  ( $\eta > 0$ ) as a set of all  $U$  that satisfy the inequality

$$\max_{|E_\alpha - E|, |E_\beta - E| \leq \Delta E} |\mathcal{O}_{\alpha\alpha} - \mathcal{O}_{\beta\beta}| \leq \|\hat{\mathcal{O}}\|_{\text{op}} d_{E, \Delta E}^{-\eta}. \quad (3.5)$$

Note that  $U \in \mathcal{U}_{\{a_i\}, \eta}$  means that the ETH holds true within  $\mathcal{H}_{E, \Delta E}$  because the maximum fluctuation of  $\mathcal{O}_{\alpha\alpha}$  vanishes exponentially (remember  $d_{E, \Delta E} \propto e^{sN}$  for the entropy density  $s$ ), but that the converse is not true.

We can show that, for almost all (typical)  $U$  over the Haar measure, the fluctuation becomes exponentially small. Indeed, we can show the following inequality

$$\mathbb{P}_U [U \notin \mathcal{U}_{\{a_i\}, \eta}] \leq 2d_{E, \Delta E} \exp \left[ -\frac{d_{E, \Delta E}^{1-2\eta}}{72\pi^3} \right], \quad (3.6)$$

where  $\mathbb{P}_U$  denotes the probability over the unitary Haar measure. Since the right-hand side becomes zero in the thermodynamic limit for  $0 < \eta < 1/2$ , almost all  $U$  satisfy  $U \in \mathcal{U}_{\{a_i\}, \eta}$ . Then, we may assume that  $U \in \mathcal{U}_{\{a_i\}, \eta}$  for  $U$  which is obtained from a physically relevant set of  $\hat{H}$  and  $\hat{\mathcal{O}}$  unless some special reasons exist, which is the statement of the typicality argument.

Let us prove Eq. (3.6). We use the following Levy's lemma [7, 227]:

$$\text{Prob} \left[ |g(\psi) - \langle g(\psi) \rangle_\psi| \geq \epsilon \right] \leq 2 \exp \left[ -\frac{\epsilon^2 (d+1)}{9\pi^3 \xi^2} \right], \quad (3.7)$$

where  $\psi \in \mathbb{S}^d \subset \mathbb{R}^{d+1}$  is a point on a  $d$ -dimensional unit sphere,  $g(\psi) : \mathbb{S}^d \rightarrow \mathbb{R}$  is a Lipschitz continuous function with a Lipschitz constant  $\xi$ , "Prob" means the uniform probability for  $\psi$  over the unit sphere, and  $\langle \cdots \rangle_\psi$  is the expectation value for the uniform measure. We here consider  $|\psi\rangle \in \mathcal{H}_{E, \Delta E}$  as a point  $\psi$  on a  $(2d_{E, \Delta E} - 1)$ -dimensional unit sphere ( $d = 2d_{E, \Delta E} - 1$ ). Then,  $g(\psi) = \langle \psi | \hat{\mathcal{P}}_{E, \Delta E} \hat{\mathcal{O}} \hat{\mathcal{P}}_{E, \Delta E} | \psi \rangle$  is a Lipschitz continuous function with

$$\xi = \Delta_{\hat{\mathcal{O}}} := \max_i a_i - \min_i a_i \quad (3.8)$$

because

$$\begin{aligned}
& |\langle \psi | \hat{\mathcal{P}}_{E,\Delta E} \hat{\mathcal{O}} \hat{\mathcal{P}}_{E,\Delta E} | \psi \rangle - \langle \psi' | \hat{\mathcal{P}}_{E,\Delta E} \hat{\mathcal{O}} \hat{\mathcal{P}}_{E,\Delta E} | \psi' \rangle| \\
&= \left| \langle \psi | \hat{\mathcal{P}}_{E,\Delta E} \hat{\mathcal{O}} \hat{\mathcal{P}}_{E,\Delta E} - X_{\hat{\mathcal{O}}}/2 | \psi \rangle - \langle \psi' | \hat{\mathcal{P}}_{E,\Delta E} \hat{\mathcal{O}} \hat{\mathcal{P}}_{E,\Delta E} - X_{\hat{\mathcal{O}}}/2 | \psi' \rangle \right| \\
&= \frac{1}{2} |(\langle \psi | + \langle \psi' |) \hat{\mathcal{O}}' (|\psi\rangle - |\psi'\rangle) + (\langle \psi | - \langle \psi' |) \hat{\mathcal{O}}' (|\psi\rangle + |\psi'\rangle)| \\
&\leq \|\hat{\mathcal{O}}'\|_{\text{op}} \cdot \left( \left\| |\psi\rangle - |\psi'\rangle \right\| + \left\| |\psi\rangle + |\psi'\rangle \right\| \right) \\
&\leq 2 \|\hat{\mathcal{O}}'\|_{\text{op}} \cdot \left\| |\psi\rangle - |\psi'\rangle \right\| \\
&= \Delta_{\hat{\mathcal{O}}} \cdot \left\| |\psi\rangle - |\psi'\rangle \right\|, \tag{3.9}
\end{aligned}$$

where

$$\hat{\mathcal{O}}' = \hat{\mathcal{P}}_{E,\Delta E} \hat{\mathcal{O}} \hat{\mathcal{P}}_{E,\Delta E} - \frac{X_{\hat{\mathcal{O}}}}{2} \tag{3.10}$$

and  $X_{\hat{\mathcal{O}}} = \max_i a_i + \min_i a_i$ . In addition, we can show that  $\langle g(\psi) \rangle_{\psi} = \text{Tr}[\hat{\rho}_{\text{mic}} \hat{\mathcal{O}}]$ . Thus, noticing that randomizing  $\psi$  is equivalent to randomizing  $U$  for some state (for which we take as the eigenstate of  $\hat{H}$ ), we obtain

$$\mathbb{P}_U \left[ \left| \langle E_{\alpha} | \hat{\mathcal{P}}_{E,\Delta E} \hat{\mathcal{O}} \hat{\mathcal{P}}_{E,\Delta E} | E_{\alpha} \rangle - \text{Tr}[\hat{\rho}_{\text{mic}} \hat{\mathcal{O}}] \right| \geq \epsilon \right] \leq 2 \exp \left[ -\frac{2\epsilon^2 d_{E,\Delta E}}{9\pi^3 \Delta_{\hat{\mathcal{O}}}^2} \right] \tag{3.11}$$

for any  $|E_{\alpha}\rangle \in \mathcal{H}_{E,\Delta E}$ .

We next notice

$$\mathbb{P} \left[ \max_k (f_k) \geq a \right] \leq \sum_k \mathbb{P} [f_k \geq a] \tag{3.12}$$

for an arbitrary set of functions  $\{f_k\}_k$ . Then, using  $\langle E_{\alpha} | \hat{\mathcal{P}}_{E,\Delta E} \hat{\mathcal{O}} \hat{\mathcal{P}}_{E,\Delta E} | E_{\alpha} \rangle = \mathcal{O}_{\alpha\alpha}$ , we have

$$\mathbb{P}_U \left[ \max_{|E_{\alpha}-E|\leq\Delta E} \left| \mathcal{O}_{\alpha\alpha} - \text{Tr}[\hat{\rho}_{\text{mic}} \hat{\mathcal{O}}] \right| \geq \epsilon \right] \leq 2d_{E,\Delta E} \exp \left[ -\frac{2\epsilon^2 d_{E,\Delta E}}{9\pi^3 \Delta_{\hat{\mathcal{O}}}^2} \right]. \tag{3.13}$$

Since

$$\frac{1}{2} \max_{|E_{\alpha}-E|\leq\Delta E, |E_{\beta}-E|\leq\Delta E} |\mathcal{O}_{\alpha\alpha} - \mathcal{O}_{\beta\beta}| \leq \max_{|E_{\alpha}-E|\leq\Delta E} |\mathcal{O}_{\alpha\alpha} - \text{Tr}[\hat{\rho}_{\text{mic}} \hat{\mathcal{O}}]|, \tag{3.14}$$

we have

$$\mathbb{P}_U \left[ \max_{|E_{\alpha}-E|\leq\Delta E, |E_{\beta}-E|\leq\Delta E} |\mathcal{O}_{\alpha\alpha} - \mathcal{O}_{\beta\beta}| > 2\epsilon \right] \leq \mathbb{P}_U \left[ \max_{|E_{\alpha}-E|\leq\Delta E} |\mathcal{O}_{\alpha\alpha} - \text{Tr}[\hat{\rho}_{\text{mic}} \hat{\mathcal{O}}]| > \epsilon \right], \tag{3.15}$$

where we have used the relation

$$\mathbb{P}[a > c] \leq [b > c] \quad (3.16)$$

for  $a \leq b$ . Substituting  $2\epsilon = \|\hat{\mathcal{O}}\|_{\text{op}} d_{E,\Delta E}^{-\eta}$  into Eq. (3.15) and using Eq. (3.13), we obtain

$$\mathbb{P}_U \left[ \max_{|E_\alpha - E| \leq \Delta E, |E_\beta - E| \leq \Delta E} |\mathcal{O}_{\alpha\alpha} - \mathcal{O}_{\beta\beta}| > \|\hat{\mathcal{O}}\|_{\text{op}} d_{E,\Delta E}^{-\eta} \right] \leq 2d_{E,\Delta E} \exp \left[ -\frac{\|\hat{\mathcal{O}}\|_{\text{op}}^2 d_{E,\Delta E}^{1-2\eta}}{18\pi^3 \Delta_{\hat{\mathcal{O}}}^2} \right]. \quad (3.17)$$

Finally, using

$$\Delta_{\hat{\mathcal{O}}} \leq 2\|\hat{\mathcal{P}}_{E,\Delta E} \hat{\mathcal{O}} \hat{\mathcal{P}}_{E,\Delta E}\|_{\text{op}} \leq 2\|\hat{\mathcal{O}}\|_{\text{op}}, \quad (3.18)$$

we obtain

$$\mathbb{P}_U \left[ \max_{|E_\alpha - E| \leq \Delta E, |E_\beta - E| \leq \Delta E} |\mathcal{O}_{\alpha\alpha} - \mathcal{O}_{\beta\beta}| > \|\hat{\mathcal{O}}\|_{\text{op}} d_{E,\Delta E}^{-\eta} \right] \leq 2d_{E,\Delta E} \exp \left[ -\frac{d_{E,\Delta E}^{1-2\eta}}{72\pi^3} \right]. \quad (3.19)$$

This is equivalent to Eq. (3.6).

### 3.3 Atypicality of most few-body observables

In the previous section, we have proven Eq. (3.6), which states that  $U \in \mathcal{U}_{\{a_i\},\eta}$  for almost all unitary matrices  $U$ . On the other hand, it is only an assumption that  $U$  obtained from the physically relevant  $\hat{H}$  and  $\hat{\mathcal{O}}$  belongs to  $\mathcal{U}_{\{a_i\},\eta}$ . Indeed, little work has existed which investigated the validity of this conjecture.

Here, we show that the typicality argument does not hold for realistic setups that possess the few-body property. Indeed, we prove that, for  $H$  with few-body interactions and most few-body  $\hat{\mathcal{O}}$ ,  $U \notin \mathcal{U}_{\{a_i\},\eta}$  holds true, as schematically illustrated in Fig. 3.1.

#### 3.3.1 Setup

We assume that the energy width  $\Delta E$  behaves as  $\Delta E \propto N^{-p}$  for a real number  $p$  and that  $d_{E,\Delta E}$  increases exponentially with  $N$ . Note that the microcanonical energy width (which Refs. [2, 30] focus on) is subextensive and thus satisfies  $-1 < p < 0$ . For simplicity, we also assume that the energy eigenvalues exist at the edges of the energy shell. This is in general made possible by changing the original width in

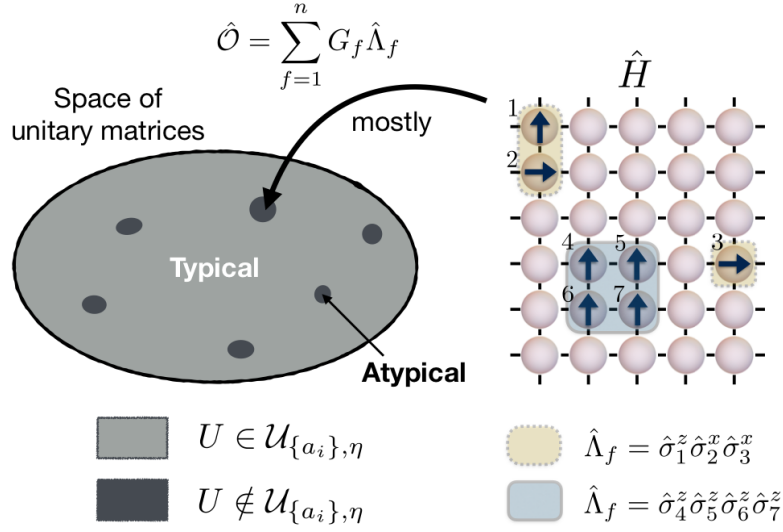


Figure 3.1: Space of unitary matrices and atypicality of most few-body observables. Almost all (*i.e.*, typical) unitary matrices  $U$  over the Haar measure belong to  $\mathcal{U}_{\{a_i\}, \eta}$ , which also implies the ETH. On the other hand, for  $H$  with few-body interactions and most few-body  $\hat{O}$ , the corresponding  $U$  behaves atypically and satisfies  $U \notin \mathcal{U}_{\{a_i\}, \eta}$ . Reproduced from Fig. 1 of Ref. [31]. ©2018 American Physical Society.

an exponentially small way, which does not change the essence of the following discussion. Then  $\max_{|E_\alpha - E|, |E_\beta - E| \leq \Delta E} |(\hat{H})_{\alpha\alpha} - (\hat{H})_{\beta\beta}| = 2\Delta E$  holds.

We consider a system with  $N$  spins on a lattice. The Hilbert space can be written as a product of local Hilbert spaces at site  $x$  as

$$\mathcal{H} = \bigotimes_{x=1}^N \mathcal{H}_x. \quad (3.20)$$

We denote  $\mathcal{L}(\mathcal{H})$  and  $\mathcal{L}(\mathcal{H}_x)$  as operator spaces that respectively act on  $\mathcal{H}$  and  $\mathcal{H}_x$ . The orthonormal basis of  $\mathcal{L}(\mathcal{H}_x)$  is given by

$$\left\{ \hat{\lambda}_x^0 := \hat{\mathbb{I}}_x, \hat{\lambda}_x^1, \dots, \hat{\lambda}_x^{S^2-1} \right\}. \quad (3.21)$$

Here,  $S = \dim[\mathcal{H}_x]$  and  $\hat{\lambda}_x^\mu$  ( $0 \leq \mu \leq S^2 - 1$ ) are  $S \times S$  Hermitian matrices that satisfy the orthonormality condition  $\text{Tr}_x[\hat{\lambda}_x^\mu \hat{\lambda}_x^{\mu'}] = S \delta_{\mu\mu'}$ . For example, for a spin-1/2 system,  $S = 2$  and  $\lambda_x^\mu$  can be taken as  $\{\hat{\mathbb{I}}, \hat{\sigma}^x, \hat{\sigma}^y, \hat{\sigma}^z\}$ . Then, the basis of

$\mathcal{L}(\mathcal{H})$  can be expressed as

$$\mathcal{B}_N = \left\{ \hat{\Lambda}'_{\mu_1, \dots, \mu_N} = \bigotimes_{x=1}^N \hat{\lambda}_x^{\mu_x} \mid 0 \leq \mu_x \leq S^2 - 1 \right\} \quad (3.22)$$

with  $\text{Tr}[\hat{\Lambda}'_{\mu_1, \dots, \mu_N} \hat{\Lambda}'_{\mu'_1, \dots, \mu'_N}] = S^N \prod_{x=1}^N \delta_{\mu_x \mu'_x}$ . For example, for the spin-1/2 system, we can take

$$\mathcal{B}_N = \{ \hat{I}, \hat{\sigma}_1^x, \hat{\sigma}_1^y, \hat{\sigma}_1^z, \hat{\sigma}_2^x, \dots, \hat{\sigma}_N^z, \hat{\sigma}_1^x \hat{\sigma}_2^x, \hat{\sigma}_1^x \hat{\sigma}_2^y, \dots, \hat{\sigma}_{N-1}^z \hat{\sigma}_N^z, \dots, \hat{\sigma}_1^z \dots \hat{\sigma}_N^z \}. \quad (3.23)$$

Let us now define the notion of  $m$ -body operators. We consider a subset  $\mathcal{B}_m$  of  $\mathcal{B}_N$  as a basis set whose elements nontrivially act on at most  $m$  sites:

$$\mathcal{B}_m = \left\{ \bigotimes_{i=1}^q \hat{\lambda}_{x_i}^{\alpha_{x_i}} \mid 1 \leq q \leq m, 1 \leq x_i \leq N, 1 \leq \alpha_{x_i} \leq S^2 - 1 \right\} \quad (3.24)$$

for  $m \geq 1$  and  $\mathcal{B}_0 = \left\{ \bigotimes_{x=1}^N \hat{\lambda}_x^0 \right\}$ . For example, for the spin-1/2 system and  $m = 2$ , we can take

$$\mathcal{B}_{m=2} = \{ \hat{I}, \hat{\sigma}_1^x, \hat{\sigma}_1^y, \hat{\sigma}_1^z, \hat{\sigma}_2^x, \dots, \hat{\sigma}_N^z, \hat{\sigma}_1^x \hat{\sigma}_2^x, \hat{\sigma}_1^x \hat{\sigma}_2^y, \dots, \hat{\sigma}_{N-1}^z \hat{\sigma}_N^z \}. \quad (3.25)$$

Then, we define  $m$ -body operators that can be written as a linear combination of elements in  $\mathcal{B}_m$  but not in  $\mathcal{B}_{m-1}$ , and *at-most*  $m$ -body operators that can be written as a linear combination of elements in  $\mathcal{B}_m$ . For example, for the spin-1/2 system,

$$\sum_{i=1}^N \hat{\sigma}_i^z + \hat{\sigma}_1^x \hat{\sigma}_5^y, \quad \sum_{i=1}^{N-1} \hat{\sigma}_i^z \hat{\sigma}_{i+1}^z, \quad \hat{\sigma}_1^x \hat{\sigma}_2^x + \hat{\sigma}_1^x + 2 \quad (3.26)$$

are two-body observables, whereas

$$\sum_{i=1}^N \hat{\sigma}_i^z, \quad \hat{\sigma}_3^z + 1 \quad (3.27)$$

are at most two-body observables but not two-body observables. Few-body operators are defined as  $m$ -body operators where  $m$  ( $m \ll N$ ) does not depend on  $N$ .

We next define randomly chosen observables from at most  $m$ -body operators. Consider a set  $\mathcal{L}_m$  of at most  $m$ -body observables. If we let  $\hat{\Lambda}_1, \dots, \hat{\Lambda}_n$  be elements in  $\mathcal{B}_m$ , where

$$n = \sum_{q=0}^m \frac{N!}{q!(N-q)!} (S^2 - 1)^q \quad (3.28)$$

is the number of the bases and  $\text{Tr}[\hat{\Lambda}_f \hat{\Lambda}_g] = S^N \delta_{fg}$ , elements in  $\mathcal{L}_m$  are written as

a linear combination of  $\hat{\Lambda}_f$ . Then we can define the random observables from  $\mathcal{L}_m$  as follows:

**Definition** (Randomly chosen observables from  $\mathcal{L}_m$ ). We take an observable  $\hat{G} \in \mathcal{L}_m$  expanded as

$$\hat{G} = \sum_{f=1}^n G_f \hat{\Lambda}_f, \quad (3.29)$$

where real random variables  $\vec{G} = (G_1, \dots, G_f, \dots, G_n)$  are chosen over a given probability distribution  $P(\vec{G})$ . If  $P(\vec{G})$  is unchanged under any  $n \times n$  orthogonal transformations,  $\hat{G}$  is called an observable randomly chosen from  $\mathcal{L}_m$ .

This definition depends on how we choose  $\{\hat{\Lambda}_f\}$  and  $P(\vec{G})$ . The following discussion holds true for an arbitrary choice of  $P(\vec{G})$  as long as  $\{\hat{\Lambda}_f\}$  possesses orthonormality and Hermiticity, and  $P(\vec{G})$  is invariant under orthogonal transformations. Thus, we may choose  $P(\vec{G})$  to suit our purpose with the invariant property. In contrast, if  $U$  is chosen from a unitary Haar measure as in the typicality argument, it is not clear from what kind of probability distributions an observable is chosen. In this sense, the operational meaning of our sampling strategy of observables is well-defined.

### 3.3.2 Proof of atypicality of most few-body observables

We now study diagonal matrix elements of random observables which we define above and compare it with the typicality argument. We consider a few-body Hamiltonian (*i.e.*, Hamiltonian that consists of few-body interactions) as well as few-body observables. Then, most few-body observables randomly chosen from  $\mathcal{L}_m$  behave atypically, *i.e.*,  $U \notin \mathcal{U}_{\{a_i\}, \eta}$ , which is understood from the following theorem:

**Theorem.** Consider a  $k$ -body Hamiltonian and sufficiently large  $N$ , and assume that  $m$  ( $k \leq m \ll N$ ) is independent of  $N$ . We now choose a random observable  $\hat{O} = \sum_f G_f \hat{\Lambda}_f$  from  $\mathcal{L}_m$ . We obtain the corresponding  $\{a_i\}$  and  $U$  from  $\hat{H}$  and  $\hat{O}$ . Then,

$$\mathbb{P}_{\mathcal{L}_m}[U \in \mathcal{U}_{\{a_i\}, \eta}] \leq \frac{\sqrt{\pi n} \|\hat{H}\|_{\text{op}} \Lambda}{2\Delta E} \frac{\Gamma(\frac{n}{2})}{\Gamma(\frac{n-1}{2})} d_{E, \Delta E}^{-\eta}. \quad (3.30)$$

Here,  $\mathbb{P}_{\mathcal{L}_m}$  means the probability with respect to  $P(\vec{G})$ , and  $\Lambda = \max_f \|\hat{\Lambda}_f\|_{\text{op}} \leq S^{m/2}$ . If  $\|\hat{H}\|_{\text{op}}$  does not increase exponentially with increasing  $N$ , the right-hand

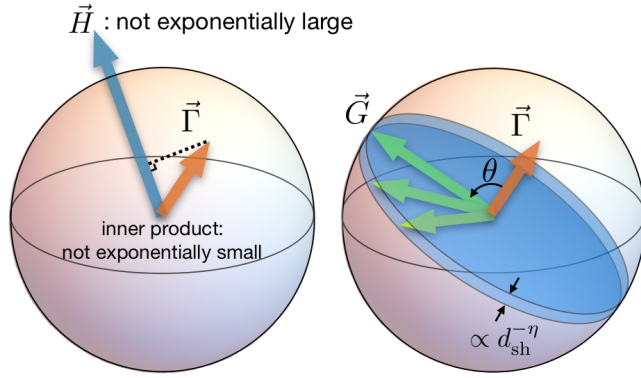


Figure 3.2: Key idea for the proof of Eq. (3.30). (Left) As a first step, we show that  $|\vec{\Gamma}|$  does not decay exponentially as we increase  $N$  unless  $|\vec{H}|$  is exponentially large. This is proven from the observation that  $|\vec{\Gamma} \cdot \vec{H}|$  does not decrease exponentially with increasing  $N$ . (Right) Next,  $\vec{G}$  has to be almost orthogonal to  $\vec{\Gamma}$  for  $|\vec{\Gamma} \cdot \vec{G}|$  to be exponentially small, *i.e.*,  $|\vec{\Gamma} \cdot \vec{G}| \leq \|\hat{O}\|_{\text{op}} d_{E,\Delta E}^{-\eta}$ , if we assume that  $|\vec{G}|$  is not exponentially large. The probability of such an event is exponentially small ( $\propto d_{E,\Delta E}^{-\eta}$ ) as long as the dimensionality  $n$  of the hypersphere is not exponentially large, which is the case for few-body observables. Reproduced from Fig. 2 of Ref. [31]. ©2018 American Physical Society.

side of the inequality (3.30) vanishes for large  $N$ , since  $d_{E,\Delta E}$  grows exponentially whereas  $n$  and  $1/\Delta E \propto N^p$  do not.

The inequality (3.30) means that  $\max_{|E_\alpha - E|, |E_\beta - E| \leq \Delta E} |\mathcal{O}_{\alpha\alpha} - \mathcal{O}_{\beta\beta}|$  does not decrease as a power of  $d_{E,\Delta E}$  for physical Hamiltonians and most few-body observables; remember the definition of  $\mathcal{U}_{\{a_i\},\eta}$  given in Eq. (3.5). This shows that the corresponding unitary  $U$  is atypical. Note that atypicality holds for arbitrary  $m$  that satisfies  $m \geq k$  and is independent of  $N$ .

The main idea is that the Hamiltonian  $\hat{H}$  is obviously an atypical operator, since maximum difference of diagonal matrix elements within the energy shell becomes equal to the energy width  $2\Delta E$ , which is assumed to decay at most polynomially. Then, since most of  $\hat{O}$  have sufficiently large overlap with  $\hat{H}$  through the few-body property, maximum difference of diagonal matrix elements for  $\hat{O}$  also behaves atypically owing to the atypicality of the Hamiltonian. This idea is quantitatively formulated in the proof below.

**Proof of Eq. (3.30) (see Fig. 3.2 for the key idea of the proof)**

As a first step, note that  $\hat{H} \in \mathcal{L}_m$  satisfies the following condition for a  $k$ -body Hamiltonian:

$$\max_{|E_\alpha - E|, |E_\beta - E| \leq \Delta E} |(\hat{H})_{\alpha\alpha} - (\hat{H})_{\beta\beta}| = 2\Delta E = \xi_d. \quad (3.31)$$

Here  $\xi_d = 2\Delta E$  does not decay faster than polynomial in the system size  $N$ . We define  $\gamma$  and  $\delta$  as labels of eigenstates satisfying  $(\hat{H})_{\gamma\gamma} - (\hat{H})_{\delta\delta} = \xi_d$ . If we define  $\Gamma_f = (\hat{\Lambda}_f)_{\gamma\gamma} - (\hat{\Lambda}_f)_{\delta\delta}$ , we obtain the expansion  $\hat{H} = \sum_{f=1}^n H_f \hat{\Lambda}_f$ , which leads to  $\vec{H} \cdot \vec{\Gamma} = \xi_d$  with  $\vec{H} = (H_1, \dots, H_n)$  and  $\vec{\Gamma} = (\Gamma_1, \dots, \Gamma_n)$ . Using

$$|\vec{H}| = \sqrt{\frac{\text{Tr}[\hat{H}^2]}{SN}} \leq \|\hat{H}\|_{\text{op}}, \quad (3.32)$$

we obtain

$$|\vec{\Gamma}| \geq \frac{\xi_d}{\|\hat{H}\|_{\text{op}}}. \quad (3.33)$$

Next,

$$\max_{|E_\alpha - E|, |E_\beta - E| \leq \Delta E} |\mathcal{O}_{\alpha\alpha} - \mathcal{O}_{\beta\beta}| \geq |\vec{G} \cdot \vec{\Gamma}| \quad (3.34)$$

leads to

$$\mathbb{P}_{\mathcal{L}_m} \left[ \max_{|E_\alpha - E|, |E_\beta - E| \leq \Delta E} |\mathcal{O}_{\alpha\alpha} - \mathcal{O}_{\beta\beta}| \leq \|\hat{\mathcal{O}}\|_{\text{op}} \epsilon \right] \leq \mathbb{P}_{\mathcal{L}_m} \left[ |\vec{G} \cdot \vec{\Gamma}| \leq \|\hat{\mathcal{O}}\|_{\text{op}} \epsilon \right] \quad (3.35)$$

for any  $\epsilon > 0$ , where we use  $\mathbb{P}[a \leq c] \geq \mathbb{P}[b \leq c]$  for  $a \leq b$ .

To evaluate Eq. (3.35), we note that the probability  $P(\vec{G})d\vec{G}$  is expressed as

$$P'(|\vec{G}|) |\vec{G}|^{n-1} d|\vec{G}| d\Omega \quad (3.36)$$

owing to the invariance under any orthogonal transformations, where  $\Omega$  is the high-dimensional solid angle. Defining the angle between  $\vec{G}$  and  $\vec{\Gamma}$  as  $\theta$ , we obtain

$$\begin{aligned} \mathbb{P}_{\mathcal{L}_m} \left[ |\vec{G} \cdot \vec{\Gamma}| \leq \|\hat{\mathcal{O}}\|_{\text{op}} \epsilon \right] &\leq \mathbb{P}_{\mathcal{L}_m} \left[ |\cos \theta| \leq \frac{\sqrt{n} \|\hat{H}\|_{\text{op}} \Lambda \epsilon}{\xi_d} \right] \\ &\leq \frac{\sqrt{\pi n} \|\hat{H}\|_{\text{op}} \Lambda \epsilon}{2\Delta E} \frac{\Gamma(\frac{n}{2})}{\Gamma(\frac{n-1}{2})}. \end{aligned} \quad (3.37)$$

Here, we have used Eq. (3.33) and

$$\begin{aligned}
\|\hat{\mathcal{O}}\|_{\text{op}} &\leq \sum_{f=1}^n |G_f| \|\hat{\Lambda}_f\|_{\text{op}} \\
&\leq \Lambda \sum_{f=1}^n |G_f| \cdot 1 \\
&\leq \Lambda |\vec{G}| \sqrt{n}.
\end{aligned} \tag{3.38}$$

Note that we have used the property of an operator norm as well as the Cauchy-Schwartz inequality. We also used

$$\begin{aligned}
\mathbb{P}_{\mathcal{L}_m}[|\cos \theta| < x] &\leq \mathbb{P}_{\mathcal{L}_m} \left[ \frac{\pi}{2}(1-x) < \theta < \frac{\pi}{2}(1+x) \right] \\
&\leq \frac{\int_{\frac{\pi}{2}(1-x)}^{\frac{\pi}{2}(1+x)} S_{n-2}(\sin \theta) d\theta}{\int_0^\pi S_{n-2}(\sin \theta) d\theta} \\
&\leq \frac{\int_{\frac{\pi}{2}(1-x)}^{\frac{\pi}{2}(1+x)} (\sin \theta)^{n-2} d\theta}{\int_0^\pi (\sin \theta)^{n-2} d\theta} \\
&\leq \sqrt{\pi} x \frac{\Gamma(\frac{n}{2})}{\Gamma(\frac{n-1}{2})},
\end{aligned} \tag{3.39}$$

where  $S_m(r) = \sqrt{\pi} \Gamma[(m+1)/2] r^m / \Gamma[(m+2)/2]$  is an area of an  $m$ -dimensional hypersphere. For  $\epsilon = d_{E, \Delta E}^{-\eta}$ , the left-hand side of (3.35) becomes  $\mathbb{P}_{\mathcal{L}_m}[U \in \mathcal{U}_{\{a_i\}, \eta}]$ . Then, with Eq. (3.37), the proof of Eq. (3.30) is completed.  $\square$

We note that our theorem applies to any  $k$ -body Hamiltonians. If we take  $\hat{H}$  as a Hamiltonian with spatially local interactions, we expect  $\|\hat{H}\|_{\text{op}} \propto N$ . Thus, for the right-hand side of Eq. (3.37) to vanish,  $\epsilon$  can instead be taken as

$$\epsilon \propto N^{-z} \sim n^{-\frac{z}{m}} \quad (z > 1 + p + m) \tag{3.40}$$

for  $\Delta E \propto N^{-p}$ , since  $\sqrt{n} \Lambda \Gamma[n/2] / \Gamma[(n-1)/2] \rightarrow n \sim N^m$  for  $N \gg 1$ . This means that the maximum fluctuation of most few-body observables actually decreases slower than

$$\sim N^{-z} \sim n^{-\frac{z}{m}} \quad (z > 1 + p + m). \tag{3.41}$$

### 3.4 Typicality of most $N$ -body observables

Our theorem of atypicality only holds true for few-body systems, where  $m$  is independent of  $N$ . If we instead consider many-body observables, the typicality argument may hold true. We here show that most random  $N$ -body observables behave typically. Indeed, we can show the following proposition:

**Proposition.** Let us consider a randomly chosen observable  $\hat{O} = \sum_f G_f \hat{\Lambda}_f$  from  $\mathcal{L}_N$ . We then obtain the corresponding  $\{a_i\}$  and  $U$ . In this case, we can show that

$$\mathbb{P}_{\mathcal{L}_N}[U \notin \mathcal{U}_{\{a_i\}, \eta}] \leq 2d \exp \left[ -\frac{dd^{-2\eta}}{72\pi^3} \right], \quad (3.42)$$

where  $d = \dim[\mathcal{H}] = S^N$ . The right-hand side vanishes for  $N \rightarrow \infty$  when  $\eta < 1/2$ .

This proposition indicates that most observables randomly chosen from  $\mathcal{L}_N$  satisfy the ETH in the energy shell. We note that recent numerical simulations indeed suggest that many-body observables can satisfy the ETH [209, 31, 28, 29], in contrast with the picture that relies on the spatial entanglement for the validity of the ETH [58].

#### Proof of Eq. (3.42)

First, we show that a random observable  $\hat{G} = \sum_f G_f \hat{\Lambda}_f$  chosen from  $\mathcal{L}_N$  has eigenstates which are distributed over the uniform Haar measure. For any  $S^N \times S^N$  transformation  $\hat{R}$  which is unitary, we have

$$\begin{aligned} \hat{R}\hat{G}\hat{R}^\dagger &= \sum_{f=1}^{S^{2N}} G_f \hat{R}\hat{\Lambda}_f\hat{R}^\dagger \\ &= \sum_{f=1}^{S^{2N}} G_f \sum_{g=1}^{S^{2N}} \mathcal{R}_{fg} \hat{\Lambda}_g \\ &= \sum_{f=1}^{S^{2N}} \tilde{G}_f \hat{\Lambda}_f, \end{aligned} \quad (3.43)$$

where  $\mathcal{R}_{fg}$  is defined by

$$\hat{R}\hat{\Lambda}_f\hat{R}^\dagger = \sum_{g=1}^{S^{2N}} \mathcal{R}_{fg} \hat{\Lambda}_g \quad (3.44)$$

and

$$\tilde{G}_f = \sum_{g=1}^{S^{2N}} G_g \mathcal{R}_{gf}. \quad (3.45)$$

Here,  $\mathcal{R}$  is an  $S^{2N} \times S^{2N}$  orthogonal matrix. Indeed, the normalization condition of  $\hat{\Lambda}_f$ ,  $\text{Tr}[\hat{\Lambda}_f \hat{\Lambda}_g] = S^N \delta_{fg}$ , leads to  $\sum_h \mathcal{R}_{fh} \mathcal{R}_{gh} = \delta_{fg}$  owing to the operator expansion of  $\hat{R} \hat{\Lambda}_f \hat{R}^\dagger \hat{R} \hat{\Lambda}_g \hat{R}^\dagger$ . In addition,  $\mathcal{R}_{fg} = \mathcal{R}_{fg}^*$  holds true because of the Hermiticity condition  $\hat{\Lambda}_f^\dagger = \hat{\Lambda}_f$ , which is known from the operator expansion of  $(\hat{R} \hat{\Lambda}_f \hat{R}^\dagger)^\dagger$ . Consequently, for randomly chosen observables from  $\mathcal{L}_N$ , the probabilities of choosing  $\hat{G}$  and  $\hat{R} \hat{G} \hat{R}^\dagger$  are equal to each other because  $P(\vec{G})$  is invariant under any orthogonal rotation, *i.e.*,  $P(\vec{G}) = P(\mathcal{R} \vec{G})$ . Thus, the eigenstates of a randomly chosen  $\hat{G}$  are uniformly distributed over the unitary Haar measure.

Now, we bound the right-hand side of Eq. (3.42). In a manner similar to the derivation of Eq. (3.6), we obtain

$$\mathbb{P}_{\mathcal{L}_N} \left[ \max_{\alpha, \beta} |\mathcal{O}_{\alpha\alpha} - \mathcal{O}_{\beta\beta}| > \|\hat{\mathcal{O}}\|_{\text{op}} d_{E, \Delta E}^{-\eta} \right] \leq 2d \exp \left[ -\frac{d d_{E, \Delta E}^{-2\eta}}{72\pi^3} \right], \quad (3.46)$$

where we have considered the unitary Haar measure for the entire Hilbert space. Because of the inequality  $\max_{\alpha, \beta} |\mathcal{O}_{\alpha\alpha} - \mathcal{O}_{\beta\beta}| \geq \max_{|E_\alpha - E|, |E_\beta - E| \leq \Delta E} |\mathcal{O}_{\alpha\alpha} - \mathcal{O}_{\beta\beta}|$ , we finally obtain

$$\begin{aligned} \mathbb{P}_{\mathcal{L}_N} \left[ \max_{|E_\alpha - E|, |E_\beta - E| \leq \Delta E} |\mathcal{O}_{\alpha\alpha} - \mathcal{O}_{\beta\beta}| > \|\hat{\mathcal{O}}\|_{\text{op}} d_{E, \Delta E}^{-\eta} \right] \\ \leq \mathbb{P}_{\mathcal{L}_N} \left[ \max_{\alpha, \beta} |\mathcal{O}_{\alpha\alpha} - \mathcal{O}_{\beta\beta}| > \|\hat{\mathcal{O}}\|_{\text{op}} d_{E, \Delta E}^{-\eta} \right]. \end{aligned} \quad (3.47)$$

Thus, Eq. (3.42) is proven.  $\square$

### 3.5 Extension of the setup with locality

Our discussion so far has focused on the few-body setup. Our results thus apply to spatially nonlocal but few-body observables, such as momentum distributions [18, 228] and structure factors [229], which are also expected to obey the standard statistical mechanics [141]. On the other hand, we may specifically be interested in spatially local observables in some cases. We here extend our theorem of atypicality for  $\mathcal{O}_{\alpha\alpha}$  to most local observables for translation-invariant locally

interacting systems.

In the following, we consider  $N$  lattice spins in one dimension, for which the label of each site is denoted as  $x = 1, \dots, N$ , for simplicity. It is straightforward to generalize the discussion to higher dimensions. Let us consider a subregion  $S_l$  which is composed of neighboring sites labeled by  $x = 1, \dots, l$ . Here, we start from  $x = 1$  without loss of generality, since we will consider a translation-invariant system in the following. If  $l (\ll N)$  is independent of  $N$ ,  $S_l$  is defined as a local subsystem. Next, we define  $\mathcal{H}_{S_l}$  as the Hilbert space of  $S_l$  and  $\mathcal{L}_l^{\text{loc}} = \mathcal{L}(\mathcal{H}_{S_l})$  as the operator space that acts on  $S_l$ . An orthonormal basis set for  $\mathcal{L}_l^{\text{loc}}$  is given as

$$\mathcal{B}_l^{\text{loc}} = \left\{ \bigotimes_{x=1}^l \hat{\lambda}_x^{\mu_x} \mid 0 \leq \mu_x \leq S^2 - 1 \right\} =: \{ \hat{\Lambda}_f^{\text{loc}} \}_{f=1}^r, \quad (3.48)$$

where  $r = S^{2l}$ . The orthonormality condition is chosen as  $\text{Tr}_{S_l}[\hat{\Lambda}_f^{\text{loc}} \hat{\Lambda}_g^{\text{loc}}] = S^l \delta_{fg}$ .

Next we define local observables randomly chosen from  $\mathcal{L}_l^{\text{loc}}$ :

**Definition** (Randomly chosen local observables from  $\mathcal{L}_l^{\text{loc}}$ ). Consider an observable  $\hat{G} \in \mathcal{L}_l^{\text{loc}}$  written as

$$\hat{G} = \sum_{f=1}^r g_f \hat{\Lambda}_f^{\text{loc}}, \quad (3.49)$$

where  $\vec{g} = (g_1, \dots, g_f, \dots, g_r)$  are random real variables chosen from a probability distribution  $P^{\text{loc}}(\vec{g})$ . If  $P^{\text{loc}}(\vec{g})$  is unchanged under an arbitrary  $r \times r$  orthogonal transformation,  $\hat{G}$  is defined as an observable randomly chosen from  $\mathcal{L}_l^{\text{loc}}$ .

Next we define an  $l'$ -local, translation-invariant Hamiltonian  $\hat{H}$  as an operator expressed as  $\hat{H} = \sum_{i=1}^N \hat{h}_{i,l'}$ , where  $\hat{h}_{1,l'}$  only acts on  $x = 1, 2, \dots, l'$  and  $\mathcal{T}[\hat{h}_{i,l'}] = \hat{h}_{i+1,l'}$ , with  $\mathcal{T}$  denoting the one-site translation.

We now prove the following theorem:

**Theorem.** Consider an  $l'$ -local translation-invariant Hamiltonian, and assume that  $l$  ( $l' \leq l \ll N$ ) is independent of  $N$  which is sufficiently large. We choose a random observable  $\hat{O} = \sum_f g_f \hat{\Lambda}_f^{\text{loc}}$  from  $\mathcal{L}_l^{\text{loc}}$ . We then obtain the corresponding  $\{a_i\}$  and  $U$  from  $\hat{H}$  and  $\hat{O}$ . Then,

$$\mathbb{P}_{\mathcal{L}_l^{\text{loc}}}[U \in \mathcal{U}_{\{a_i\}, \eta}] \leq \frac{\sqrt{\pi r N} \|\hat{h}\|_{\text{op}} \Lambda}{2\Delta E} \frac{\Gamma(\frac{r}{2})}{\Gamma(\frac{r-1}{2})} d_{E, \Delta E}^{-\eta}, \quad (3.50)$$

where  $\mathbb{P}_{\mathcal{L}_l^{\text{loc}}}$  means a probability over  $P^{\text{loc}}(\vec{g})$  and  $\Lambda = \max_f \|\hat{\Lambda}_f\|_{\text{op}} \leq S^{\frac{l}{2}} = r^{1/4}$ . If  $\|\hat{h}\|_{\text{op}} = \|\hat{h}_{1,l'}\|_{\text{op}}$  does not increase exponentially with increasing  $N$ , the right-hand side vanishes in the thermodynamic limit.

**Proof of Eq. (3.50)**

We first note that  $\hat{h}_{1,l'}$  belongs to  $\mathcal{L}_l^{\text{loc}}$  and satisfies the following:

$$\begin{aligned} (\hat{h}_{1,l'})_{\gamma\gamma} - (\hat{h}_{1,l'})_{\delta\delta} &= \frac{1}{N} \sum_i [(\hat{h}_{i,l'})_{\gamma\gamma} - (\hat{h}_{i,l'})_{\delta\delta}] \\ &= \frac{1}{N} [(\hat{H})_{\gamma\gamma} - (\hat{H})_{\delta\delta}] = \frac{2\Delta E}{N}, \end{aligned} \quad (3.51)$$

where  $\gamma$  and  $\delta$  label the maximum and minimum eigenvalues within the energy shell, respectively. Let us define

$$\gamma_f = (\hat{\Lambda}_f^{\text{loc}})_{\gamma\gamma} - (\hat{\Lambda}_f^{\text{loc}})_{\delta\delta}. \quad (3.52)$$

Then,  $\hat{h}_{1,l'} = \sum_{f=1}^r h_f \hat{\Lambda}_f^{\text{loc}}$  leads to

$$\vec{h} \cdot \vec{\gamma} = \frac{2\Delta E}{N}, \quad (3.53)$$

where  $\vec{h} = (h_1, \dots, h_r)$  and  $\vec{\gamma} = (\gamma_1, \dots, \gamma_r)$ . Since

$$|\vec{h}| = \sqrt{\frac{\text{Tr}_S[\hat{h}_{1,l'}^2]}{S^l}} \leq \|\hat{h}_{1,l'}\|_{\text{op}} = \|\hat{h}\|_{\text{op}}, \quad (3.54)$$

we have

$$|\vec{\gamma}| \geq \frac{2\Delta E}{N\|\hat{h}\|_{\text{op}}}. \quad (3.55)$$

We now discuss the right-hand side of Eq. (3.50). Since

$$\max_{|E_\alpha - E|, |E_\beta - E| \leq \Delta E} |\mathcal{O}_{\alpha\alpha} - \mathcal{O}_{\beta\beta}| \geq |\vec{g} \cdot \vec{\gamma}|, \quad (3.56)$$

we have

$$\mathbb{P}_{\mathcal{L}_l^{\text{loc}}} \left[ \max_{|E_\alpha - E|, |E_\beta - E| \leq \Delta E} |\mathcal{O}_{\alpha\alpha} - \mathcal{O}_{\beta\beta}| \leq \|\hat{\mathcal{O}}\|_{\text{op}} \epsilon \right] \leq \mathbb{P}_{\mathcal{L}_l^{\text{loc}}} \left[ |\vec{g} \cdot \vec{\gamma}| \leq \|\hat{\mathcal{O}}\|_{\text{op}} \epsilon \right]. \quad (3.57)$$

Defining the angle between  $\vec{g}$  and  $\vec{\gamma}$  as  $\phi$ , we have

$$\begin{aligned} \mathbb{P}_{\mathcal{L}_l^{\text{loc}}} \left[ |\vec{g} \cdot \vec{\gamma}| \leq \|\hat{\mathcal{O}}\|_{\text{op}} \epsilon \right] &\leq \mathbb{P}_{\mathcal{L}_l^{\text{loc}}} \left[ |\cos \phi| \leq \frac{\sqrt{r} N \|\hat{h}\|_{\text{op}} \Lambda \epsilon}{2\Delta E} \right] \\ &\leq \frac{\sqrt{\pi r} N \|\hat{h}\|_{\text{op}} \Lambda \epsilon}{2\Delta E} \frac{\Gamma(\frac{r}{2})}{\Gamma(\frac{r-1}{2})}. \end{aligned} \quad (3.58)$$

Note that we have used

$$\|\hat{\mathcal{O}}\|_{\text{op}} \leq \Lambda |\vec{g}| \sqrt{r} \quad (3.59)$$

as in Eq. (3.38) and that  $P^{\text{loc}}(\vec{g})$  is invariant under orthogonal transformations.

Using Eqs. (3.57) and (3.58) and taking  $\epsilon = d_{E,\Delta E}^{-\eta}$ , we can show that the left-hand side of (3.57) becomes  $\mathbb{P}_{\mathcal{L}^{\text{loc}}}[U \in \mathcal{U}_{\{a_i\},\eta}]$ , which completes the proof of Eq. (3.50).  $\square$

Equations (3.57) and (3.58) also tell us how slowly the maximum fluctuation of  $O_{\alpha\alpha}$  decays. Let us choose  $\Delta E = \|\hat{h}\|_{\text{op}} N^{-p} (-1 < p)$ . Since  $\sqrt{\pi r} \Lambda \Gamma(r/2)/2\Gamma((r-1)/2)$  is independent of  $N$ , we can choose  $\epsilon = N^{-z}$  ( $z > 1 + p$ ) so that the left-hand side of (3.57) may vanish for  $N \rightarrow \infty$ .

## 3.6 Discussions

We have examined the validity of the typicality argument, which is based on the unitary Haar measure, for the few-body (or local) setting. We have rigorously proven that diagonal matrix elements  $O_{\alpha\alpha}$  behave atypically for most few-body observables when the energy width decreases at most algebraically with increasing  $N$ , which is demonstrated by Eq. (3.30) (or Eq. (3.50)). We have also shown, on the other hand, that the typicality argument can hold true for many-body observables (see Eq. (3.42)).

We now discuss the meaning of our atypicality and the relation between previous works. The results that we have obtained suggest that the typicality argument does not hold true for physical Hamiltonians and few-body observables when the width of the energy shell decays at most polynomially. Thus, the typicality argument cannot explain the ETH in realistic nonintegrable systems, contrary to the arguments in *e.g.*, Ref. [30]. We note, however, that we do not deny the ETH itself. Indeed, we do not exclude the possibility that the maximum fluctuation of  $O_{\alpha\alpha}$  decays algebraically with increasing  $N$ . Our results thus indicate that a different approach which does not rely on the typicality argument is required for justifying the ETH. We also note that our present study does not judge whether the original work by von Neumann [2] is valid. In fact, he considered modified observables that are obtained from the coarse-graining of the original macroscopic observables. This procedure adds subextensive corrections to the observables, which are negligible in discussing thermalization in macroscopic systems but Eq. (3.30) becomes no longer applicable.

We next discuss the relation with Srednicki's conjecture in Eq. (2.27). If we assume that the "slope"  $d\mathcal{A}(E)/dE$  in this conjecture does not decay exponentially, the atypicality holds true. Indeed, Srednicki's conjecture with this assump-

tion leads to the maximum fluctuation of the diagonal matrix elements that is estimated to be  $d\mathcal{A}(E)/dE \times 2\Delta E$  in the thermodynamic limit, which does not decrease exponentially small for  $\Delta E \propto N^{-p}$ . However, our proof of atypicality is rigorously obtained solely from quantum mechanics without relying on any conjecture or assumption about matrix elements. From a different perspective, our results rigorously show that the random-matrix behavior of matrix elements  $O_{\alpha\beta}$  should not hold for few-body observables unless the energy width decays exponentially with the system size. Note that the previous numerical simulations that argued random-matrix-type (exponentially small) fluctuation of diagonal matrix elements do not contradict with our results because they used a different measure of fluctuations of  $O_{\alpha\alpha}$ , which essentially subtracts the effect of the slope  $d\mathcal{A}(E)/dE$  that causes atypicality. Recent numerical simulation [230] indeed demonstrated that the random-matrix-type behavior appears only after we get rid of atypical structures of  $O_{\alpha\alpha}$  that is expressed as an overlap of the Hamiltonian and observables, which is consistent with our discussion.

Our results in Eq. (3.30) (or Eq. (3.50)) and Eq. (3.42) explicitly demonstrate that few-body properties of observables and the Hamiltonian are very important for the statistics of matrix elements. This fact was not pointed out in the previous literatures. It is indicated from our results that the assumption for the slope  $d\mathcal{A}(E)/dE$  in the previous paragraph usually seems to hold in numerics [70, 25] because they mainly consider few-body observables. On the other hand, if many-body observables are concerned, the slope can be much smaller as a function of energy [31]. We also note that the slope can be small even for few-body observables [231, 232] in Floquet nonintegrable systems ( $\tilde{E}$  represents the quasienergy), for which the energy is not conserved and our results do not apply.

# Chapter 4

## Review: theory of open quantum systems

While there are systems which are nearly isolated such as cold atom systems, no systems are perfectly isolated because of the existence of couplings with external environments. Such open quantum systems obey non-unitary time evolutions, which cannot be understood within the framework discussed in the previous chapters. Indeed, dissipation can drive systems; the obtained state may be trivial (*e.g.*, maximally mixed) states, but in turn it can be highly out-of-equilibrium states (*e.g.*, non-equilibrium steady states). It is a long-standing and challenging problem to establish nonequilibrium statistical mechanics, which may emerge as a consequence of external environments. The ETH, though being successful in closed quantum systems, is apparently not sufficient to explain such complicated situations.

In a modern perspective, dissipation and measurements have been controlled in recent experiments of many-body systems using cold atoms, trapped ions, etc., as mentioned in Chapter 1. These experiments provide a suitable setup to pursue statistical mechanics and thermalization in open quantum many-body systems. For example, as detailed later, decay of the MBL obeying the Lindblad master equation with a dephasing type of dissipation has been investigated both theoretically and experimentally.

It is also important to note that certain experimental setups, represented by continuously measured open quantum systems, can access each quantum trajectory that keeps individual measurement outcomes [233]. Dynamics of such a quantum trajectory may behave differently from the conventional dynamics, for which all measurement outcomes are averaged out. This will be clarified in Sec-

tion 4.1, where we discuss the dynamics of non-Hermitian systems as a special case of quantum trajectories. In addition, we comment that quantum trajectories are necessary to discuss closed-loop feedback control depending on measurement outcomes, which has experimentally been realized in quantum many-body systems using Rydberg atoms [105, 106].

In this chapter, we review the basic theory and recent developments in open quantum systems. In Section 4.1, we formulate dynamics of quantum trajectories in repetitively or continuously measured open quantum systems. In Section 4.2, we review properties of non-Hermitian systems, which can be regarded as the simplest case of quantum trajectories. In Section 4.3, we discuss recent developments on thermalization of open quantum many-body dynamics.

## 4.1 Repeatedly or continuously measured open quantum systems

### 4.1.1 Repeatedly measured quantum systems

We here formulate time evolution of quantum systems under indirect repeated measurements. Here, we model the indirect measurement as the following cycle:

1. (Preparation) We attach an ancilla state  $\hat{\rho}_A$  (such as photons) to the system  $\hat{\rho}_S$  (such as bosons). The total state  $\hat{\rho}_{\text{tot}}$  is given by

$$\hat{\rho}_{\text{tot},0} = \hat{\rho}_S \otimes \hat{\rho}_A. \quad (4.1)$$

2. (Interaction) We let the system and the ancilla interact with a unitary time evolution operator  $\hat{U}_{SA}$ . Then the entire system becomes

$$\hat{\rho}_{\text{tot},0} \rightarrow \hat{U}_{SA}(\hat{\rho}_S \otimes \hat{\rho}_A)\hat{U}_{SA}^\dagger. \quad (4.2)$$

3. (Measurement) We perform a projective measurement on the ancilla. We introduce a set of projective operators  $\hat{P}_A(\eta)$  depending on a measurement result  $\eta$ . The normalization condition is given by  $\sum_\eta \hat{P}_A(\eta) = \hat{\mathbb{I}}_A$ , where  $\hat{\mathbb{I}}_{A/S}$  is the identity operator of the ancilla/system Hilbert space.

The state after the measurement with an outcome  $\eta$  can be written as

$$\hat{\rho}_{\text{tot},\eta} = \frac{\hat{P}_A(\eta)\hat{U}_{SA}(\hat{\rho}_S \otimes \hat{\rho}_A)\hat{U}_{SA}^\dagger\hat{P}_A(\eta)}{p_\eta} \quad (4.3)$$

with the probability of the measurement result  $\eta$  given by

$$p_\eta = \text{Tr}[\hat{P}_A(\eta)\hat{U}_{SA}(\hat{\rho}_S \otimes \hat{\rho}_A)\hat{U}_{SA}^\dagger \hat{P}_A(\eta)]. \quad (4.4)$$

4. (Detachment of the ancilla) Finally, we trace out the Hilbert space of the ancilla and obtain

$$\hat{\rho}_{S,\eta} = \tilde{\mathcal{E}}_\eta(\hat{\rho}_S) = \text{Tr}_A[\hat{\rho}_{\text{tot},\eta}] \quad (4.5)$$

for the measurement outcome  $\eta$ . Therefore, the state after the ensemble average over the measurement outcome  $\eta$  is given by

$$\hat{\rho}'_S = \sum_\eta p_\eta \hat{\rho}_{S,\eta} = \sum_\eta p_\eta \tilde{\mathcal{E}}_\eta(\hat{\rho}_S) = \sum_\eta \text{Tr}_A[\hat{P}_A(\eta)\hat{U}_{SA}(\hat{\rho}_S \otimes \hat{\rho}_A)\hat{U}_{SA}^\dagger \hat{P}_A(\eta)]. \quad (4.6)$$

The map  $\hat{\rho}_S \rightarrow \hat{\rho}'_S = \mathcal{E}(\hat{\rho}_S)$  defines one cycle of the measurement process.

Next, let us perform the spectral decompositions of  $\hat{\rho}_A$  and  $\hat{P}_A(\eta)$  as follows:

$$\begin{aligned} \hat{\rho}_A &= \sum_a \rho_{A,a} |\rho_{A,a}\rangle \langle \rho_{A,a}|, \\ \hat{P}_A(\eta) &= \sum_b |\pi_{A,\eta,b}\rangle \langle \pi_{A,\eta,b}|, \end{aligned} \quad (4.7)$$

where  $a$  and  $b$  are the labels of eigenstates that diagonalize  $\hat{\rho}_A$  and  $\hat{P}_A(\eta)$ , respectively. Then, introducing the operators

$$\hat{M}_{\eta,c} = \sqrt{\rho_{A,a}} \langle \pi_{A,\eta,b} | \hat{U}_{SA} | \rho_{A,a} \rangle \quad (4.8)$$

with  $c = (a, b)$ , we obtain

$$\hat{\rho}_{S,\eta} = \tilde{\mathcal{E}}_\eta(\hat{\rho}_S) = \frac{\sum_c \hat{M}_{\eta,c} \hat{\rho}_S \hat{M}_{\eta,c}^\dagger}{p_\eta} \quad (4.9)$$

and

$$\hat{\rho}'_S = \mathcal{E}(\hat{\rho}_S) = \sum_{\eta,c} \hat{M}_{\eta,c} \hat{\rho}_S \hat{M}_{\eta,c}^\dagger \quad (4.10)$$

where

$$\sum_{\eta,c} \hat{M}_{\eta,c}^\dagger \hat{M}_{\eta,c} = \hat{\mathbb{I}}_S \quad (4.11)$$

is satisfied. Note that the map  $\mathcal{E}$  is completely positive and trace-preserving.

Suppose that we repeat the above measurement cycles  $n$  times. A quantum

trajectory with the outcomes  $\eta_1, \eta_2, \dots, \eta_n$  can be written as

$$\tilde{\mathcal{E}}_{\eta_n}(\dots(\tilde{\mathcal{E}}_{\eta_1}(\hat{\rho}_S))\dots). \quad (4.12)$$

On the other hand, the averaged dynamics over all quantum trajectories can be simply written as

$$\mathcal{E}^n(\hat{\rho}_S). \quad (4.13)$$

### 4.1.2 Continuously measured quantum systems

Next, we assume that each of the above cycles is performed in a very short time  $dt$ . We consider a situation in which the initial state of the ancilla is  $\hat{\rho}_A = |0\rangle\langle 0|$ . Then,  $\eta = 0$  corresponds to the case for the null measurement outcome and  $\eta \geq 1$  corresponds to the case for which some signal is observed. We also assume that the measurement process is characterized by the operators  $\hat{M}_0, \hat{M}_1, \dots$  given by

$$\begin{aligned} \hat{M}_0 &= \hat{\mathbb{I}}_S + (\hat{K} - i\hat{H})dt, \\ \hat{M}_{\eta \geq 1} &= \hat{L}_\eta \sqrt{dt}. \end{aligned} \quad (4.14)$$

Here,  $\hat{H}$  and  $\hat{K}$  are Hermitian and we have omitted  $c = (a, b)$  in Eq. (4.8) by assuming that the initial ancilla state is pure and that each of the projective operators  $\hat{P}_A(\eta)$  has rank 1. It follows from the normalization condition in Eq. (4.11) that

$$\hat{K} = -\frac{1}{2} \sum_{\eta \geq 1} \hat{L}_\eta^\dagger \hat{L}_\eta. \quad (4.15)$$

As we mentioned above,  $\eta = 0$  corresponds to the case for which no outcome is obtained, and  $\eta \neq 0$  corresponds to the case with outcome  $\eta$ . Indeed, for  $\eta = 0$ , the state evolves as

$$\begin{aligned} \hat{\rho}_0(t + dt) &= \frac{\hat{M}_0 \hat{\rho}(t) \hat{M}_0^\dagger}{p_{\eta=0}} \\ &= \hat{\rho}(t) + (-i[\hat{H}, \hat{\rho}(t)] + \{\hat{K}, \hat{\rho}(t)\} - 2\text{Tr}[\hat{\rho}(t)\hat{K}]) dt + o(dt) \end{aligned} \quad (4.16)$$

with

$$p_{\eta=0} = \text{Tr}[\hat{\rho}(t)\hat{M}_0^\dagger\hat{M}_0] = 1 + 2\text{Tr}[\hat{\rho}(t)\hat{K}]dt + o(dt). \quad (4.17)$$

Thus, the state evolves continuously as a function of time. On the other hand, for

$\eta \geq 1$ , the state becomes

$$\begin{aligned}\hat{\rho}_{\eta \geq 1}(t + dt) &= \frac{\hat{M}_\eta \hat{\rho}(t) \hat{M}_\eta^\dagger}{p_\eta} \\ &= \frac{\hat{L}_\eta \hat{\rho}(t) \hat{L}_\eta^\dagger}{\text{Tr}[\hat{\rho}(t) \hat{L}_\eta^\dagger \hat{L}_\eta]}\end{aligned}\quad (4.18)$$

with probability

$$p_\eta = \text{Tr}[\hat{\rho}(t) \hat{M}_\eta^\dagger \hat{M}_\eta] = \text{Tr}[\hat{\rho}(t) \hat{L}_\eta^\dagger \hat{L}_\eta] dt. \quad (4.19)$$

Thus, the state evolves discontinuously as a function of time, which is called the quantum jump.

The dynamics for which all measurement outcomes  $\eta$  are averaged out can be written as

$$\begin{aligned}\frac{d\hat{\rho}(t)}{dt} &= -i[\hat{H}, \hat{\rho}(t)] - \frac{1}{2} \left\{ \sum_{\eta \geq 1} \hat{L}_\eta^\dagger \hat{L}_\eta, \hat{\rho}(t) \right\} + \sum_{\eta \geq 1} \hat{L}_\eta \hat{\rho}(t) \hat{L}_\eta^\dagger \\ &= -i\hat{H}_{\text{NH}} \hat{\rho}(t) + i\hat{\rho}(t) \hat{H}_{\text{NH}}^\dagger + \sum_{\eta \geq 1} \hat{L}_\eta \hat{\rho}(t) \hat{L}_\eta^\dagger,\end{aligned}\quad (4.20)$$

where we have introduced a non-Hermitian Hamiltonian

$$\hat{H}_{\text{NH}} = \hat{H} - \frac{i}{2} \sum_{\eta \geq 1} \hat{L}_\eta^\dagger \hat{L}_\eta. \quad (4.21)$$

The equation Eq. (4.20) is nothing but the Lindblad equation.

When we instead focus on quantum trajectories with individual measurement outcomes, the dynamics can be written as the stochastic time evolution. If we assume that the state is pure, its dynamics is given by

$$d|\psi\rangle = \left( \hat{\mathbb{I}}_S - i\hat{H}_{\text{NH}} + \frac{1}{2} \sum_{\eta \geq 1} \langle \psi | \hat{L}_\eta^\dagger \hat{L}_\eta | \psi \rangle \right) |\psi\rangle dt + \sum_{\eta \geq 1} \left( \frac{\hat{L}_\eta |\psi\rangle}{\langle \psi | \hat{L}_\eta^\dagger \hat{L}_\eta | \psi \rangle} - |\psi\rangle \right) dN_\eta. \quad (4.22)$$

Here, the event of quantum jump  $dN_\eta$  is defined as a stochastic calculus satisfying

$$\begin{aligned}dN_\eta dN_{\eta'} &= \delta_{\eta\eta'} dN_\eta, \\ \mathbb{E}[dN_\eta] &= \langle \psi | \hat{L}_\eta^\dagger \hat{L}_\eta | \psi \rangle dt,\end{aligned}\quad (4.23)$$

where  $\mathbb{E}$  denotes the average over samples. The quantum trajectory is composed of no-jump intervals, where the dynamics is governed by the non-Hermitian Hamiltonian in Eq. (4.21), and the quantum jumps, at which the state suddenly

changes owing to the second term in Eq. (4.22). Note that the averaged dynamics of  $\hat{\rho}(t) = \mathbb{E}[|\psi\rangle\langle\psi|]$  satisfies the Lindblad equation in Eq. (4.20).

When there are no quantum jumps, *i.e.*,  $dN_\eta = 0$ , the dynamics of the quantum trajectory is simply given by

$$\frac{d|\psi\rangle}{dt} = \left( -i\hat{H}_{\text{NH}} + \frac{1}{2} \sum_{\eta \geq 1} \langle \psi | \hat{L}_\eta^\dagger \hat{L}_\eta | \psi \rangle \right) |\psi\rangle, \quad (4.24)$$

whose solution is

$$|\psi(t)\rangle = \frac{e^{-i\hat{H}_{\text{NH}}t} |\psi(0)\rangle}{\|e^{-i\hat{H}_{\text{NH}}t} |\psi(0)\rangle\|}. \quad (4.25)$$

Thus, the dynamics of a quantum trajectory with no jump processes is determined by the non-Hermitian Hamiltonian  $\hat{H}_{\text{NH}}$ .

## 4.2 Non-Hermitian systems

We have seen above that the non-Hermitian dynamics is important for the dynamics of quantum trajectories. In fact, non-Hermitian Hamiltonians generally show up in various types of open systems, both in classical and quantum systems. In this section, we review basic properties and applications of non-Hermitian Hamiltonians.

### 4.2.1 Basic aspects of non-Hermitian matrices

Let us consider a very simple example. We take a non-Hermitian matrix

$$H = \sigma^z + ig\sigma^y = \begin{pmatrix} 1 & g \\ -g & -1 \end{pmatrix} \quad (4.26)$$

with  $g \in \mathbb{R}$  ( $g \neq 0$ ). The matrix has eigenvalues

$$\lambda_+ = \sqrt{1 - g^2}, \quad \lambda_- = -\sqrt{1 - g^2} \quad (4.27)$$

which correspond to two right eigenstates (*i.e.*,  $H\vec{\phi}_\pm = \lambda_\pm\vec{\phi}_\pm$ ),

$$\vec{\phi}_+ \propto \begin{pmatrix} -g \\ 1 - \sqrt{1 - g^2} \end{pmatrix}, \quad \vec{\phi}_- \propto \begin{pmatrix} -g \\ 1 + \sqrt{1 - g^2} \end{pmatrix}. \quad (4.28)$$

On the other hand, left eigenstates, which satisfy  $\vec{\chi}_\pm^\dagger H = \lambda_\pm \vec{\chi}_\pm^\dagger$ , are given by

$$\vec{\chi}_+^\dagger \propto \left( g \quad 1 - \sqrt{1 - g^2} \right), \quad \vec{\chi}_-^\dagger \propto \left( g \quad 1 + \sqrt{1 - g^2} \right). \quad (4.29)$$

There are some important properties to note:

1. Left and right eigenstates are in general different, *i.e.*,  $\vec{\phi}_\alpha$  and  $\vec{\chi}_\alpha$  are not proportional to each other.
2. Three normalization conditions  $\vec{\chi}_\alpha^\dagger \vec{\phi}_\alpha = 1$ ,  $\vec{\phi}_\alpha^\dagger \vec{\phi}_\alpha = 1$ , and  $\vec{\chi}_\alpha^\dagger \vec{\chi}_\alpha = 1$  cannot simultaneously be satisfied. In the following, we assume  $\vec{\chi}_\alpha^\dagger \vec{\phi}_\alpha = 1$  and  $\vec{\phi}_\alpha^\dagger \vec{\phi}_\alpha = 1$ , but  $\vec{\chi}_\alpha^\dagger \vec{\chi}_\alpha \neq 1$ .
3. (Biothogonality) Under the normalization condition above, one obtains

$$\vec{\chi}_\alpha^\dagger \vec{\phi}_\beta = \delta_{\alpha\beta}, \quad (4.30)$$

*i.e.*, the biothogonality between right and left eigenstates.

4. (Non-orthogonality) On the other hand, there is no orthogonality between two right (left) eigenstates in general,

$$\vec{\phi}_\alpha^\dagger \vec{\phi}_\beta \neq 0, \quad \vec{\chi}_\alpha^\dagger \vec{\chi}_\beta \neq 0. \quad (4.31)$$

These properties are common to general non-Hermitian matrices.

In addition, the Hamiltonian in Eq. (4.26) has the following important properties owing to the reality condition  $H = H^*$ :

1. For  $|g| < 1$ , both eigenvalues stay real, *i.e.*,  $\lambda_\pm \in \mathbb{R}$ , even in the presence of the non-Hermiticity. Each of the two eigenstates is invariant under the complex-conjugate operation,  $\vec{\phi}_\alpha^* = \vec{\phi}_\alpha$ .
2. For  $|g| > 1$ , two eigenvalues are complex-conjugate to each other, *i.e.*,  $\lambda_+^* = \lambda_-$ . In this case, the corresponding eigenstates are also connected by the complex conjugation,  $\vec{\phi}_+^* = \vec{\phi}_-$ .
3. For  $|g| = 1$ , two eigenstates and eigenvalues coincide, or “coalesce”. In contrast with the degeneracy that can occur in Hermitian systems, this coincidence is accompanied by the reduction of the rank of the matrix. Indeed, since eigenstates coincide, they cannot span the entire Hilbert space, which means that the completeness of the eigenstates is lost. These special points are called exceptional points.

These properties are known to occur if the system respects time-reversal symmetry  $\hat{T} = \hat{\mathcal{T}}_+ \hat{K}$ , where  $\hat{K}$  is a complex-conjugation operator and  $\hat{\mathcal{T}}_+$  ( $\hat{\mathcal{T}}_+ \hat{\mathcal{T}}_+^* = \pm \hat{\mathbb{1}}$ ) is a unitary operator, namely

$$\hat{\mathcal{T}}_+ \hat{H}^* \hat{\mathcal{T}}_+^{-1} = \hat{H}. \quad (4.32)$$

Note that  $\hat{\mathcal{T}}_+$  is the identity in the example in Eq. (4.26). When  $\hat{H} |\phi_\alpha\rangle = E_\alpha |\phi_\alpha\rangle$ , we have  $\hat{H}^* |\phi_\alpha\rangle^* = E_\alpha^* |\phi_\alpha\rangle^*$  and thus

$$\begin{aligned} \hat{H} \hat{\mathcal{T}}_+ |\phi_\alpha\rangle^* &= \hat{\mathcal{T}}_+ \hat{H}^* |\phi_\alpha\rangle^* \\ &= E_\alpha^* \hat{\mathcal{T}}_+ |\phi_\alpha\rangle^*. \end{aligned} \quad (4.33)$$

Thus,  $\hat{H}$  has an eigenstate  $\hat{\mathcal{T}}_+ |\phi_\alpha\rangle^*$  with an eigenvalue  $E_\alpha^*$ . This means that eigenvalues necessarily appear as real ones or form complex-conjugate pairs. We note that these properties appear also for matrices with the pseudo-Hermiticity [234], *i.e.*,

$$\hat{\eta} \hat{H}^\dagger \hat{\eta}^{-1} = \hat{H} \quad (4.34)$$

for a unitary matrix  $\hat{\eta}$  with  $\hat{\eta}^2 = 1$ . In this case, when  $\langle \chi_\alpha | \hat{H} = E_\alpha \langle \chi_\alpha |$ , the vector  $\eta |\chi_\alpha\rangle^*$  becomes a right eigenstate of  $\hat{H}$  with an eigenvalue  $E_\alpha^*$ .

Let us go back to the simple example in Eq. (4.26). If we increase  $g$  from 0, two real eigenvalues first approach each other. Then, the eigenvalues coalesce at  $g = 1$  and then become complex for  $g > 1$ . In other words, eigenvalues can be complex only through the exceptional point. This is in contrast with the matrix without such time-reversal symmetry, where eigenvalues themselves are, in general, complex.

The real-complex transition was already discussed in the seminal paper by Hatano and Nelson [235, 236, 237], who investigated an asymmetric hopping model with disorder (see Chapter 5) that keeps time-reversal symmetry. The importance of the symmetry was first stressed in Ref. [38], who considered a single particle in a non-Hermitian potential with parity and time-reversal (PT) symmetry. In that case, the real-complex transition is called the PT-symmetry breaking. The case for which eigenvalues are real is called the PT-symmetry unbroken phase; the case for which eigenvalues form a complex-conjugate pair is called the PT-symmetry broken phase, since eigenstates are no longer invariant under PT operation while the Hamiltonian is.

## 4.2.2 Non-Hermitian quantum dynamics

Let us consider time evolution of a non-Hermitian quantum system that obeys Eq. (4.25). By expanding the Hamiltonian in terms of its energy eigenstates, the state becomes

$$|\psi(t)\rangle = \frac{\sum_{\alpha} \langle E_{\alpha}^L | \psi(0) \rangle e^{-iE_{\alpha}t} |E_{\alpha}^R\rangle}{\left\| \sum_{\alpha} \langle E_{\alpha}^L | \psi(0) \rangle e^{-iE_{\alpha}t} |E_{\alpha}^R\rangle \right\|}, \quad (4.35)$$

where  $|E_{\alpha}^R\rangle$  and  $|E_{\alpha}^L\rangle$  are right and left eigenstates of  $\hat{H}_{\text{NH}}$ , respectively. When one of the eigenvalues  $E_{\alpha}$  have nonzero imaginary parts, the state will eventually be dominated by the particular mode  $|\tilde{E}_{\alpha}^R\rangle$ , where  $\tilde{E}_{\alpha}$  is the energy eigenvalue with the maximum positively imaginary part. When all of the eigenvalues are real (*e.g.*, in a PT-symmetry unbroken phase), there is no such eventual dominance of the state. On the other hand, even such a case can exhibit an interesting dynamics which is absent in closed quantum systems. For example, even for an observable  $\hat{O}$  that satisfies  $[\hat{H}_{\text{NH}}, \hat{O}] = 0$ , its expectation value is not necessary conserved if  $|\psi(0)\rangle$  is not an eigenstate of  $\hat{O}$ . Indeed, we have

$$\langle \psi(t) | \hat{O} | \psi(t) \rangle = \frac{\langle \psi(0) | e^{i\hat{H}_{\text{NH}}^{\dagger}t} e^{-i\hat{H}_{\text{NH}}t} \hat{O} | \psi(0) \rangle}{\langle \psi(0) | e^{i\hat{H}_{\text{NH}}^{\dagger}t} e^{-i\hat{H}_{\text{NH}}t} | \psi(0) \rangle}, \quad (4.36)$$

which is, in general, time dependent.

## 4.2.3 Other non-Hermitian systems

We have seen above that non-Hermitian matrices come into play in quantum-trajectory theory for continuously measured quantum systems. On the other hand, non-Hermitian systems appear in many other situations. In fact, non-Hermitian systems have actively been studied in the context of classical optics [238, 239, 240, 241, 242, 243, 39]. For example, in Ref. [242], electric fields in the absorbing media (with a complex refractive index) obey an effective non-Hermitian Schrodinger equation. These systems are expected to be suitable playgrounds for interesting non-Hermitian phenomena, such as PT-symmetry breaking and non-Hermitian topological effect [244, 245, 246].

Non-Hermitian matrices also naturally appear in dissipative [247, 248] systems. If we consider classical Markov dynamics, its transition matrix is, in general, non-Hermitian. For another example, the Lindblad superoperator for quantum systems can also be mapped to non-Hermitian operator (see Chapter 6 as an example). Non-Hermiticity also appears in linearized hydrodynamics [249]. In

addition, non-Hermitian matrices are relevant for other fields of science, such as biology [250] and information science [251].

## 4.3 Previous studies on thermalization of open quantum many-body systems

In the previous sections we have discussed basic formulations of open quantum systems. We here review studies on the problem of thermalization, such as stationary states, in open quantum many-body systems.

### 4.3.1 Thermalization under the Lindblad equations

We first consider the stationary states of the Lindblad equations. The simplest case is that the operator  $\hat{L}_\eta$  for each  $\eta$  is Hermitian. In this case, the maximally mixed state  $\hat{\rho} \propto \hat{\mathbb{I}}$  becomes a solution of the Lindblad equation. More generally, a sufficient condition (called quantum generalization of the detailed-balance condition) for a Lindblad operator to have the Gibbs state as a stationary-state solution is also obtained [252].

Recently, it has been reported numerically that even systems without the quantum generalization of the detailed-balance condition sometimes relax to a thermal state for a weak coupling limit  $\|\hat{L}_\eta\| \rightarrow 0$  [253]. However, it is still not fully understood when a system relaxes to thermal equilibrium for a general setup.

There are other cases for which the stationary-state solutions of the Lindblad equation are known. One of the important examples is the case that dark states appear. Namely, if the state  $\hat{\rho}$  is eliminated by all of the jump operators

$$\hat{L}_\eta \hat{\rho} = 0 \tag{4.37}$$

and if it is invariant under the Hamiltonian part

$$[\hat{\rho}, \hat{H}] = 0, \tag{4.38}$$

$\hat{\rho}$  is a stationary state of the Lindblad equation. This technique is used to create a desired state by controlling dissipation [254, 255, 256].

In many cases, however, the stationary state emerges as a complicated competition of the unitary dynamics and dissipation. For example, by tuning the dissipation, the stationary state of dissipative many-body systems (*e.g.*, locally interacting spin systems) can exhibit nontrivial phase transitions [257, 258]. We

can also create highly nonequilibrium stationary states, such as current-carrying stationary states [259, 260] or time-crystalline states [261, 262]. While analytical [263, 264] and numerical [265, 266, 267, 268, 269, 270, 271, 258, 272, 273, 274, 275] techniques for finding such stationary states are rapidly developing, it is still an interesting open problem to elucidate stationary states of Lindblad equations in general setups.

### 4.3.2 Decay of the many-body localization under the Lindblad dynamics

Here, as one of the most important cases of thermalization in open systems, we discuss the effect of dissipation on the MBL system.

The MBL under dissipation was first considered in Ref. [276], which investigated interacting disordered Fermionic systems with a dephasing-type dissipation ( $\hat{L}_l = \hat{n}_l$ )

$$\dot{\hat{\rho}}(t) = -i[\hat{H}, \hat{\rho}(t)] + \gamma \sum_{l=1}^N \left[ \hat{n}_l \hat{\rho}(t) \hat{n}_l - \frac{1}{2} \{ \hat{n}_l, \hat{\rho}(t) \} \right], \quad (4.39)$$

where

$$\hat{H} = -J \sum_{l=1}^N (\hat{c}_l^\dagger \hat{c}_{l+1} + \hat{c}_{l+1}^\dagger \hat{c}_l) + V \sum_{l=1}^N \hat{n}_l \hat{n}_{l+1} + 2 \sum_{l=1}^N h_l \hat{n}_l. \quad (4.40)$$

In this case, the stationary state is trivially an infinite-temperature state because  $\hat{n}_l$  is Hermitian. On the other hand, using numerical simulations for finite-size systems, the authors of Ref. [276] claimed that the dynamics in the strong-disorder regime is different from that in the weak-disorder regime. For example, they found that the von-Neumann entropy of  $\hat{\rho}(t)$  grows logarithmically as  $\sim \log(\gamma t)$ , which indicates the exponentially long relaxation time as in Hermitian MBL cases, although the relaxation time depends on the dissipation. They also found that the imbalance of particle numbers between odd and even sites asymptotically exhibits a stretched exponential decay ( $\sim \exp(-\mu t^\alpha)$  for some  $\mu$  and  $\alpha$ ).

Subsequently, there appeared several works that investigate the same models using an effective classical dynamics. In Ref. [277], the authors investigated the long-time behavior by analyzing the low-lying eigenstates (near stationary states) by using the degenerate perturbation theory. After showing that the long-time dynamics is effectively described by a classical Markov process, they argued that Renyi-2 entropy becomes thermal values and do not exhibit MBL signatures (in

contrast with the finding in Ref. [276]). Reference [278] investigated the long-time dynamics by assuming that off-diagonal quantum coherence in the basis that diagonalizes quasilocal conserved quantities rapidly decays owing to dephasing. Then, the dynamics is governed by the classical rate equation for the particle density at each site. Using this effective equation, they numerically showed that the local imbalance exhibits a stretched exponential decay, which is consistent with the finding in Ref. [276]. Such a stretched exponential decay was later observed in a controlled experiment of ultracold atoms [104].

We note that, by tuning the dissipation (that is non-Hermitian) such that it drives the system into a nonequilibrium steady state, we can find the localization signature even in stationary states of open systems [279, 280]. For example, by choosing

$$\hat{L}_l = (\hat{c}_l^\dagger + \hat{c}_{l+1}^\dagger)(\hat{c}_l - \hat{c}_{l+1}) \quad (4.41)$$

for the jump operators instead of  $\hat{L}_l = \hat{n}_l$  in Eq. (4.39), the stationary state is shown to exhibit MBL signatures for, *e.g.*, the imbalance of particles [280].

### 4.3.3 Thermalization dynamics without ensemble averaging

We have explained the dynamics of the Lindblad equation, which describes the averaged dynamics over all quantum jumps. Here, we discuss a few theoretical progresses which treat thermalization of open many-body systems at the level of quantum trajectories.

#### Dynamics of quantum trajectories

One of the simplest scenario is that each quantum trajectory will heat up owing to the energy injection by quantum jumps (*i.e.*, measurement backaction). The authors of Ref. [281] showed that a typical quantum trajectory in the Bose-Hubbard model with very weak dissipation, which ensures the long-time interval between quantum jumps, heats up to a state described by the infinite-temperature state. To see this, we remind that the dynamics of quantum trajectories consists of time evolutions by a non-Hermitian Hamiltonian (which is approximated by the Hermitian Hamiltonian of the Bose-Hubbard model under the weak-dissipation condition) and stochastic quantum jumps. Since the quantum jumps are regarded as stochastic quench operations of the system and the ETH is satisfied owing to the nonintegrability of the Hermitian, the quantum trajectories after a sufficiently

long time are described by thermal states, whose energy eventually grows.

Another interesting consequence of quantum jumps is that it can disentangle a quantum state. References [282, 283, 284] considered random quantum circuits which are composed of unitary parts (explained in Chapter 2) and non-unitary projective measurements. Intuitively, if the occurrence of the projective measurement is sufficiently rare, quantum trajectories will be entangled owing to the interaction of the unitary time evolution. On the other hand, for frequent local measurements, quantum trajectories will be disentangled owing to the collapse of the state. Indeed, it was found that the competition between interactions and measurements leads to a novel critical phase transition of the growth of the entanglement entropy  $S(t)$  of quantum trajectories. Namely,  $S(t) \propto O(t^1)$  is found for infrequent measurements but  $S(t) \sim O(t^0)$  for frequent measurements. At the critical point,  $S(t)$  exhibits the logarithmic behavior as  $S(t) \sim \log t$ . This behavior is also related with the classical percolation theory [283]. The entanglement phase transition has actively been studied in various setups recently, such as the case for indirect measurements [285] and specific bosonic systems [286]. It is also related to quantum information theory, such as information scrambling and the error correction [287, 288, 289, 290].

### **Non-Hermitian dynamics**

While the phenomena discussed above are explained by the effects of stochastic quantum jumps, interesting features can also result from the continuous-time evolution described by non-Hermitian Hamiltonians. In fact, several works investigated consequences brought by purely non-Hermitian dynamics, which corresponds to postselected quantum trajectories with no jumps (see Eq. (4.25)). For example, Ref. [291] showed that the Lieb-Robinson bound, which holds true for unitary time evolution and the Lindblad dynamics, breaks down for non-Hermitian time evolutions, reflecting the non-orthogonality of eigenstates. In Ref. [292], it was demonstrated that quantum magnetism which corresponds to negative temperature is dynamically stabilized in the Hubbard model with a non-Hermitian interaction, since an eigenvalue for such a negative-temperature state has the maximum imaginary part among the spectrum.

# Chapter 5

## Non-Hermitian many-body localization

### 5.1 Motivation

In the previous chapter, we have seen that non-Hermitian Hamiltonians appear in open systems, e.g., continuously measured quantum systems with null outcome. As explained there, non-Hermiticity leads to many unique properties, such as the real-complex phase transition of two eigenvalues under time-reversal symmetry (TRS), which also affect properties of nonequilibrium dynamics.

One of the important classes of non-Hermitian systems that exhibit the real-complex transition owing to TRS was proposed by Hatano and Nelson in 1996 [235, 236, 237]. This model is a single-particle disordered model with asymmetric hopping. In this model, a real-complex phase transition of the single-particle spectrum and a non-Hermitian generalization of the Anderson localization coincide.

While the Hatano-Nelson model is a seminal one which has been followed by many researchers [293, 294, 295, 296, 297, 298, 299], it is unknown if a real-complex transition owing to TRS and a localization transition owing to disorder occur in non-Hermitian many-body systems. As discussed in Chapter 2, many-body interaction and localization lead to the nontrivial consequence of many-body localization (MBL), which is characterized by the transition of a many-body spectrum. It is an intriguing problem how the competition between interaction, localization, and non-Hermiticity affects many-body properties of the system.

This question is also related to the problem of thermalization in open quantum many-body systems. As discussed in Chapter 4, MBL in open systems has been studied in the Lindblad master-equation formalism, which shows that the

MBL may be destroyed by certain dissipation [278, 276, 277, 104, 300]. On the other hand, non-Hermitian setups are relevant for quantum trajectories (with no quantum jumps) in continuously measured quantum many-body systems, where measurement outcomes are not averaged out, and describe physics distinct from the master-equation approach. It is nontrivial whether disorder affects the dynamics of such non-Hermitian open systems.

In this chapter, we discuss MBL in non-Hermitian systems. We demonstrate that imaginary parts of many-body energy eigenvalues of non-Hermitian many-body systems with TRS are suppressed by localization. We find that interacting systems with disorder and asymmetric hopping exhibit a novel real-complex phase transition: almost all energy eigenvalues become complex for weak disorder, and almost all energy eigenvalues become real for strong disorder (see Fig. 5.1(a) and (b)). In the real-eigenvalue phase, absorption and emission of energy disappear despite non-Hermiticity, and the dynamics becomes unstable. We then show the presence of a non-Hermitian MBL transition, which is characterized by level-spacing distributions and entanglement entropy, near the real-complex phase transition point. We conjecture that points of the two transitions coincide in the thermodynamic limit using an analytical discussion on eigenstate stability. We also show the absence of the real-complex transition in non-Hermitian systems with gain and/or loss since they do not possess TRS, although non-Hermitian MBL still persists (see Fig. 5.1(c)). We summarize the results in Fig. 5.1(d).

## 5.2 Brief review of the Hatano-Nelson model

Before stating our main results, we first review the Hatano-Nelson model. The original continuum Hamiltonian is given by

$$\hat{H}_{\text{con}} = \frac{(\hat{p} - ig)^2}{2m} + V(\hat{x}), \quad (5.1)$$

where  $V(\hat{x})$  is a random potential and we consider a one-dimensional system for simplicity. In addition, the "imaginary gauge field"  $ig$  controls the strength of non-Hermiticity (note that the sign of  $g$  is reversed from Ref. [235]). The discrete second-quantized version with the tight-binding approximation is

$$\hat{H} = \sum_{i=1}^L \left[ -J \left( e^{-g} \hat{b}_{i+1}^\dagger \hat{b}_i + e^g \hat{b}_i^\dagger \hat{b}_{i+1} \right) + h_i \hat{n}_i \right], \quad (5.2)$$

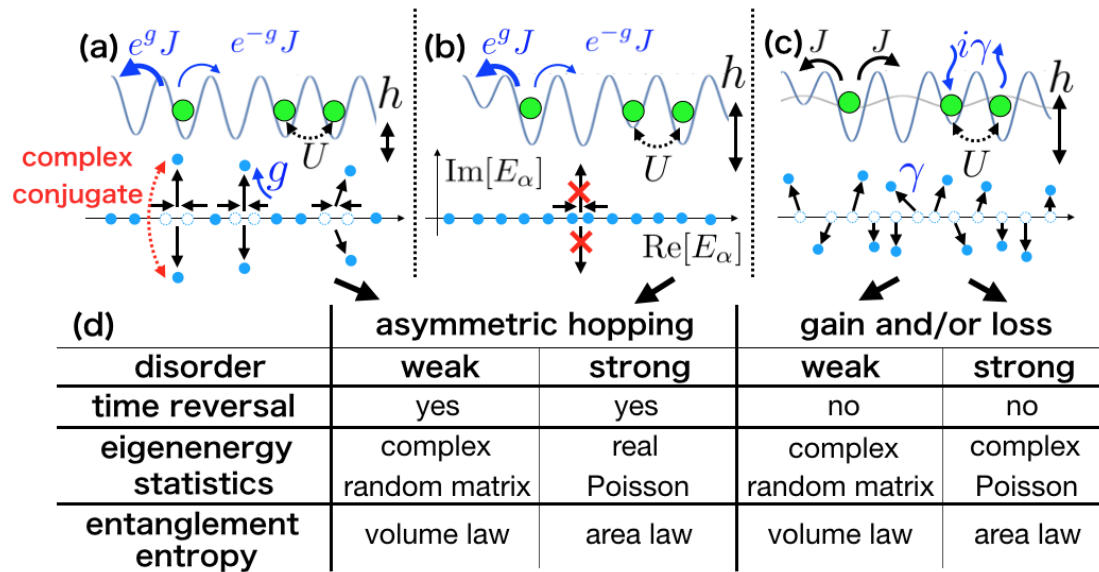


Figure 5.1: (a) A model with weak disorder and asymmetric hopping. A non-Hermitian perturbation makes two energy eigenvalues coalesce and become complex conjugate to each other. (b) A model with strong disorder and asymmetric hopping. Localization prohibits coalescence of energy eigenvalues owing to perturbation. (c) A model with strong disorder and gain and/or loss. In the absence of TRS, energy eigenvalues with nonzero imaginary parts can appear without coalescence, even when localization occurs. (d) Statistics of energy eigenvalues and entanglement entropy of energy eigenstates for a model with asymmetric hopping (Eq. (5.6)) or a model with gain and/or loss (Eq. (5.29)) for different strengths of disorder. Reproduced from Fig. 1 of Ref. [111]. ©2019 American Physical Society with a slight modification.

where  $\hat{n}_i = \hat{b}_i^\dagger \hat{b}_i$  is the number operator of particles at site  $i$  ( $\hat{b}_i$  is the annihilation operator),  $g$  represents non-Hermitian asymmetric hopping, and  $h_i$  denotes the disorder strength which is randomly chosen from  $[-h, h]$ . We also consider the periodic boundary condition. Note that this model becomes the Anderson model for  $g = 0$ .

The Hatano-Nelson model shows an interesting spectral transition as a function of disorder (see Fig. 5.2). If disorder is weak enough compared with the non-Hermiticity, the eigenstates become delocalized and the corresponding eigenvalues become complex. If disorder is strong enough compared with the non-Hermiticity, the eigenstates become localized and the corresponding eigenvalues become real.

Let us discuss an intuitive reason why non-Hermiticity leads to the breakdown of localization. Since Eq. (5.1) describes a particle in the imaginary gauge field, we may perform the following "imaginary gauge transformation" and make the field vanish:

$$\begin{aligned}\hat{\mathcal{V}} &= e^{\frac{gx}{\hbar}}, \\ \hat{\mathcal{V}}\hat{H}_{\text{con}}\hat{\mathcal{V}}^{-1} &= \frac{\hat{p}^2}{2m} + V(\hat{x}).\end{aligned}\quad (5.3)$$

Since this operation is a similarity transformation which does not alter the eigenvalues and the transformed Hamiltonian is Hermitian,  $\hat{H}_{\text{con}}$  has real eigenvalues when this transformation is applicable. To see when this transformation becomes inapplicable, let us start from  $g = 0$ , where all of the eigenvalues are delocalized in one dimension owing to the Anderson localization. In that case, a localized eigenstate can be written as

$$\psi(x) \sim \exp\left(-\frac{|x - x_0|}{\xi_{\text{loc}}}\right) \quad (5.4)$$

for some  $x_0$ . For  $g > 0$ , the eigenstate becomes

$$\psi^g(x) = \hat{\mathcal{V}}^{-1}\psi(x) \sim \exp\left(\frac{gx}{\hbar} - \frac{|x - x_0|}{\xi_{\text{loc}}}\right). \quad (5.5)$$

For  $g/\hbar < 1/\xi_{\text{loc}}$ ,  $\psi^g(x)$  can be safely normalized because  $|\psi^g(x)|$  decays exponentially for large  $|x|$ . In that case, the shape of the eigenstate is deformed but it is still localized, and the corresponding eigenvalue remains real. On the other hand, for  $g/\hbar > 1/\xi_{\text{loc}}$ ,  $\psi^g(x)$  exponentially diverges for either large positive  $x$  or large negative  $x$ , which is incompatible with the periodic boundary condition. This means that the above gauge transformation cannot be applied, which allows com-

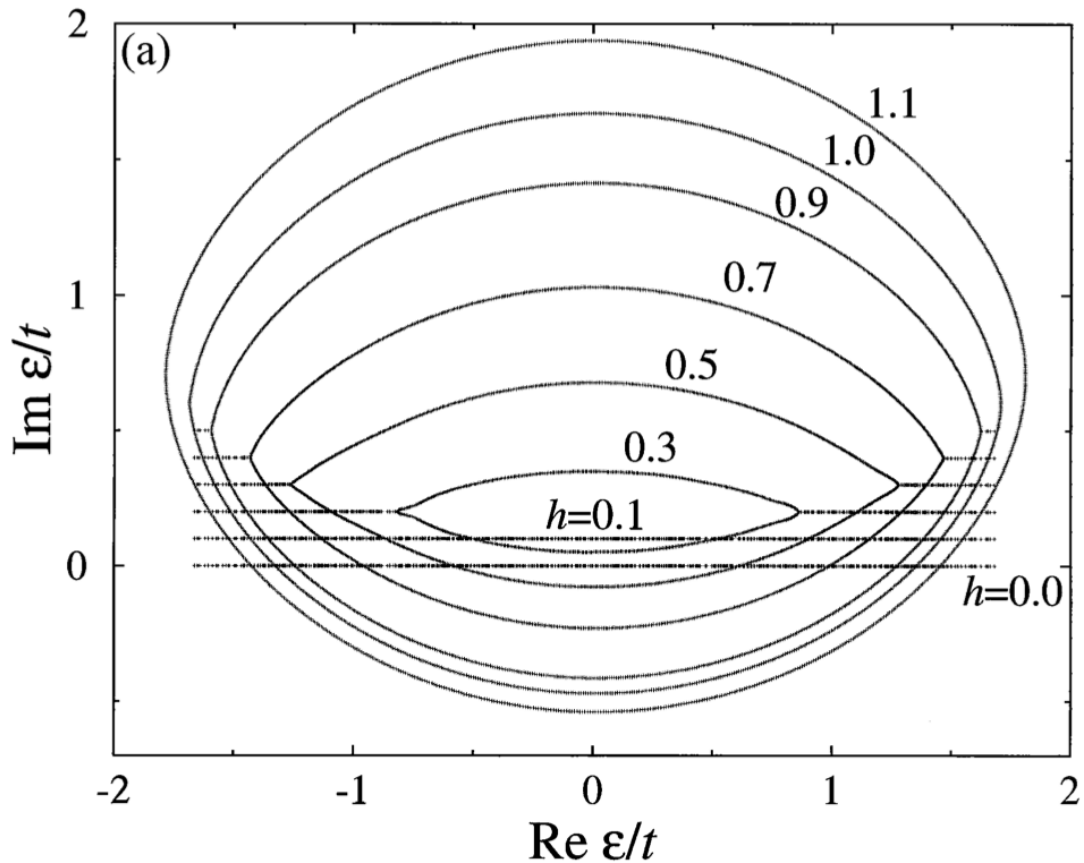


Figure 5.2: Single-particle spectra of the Hatano-Nelson model [235]. Note that  $h$  in the figure corresponds to  $-g$  in Eq. (5.2), which is not the disorder strength. For  $h = 0$ , all of the energy eigenvalues are real, and all of the eigenstates become localized. For nonzero  $h$ , complex eigenvalues appear, which correspond to delocalized eigenstates. Note that imaginary parts are shifted for  $h > 0$  for clarity. Reproduced from Fig. 2 of Ref. [235]. ©1996 American Physical Society. Reprinted figure with permission from Fig.2(a) of [Naomichi Hatano and David R. Nelson. Localization Transitions in Non-Hermitian Quantum Mechanics. Physical Review Letters, 77, 570, Jul 1996 (Ref. [235])] Copyright 1996 by the American Physical Society.

plex eigenvalues. In that case, the eigenstate is no longer localized but extended (delocalized) to the entire space.

The Hatano-Nelson model was originally proposed to describe the depinning transition of vortices in type-II superconductors. Indeed, it can be argued that the asymmetric hopping takes the role of the tilting field imposed on the vortices, and that the real-complex phase transition corresponds to the pinning-depinning transition owing to the tilting field. The Hatano-Nelson model is also arguably relevant for other contexts, such as population biology [250], quantum chaos [293], mathematics [294, 295, 297], quantum chromodynamics [296], and optics [298, 299].

### 5.3 Real-complex phase transition in an interacting model with asymmetric hopping

We now show that a real-complex transition and a localization transition occur at the level of many-body spectra (in stark contrast with the single-particle spectra of the Hatano-Nelson model) for an interacting model with disorder and asymmetric hopping. The Hamiltonian that we consider is

$$\hat{H} = \sum_{i=1}^L \left[ -J(e^{-g}\hat{b}_{i+1}^\dagger \hat{b}_i + e^g\hat{b}_i^\dagger \hat{b}_{i+1}) + U\hat{n}_i\hat{n}_{i+1} + h_i\hat{n}_i \right], \quad (5.6)$$

where  $\hat{b}_i$  represents the annihilation operator for a hard-core boson (the following discussion on the real-complex phase transition also holds true for the case of the Bose-Hubbard model, as shown in Appendix A). This model becomes the Hatano-Nelson model for  $U = 0$ , which is the disordered XXZ model exhibiting the Hermitian MBL for  $g = 0$ , and the asymmetric XXZ model for  $h = 0$  [301]. The model respects TRS because it can be written as a real matrix. In addition, the model can be realized in state-of-the-art experiments of ultracold atoms that are measured continuously, since strong disorder has been realized [61] and asymmetric hopping is also proposed to be implemented [244]. In the following, we focus on the subspace where a number of particles is fixed as  $M = L/2$  (half-filling) and the parameters as  $J = 1$ ,  $g = 0.1$ , and  $U = 2$ . See Appendix A for other values of the parameters.

We first show the many-body energy eigenvalues of the above Hamiltonian in Fig. 5.3(a). Note that the spectrum always has a reflection symmetry about the real axis, since the system respects TRS. On the other hand, the number of energy

eigenvalues with nonzero imaginary parts evidently decreases as  $h$  increases.

### 5.3.1 Fraction of complex energy eigenvalues

To quantify the real-complex property of energy eigenvalues, we consider the following fraction

$$f_{\text{Im}} = \frac{\overline{D_{\text{Im}}}}{D}. \quad (5.7)$$

Here,  $D_{\text{Im}}$  denotes the number of energy eigenvalues with nonzero imaginary parts,  $D$  is the dimension of the Hilbert space, and the overline means the average over disorder. Note that we consider the average over energy eigenvalues for the entire energy range to simplify our discussion. This means that we essentially discuss the energy scale that corresponds to the infinite temperature, where the density of states becomes maximal, for sufficiently large systems.

We show in Fig. 5.3(b) the dependence of  $f_{\text{Im}}$  on  $h$  for different system sizes  $L$ . When we increase the system size,  $f_{\text{Im}}$  increases when  $h \lesssim h_c^{\text{R}} \simeq 8$  and decreases when  $h \gtrsim h_c^{\text{R}}$ . This means a real-complex critical phase transition for many-body eigenvalues at  $h = h_c^{\text{R}}$  in the thermodynamic limit  $L \rightarrow \infty$ . Moreover, we can confirm the scaling behavior around the critical point when we consider  $f_{\text{Im}}$  as a function of  $(h - h_c^{\text{R}})L^{1/\nu}$ , where we obtain  $\nu = 0.5$  here. It is a future problem to investigate what determines the universality class defined from this critical exponent.

In conclusion, almost all energy eigenvalues are complex when  $h < h_c^{\text{R}}$  and real when  $h > h_c^{\text{R}}$ . Note that this transition is defined from the statistics of many-body spectra in the thermodynamic limit. This is quite different from the usual PT symmetry transition, for which the transition point is identified by the coalescence of two eigenstates, not by statistics of many eigenstates. We note that the maximum imaginary value among all energy eigenvalues shows a similar transition, as shown in Appendix A.

### 5.3.2 Transition of dynamical stability

The above transition means that, for large disorder, almost all energy eigenvalues suddenly become real. This transition considerably affects the stability of the time evolution of the system. To see this, we consider the following non-Hermitian

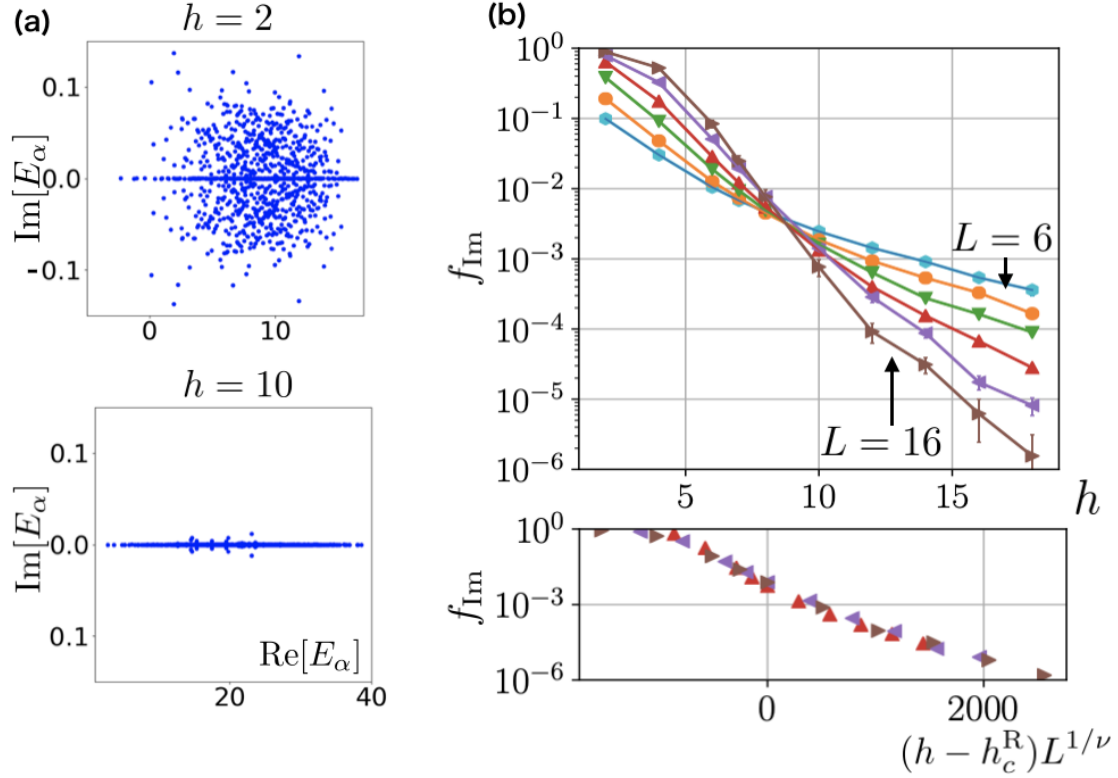


Figure 5.3: (a) Energy eigenvalues of the non-Hermitian Hamiltonian (5.6) for different disorder strength ( $h = 2, 10$ ) with  $L = 12$ . (b) (top) Dependence of the fraction  $f_{\text{Im}}$  on disorder strength  $h$  for  $L = 6, 8, 10, 12, 14$ , and 16. and small for  $h \gtrsim h_c^{\text{R}}$ . (bottom) As a function of  $(h - h_c^{\text{R}})L^{1/\nu}$ ,  $f_{\text{Im}}$  exhibits the critical scaling collapse, where  $h_c^{\text{R}} = 8.0$  and  $\nu = 0.5$  are used. Note that we determine  $f_{\text{Im}}$  using a cutoff of the imaginary part  $C = 10^{-13}$ , with which machine errors ( $|\text{Im}E_\alpha| \ll C$ ) and pure complex eigenvalues ( $|\text{Im}E_\alpha| \gg C$ ) can be separated clearly. We show the data that are averaged over  $N_{\text{sam}}$  samples for different disorder realizations. Here,  $N_{\text{sam}} = 10000$  for  $L = 6, 8, 10, 12$ ,  $N_{\text{sam}} = 1000$  for  $L = 14$ , and  $N_{\text{sam}} = 100$  for  $L = 16$ .

time evolution:

$$|\psi(t)\rangle = \frac{e^{-i\hat{H}t} |\psi_0\rangle}{\|e^{-i\hat{H}t} |\psi_0\rangle\|}, \quad (5.8)$$

which describes to the quantum trajectories with no jump processes for systems that are continuously measured, as discussed in Chapter 4. In the following, we assume that the initial state  $|\psi_0\rangle$  is a charge-density-wave state

$$|\psi_0\rangle = |1010 \cdots 10\rangle. \quad (5.9)$$

In Fig. 5.4(a), we show the dynamics of the real part of the energy,

$$E^R(t) = \text{Re}[\overline{\langle \psi(t) | \hat{H} | \psi(t) \rangle}]. \quad (5.10)$$

We first note that  $E^R(t)$  does not change because of the conservation of energy in the Hermitian case, i.e., in the case with  $g = 0$ . If we add non-Hermiticity, however,  $E^R(t)$  dramatically changes for  $h \lesssim h_c^R$ . This indicates the instability of the system in the complex-eigenvalue phase owing to energy absorption and emission. In contrast, the system is stable if  $h \gtrsim h_c^R$ , in that the energy is kept almost constant with only small oscillations. This comes from the fact that almost all energy eigenvalues are real.

We can also consider the dynamics of the half-chain entanglement entropy

$$S(t) := \overline{\text{Tr}_{L/2}[|\psi(t)\rangle \langle \psi(t)|]}. \quad (5.11)$$

In Fig. 5.4(b), we show that  $S(t)$  increases similarly for both the Hermitian ( $g = 0$ ) and non-Hermitian ( $g = 0.1$ ) cases for short time ( $t \lesssim 4$ ) if disorder is weak ( $h = 2$ ). In the longer time ( $t \gtrsim 10$ ), however,  $S(t)$  behaves differently: while  $S(t)$  saturates for  $g = 0$ , it gradually decays for  $g = 0.1$ . This decrease again demonstrates that this non-Hermitian model is unstable for weak disorder. For the strong-disorder case ( $h = 14$ ),  $S(t)$  shows a logarithmic growth for a long time, in a manner similar to the Hermitian case [302, 162], which again demonstrates that the system becomes dynamically stable despite its non-Hermiticity for strong disorder.

Finally, Fig. 5.4(c) show the dynamics of the local density of particles,

$$m(t) = \overline{\langle \psi(t) | \hat{n}_1 | \psi(t) \rangle}. \quad (5.12)$$

For the weak disorder ( $h = 2$ ),  $m(t)$  saturates for  $g = 0$  and decreases for a long time for  $g = 0.1$ . For the strong disorder ( $h = 14$ ),  $m(t)$  shows similar behavior for  $g = 0$  and  $g = 0.1$ .

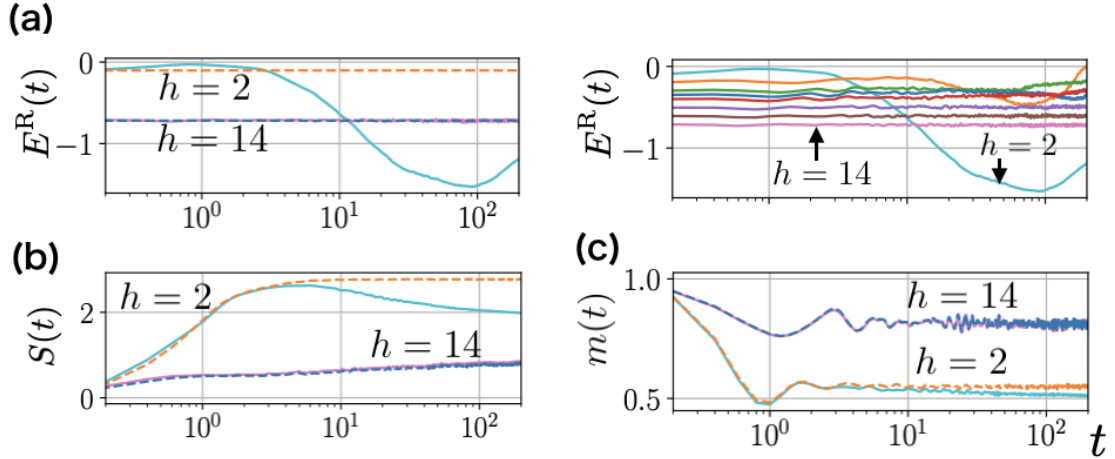


Figure 5.4: (a) (left) Dynamics of the real part of the energy  $E^R(t)$  in Eq. (5.10) for different non-Hermitian strength  $g$  (dashed lines are for  $g = 0$  and solid lines are for  $g = 0.1$ ). (right) Time evolution of  $E^R(t)$  for  $h = 2, 4, 6, 7, 8, 10, 12$ , and  $14$  for  $g = 0.1$ . (b) Dynamics of the half-chain entanglement entropy  $S(t)$  in Eq. (5.11). (c) Dynamics of the local particle density  $m(t)$  in Eq. (5.12). For the weak disorder  $h = 2$ ,  $m(t)$  saturates for  $g = 0$  but keeps decreasing for  $g = 0.1$  in the long time. All the data show the results that are averaged over  $N_{\text{sam}} = 100$  samples for  $L = 12$ .

Whereas the non-Hermitian time evolution and the Hermitian one are different, our results imply that the dynamics as well as stationary states are distinct in the two phases. These results provide a first step toward understanding thermalization of such open quantum systems with disorder. For instance, recurrence phenomena do not occur in the complex-eigenvalue phase but it can occur in the real-eigenvalue phase.

## 5.4 Non-Hermitian many-body localization

We have discussed the real-complex transition so far. We next discuss yet another transition, namely, the MBL transition in our system. Though it is nontrivial how we can characterize MBL with non-Hermiticity, we will demonstrate that some of the known method for characterizing MBL in Hermitian systems can be extended to the non-Hermitian systems.

Firstly, we consider the level-spacing distribution of energy eigenvalues. Since eigenvalues become complex for small  $h$ , we need to consider the level-spacing distributions on the complex plane in that case. We use the spacings on the real axis for large  $h$ . Here, a level spacing for an energy eigenvalue  $E_\alpha$  on the complex

plane is essentially given by the minimum distance  $d_1 = \min_{\beta} |E_{\alpha} - E_{\beta}|$ . Note that we need to perform the unfolding procedure to obtain the normalized level spacing  $s$  from the bare distance  $d_1$ . To do this task, we follow Ref. [145]. We first note that a local mean density of energy eigenvalues can be estimated as

$$\bar{\rho} = \frac{n}{\pi d_n^2}, \quad (5.13)$$

where  $n$  is sufficiently larger than unity (but not too large) and  $d_n$  is the distance of the  $n$ th nearest neighbor from  $E_{\alpha}$ . Then,  $s$  is defined as [145]

$$s = d_1 \sqrt{\bar{\rho}}, \quad (5.14)$$

with which the dependence of local density of eigenvalues vanishes.

In Fig. 5.5(a), we show level-spacing distributions for different disorder strength. When disorder is weak, the distribution obeys the Ginibre distribution, which is the Gaussian random matrix ensemble for non-Hermitian matrices [145, 303] (see Chapter 6 for details). Concretely, the level-spacing distribution is given by [304, 145, 296]

$$P_{\text{Gin}}^{\text{C}}(s) = cp(cs), \quad (5.15)$$

where

$$p(s) = \lim_{N \rightarrow \infty} \left[ \prod_{n=1}^{N-1} e_n(s^2) e^{-s^2} \right] \sum_{n=1}^{N-1} \frac{2s^{2n+1}}{n! e_n(s^2)} \quad (5.16)$$

with

$$e_n(x) = \sum_{m=0}^n \frac{x^m}{m!} \quad (5.17)$$

and

$$c = \int_0^{\infty} ds s p(s) = 1.1429 \dots, \quad (5.18)$$

rather than a Poisson statistics

$$P_{\text{Po}}^{\text{C}}(s) = \frac{\pi s}{2} e^{-\frac{\pi}{4}s^2}, \quad (5.19)$$

on the complex plane. This result shows a non-Hermitian extension of the Bohigas-Giannoni-Schmit conjecture [145, 119, 57], which states that level-spacing distributions of chaotic systems obey the Wigner-Dyson distribution in Hermitian systems. We also find that, for large disorder strength, the level-spacing distribution

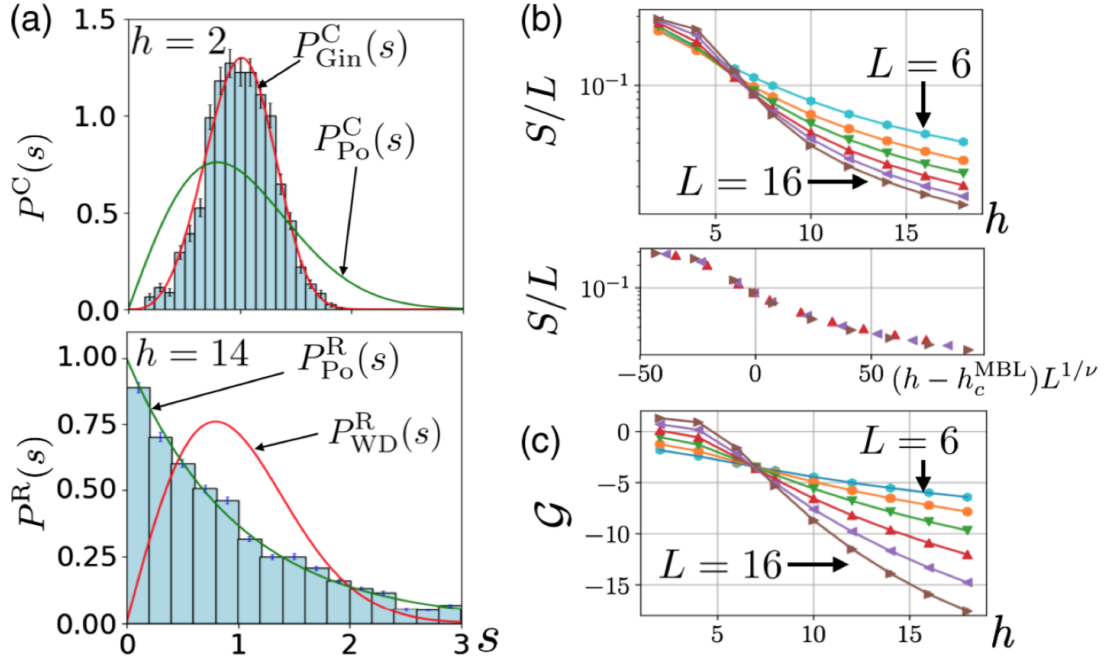


Figure 5.5: (a) Level-spacing distribution  $P(s)$  of energy eigenvalues on the complex plane ( $h = 2$ ) and that of energy eigenvalues on the real axis ( $h = 14$ ), where the system size is  $L = 16$ . We take statistics from energy eigenvalues that lie within  $\pm 10\%$  in the middle of the spectrum with respect to real and imaginary parts. (b) (top) Half-chain entanglement entropy  $S/L$  calculated from the average of  $S_\alpha/L$  over disorder and eigenstates whose energy eigenvalues are within  $\pm 2\%$  from the middle of the real part of the spectrum. (bottom) Scaling collapse as a function of  $(h - h_c^{\text{MBL}})L^{1/\nu}$ , where  $h_c^{\text{MBL}} = 7.1$  and  $\nu = 1.3$  are used. (c) Eigenstate stability  $\mathcal{G}$  for different system sizes, where  $\hat{V}_{\text{NH}} = \hat{b}_i^\dagger \hat{b}_{i+1}$ . Reproduced from Fig. 3 of Ref. [111]. ©2019 American Physical Society.

on the real axis obeys the Poisson distribution

$$P_{\text{Po}}^{\text{R}}(s) = e^{-s}, \quad (5.20)$$

rather than the Wigner-Dyson statistics

$$P_{\text{WD}}^{\text{R}}(s) = \frac{\pi s}{2} e^{-\frac{\pi}{4}s^2}. \quad (5.21)$$

We next investigate half-chain entanglement entropy of  $|E_\alpha^{\text{R}}\rangle$ ,

$$S_\alpha = \text{Tr}_{L/2}[|E_\alpha^{\text{R}}\rangle \langle E_\alpha^{\text{R}}|], \quad (5.22)$$

which is calculated from a right eigenstate. Note that we obtain similar results for left eigenstates. Here, we have a normalization condition that  $\langle E_\alpha^{\text{R}} | E_\alpha^{\text{R}} \rangle = 1$ . In Fig. 5.5(b), we illustrate the dependence on  $L$  of  $S_\alpha/L$  that is averaged over

the eigenstates in the middle of the spectrum, which is denoted by  $S/L$ . We can confirm that  $S$  shows a crossover from the volume law to the area law for  $h \simeq h_c^{\text{MBL}} \simeq 7.1$ . We also find the scaling collapse around the critical point by rewriting the entropy as a function of  $(h - h_c^{\text{MBL}})L^{1/\nu}$ , where we find  $\nu = 1.3$ . From these results, we can distinguish the delocalized and MBL phases by  $S(t)$  even in non-Hermitian systems, as in the Hermitian case [159, 173]. If the system is delocalized, eigenstates of non-Hermitian systems are predicted by those of non-Hermitian random matrices, which are expected to satisfy the volume law just as the Hermitian counterpart. If the system is localized, eigenstates are determined by quasilocal conserved quantities even for non-Hermitian systems and the area law holds. It is a future problem to investigate how the universality class of this transition changes from the Hermitian counterpart.

## 5.5 Relation between two transition points

Finally, we discuss the stability of eigenstates against small perturbations in delocalized and localized phases, which elucidate why the complex energy eigenvalues are suppressed in the localized system with TRS.

To discuss this in a general setup, we consider a decomposition of a Hamiltonian into an unperturbed part and a non-Hermitian perturbation as

$$\hat{H} = \hat{H}_0 + \hat{V}_{\text{NH}}. \quad (5.23)$$

Here,  $\hat{H}_0$  may also be non-Hermitian. Let us consider a set of real eigenvalues  $\{\mathcal{E}_a\}$  of  $\hat{H}_0$ , where the right and left eigenstates can be written as  $|\mathcal{E}_a^R\rangle$  and  $|\mathcal{E}_a^L\rangle$ , respectively. Note that they satisfy the biorthonormality,  $\langle \mathcal{E}_a^L | \mathcal{E}_b^R \rangle = \delta_{ab}$  [305].

We now add the perturbation  $\hat{V}_{\text{NH}}$ . The first-order energy deviation is given by

$$\langle \mathcal{E}_a^L | \hat{V}_{\text{NH}} | \mathcal{E}_a^R \rangle, \quad (5.24)$$

which is, in general, complex. On the other hand, if the system respects TRS, it becomes real because

$$\begin{aligned} \langle \mathcal{E}_a^L | \hat{V}_{\text{NH}} | \mathcal{E}_a^R \rangle &= (|\mathcal{E}_a^L\rangle, \hat{V}_{\text{NH}} |\mathcal{E}_a^R\rangle) \\ &= (\hat{T} |\mathcal{E}_a^L\rangle, \hat{T} \hat{V}_{\text{NH}} |\mathcal{E}_a^R\rangle)^* \\ &= (|\mathcal{E}_a^L\rangle, \hat{V}_{\text{NH}} |\mathcal{E}_a^R\rangle)^* \\ &= \langle \mathcal{E}_a^L | \hat{V}_{\text{NH}} | \mathcal{E}_a^R \rangle^*, \end{aligned} \quad (5.25)$$

where we have used  $[\hat{H}_0, \hat{T}] = [\hat{V}_{\text{NH}}, \hat{T}] = 0$  and  $\hat{T} |\mathcal{E}_a^{R/L}\rangle = |\mathcal{E}_a^{R/L}\rangle$ . This means that energy eigenvalues of systems with TRS cannot be complex at the level of the first-order energy deviation, i.e., if we do not consider the mixing with other eigenstates.

Even with TRS, however, eigenvalues can be complex owing to coalescence of two eigenvalues for sufficiently large  $\hat{V}_{\text{NH}}$ , as reviewed in Chapter 4. This coalescence results from the mixing of two eigenstates, which are relevant for higher-order perturbations. To evaluate the perturbation of energy eigenstates, we write the Hamiltonian as

$$\hat{H} = \hat{H}_0 + \hat{V}_{\text{NH}} = \sum_a (\mathcal{E}_a + \Delta E_a^{(0)}) |\mathcal{E}_a^R\rangle \langle \mathcal{E}_a^L| + \hat{V}_{\text{NH}} - \sum_a \Delta E_a^{(0)} |\mathcal{E}_a^R\rangle \langle \mathcal{E}_a^L| \quad (5.26)$$

with  $\Delta E_a^{(0)} = \langle \mathcal{E}_a^L | \hat{V}_{\text{NH}} | \mathcal{E}_a^R \rangle$ . Let us consider the second and third terms on the right-hand side as a perturbation. We then obtain the following perturbed eigenstate:

$$|\mathcal{E}_{a,\text{perturbed}}^R\rangle = |\mathcal{E}_a^R\rangle + \sum_{b(\neq a)} \frac{\langle \mathcal{E}_b^L | \hat{V}_{\text{NH}} | \mathcal{E}_a^R \rangle}{\mathcal{E}'_b - \mathcal{E}'_a} |\mathcal{E}_b^R\rangle. \quad (5.27)$$

Here, we have used the normalization conditions  $\langle \mathcal{E}_a^L | \mathcal{E}_b^R \rangle = \delta_{ab}$  and  $\langle \mathcal{E}_a^R | \mathcal{E}_a^R \rangle = 1$  (note that  $\langle \mathcal{E}_a^L | \mathcal{E}_a^L \rangle \neq 1$ ). For the perturbation series to converge, the magnitude of the second term should be small enough. We particularly take  $b = a + 1$  and define its logarithm to discuss the localization transition, which leads to

$$\mathcal{G} = \ln \frac{|\langle \mathcal{E}_{a+1}^L | \hat{V}_{\text{NH}} | \mathcal{E}_a^R \rangle|}{|\mathcal{E}'_{a+1} - \mathcal{E}'_a|}. \quad (5.28)$$

Note that this is a generalized stability measure for the Hermitian counterpart of Ref. [185], which has been discussed in Chapter 2. If  $\mathcal{G}$  is large enough, it is expected that eigenvalues coalesce and that many complex eigenvalues appear. Note that an exception to this expectation is realized by assuming the Hamiltonian which can be written as  $\hat{H} = \hat{\mathcal{V}}^{-1} \hat{H}_{\text{H}} \hat{\mathcal{V}}$ , where  $\hat{H}_{\text{H}}$  is Hermitian and  $\hat{\mathcal{V}}$  is a non-unitary invertible operator, since  $\hat{H}$  and  $\hat{H}_{\text{H}}$  have the same eigenvalues, as shown in Appendix A. Nevertheless, our discussion is applicable to generic non-Hermitian systems without this structure. Indeed, our discussion is consistent with numerics for the Lindblad operators [306, 264, 261, 244, 307], which are mapped to non-Hermitian matrices.

Just as in the Hermitian situation [185], we find that the stability measure in Eq. (5.28) becomes small only when the system is in an MBL phase. In Fig. 5.5(c),

we show the dependence of  $\mathcal{G}$  on  $h$ . It is found that  $\mathcal{G} \sim \alpha L$  ( $\alpha > 0$ ) and  $\mathcal{G} \sim -\beta L$  ( $\beta > 0$ ) for the delocalized and localized phases, respectively. This is similar to the case for the Hermitian counterpart [185]. The non-Hermitian MBL transition point is evaluated as  $h_c^{\text{MBL}} \simeq 7 \pm 1$  from the point where  $\mathcal{G}$  becomes independent of  $L$ .

We conjecture that the points of the real-complex transition  $h_c^{\text{R}}$  and the MBL transition  $h_c^{\text{MBL}}$  coincide in the thermodynamic limit. In fact, from the discussions for the stability of eigenstates above, the process through which two adjacent eigenstates coalesce is suppressed by the MBL. Moreover, we can argue that the coalescence is suppressed even for non-adjacent eigenstates and thus the entire spectra become real in our asymmetric hopping model (see Appendix A). We note that the two transition points are close ( $h_c^{\text{R}} \simeq 8 \pm 1$  and  $h_c^{\text{MBL}} \simeq 7 \pm 1$  for  $g = 0.1$ ) to each other but slightly different in our numerical calculations up to  $L = 16$ . From the analytical arguments of the stability above, we suppose that this small deviation is a consequence of a finite-system size.

Finally, we make two remarks concerning the above discussion. First, the discussion is expected to apply for the Hatano-Nelson model;  $\mathcal{G}$  can be the signature of the localization transition and this transition leads to the suppression of coalescence of eigenvalues and thus the real-complex transition for a single-particle level. Second, as mentioned in Chapter 2, there can be higher-order perturbation effects that alters the nature of the localization [180], which we have neglected for simplifying the discussion.

## 5.6 A gain-and-loss model

We have considered the system with TRS. Finally, we discuss that the real-complex transition does not occur while the non-Hermitian MBL still occurs if we break TRS. We consider the following model with gain and loss, which becomes feasible in state-of-the-art experiments [308, 98]:

$$\hat{H} = \sum_{i=1}^L -J(\hat{b}_{i+1}^\dagger \hat{b}_i + \text{H.c.}) + U\hat{n}_i\hat{n}_{i+1} + (h_i - i\gamma(-1)^i)\hat{n}_i. \quad (5.29)$$

This model does not possess TRS because of the gain and loss terms at odd and even sites, respectively, which tend to decrease and increase the number of particles at these sites. In Fig. 5.6(a), we show the spectra of this model for different values of  $h$ , which indicates that all energy eigenvalues are complex for any  $h$  and

$L$ , i.e.,  $f_{\text{Im}} = 1$  for all cases. Thus, it is expected that the system is always unstable in that it drastically changes its energy.

Despite the absence of the real-complex phase transition, the non-Hermitian MBL still occurs. In Fig. 5.6(b), we show the level-spacing distributions on the complex plane for different disorder strength  $h$ . When  $h \lesssim h_c^{\text{MBL}}$  ( $h_c^{\text{MBL}} \gtrsim 4$ ), the distribution obeys non-Hermitian random matrix theory with transposition symmetry, which is distinct from  $P_{\text{Gin}}^{\text{C}}(s)$  as will be discussed in Chapter 6. When  $h \gtrsim h_c^{\text{MBL}}$ , it is a Poisson distribution in the complex plane,  $P_{\text{Po}}^{\text{C}}(s)$  (note that this distribution coincides with the Wigner-Dyson distribution for Hermitian matrices). This transition implies the presence of the non-Hermitian MBL. We also find that the half-chain entanglement entropy exhibits a transition from the volume to the area law around  $h \sim h_c^{\text{MBL}} = 4.2$  (see Fig. 5.6(c)), with the scaling collapse as a function of  $(h - h_c^{\text{MBL}})L^{1/\nu}$ , where we find  $\nu = 1.8$ . It is a future problem to investigate whether the universality class for this transition in the gain-and-loss model is different from that in the asymmetric hopping model.

## 5.7 Discussions

We have demonstrated that MBL which is extended to non-Hermitian systems suppresses the imaginary part of energy eigenvalues for generic non-Hermitian interacting Hamiltonians with TRS. Using the system with asymmetric hopping, we have shown that a novel real-complex transition occurs and changes the dynamical stability of the system. In addition, non-Hermitian MBL has been shown to be characterized by the level-spacing distributions and entanglement entropy as in the Hermitian case. The discussion on stability of eigenstates allows us to argue that two transition points coincide in the thermodynamic limit. We have also provided numerical evidence for the absence of real-complex transitions for models with gain and/or loss without TRS, although the non-Hermitian MBL occurs.

The real-complex transition discussed in this chapter is conceptually novel since it cannot occur in closed, clean, or few-body systems. As a related fact, there is a transition in the dynamical stability, where the important notion of Hermitian thermalization such as recurrence can be discussed even in non-Hermitian systems (which are relevant for continuously measured quantum systems). Moreover, there are many other features of the non-Hermitian MBL represented by the critical phenomena, which are indicated by our critical scaling collapse and may

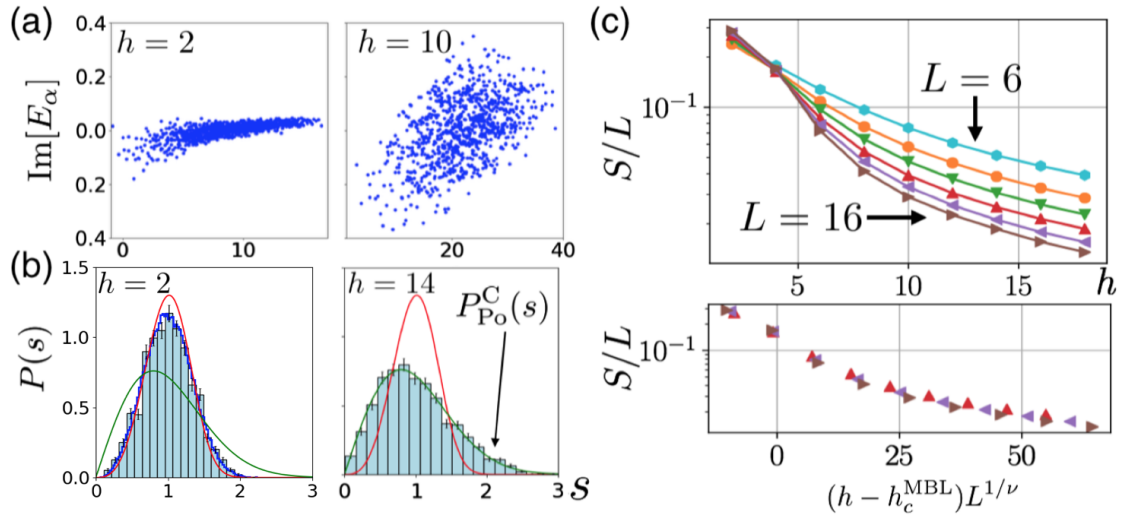


Figure 5.6: (a) Energy eigenvalues of the non-Hermitian Hamiltonian without TRS in Eq. (5.29) for  $\gamma = 0.1$ . (b) Level-spacing distributions on the complex plane for energy eigenvalues. We take the statistics from the eigenstates whose eigenvalues are within  $\pm 10\%$  from the middle of the spectrum (single-disorder realization with  $L = 16$ ). (c) (top) Dependence on  $h$  of  $S/L$  averaged over the eigenstates from the middle of the real part of the spectrum for different system sizes  $L$  and  $\gamma = 0.1$ . (bottom) The scaling collapse of  $S/L$  as a function of  $(h - h_c^{\text{MBL}})L^{1/\nu}$  around the critical point, where we use  $h_c^{\text{MBL}} = 4.2$  and  $\nu = 1.8$ . Reproduced from Fig. 4 of Ref. [111]. ©2019 American Physical Society with a slight modification.

differ from the conventional Hermitian transitions. Our results are also related to quantum chaos [119, 247, 141] in open systems described by non-Hermitian interacting Hamiltonians, as implied by its random-matrix-type level-spacing distributions.

# Chapter 6

## The threefold way in non-Hermitian random matrices

### 6.1 Motivation

As we have seen in the previous chapter, delocalized phases of the non-Hermitian many-body systems are characterized by universality of non-Hermitian random matrices. Furthermore, universality of non-Hermitian random matrices is known to appear in various systems including mesoscopic systems [303], dissipative systems [247, 248, 249], and neural networks [251].

As fundamental ensembles of non-Hermitian random matrices, Ginibre introduced three different ensembles based on time-reversal symmetry (TRS), which are called GinUE, GinOE, and GinSE [309]. This is a natural generalization of Dyson's threefold way in Hermitian random matrices, where three ensembles distinguished by TRS are called GUE, GOE, and GSE (see Chapter 2).

On the other hand, the three symmetry classification by Ginibre does not lead to three distinct universality classes for local correlations. In fact, all of Ginibre's three symmetry classes lead to the same universality class for level-spacing distributions on the complex plane, in contrast with Dyson's three symmetry classes, for which three different symmetry classes appear. Given the diverse applications of universality of random matrices, it is fundamentally important to study whether other universality classes exist for non-Hermitian random matrices if we consider symmetries which are different from TRS. Note that symmetry classification is determined only from algebraic structures of matrices, but that universality classification is determined from statistics of the spectra that do not depend on the detailed structure of matrices.

In this chapter, we show that three different universality classes, namely Ginibre's class and the other two new classes, appear by considering transposition symmetry, which is distinct from the complex conjugation symmetry (TRS) for non-Hermitian matrices. We first review previous results on non-Hermitian random matrices and its symmetry classification (characterized by non-Hermitian extension of the Altland-Zirnbauer symmetry classes [310]) in the following two sections. We then demonstrate our main numerical results of new universality classes of level-spacing distributions for non-Hermitian random matrices with transposition symmetry. We discuss that transposition symmetry affects interactions between two close eigenvalues and changes level-spacing distributions, while the other symmetries including TRS can only affect correlations of nonlocal eigenvalues (see Fig. 6.1), which is supported by the analysis of small matrices. It is also shown that the new universality classes that we find manifest themselves in dissipative quantum nonintegrable systems described by Lindblad many-body equations and non-Hermitian many-body Hamiltonians.

## 6.2 Review on Ginibre's symmetry classes

### 6.2.1 Definition

We first review Ginibre's three non-Hermitian random-matrix symmetry classes with TRS, called the classes A, AI, and AII.

#### Class A

Let us first consider a symmetry class of non-Hermitian matrices without any symmetry constraint, which is called the class A. By dropping the Hermiticity condition for GOE by Dyson, whose probability distribution can be written as

$$P(\hat{H}) d\hat{H} \propto e^{-\beta \text{Tr}[\hat{H}^2]} d\hat{H} \propto \exp \left[ -\beta \sum_i H_{ii}^2 - 2\beta \sum_{i>j} |H_{ij}|^2 \right] \prod_i dH_{ii} \prod_{i>j} dH_{ij} dH_{ij}^*, \quad (6.1)$$

Ginibre introduced GinOE characterized by

$$P(\hat{H}) d\hat{H} \propto e^{-\beta \text{Tr}[\hat{H}^\dagger \hat{H}]} d\hat{H} \propto \exp \left[ -\beta \sum_{i,j} |H_{ij}|^2 \right] \prod_{i,j} dH_{ij} dH_{ij}^*. \quad (6.2)$$

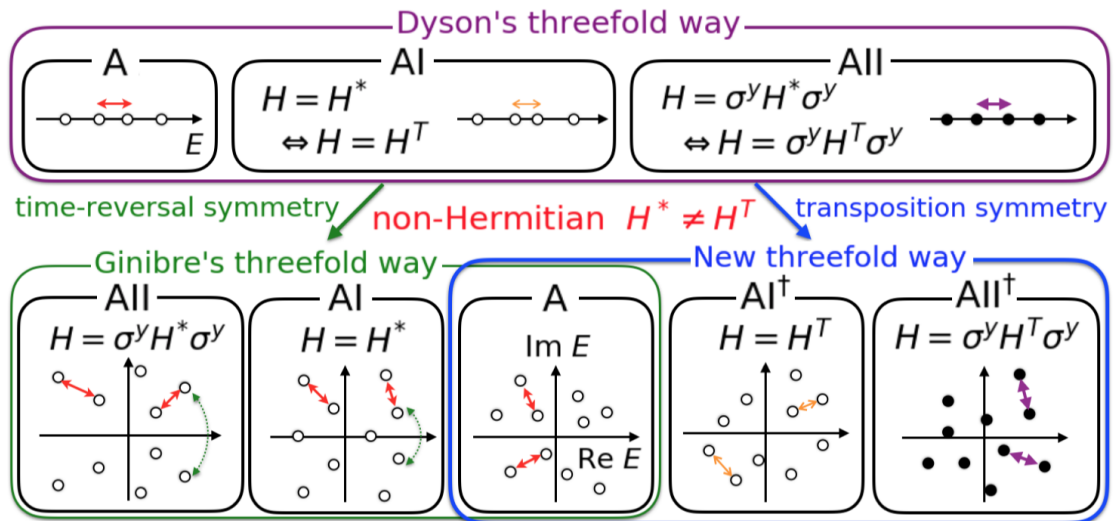


Figure 6.1: Dyson's threefold way with respect to time-reversal symmetry (TRS) and its two different kinds of non-Hermitian extensions. Open circles denote individual eigenvalues and filled circles indicate Kramers pairs of eigenvalues. In Dyson's three classes, repulsive interactions between neighboring eigenvalues are different from one another. However, the difference does not appear when we consider Ginibre's threefold way of non-Hermitian matrices. This is because TRS only influences the global symmetry of eigenvalues (green arrows). On the other hand, transposition symmetry ( $\text{TRS}^\dagger$ ) is different from TRS because of the absence of Hermiticity and results in another threefold universality. In this case, the interaction between neighboring eigenvalues becomes weaker for the class  $\text{AI}^\dagger$  and stronger for  $\text{AII}^\dagger$  than that for the class A, as indicated by the arrows with different colors. Taken from Fig. 1 in the fourth version of Ref. [112].

Note that we can consider other probability distributions in the class A. For example, for a non-Hermitian Bernoulli ensemble, matrix elements are randomly chosen from

$$H_{ij} = \begin{cases} 1 + i; \\ 1 - i; \\ -1 + i; \\ -1 - i \end{cases} \quad (6.3)$$

with equal probabilities.

### Class AI

For the class AI, there exists a TRS  $\hat{T} = \hat{\mathcal{T}}_+ \hat{K}$  that satisfies  $\hat{T}^2 = +\hat{\mathbb{1}}$  and  $[\hat{T}, \hat{H}] = 0$ . In other words, there exists a unitary operator  $\hat{\mathcal{T}}_+$  that satisfies

$$\hat{\mathcal{T}}_+ \hat{H}^* \hat{\mathcal{T}}_+^{-1} = \hat{H}, \quad \hat{\mathcal{T}}_+^* \hat{\mathcal{T}}_+ = +\hat{\mathbb{1}}. \quad (6.4)$$

As we have seen in the previous chapters, this symmetry leads to eigenvalues that are either real or form complex-conjugate pairs.

We can assume that  $\hat{\mathcal{T}}_+$  is an identity operator without loss of generality, from which we obtain the condition for real matrices

$$H_{ij} = H_{ij}^*, \quad (6.5)$$

if we consider Gaussian ensembles. In fact, from Eq. (6.4) we can prove that  $\hat{U}^{-1} \hat{H} \hat{U}$  is real for a unitary operator  $\hat{U} = \sqrt{\hat{\mathcal{T}}_+}$ . Since Gaussian ensembles  $P(\hat{H})$  satisfy  $P(\hat{H}) d\hat{H} = P(\hat{U}^{-1} \hat{H} \hat{U}) d(\hat{U}^{-1} \hat{H} \hat{U})$ , we can assume an ensemble of real matrices. Thus, we can study the probability distribution of Gaussian real matrices (GinOE) given by

$$P(\hat{H}) d\hat{H} \propto \exp \left[ -\beta \sum_{i,j} H_{ij}^2 \right] \prod_{i,j} dH_{ij}. \quad (6.6)$$

Though a Bernoulli ensemble explicitly depends on  $\hat{\mathcal{T}}_+$ , we consider  $\hat{\mathcal{T}}_+ = \hat{\mathbb{1}}$  in the following discussions. Then, the matrix elements are randomly chosen as

$$H_{ij} = \begin{cases} 1; \\ -1 \end{cases} \quad (6.7)$$

with equal probabilities.

Here, we note the relation between the class AI and another class called D<sup>†</sup> in

Ref. [246]. Matrices in class  $D^\dagger$  satisfy the condition

$$\hat{\mathcal{T}}_- \hat{H}^* \hat{\mathcal{T}}_-^{-1} = -H, \quad \hat{\mathcal{T}}_- \hat{\mathcal{T}}_-^* = \hat{\mathbb{I}}, \quad (6.8)$$

where  $\hat{\mathcal{T}}_-$  is called a conjugate of particle-hole symmetry (PHS<sup>†</sup>) [246]. Importantly, the symmetry the classes AI and  $D^\dagger$  are in one-to-one correspondence [245] in the following sense: if  $H$  belongs to the class AI, another matrix  $iH$  belongs to class  $D^\dagger$ . In particular, the level-spacing distributions for both of these classes are identical, considering the rotation of the spectrum by the angle  $\pi/2$  in the complex plane.

### Class AII

For the class AII, matrices have TRS given as

$$\hat{\mathcal{T}}_+ \hat{H}^* \hat{\mathcal{T}}_+^{-1} = \hat{H}, \quad \hat{\mathcal{T}}_+^* \hat{\mathcal{T}}_+ = -\hat{\mathbb{I}}. \quad (6.9)$$

In a manner similar to the class AI, eigenvalues form complex-conjugate pairs  $(E_\alpha, E_\alpha^*)$ . In contrast with the class AII in the Hermitian case, the two-fold degenerate Kramers pairs appear only for eigenvalues that stay real for the class AII in the non-Hermitian case. Furthermore, Kramers pairs on the real axis are absent for typical random matrices in the non-Hermitian the class AII owing to the level repulsions of eigenvalues that occur for generic matrices.

We can choose  $\hat{\mathcal{T}}_+$  as the Pauli matrix  $\hat{\sigma}^y$  just as in the case for the class AI for Gaussian ensembles. We obtain

$$\hat{H} = \hat{\mathbb{I}}_{2 \times 2} \otimes \hat{a} + i\hat{\sigma}^x \otimes \hat{b} + i\hat{\sigma}^y \otimes \hat{c} + i\hat{\sigma}^z \otimes \hat{d}, \quad (6.10)$$

where  $\hat{a}$ ,  $\hat{b}$ ,  $\hat{c}$ , and  $\hat{d}$  denote non-Hermitian matrices whose elements are real. The Gaussian probability distribution is then given by

$$P(\hat{H}) d\hat{H} \propto \exp \left[ -\beta \sum_{i,j} \left( a_{ij}^2 + b_{ij}^2 + c_{ij}^2 + d_{ij}^2 \right) \right] \prod_{i,j} da_{ij} db_{ij} dc_{ij} dd_{ij}. \quad (6.11)$$

In contrast, for a Bernoulli ensemble, matrix elements are randomly chosen as

$$a_{ij}, b_{ij}, c_{ij}, d_{ij} = \begin{cases} 1; \\ -1 \end{cases} \quad (6.12)$$

with equal probabilities.

We note the equivalence between the class AII and class  $C^\dagger$ , the latter of which

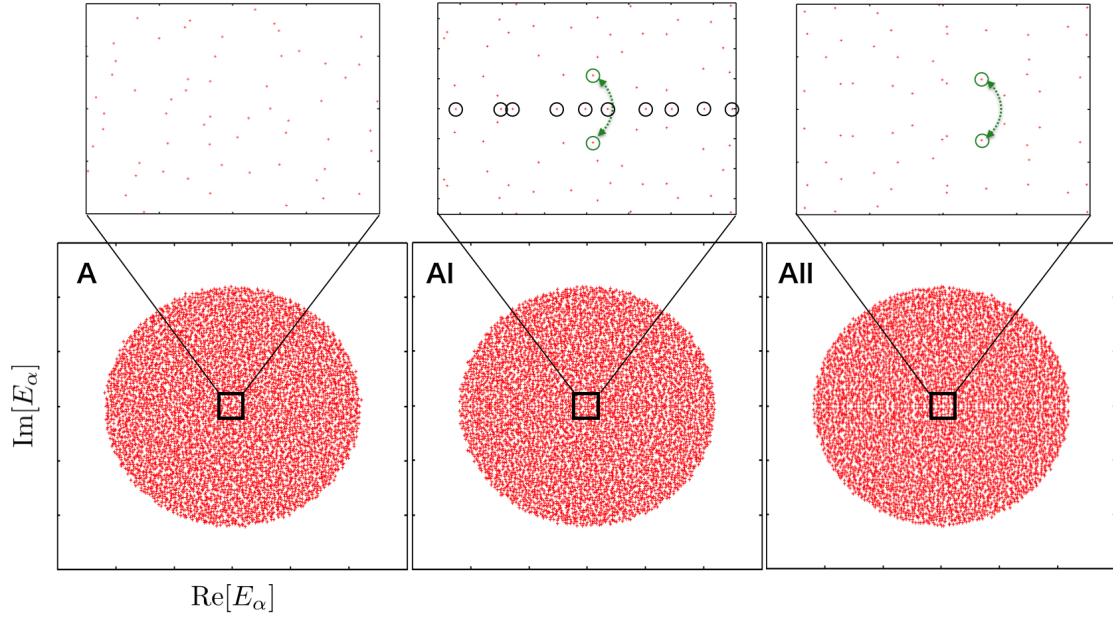


Figure 6.2: Eigenvalue plots for non-Hermitian Gaussian random matrices in the classes A, AI, and AII. In the enlarged figures, we can see that real eigenvalues exist for the class AI, and complex-conjugate pairs appear for the classes AI and AII.

respects PHS<sup>†</sup>,

$$\hat{\mathcal{T}}_- \hat{H}^* \hat{\mathcal{T}}_-^{-1} = -\hat{H}, \quad \hat{\mathcal{T}}_- \hat{\mathcal{T}}_-^* = -\hat{\mathbb{I}}, \quad (6.13)$$

in the sense discussed previously for the classes AI and D<sup>†</sup>, that is, the level-spacing distributions for both of these classes are the same, considering the rotation of the spectrum by the angle  $\pi/2$  in the complex plane.

## 6.2.2 Spectral properties

The properties of Ginibre's ensembles have thoroughly been investigated [311, 312, 313, 314, 315, 316]. For example, the density of states in each of the three ensembles is well described by the circular law, where eigenvalues spread uniformly within a circle with a radius proportional to  $\sqrt{N}$ , where  $N$  is the matrix size (see Fig. 6.2).

As an important property, let us consider the joint probability distribution of eigenvalues for GinUE, which is known as

$$P_{\text{jpdf, GinUE}}(E_1, \dots, E_N) d^2 E_1 \cdots d^2 E_N \propto e^{-\sum_{j=1}^N |E_j|^2} \prod_{1 \leq i < j \leq N} |E_i - E_j|^2 d^2 E_1 \cdots d^2 E_N. \quad (6.14)$$

The factor  $|E_i - E_j|^2$  represents a cubic level-repulsion factor between eigenvalues (note the extra factor which comes from  $d^2E_i d^2E_j$ ), which is reflected in the level-spacing distribution. In fact, the level-spacing distribution, which is given by Eq. (5.15), is derived from this joint distribution.

Next, the joint probability distribution for GinOE is given by [311]

$$P_{\text{jpdf, GinOE}}(E_1, \dots, E_N) \propto \sqrt{\prod_{j=1}^N \operatorname{erfc}\left(\frac{|E_j - E_j^*|}{\sqrt{2}}\right) e^{-\frac{E_j^2 + E_j^{*2}}{2}}} \prod_{1 \leq i < j \leq N} (E_i - E_j), \quad (6.15)$$

where

$$\operatorname{erfc}(x) = \frac{2}{\sqrt{\pi}} \int_x^\infty e^{-t^2} dt. \quad (6.16)$$

For eigenvalues that are real or almost real, the distribution qualitatively differs from that for GinUE. On the other hand, eigenvalues in the bulk of the spectrum (i.e., far away from the real axis) behave similarly compared with GinUE. For example, if we focus on the eigenvalues  $E_1$  and  $E_2$ , both of which are assumed to be in the bulk of the upper circle, we find a level-repulsion factor  $|E_1 - E_2|^2$  as in GinUE. In addition, we obtain the coefficient  $e^{-|E_1|^2 - |E_2|^2}$  as in GinUE by using  $\operatorname{erfc}(x) \rightarrow \frac{e^{-x^2}}{x\sqrt{\pi}}$  for large  $x$ .

More intuitively, TRS creates global correlations between eigenvalues that are complex conjugate with each other, but they do not affect local correlations of eigenvalues away from the real axis. A similar discussion can be made for GinSE. Then, in particular, the level-spacing distributions (in the bulk of the spectrum) for Ginibre's three classes are argued to be the same [145], in contrast with the Hermitian case.

## 6.3 Review on non-Hermitian symmetry classes

### 6.3.1 Overview

As we have seen in the previous section, Ginibre's three classes A, AI, AII classified by TRS do not lead to distinct universality classes of the level-spacing distribution. On the other hand, it has recently been recognized that symmetries are enriched in non-Hermitian matrices [317, 318, 246]. As a prime example, we first note that  $\hat{H}^* \neq \hat{H}^T$  for non-Hermitian matrices. Then, instead of TRS in Eq. (6.4), we can

Table 6.1: Symmetry classes, constraints (where the corresponding unitary operators are taken as the simplest ones), and level-spacing distributions. The sign (plus or minus) indicates whether the symmetry operator squared is  $+\hat{\mathbb{I}}$  or  $-\hat{\mathbb{I}}$ . Only the classes  $\text{AI}^\dagger$  and  $\text{AII}^\dagger$  exhibit the distributions distinct from that of  $\text{GinUE}$ .

Class	Symmetry	Constraint	$p_{\text{GinUE}}(s)$ ?
A	None	-	Yes [309]
$\text{AI} (\text{D}^\dagger)$	$\text{TRS}, + (\text{PHS}^\dagger, +)$	$\hat{H} = \hat{H}^*$	Yes [248]
$\text{AII} (\text{C}^\dagger)$	$\text{TRS}, - (\text{PHS}^\dagger, -)$	$\hat{H} = \hat{\sigma}^y \hat{H}^* \hat{\sigma}^y$	Yes [309]
$\text{AI}^\dagger$	$\text{TRS}^\dagger, +$	$\hat{H} = \hat{H}^T$	<b>No</b>
$\text{AII}^\dagger$	$\text{TRS}^\dagger, -$	$\hat{H} = \hat{\sigma}^y \hat{H}^T \hat{\sigma}^y$	<b>No</b>
D	$\text{PHS}, +$	$\hat{H} = -\hat{H}^T$	Yes
C	$\text{PHS}, -$	$\hat{H} = -\hat{\sigma}^y \hat{H}^T \hat{\sigma}^y$	Yes
AIII	CS (pH)	$\hat{H} = -\hat{\sigma}^z \hat{H}^\dagger \hat{\sigma}^z$	Yes
AIII $^\dagger$	SLS (CS $^\dagger$ )	$\hat{H} = -\hat{\sigma}^z \hat{H} \hat{\sigma}^z$	Yes

consider complex-conjugate TRS ( $\text{TRS}^\dagger$ ) defined by transposition as follows:

$$\hat{C}_+ \hat{H}^T \hat{C}_+^{-1} = \hat{H}, \quad \hat{C}_+^* \hat{C}_+ = +\hat{\mathbb{I}}, \quad (6.17)$$

which is called the class  $\text{AI}^\dagger$ .

In general, we can consider a non-Hermitian extension of the Altland-Zirnbauer (AZ) tenfold symmetry classes for Hermitian matrices [310]. Within Hermitian AZ classes, five symmetry classes (AIII, AI, D, AII, and C) possess only one symmetry, i.e., TRS, particle-hole symmetry (PHS), or chiral symmetry (CS). By considering the above ramification for non-Hermitian matrices, we obtain another set of five classes ( $\text{AIII}^\dagger$ ,  $\text{AI}^\dagger$ ,  $\text{D}^\dagger$ ,  $\text{AII}^\dagger$ , and  $\text{C}^\dagger$ ). On the other hand, as we have seen above, the classes AI and  $\text{D}^\dagger$  as well as the classes AII and  $\text{C}^\dagger$ , are equivalent. Thus, adding the class A, we have nine non-Hermitian symmetry classes with up to one symmetry. Note that combination of more than one symmetry leads to the other 29 classes, which defines 38 different classes [246]. In the following, we especially focus on non-Hermitian matrices for the above 9 classes. The property of the 9 classes is summarized in Table 6.1.

### 6.3.2 Detailed classification

Here, we present detailed properties of the classes  $\text{AI}^\dagger$ ,  $\text{AII}^\dagger$ , D, C, AIII, and  $\text{AIII}^\dagger$  introduced in Ref. [246]. We also introduce explicit forms of Gaussian and Bernoulli ensemble for each class, which is a part of our work.

### Class AI<sup>†</sup>

For class AI<sup>†</sup>, there exists a unitary matrix  $\hat{C}_+$  for which Eq. (6.17) is satisfied. By taking the transpose of the eigenequation for the left eigenvector

$$\langle \chi_\alpha | \hat{H} = E_\alpha \langle \chi_\alpha |, \quad (6.18)$$

we have

$$\hat{H}^T |\chi_\alpha\rangle^* = E_\alpha |\chi_\alpha\rangle^*. \quad (6.19)$$

When TRS<sup>†</sup> is present, we thereby obtain

$$\hat{H} \left( \hat{C}_+ |\chi_\alpha\rangle^* \right) = \hat{C}_+ \hat{H}^T |\chi_\alpha\rangle^* = E_\alpha \left( \hat{C}_+ |\chi_\alpha\rangle^* \right). \quad (6.20)$$

Thus,  $\hat{C}_+ |\chi_\alpha\rangle^*$  also becomes an eigenstate of  $\hat{H}$  with the same eigenvalue  $E_\alpha$  as  $|\phi_\alpha\rangle$ . Assuming no degeneracy, we obtain the constraint between right and left eigenstates as

$$\hat{C}_+ |\chi_\alpha\rangle^* \propto |\phi_\alpha\rangle. \quad (6.21)$$

Note that this constraint is imposed on all the eigenstates, which results in a new universality class of the level-spacing distribution as discussed in the next section.

We can assume without loss of generality that  $\hat{C}_+$  is the identity for the Gaussian ensemble, which leads to the condition for a symmetric matrix:

$$H_{ij} = H_{ji}. \quad (6.22)$$

The probability distribution in this case is given by

$$P(\hat{H}) d\hat{H} \propto \exp \left[ -\beta \left( \sum_i |H_{ij}|^2 + \sum_{i>j} 2|H_{ij}|^2 \right) \right] \prod_{i \geq j} dH_{ij} dH_{ij}^*. \quad (6.23)$$

For a Bernoulli ensemble, on the other hand, matrix elements are randomly chosen as

$$H_{ij} = \begin{cases} 1 + i; \\ 1 - i; \\ -1 + i; \\ -1 - i \end{cases} \quad (6.24)$$

with equal probabilities under the constraint in Eq. (6.22).

Note that the class AI<sup>†</sup> naturally appears in experiments. For example, optical systems with gain and loss are in the class AI<sup>†</sup> because gain and loss only introduce non-Hermitian imaginary terms on the diagonal matrix elements, which keeps the symmetric structure under transposition. Another example is the Rydberg

systems with dissipation, which is described by a Lindblad equation, as discussed later.

### Class AII<sup>†</sup>

In class AII<sup>†</sup>, matrices have TRS<sup>†</sup> defined as

$$\hat{C}_+ \hat{H}^T \hat{C}_+^{-1} = \hat{H}, \quad \hat{C}_+ \hat{C}_+^* = -\hat{\mathbb{I}}. \quad (6.25)$$

In this case, we can prove a non-Hermitian extension of the Kramers degeneracy theorem [319, 320]. Indeed, from  $\hat{C}_+^T \hat{C}_+^{-1} = -\hat{\mathbb{I}}$ , we obtain

$$\langle \chi_\alpha | \hat{C}_+ (|\chi_\alpha\rangle^*) = \left( \langle \chi_\alpha | \hat{C}_+ (|\chi_\alpha\rangle^*) \right)^T = \langle \chi_\alpha | \hat{C}_+^T (|\chi_\alpha\rangle^*) = -\langle \chi_\alpha | \hat{C}_+ (|\chi_\alpha\rangle^*), \quad (6.26)$$

which leads to  $\langle \chi_\alpha | \hat{C}_+ (|\chi_\alpha\rangle^*) = 0$ . Hence, the eigenvectors  $|\phi_\alpha\rangle$  and  $\hat{C}_+ |\chi_\alpha\rangle^*$  satisfy biorthogonal and linear-independent conditions. This indicates that all the eigenstates have at least two-fold degeneracy when TRS<sup>†</sup> with  $\hat{C}_+ \hat{C}_+^* = -\hat{\mathbb{I}}$  is present.

We can take  $\hat{C}_+$  as the Pauli matrix  $\hat{\sigma}^y$ , which enables us to describe the Gaussian distribution for arbitrary  $\hat{C}_+$  with  $\hat{C}_+ \hat{C}_+^* = -\hat{\mathbb{I}}$  as we have seen so far. We then have

$$\hat{H} = \begin{pmatrix} \hat{a} & \hat{b} \\ \hat{c} & \hat{d} \end{pmatrix}, \quad (6.27)$$

where  $\hat{a}$ ,  $\hat{b}$ ,  $\hat{c}$ , and  $\hat{d}$  satisfy

$$\hat{a} = \hat{d}^T, \quad \hat{b} = -\hat{b}^T, \quad \hat{c} = -\hat{c}^T. \quad (6.28)$$

Then, the probability distribution of a Gaussian ensemble is defined by

$$P(\hat{H}) d\hat{H} \propto \exp \left\{ -2\beta \left[ \sum_i |a_{ii}|^2 + \sum_{i>j} (|a_{ij}|^2 + |b_{ij}|^2 + |c_{ij}|^2 + |d_{ij}|^2) \right] \right\} \\ \times \prod_i da_{ii} da_{ii}^* \prod_{i>j} da_{ij} da_{ij}^* db_{ij} db_{ij}^* dc_{ij} dc_{ij}^* dd_{ij} dd_{ij}^*. \quad (6.29)$$

For a Bernoulli ensemble, matrix elements are randomly chosen as

$$a_{ij}, b_{ij}, c_{ij}, d_{ij} = \begin{cases} 1 + i; \\ 1 - i; \\ -1 + i; \\ -1 - i \end{cases} \quad (6.30)$$

with equal probabilities under the constraint in Eq. (6.28).

### Class D

In the class D, matrices have particle-hole symmetry (PHS) given as

$$\hat{C}_- \hat{H}^T \hat{C}_-^{-1} = -\hat{H}, \quad \hat{C}_- \hat{C}_-^* = +\hat{\mathbb{I}}, \quad (6.31)$$

with a unitary matrix  $\hat{C}_-$ .

Just as in the classes AI<sup>†</sup> and AII<sup>†</sup>, we obtain

$$\hat{H} \left( \hat{C}_- |\chi_\alpha\rangle^* \right) = -\hat{C}_- \hat{H}^T |\chi_\alpha\rangle^* = -E_\alpha \left( \hat{C}_- |\chi_\alpha\rangle^* \right). \quad (6.32)$$

Hence,  $\hat{C}_- |\chi_\alpha\rangle^*$  again becomes an eigenstate of  $\hat{H}$  with an eigenvalue  $-E_\alpha$ . Thus, eigenvalues constitute  $(E_\alpha, -E_\alpha)$  pairs. In other words, PHS creates eigenvalue-pairs  $(E_\alpha, -E_\alpha)$  but does not impose local constraints on eigenstates away from the zero eigenvalue, in analogy with TRS and PHS<sup>†</sup>.

We assume that  $\hat{C}_-$  is the identity operator without loss of generality for Gaussian ensembles. We then obtain

$$H_{ij} = -H_{ji}. \quad (6.33)$$

In other words, they can be regarded as antisymmetric matrices. Then, the probability distribution is given as

$$P(\hat{H}) d\hat{H} \propto \exp \left[ -2\beta \sum_{i>j} |H_{ij}|^2 \right] \prod_{i>j} dH_{ij} dH_{ij}^*. \quad (6.34)$$

For a Bernoulli ensemble, on the other hand, matrix elements are randomly chosen as

$$H_{ij} = \begin{cases} 1 + i; \\ 1 - i; \\ -1 + i; \\ -1 - i \end{cases} \quad (6.35)$$

with equal probabilities which obey the constraint in Eq. (6.33).

### Class C

In the class C, matrices have PHS given by

$$\hat{C}_- \hat{H}^T \hat{C}_-^{-1} = -\hat{H}, \quad \hat{C}_- \hat{C}_-^* = -\hat{\mathbb{I}}, \quad (6.36)$$

with a unitary matrix  $\hat{C}_-$ . In a manner similar to the class D, there appear eigenvalue-pairs  $(E_\alpha, -E_\alpha)$ .

We assume that  $\hat{C}_-$  is the Pauli operator  $\hat{\sigma}^y$  without loss of generality for Gaussian ensembles. We then obtain

$$\hat{a} = -\hat{d}^T, \quad \hat{b} = \hat{b}^T, \quad \hat{c} = \hat{c}^T \quad (6.37)$$

for a matrix form in Eq. (6.27). Then, the probability distribution is

$$P(\hat{H}) d\hat{H} \propto \exp \left\{ -2\beta \left[ \sum_i (|a_{ii}|^2 + |b_{ii}|^2/2 + |c_{ii}|^2/2) + \sum_{i>j} (|a_{ij}|^2 + |b_{ij}|^2 + |c_{ij}|^2 + |d_{ij}|^2) \right] \right\} \\ \times \prod_i da_{ii} da_{ii}^* db_{ii} db_{ii}^* \prod_{i>j} da_{ij} da_{ij}^* db_{ij} db_{ij}^* dc_{ij} dc_{ij}^* dd_{ij} dd_{ij}^*. \quad (6.38)$$

For a Bernoulli ensemble, on the other hand, matrix elements are randomly chosen as

$$a_{ij}, b_{ij}, c_{ij}, d_{ij} = \begin{cases} 1 + i; \\ 1 - i; \\ -1 + i; \\ -1 - i \end{cases} \quad (6.39)$$

with equal probabilities which obey the constraint in Eq. (6.37).

### Class AIII

In the class AIII, matrices have chiral symmetry (CS) defined by

$$\hat{\Gamma} \hat{H}^\dagger \hat{\Gamma}^{-1} = -\hat{H}, \quad \hat{\Gamma}^2 = \hat{\mathbb{I}}, \quad (6.40)$$

with a unitary matrix  $\hat{\Gamma}$ . In a manner similar to the class D, there appear eigenvalue-pairs  $(E_\alpha, -E_\alpha)$ . In this case, we obtain

$$\hat{H} (\hat{\Gamma} |\chi_\alpha\rangle) = -\hat{\Gamma} \hat{H}^\dagger |\chi_\alpha\rangle = -E_\alpha^* (\hat{\Gamma} |\chi_\alpha\rangle). \quad (6.41)$$

Thus,  $\hat{\Gamma} |\chi_\alpha\rangle$  becomes an eigenstate of  $\hat{H}$  with an eigenvalue  $-E_\alpha^*$ . In other words, there appear eigenvalue pairs  $(E_\alpha, -E_\alpha^*)$ . In a manner similar to the equivalence between TRS and PHS<sup>†</sup> [245] mentioned before, CS is equivalent to pseudo-Hermiticity [234], which is defined by the following conditions

$$\hat{\eta} \hat{H}^\dagger \hat{\eta}^{-1} = \hat{H}, \quad \hat{\eta}^2 = \hat{\mathbb{I}} \quad (6.42)$$

for some unitary operator  $\hat{\eta}$ . This condition indicates that the pairs  $(E_\alpha, E_\alpha^*)$  are present in the complex plane.

We can assume that  $\hat{\Gamma}$  is a Pauli matrix  $\hat{\sigma}^z$  for obtaining a nontrivial consequence, which results in Eq. (6.27) with

$$\hat{a} = -\hat{a}^\dagger, \quad \hat{b} = \hat{c}^\dagger, \quad \hat{c} = \hat{b}^\dagger, \quad \hat{d} = -\hat{d}^\dagger. \quad (6.43)$$

Since  $\hat{H}$  always becomes an anti-Hermitian matrix for a specific case  $\hat{\Gamma} = \hat{\mathbb{I}}$ , which becomes the class A in Hermitian systems (by considering  $i\hat{H}$ ), we do not consider that case here. Then, the Gaussian probability distribution is given as

$$\begin{aligned} P(\hat{H}) d\hat{H} \\ \propto \exp \left\{ -\beta \left[ \sum_i (|a_{ii}|^2 + |d_{ii}|^2 + 2|b_{ii}|^2) + 2 \sum_{i>j} (|a_{ij}|^2 + |b_{ij}|^2 + |c_{ij}|^2 + |d_{ij}|^2) \right] \right\} \\ \times \prod_i da_{ii} dd_{ii} db_{ii} db_{ii}^* \prod_{i>j} da_{ij} da_{ij}^* db_{ij} db_{ij}^* dc_{ij} dc_{ij}^* dd_{ij} dd_{ij}^*. \end{aligned} \quad (6.44)$$

For a Bernoulli ensemble, on the other hand, matrix elements are randomly chosen as

$$a_{ij}, b_{ij}, c_{ij}, d_{ij} = \begin{cases} 1 + i; \\ 1 - i; \\ -1 + i; \\ -1 - i \end{cases} \quad (6.45)$$

with equal probabilities under the constraint in Eq. (6.43).

### Class AIII<sup>†</sup>

In the class AIII<sup>†</sup>, matrices have sublattice symmetry (SLS) given by

$$\hat{S}\hat{H}\hat{S}^{-1} = -\hat{H}, \quad \hat{S}^2 = 1 \quad (6.46)$$

with a unitary matrix  $\hat{S}$ . In this case, we obtain

$$\hat{H}(\hat{S}|\phi_\alpha\rangle) = -\hat{S}\hat{H}|\phi_\alpha\rangle = -E_\alpha(\hat{S}|\phi_\alpha\rangle). \quad (6.47)$$

Thus,  $\hat{S}|\phi_\alpha\rangle$  is an eigenstate of  $\hat{H}$  with an eigenvalue  $-E_\alpha$  and there appear eigenvalue pairs  $(E_\alpha, -E_\alpha)$ .

We can assume that  $\hat{S}$  is a Pauli matrix  $\hat{\sigma}^z$  to obtain a nontrivial consequence,

which results in Eq. (6.27) with

$$\hat{a} = \hat{d} = 0. \quad (6.48)$$

Since  $\hat{H}$  always becomes a zero matrix for a specific case  $\hat{\Gamma} = \hat{\mathbb{1}}$ , we do not consider that case here. Then, the Gaussian probability distribution is given as

$$P(\hat{H}) d\hat{H} \propto \exp \left[ -\beta \sum_{i,j} (|b_{ij}|^2 + |c_{ij}|^2) \right] \prod_{i,j} db_{ij} dc_{ij}. \quad (6.49)$$

For a Bernoulli ensemble, on the other hand, matrix elements are randomly chosen as

$$b_{ij}, c_{ij} = \begin{cases} 1 + i; \\ 1 - i; \\ -1 + i; \\ -1 - i \end{cases} \quad (6.50)$$

with equal probabilities under the constraint in Eq. (6.48).

## 6.4 New threefold way in non-Hermitian random matrices and universality of level-spacing distributions

We now show that there appear three different universality classes of level-spacing distributions if we consider transposition symmetry (TRS<sup>†</sup>). The level-spacing distribution is defined in Chapter 5. In the following, we focus on the Gaussian and Bernoulli distributions defined in the previous section. Examples of matrices taken from these ensembles are given in Fig. 6.3(A), which shows that matrix elements behave differently from each other's ensemble.

In Fig. 6.3(B), we show the distribution  $p(s)$  for each of the three symmetry classes A, AI<sup>†</sup>, and AII<sup>†</sup>. We first find that, the distributions behave similarly for the Gaussian and Bernoulli ensembles if the symmetry class is the same, which indicates the universality of each class. Secondly, three different symmetry classes lead to three different universality classes for  $p(s)$ , which can be found from e.g., the peak height and the width of the distribution. This is similar to Dyson's threefold way but in stark contrast with Ginibre's classification. In Fig. 6.3(C), we show the level-spacing distribution for the other classes with a single symmetry, i.e., the classes AI, AII, D, C, AIII, and AIII<sup>†</sup> for the Gaussian ensembles (the Bernoulli

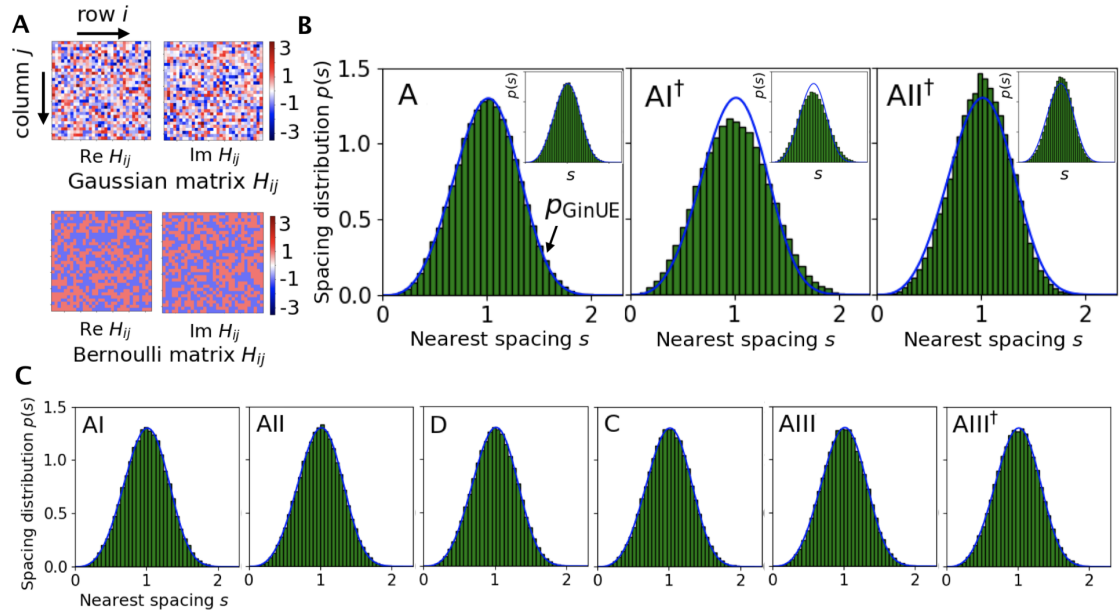


Figure 6.3: (A) A single realization of a matrix sampled from the Gaussian and Bernoulli random  $32 \times 32$  matrices for the class A (real and imaginary parts). (B) Level-spacing distributions  $p(s)$  calculated for random matrices that belong to the classes A,  $AI^\dagger$ , and  $AII^\dagger$ . The matrix elements obey Gaussian and Bernoulli distributions for main panels and insets, respectively. (C) Level-spacing distributions  $p(s)$  calculated for random matrices that belong to the classes AI, AII, D, C, AIII and  $AIII^\dagger$ . They obey distributions described by GinUE. We obtain the results by diagonalizing  $2000 \times 2000$  matrices and from averages over 1000 samples. Statistics are chosen from eigenvalues which are away from the edges of the spectrum and from the symmetric line (i.e., the real or imaginary axes). The Level-spacing distribution for the class  $AII^\dagger$  is computed by identifying the Kramers degeneracies. Taken from Fig. 2 in the first version of Ref. [112].

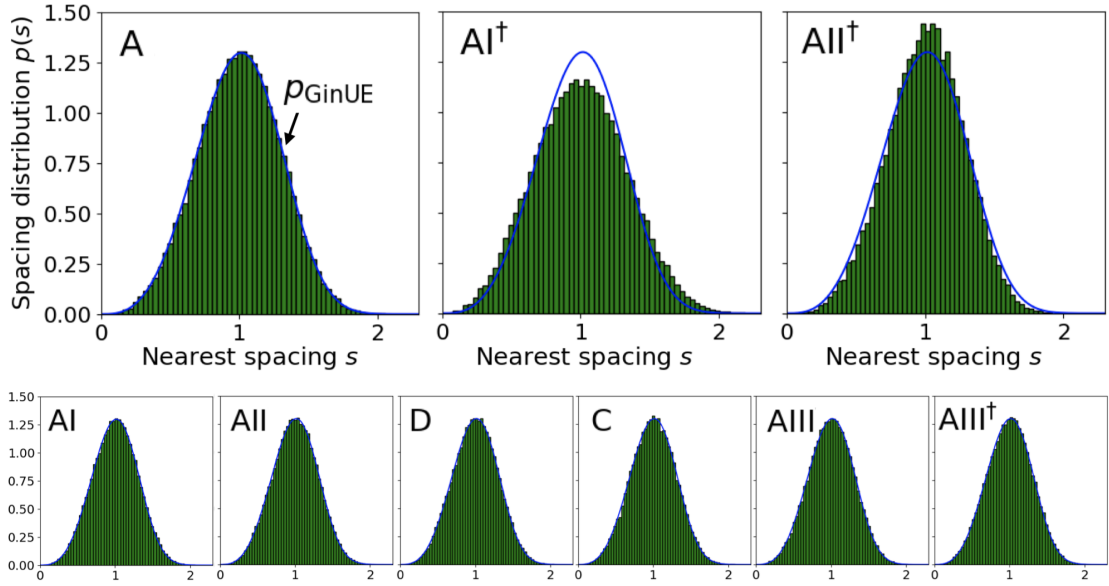


Figure 6.4: Level-spacing distributions  $p(s)$  calculated for random matrices that belong to the classes A,  $AI^\dagger$ ,  $AII^\dagger$ , AI, AII, D, C, AIII and  $AIII^\dagger$ . The results are computed from diagonalizing  $6000 \times 6000$  matrices and from averages over 300 samples. Statistics are chosen from eigenvalues which are away from the edges of the spectrum and from the symmetric line (i.e., the real or imaginary axes). The level spacing for the class  $AII^\dagger$  is calculated from the minimum distance between two Kramers pairs, each of which is doubly degenerate. Taken from Fig. S-1 in the first version of Ref. [112].

ensembles give the similar results). They are well described by the distributions of GinUE (the class A)  $p_{\text{GinUE}}(s)$ . This means that nonlocal pairs of eigenvalues such as  $(E_\alpha, E_\alpha^*)$  indeed cannot alter the local correlation of eigenvalues measured by  $p(s)$  away from the symmetric line, i.e., the real or imaginary axis.

To strengthen the evidence of the universality and the existence of the three-fold universality classes, we show the results for a larger matrix in Fig. 6.4 size than those in Fig. 6.3. We find that similar results are obtained for such larger matrices, which indicates that the three distinctive universality classes are not the consequence of the finite-size effect.

Furthermore, we quantitatively confirm this threefold universality by up to the fourth cumulants of  $p(s)$ . The second, third, and fourth cumulants are defined as

$$c_2 = m_2 - m_1^2 \quad (6.51)$$

$$c_3 = m_3 - 3m_1m_2 + 2m_1^3 \quad (6.52)$$

$$c_4 = m_4 - 4m_1m_3 - 3m_2^2 + 12m_1^2m_2 - 6m_1^4, \quad (6.53)$$

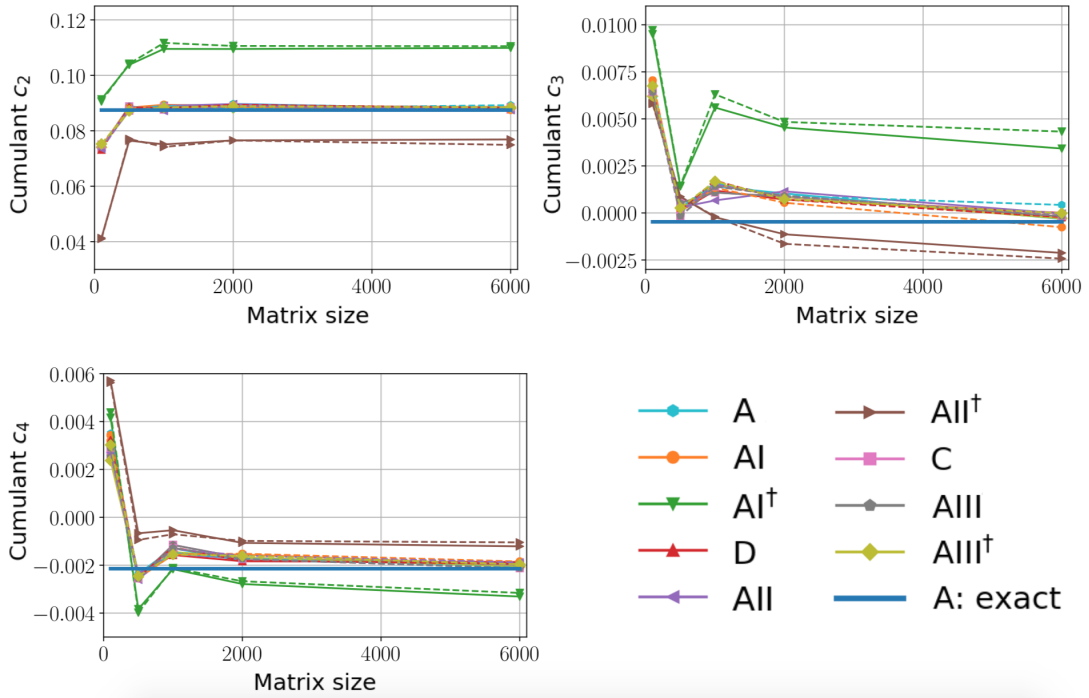


Figure 6.5: Second, third, and fourth cumulants of  $p(s)$  for different matrix sizes. We consider the nine symmetry classes and two different matrix ensembles (solid/dashed lines denote the Gaussian/Bernoulli ensembles). Thick solid lines are the results computed from the exact result of  $p_{GinUE}(s)$ . Statistics are chosen from eigenvalues which are away from the edges of the spectrum and from the symmetric line (i.e., the real or imaginary axes). The data show averaged results over 20000, 4000, 2000, 1000, 300 matrices whose sizes are 100, 500, 1000, 2000, 6000, respectively. Taken from Fig. S-2 in the fourth version of Ref. [112].

where

$$m_k = \int_0^\infty ds s^k p(s) \quad (6.54)$$

denotes the  $k$ th moment. From Fig. 6.5, we find the following results which strengthen the argument on the threefold universality:

1. The Gaussian and Bernoulli ensembles that belong to the same symmetry class lead to the same results for all of the cases. Small deviations for the largest matrix size can be ascribed to the fact that the number of samples is limited.
2. For matrix sizes that are large enough, three distinct universality classes are found to appear even in cumulants with high orders; while the cumulants of the classes A, AI, AII, D, C, AIII, and AIII<sup>†</sup> are the same, those for the classes AI<sup>†</sup> and AII<sup>†</sup> are different.
3. The cumulants  $c_{A,2}$ ,  $c_{A,3}$ , and  $c_{A,4}$  for the classes A, AI, AII, D, C, AIII, and AIII<sup>†</sup> are close to the values computed from the exact GinUE distribution  $p_{\text{GinUE}}(s)$  ( $c_{A,2} = 0.0875$ ,  $c_{A,3} = 0.000471$ , and  $c_{A,4} = 0.00215$ ). On the other hand, the classes AI<sup>†</sup> and AII<sup>†</sup> have cumulants that have different values, which imply that they are distinct from that of the GinUE even when we consider the infinite matrix size. From Fig. 6.5, we conjecture that  $c_{\text{AI}^\dagger,2} \simeq 0.11$ ,  $c_{\text{AII}^\dagger,2} \simeq 0.075$ ,  $c_{\text{AI}^\dagger,3} \simeq 0.004$ ,  $c_{\text{AII}^\dagger,3} \simeq -0.0025$ ,  $c_{\text{AI}^\dagger,4} \simeq -0.003$ , and  $c_{\text{AII}^\dagger,4} \simeq -0.001$ .

## 6.5 Analysis for small matrices

In this section, we argue that we can understand the main feature of our results by analyzing small matrices, i.e, by calculating  $p(s)$  obtained from  $2 \times 2$  (or  $4 \times 4$ ) matrices. Even though small matrices give quantitatively different results from larger matrices [145], it is expected that we can understand some *qualitative* features of level-spacing distributions [248], e.g., how TRS<sup>†</sup> changes the height and width of  $p(s)$ . This is because the repulsive interaction owing to perturbations between two eigenvalues that are close with each other is qualitatively understood by diagonalization of the  $2 \times 2$  (or  $4 \times 4$ ) transition matrix [248].

Let us consider a situation that a random matrix  $\hat{H}$  is slightly perturbed with  $\hat{V}$ , which is assumed to preserve symmetry. To evaluate the correlation of two eigenvalues induced by  $\hat{V}$ , assume that these two eigenvalues are much closer to each

other than to the others. In this case, the repulsive interactions of these eigenvalues can be estimated by diagonalizing  $\hat{V}$  in the subspace which is spanned by the corresponding eigenstates. We expect that this method can describe qualitative feature of the level-spacing distributions.

Using the above method, we obtain matrices that are dependent on the symmetry of  $\hat{H}$  (or equivalently  $\hat{V}$ ). Firstly, consider the simplest case of the class A. When we denote  $|\phi_1\rangle$  ( $|\chi_1\rangle$ ) and  $|\phi_2\rangle$  ( $|\chi_2\rangle$ ) as the corresponding right (left) eigenstates, the two-by-two matrix which we want can be written as

$$\begin{pmatrix} \langle \chi_1 | \hat{V} | \phi_1 \rangle & \langle \chi_1 | \hat{V} | \phi_2 \rangle \\ \langle \chi_2 | \hat{V} | \phi_1 \rangle & \langle \chi_2 | \hat{V} | \phi_2 \rangle \end{pmatrix} =: \begin{pmatrix} a & b \\ c & d \end{pmatrix}. \quad (6.55)$$

Since  $|\phi_1\rangle$  and  $|\phi_2\rangle$  are regarded as independent random vectors for large  $\hat{H}$  and there is in general no direct relation between  $|\phi_\alpha\rangle$  and  $|\chi_\alpha\rangle$ ,  $a, b, c, d \in \mathbb{C}$  can be treated as random independent variables. By taking  $a, b, c$ , and  $d$  as Gaussian random variables, we define

$$\hat{H}_{\text{small,A}} =: \begin{pmatrix} a & b \\ c & d \end{pmatrix}. \quad (6.56)$$

Let us consider the class AI next. While TRS imposes the constraint on two eigenvalues that are complex conjugate to each other, it does not on two close eigenstates that are away from the real axis. Consequently, the obtained matrix that characterizes the interaction of eigenvalues for the class AI also has the form of  $\hat{H}_{\text{small,A}}$ . We note that  $\hat{H}_{\text{small,A}}$  becomes a complex matrix despite TRS of  $\hat{V}$ , since the eigenstates  $|\phi_1\rangle$  and  $|\phi_2\rangle$  spontaneously break TRS. We obtain similar discussions for the classes AII, D, C, AIII, and AIII<sup>†</sup>: the eigenstates  $|\phi_1\rangle$  and  $|\phi_2\rangle$  no longer preserve the symmetry constraint of  $\hat{V}$ , and  $\hat{H}_{\text{small,A}}$  describes the relevant interaction. In other words, a global symmetry of the spectrum cannot influence the local statistics that are away from the real axis [145].

On the other hand, we face a different situation for classes with transposition symmetry (TRS<sup>†</sup>). Let us consider the class AI<sup>†</sup>, where a condition  $\hat{C}_+ |\chi_\alpha\rangle^* = |\phi_\alpha\rangle$  is satisfied as noted in Eq. (6.21) (we have taken a proportional coefficient to be one). Then, whereas  $\langle \chi_1 | \hat{V} | \phi_1 \rangle$  and  $\langle \chi_2 | \hat{V} | \phi_2 \rangle$  become independent complex

variables, the following relation applies for the off-diagonal terms:

$$\begin{aligned}
\langle \chi_1 | \hat{V} | \phi_2 \rangle &= (\langle \chi_1 | \hat{V} | \phi_2 \rangle)^T \\
&= (\langle \phi_2 |^*) \hat{V} | \chi_1 \rangle^* \\
&= \langle \chi_2 | \hat{C}_+^T \hat{V}^T \hat{C}_+^{-1} | \phi_1 \rangle \\
&= \langle \chi_2 | \hat{C}_+ \hat{V}^T \hat{C}_+^{-1} | \phi_1 \rangle \\
&= \langle \chi_2 | \hat{V} | \phi_1 \rangle, \tag{6.57}
\end{aligned}$$

where we have used the relation  $\hat{C}_+^T = \hat{C}_+$ , which holds for the class AI<sup>†</sup>. Hence, a symmetric matrix with  $b = c$ , i.e.,

$$\hat{H}_{\text{small,AI}} =: \begin{pmatrix} a & b \\ b & d \end{pmatrix} \tag{6.58}$$

is obtained.

Finally, for the class AII<sup>†</sup>, we need a four-by-four matrix to deal with the Kramers degeneracy. Let us assume that matrices are spanned by  $|\phi_1\rangle, |\bar{\phi}_1\rangle, |\phi_2\rangle, |\bar{\phi}_2\rangle$ , where the corresponding left eigenstates are denoted as  $|\chi_1\rangle, |\bar{\chi}_1\rangle, |\chi_2\rangle, |\bar{\chi}_2\rangle$ . Here, we note that the following relations hold:

$$|\bar{\phi}_\alpha\rangle = \hat{C}_+ |\chi_\alpha\rangle^*, \quad \langle \bar{\chi}_\alpha | = (\langle \phi_\alpha |^*) \hat{C}_+^{-1}. \tag{6.59}$$

We also note that  $\hat{C}_+^T = -\hat{C}_+$  for the class AII<sup>†</sup>. In this case, we obtain

$$\begin{aligned}
\langle \bar{\chi}_\alpha | \hat{V} | \bar{\phi}_\beta \rangle &= (\langle \phi_\alpha |^*) \hat{C}_+^{-1} \hat{V} \hat{C}_+ (|\chi_\alpha\rangle^*) \\
&= [(\langle \phi_\alpha |^*) \hat{C}_+^{-1} \hat{V} \hat{C}_+ (|\chi_\alpha\rangle^*)]^T \\
&= \langle \chi_\beta | \hat{C}_+^T \hat{V}^T (\hat{C}_+^T)^{-1} | \phi_\alpha \rangle \\
&= \langle \chi_\beta | \hat{C}_+ \hat{V}^T (\hat{C}_+)^{-1} | \phi_\alpha \rangle \\
&= \langle \chi_\beta | \hat{V} | \phi_\alpha \rangle. \tag{6.60}
\end{aligned}$$

We also have

$$\begin{aligned}
\langle \chi_\alpha | \hat{V} | \bar{\phi}_\beta \rangle &= [\langle \chi_\alpha | \hat{V} \hat{C}_+ (|\chi_\alpha\rangle^*)]^T \\
&= \langle \chi_\beta | \hat{C}_+^T \hat{V}^T (|\chi_\alpha\rangle^*) \\
&= -\langle \chi_\beta | \hat{C}_+ \hat{V}^T (|\chi_\alpha\rangle^*) \\
&= -\langle \chi_\beta | \hat{V} \hat{C}_+ (|\chi_\alpha\rangle^*) \\
&= -\langle \chi_\beta | \hat{V} | \phi_\alpha \rangle \tag{6.61}
\end{aligned}$$

and

$$\begin{aligned}
\langle \bar{\chi}_\alpha | \hat{V} | \phi_\beta \rangle &= [(\langle \phi_\alpha |)^* \hat{C}_+^{-1} \hat{V} | \phi_\beta \rangle]^T \\
&= (\langle \phi_\beta |)^* \hat{C}_+^{-1} \hat{V}^T (\hat{C}_+^T)^{-1} | \phi_\alpha \rangle \\
&= -(\langle \phi_\beta |)^* \hat{C}_+^{-1} \hat{V}^T (\hat{C}_+)^{-1} | \phi_\alpha \rangle \\
&= -(\langle \phi_\beta |)^* \hat{C}_+^{-1} (\hat{C}_+)^{-1} \hat{V} | \phi_\alpha \rangle \\
&= -\langle \bar{\chi}_\beta | \hat{V} | \phi_\alpha \rangle.
\end{aligned} \tag{6.62}$$

To sum up, the relevant matrix can be written as

$$H_{\text{small, AII}^\dagger} = \begin{pmatrix} a & 0 & e & b \\ 0 & a & c & g \\ g & -b & d & 0 \\ -c & e & 0 & d \end{pmatrix}, \tag{6.63}$$

where  $a, b, c, d, e, g \in \mathbb{C}$ .

The distance between two eigenvalues (or Kramers pairs of eigenvalues) in these three cases can be written as

$$|E_1 - E_2| = \left| \sqrt{(a-d)^2 + 4bc} \right| \tag{6.64}$$

for the class A (and AI, AII, D, C, AIII, and AIII<sup>†</sup>),

$$|E_1 - E_2| = \left| \sqrt{(a-d)^2 + 4b^2} \right| \tag{6.65}$$

for the class AI<sup>†</sup>,

$$|E_1 - E_2| = \left| \sqrt{(a-d)^2 + 4ef - 4bc} \right| \tag{6.66}$$

and for the class AII<sup>†</sup>. We can see that the distributions of  $|E_1 - E_2|$  are different in the three cases, since the different numbers of free parameters are involved. This is similar to the Hermitian case, in which the number of degrees of freedom that changes with symmetry affects the level-spacing distributions. To summarize, the transposition symmetry (not TRS) can change the interactions of two eigenvalues and alter the level-spacing distributions through the change of the number of degrees of freedom even in the non-Hermitian case.

Figure 6.6 indeed shows that the (normalized) level-spacing distributions for matrices  $\hat{H}_{\text{small, A}}$ ,  $\hat{H}_{\text{small, AI}^\dagger}$ , and  $\hat{H}_{\text{small, AII}^\dagger}$  are distinct from one another. The properties for the peak and variance for these small matrices also apply to the calculations of large matrices as we have seen previously, which is demonstrated as suppression or enhancement of the GinUE distribution in Fig. 6.3 [321].

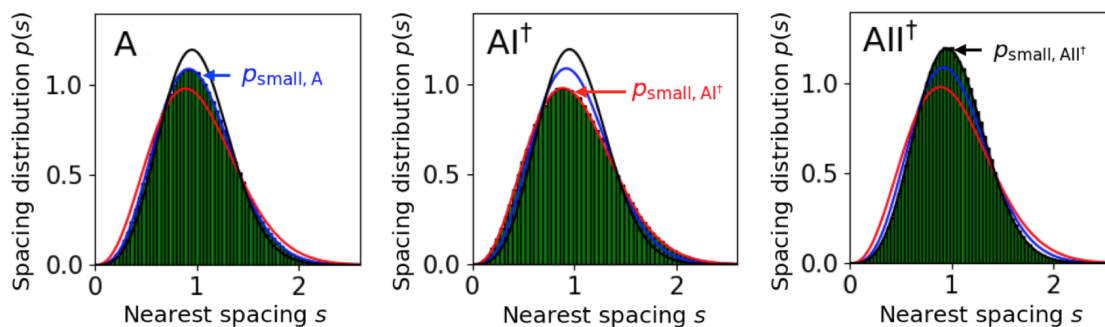


Figure 6.6: Level-spacing distributions for  $\hat{H}_{\text{small},A}$ ,  $\hat{H}_{\text{small},AI^\dagger}$ , and  $\hat{H}_{\text{small},AII^\dagger}$ . Histograms that are numerically obtained agree excellently with analytical predictions in Eq. (6.76). We obtain the results from averages over  $10^6$  ensembles. Taken from Fig. S-3 in the fourth version of Ref. [112].

### 6.5.1 Detailed analysis

[Note: the results of this subsection, in particular Eq. (6.76), are mainly obtained by Mr. Naoto Kura. My contribution is the physical interpretation of the obtained results.]

In this subsection, we give a more detailed analysis for non-Hermitian small matrices and compare similarity to and difference from the Hermitian case. Let us first reparametrize  $\hat{H}_{\text{small}}$  by expanding it using an appropriate basis set  $\{\hat{\lambda}^\nu\}$  of the matrix space:

$$\hat{H}_{\text{small}} = z_0 \hat{\mathbb{I}} + \sum_{\nu=1}^f z_\nu \hat{\lambda}^\nu. \quad (6.67)$$

Here,  $z_\nu \in \mathbb{C}$  and  $\hat{\lambda}^\nu$  satisfy the Hermiticity, the traceless condition, and the orthonormality

$$\text{Tr}[\hat{\lambda}^\nu] = 0, \quad \text{Tr}[\hat{\lambda}^\nu \hat{\lambda}^\sigma] = S \delta_{\nu\sigma}, \quad (6.68)$$

where  $S = 2$  for two-by-two matrices and  $S = 4$  for four-by-four matrices. The matrix bases  $\{\hat{\lambda}^\nu\}$  for the three classes A,  $AI^\dagger$  and  $AII^\dagger$  are summarized in Table 6.2.

We consider  $z_\nu$  as random variables instead of  $a, b, \dots$  in the previous section. We first note that

$$P(\hat{H}) \propto e^{-\beta \text{Tr}[\hat{H}^\dagger \hat{H}]} = e^{-S\beta \sum_{\nu=1}^f |z_\nu|^2}. \quad (6.69)$$

Since  $z_0 \hat{\mathbb{I}}$  does not affect the level-spacing distributions, we can consider (instead

Table 6.2: Matrix bases  $\{\hat{\lambda}^v\}$  for three different classes  $\text{AI}^\dagger$ ,  $\text{A}$ , and  $\text{AII}^\dagger$ . Here,  $\sigma^{x,y,z}$  and  $\gamma^{1,2,3,4,5}$  are the Pauli and the Dirac matrices, respectively. We follow the notation of Ref. [322].

Class	$f$	Basis
$\text{AI}^\dagger$	2	$\sigma^x, \sigma^z$
$\text{A}$	3	$\sigma^x, \sigma^y, \sigma^z$
$\text{AII}^\dagger$	5	$\gamma^1, \gamma^2, \gamma^3, \gamma^4, \gamma^5$

of  $\hat{H}_{\text{small}}$ )

$$\hat{H}'_{\text{small}} = \sum_{v=1}^f z_v \hat{\lambda}^v \quad (6.70)$$

which is traceless. We obtain

$$(\hat{H}'_{\text{small}})^2 = \sum_{v=1}^f z_v^2 \hat{\mathbb{I}} \quad (6.71)$$

owing to the anticommutation relation

$$\hat{\lambda}^v \hat{\lambda}^\sigma + \hat{\lambda}^\sigma \hat{\lambda}^v = 2\delta_{v\sigma} \hat{\mathbb{I}} \quad (6.72)$$

for the basis in Table 6.2. At the same time, owing to the traceless condition,  $\hat{H}'_{\text{small}}$  has eigenvalues  $(\epsilon, -\epsilon)$  (or  $(\epsilon, \epsilon, -\epsilon, -\epsilon)$  for the classes  $\text{AII}^\dagger$ ). Then,  $\hat{H}'_{\text{small}}$  satisfies

$$(\hat{H}'_{\text{small}})^2 = \epsilon^2 \hat{\mathbb{I}}. \quad (6.73)$$

Combining the results above, we obtain that the level-spacing  $s$  (before unfolding) can be written as

$$s = 2|\epsilon| = 2|X_f|^{1/2}, \quad (6.74)$$

where

$$X_f = \sum_{v=1}^f z_v^2. \quad (6.75)$$

Thus, the level-spacing distributions are determined by the sum of  $f$  complex-valued degrees of freedom which are chosen from the Gaussian distribution. Here,  $f = 3$  for the class  $\text{A}$ ,  $f = 2$  for the class  $\text{AI}^\dagger$ , and  $f = 5$  for the class  $\text{AII}^\dagger$ . Importantly, this is a straightforward extension of the Hermitian case, in which the level spacings turn out to be described by the sum of  $f$  real-valued degrees of freedom. In that case,  $f = 3$  for the class  $\text{A}$ ,  $f = 2$  for the class  $\text{AI}$ , and  $f = 5$  for the class  $\text{AII}$ .

The normalized level-spacing distributions are calculated from the representation in Eq. (6.74). The straightforward calculation gives (see Appendix B for the derivation)

$$p_{\text{small}}(s) = \frac{(C_f s)^3}{\mathcal{N}_f} K_{\frac{f-2}{2}} \left( (C_f s)^2 \right), \quad (6.76)$$

where

$$K_\alpha(x) = \int_0^\infty e^{-x \cosh z} \cosh(\alpha z) \quad (6.77)$$

is the modified Bessel function, and  $C_f$  and  $\mathcal{N}_f$  are normalization constants. The analytical result in Eq. (6.76) well describes the numerical results in Fig. 6.6. We note that  $p_{\text{small}}$  for a Hermitian random matrix involves the chi-squared distribution instead of the modified Bessel distribution, after the evaluation of the sum of  $f$  real-valued degrees of freedom. In fact, it can be written in a form

$$p_{\text{small}}(s) = A_f s \chi_f^2 \left[ (B_f s)^2 \right]. \quad (6.78)$$

Let us state some properties of  $p_{\text{small}}$ . Firstly, the level-repulsion factor for non-Hermitian  $p_{\text{small}}(s \rightarrow 0)$  is universally  $\simeq s^3$  [248] irrespective of symmetry (with an additional factor of  $\log s$  only for the class  $\text{AI}^\dagger$ ), in contrast with the Hermitian case in which  $p_{\text{small}}(s \rightarrow 0) \propto s^{f-1}$ . This comes from the difference between the modified Bessel function and the chi-squared distribution, where only the latter leads to the  $f$ -dependent power of  $s$  in the  $s \rightarrow 0$  limit.

On the other hand, the entire distribution depends on the three symmetry classes even in the non-Hermitian case as in Dyson's Hermitian case, which means that  $\text{TRS}^\dagger$  alters repulsive interactions. In fact,  $p_{\text{small},\text{AI}^\dagger}$  and  $p_{\text{small},\text{AII}^\dagger}$  respectively have lower and higher peaks than  $p_{\text{small},\text{A}}$ . In addition,  $p_{\text{small},\text{AI}^\dagger}$  and  $p_{\text{small},\text{AII}^\dagger}$  respectively have larger and smaller variances than  $p_{\text{small},\text{A}}$ . The figures of Fig. 6.6 at relatively small  $s$  actually indicate that the repulsive interaction is smaller for the class  $\text{AI}^\dagger$  and larger for the class  $\text{AII}^\dagger$  than that for the class A. This is very similar to the Hermitian case, where the repulsive interaction is smaller for the class  $\text{AI}$  and larger for the class  $\text{AII}$  than that for the class A.

## 6.6 Universality in dissipative many-body systems

As we have seen in Chapter 2, local spectral statistics of eigenvalues, such as the level-spacing statistics for Hermitian quantum nonintegrable Hamiltonians, are

conjectured to obey those of random matrices [121, 119, 323, 143, 16, 116, 147, 18, 324, 57, 22, 24, 192, 26, 141, 27, 325, 149, 142, 31]. As a natural extension of this conjecture, the level-spacing statistics of non-Hermitian random matrices are supposed to characterize the transition between nonintegrability and integrability, and the transition between chaos and localization, in dissipative quantum systems [247, 296, 111]. On the other hand, the effect of symmetry for the universality has not been investigated so far. In this section, we show that new universality classes of level-spacing distributions indeed appear in dissipative quantum nonintegrable many-body systems.

### 6.6.1 Non-Hermitian many-body systems

We first consider locally interacting non-Hermitian spin models that realize the classes A,  $\text{AI}^\dagger$ , and  $\text{AII}^\dagger$  by changing the parameters (see Fig. 6.7(a)). The Hamiltonian is given by

$$\begin{aligned}\hat{H} &= \hat{H}_I + \hat{H}_F + \hat{H}_{\text{DM}}, \tag{6.79} \\ \hat{H}_I &= - \sum_{j=1}^{N-1} (1 + iJ\epsilon_j) \hat{\sigma}_j^z \hat{\sigma}_{j+1}^z, \\ \hat{H}_F &= - \sum_{j=1}^N (h' \hat{\sigma}_j^x + h \hat{\sigma}_j^z), \\ \hat{H}_{\text{DM}} &= \sum_{j=1}^{N-1} \vec{D} \cdot (\vec{\sigma}_j \times \vec{\sigma}_{j+1}),\end{aligned}$$

where  $\epsilon_j$  is randomly chosen from  $[-1, 1]$ ,  $h' = -2.1h$ , and  $\vec{D} = D(\vec{e}_x + \vec{e}_z)/\sqrt{2}$ . Note that this is a non-Hermitian generalization of Eq. (2.34) (where we consider  $J \neq 0$ ).

The symmetry class of this model changes with  $h$  and  $D$ . The model belongs to (i) the class A for  $D \neq 0, h \neq 0$ , (ii) the class  $\text{AI}^\dagger$  for  $D = 0, h \neq 0$  since  $\hat{H} = \hat{H}^T$  holds, and (iii) the class  $\text{AII}^\dagger$  for  $h = 0, D \neq 0$  when  $L$  is odd since

$$\hat{H} = \left( \prod_{i=1}^L \hat{\sigma}_i^y \right) \hat{H}^T \left( \prod_{i=1}^L \hat{\sigma}_i^y \right)^{-1} \tag{6.80}$$

with

$$\left( \prod_{i=1}^L \hat{\sigma}_i^y \right) \left( \prod_{i=1}^L \hat{\sigma}_i^y \right)^* = (-1)^L. \tag{6.81}$$

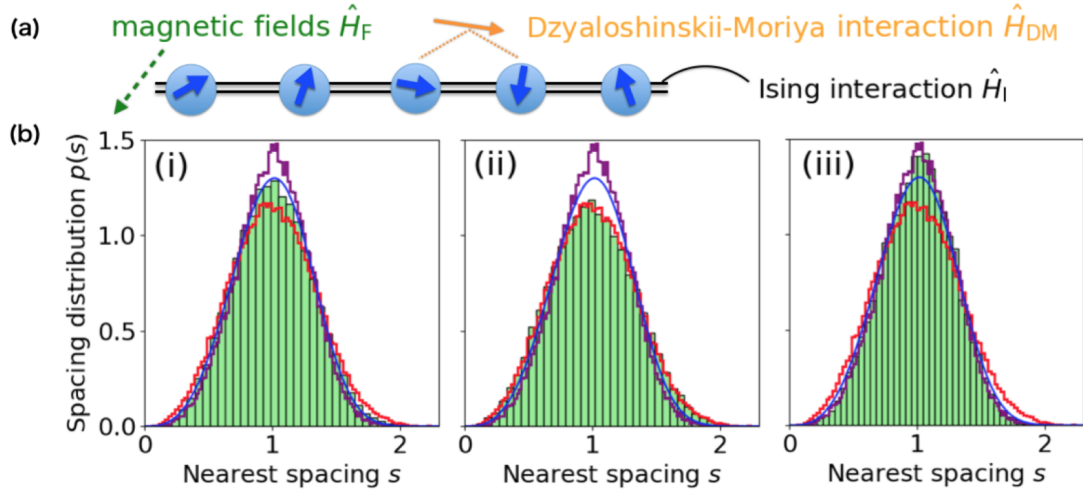


Figure 6.7: (a) Schematic illustration of the non-Hermitian spin chain with local interactions in Eq. (6.79). (b) Level-spacing distributions  $p(s)$  for three different models (i), (ii), and (iii) after the unfolding procedure of eigenvalues. The blue, red, and purple lines are the results for the classes A,  $AI^\dagger$ , and  $AII^\dagger$ , respectively (for the classes  $AI^\dagger$  and  $AII^\dagger$ , we show the same numerical data obtained in Fig. 6.3(B)). The parameters are chosen as  $h = 0.5, D = 0$  for the model (i),  $h = 0.5, D = 0.9$  for the model (ii), and  $h = 0, D = 0.9$  for the model (iii). In addition,  $J = 0.2$  and  $L = 13$  are used for all the models. We obtain the results from averages over 30 samples. We take statistics from eigenvalues that are away from the upper and lower edges of the spectrum. Taken from Fig. S-4 in the fourth version of Ref. [112].

In general, the three non-Hermitian classes A,  $AI^\dagger$  and,  $AII^\dagger$  are obtained by adding non-Hermiticity to diagonal terms of Hermitian systems that belong to the classes A, AI, and AII, respectively.

We show in Fig. 6.7 the distributions  $p(s)$  for the above three models after the unfolding procedure (see Chapter 5) of eigenvalues [145]. There appear clearly distinct three types of distributions, which correspond to the universality classes of random-matrix ensembles (see Fig. 6.3(b)) that belong to the same symmetry classes. Indeed, model (i) obeys the universality of class A (blue line), model (ii) obeys that of the class  $AI^\dagger$  (red line, which is the same data with the middle main panel in Fig. 6.3(B)), and model (iii) obeys the universality of the class  $AII^\dagger$  (purple line, which is the same data with the right main panel in Fig. 6.3(B)). Our results show that local correlations of eigenvalues of nonintegrable non-Hermitian many-body systems are predicted by the universality of non-Hermitian random matrices with the same symmetry.

## 6.6.2 Lindblad many-body dynamics

Next, we demonstrate that the universality of non-Hermitian random matrices also appears in a completely different type of dissipative many-body systems, i.e., dissipative systems described by the Lindblad equation (see Fig. 6.8):

$$\frac{d\hat{\rho}}{dt} = \mathcal{L}[\hat{\rho}] = -i[\hat{H}, \hat{\rho}] + \sum_{j=1}^L \gamma \left[ \hat{\Gamma}_j \hat{\rho} \hat{\Gamma}_j^\dagger - \frac{1}{2} \{ \hat{\Gamma}_j^\dagger \hat{\Gamma}_j, \hat{\rho} \} \right], \quad (6.82)$$

where  $\hat{\Gamma}_j$  denotes a dissipation operator that acts on the site  $j$ , and  $\gamma$  is the strength of dissipation (see Chapter 4). We consider a dissipative spin-1/2 model in one dimension (see Fig. 6.8(a)). The Lindblad superoperator [326] above consists of the Hamiltonian

$$\hat{H} = - \sum_{j=1}^{L-1} (1 + \epsilon_j) \hat{\sigma}_j^z \hat{\sigma}_{j+1}^z - \sum_{j=1}^L \left( -1.05 \hat{\sigma}_j^x + 0.2 \hat{\sigma}_j^z \right), \quad (6.83)$$

where  $\epsilon_j$  is randomly chosen from  $[-0.1, 0.1]$ , and dissipation that is either (i) dephasing

$$\hat{\Gamma}_j = \hat{\sigma}_j^z \quad (6.84)$$

or (ii) damping

$$\hat{\Gamma}_j = \hat{\sigma}_j^-. \quad (6.85)$$

This model can be realized with Rydberg atoms [327].

Instead of the eigenvalue equation of the Hamiltonian, we consider the supereigenvalue equation for the Lindblad superoperator,

$$\mathcal{L}[\hat{v}_\alpha] = \eta_\alpha \hat{v}_\alpha, \quad (6.86)$$

where  $\eta_\alpha$  is the supereigenvalue for the supereigenstate  $\hat{v}_\alpha$ . To know the symmetry of the Lindblad superoperator, it is convenient to employ the operator representation of superoperators. This can be done by considering the following isomorphism:

$$\hat{A} |i\rangle \langle j| \hat{B} \rightarrow (\hat{A} \otimes \hat{B}^T) |i\rangle \otimes |j\rangle, \quad (6.87)$$

where we have duplicated the Hilbert space by introducing a dual space.

The Lindblad superoperator can then be written as

$$\mathcal{L} \rightarrow \hat{\mathcal{L}} = -i(\hat{H} \otimes \mathbb{I} - \hat{\mathbb{I}} \otimes \hat{H}^T) + \gamma \sum_{j=1}^L \left[ \hat{\Gamma}_j \otimes \hat{\Gamma}_j^* - \frac{1}{2} \hat{\Gamma}_j^\dagger \hat{\Gamma}_j \otimes \hat{\mathbb{I}} - \hat{\mathbb{I}} \otimes \hat{\Gamma}_j^T \hat{\Gamma}_j^* \right], \quad (6.88)$$

whose eigenvalues equal  $\lambda_\alpha$ .

For any  $\hat{\Gamma}_j$ ,  $\hat{\mathcal{L}}$  has TRS whose square equals one. In fact, if we consider the "SWAP" unitary operator  $\hat{\mathcal{T}}_+$  which exchanges the original and the dual Hilbert spaces, i.e.,

$$\hat{\mathcal{T}}_+(\hat{A} \otimes \hat{B})\hat{\mathcal{T}}_+^{-1} = \hat{B} \otimes \hat{A}, \quad (6.89)$$

we obtain

$$\hat{\mathcal{T}}_+ \hat{\mathcal{L}}^* \hat{\mathcal{T}}_+^{-1} = \hat{\mathcal{L}} \quad (6.90)$$

along with

$$\hat{\mathcal{T}}_+ \hat{\mathcal{T}}_+^* = 1. \quad (6.91)$$

In addition, for our model,  $\hat{\mathcal{L}}$  can have TRS<sup>†</sup> depending on the dissipator  $\hat{\Gamma}_j$ . In fact, since  $\hat{H} = \hat{H}^T$  (in the Fock basis), we have

$$\hat{\mathcal{L}}^T = -i(\hat{H} \otimes \mathbb{I} - \hat{\mathbb{I}} \otimes \hat{H}^T) + \gamma \sum_{j=1}^L \left[ \hat{\Gamma}_j^T \otimes \hat{\Gamma}_j^\dagger - \frac{1}{2} \hat{\Gamma}_j^T \hat{\Gamma}_j^* \otimes \hat{\mathbb{I}} - \hat{\mathbb{I}} \otimes \hat{\Gamma}_j^\dagger \hat{\Gamma}_j \right]. \quad (6.92)$$

Hence, if

$$\hat{\Gamma}_j^T = \hat{\Gamma}_j \quad \text{and} \quad (\hat{\Gamma}_j^\dagger \hat{\Gamma}_j)^T = \hat{\Gamma}_j^\dagger \hat{\Gamma}_j, \quad (6.93)$$

the transposition remains, i.e.,  $\hat{\mathcal{L}}^T = \hat{\mathcal{L}}$ . This condition is satisfied only for (i) dephasing  $\hat{\Gamma}_j = \hat{\sigma}_j^z$  and not for (ii) damping  $\hat{\Gamma}_j = \hat{\sigma}_j^-$ .

We show in Fig. 6.8(b) the level-spacing distributions  $p(s)$  for the two models (i) and (ii). It is evident that, while model (i) obeys the universality of the class AI<sup>†</sup>, model (ii) obeys the universality of the class A. These results demonstrate that local correlations of (super)eigenvalues of nonintegrable dissipative Lindblad superoperator are also described by the universality of non-Hermitian random matrices considering TRS<sup>†</sup>. Note that the additional TRS (the swap symmetry) is irrelevant for the level-spacing distribution away from the real axis because it only creates nonlocal pairs of eigenvalues.

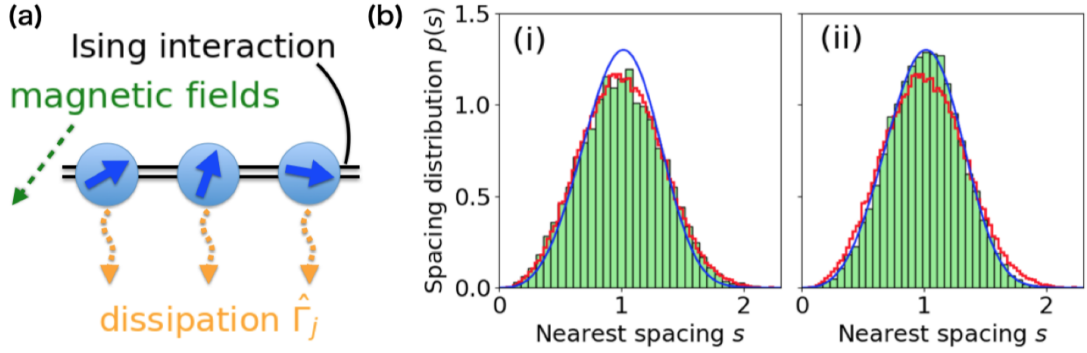


Figure 6.8: (a) Schematic figure of a locally interacting system governed by the Lindblad equation in Eq. (6.83). (b) Level-spacing distributions  $p(s)$  for two different types of dissipators (Eq. (6.84) for (i) and Eq. (6.85) for (ii)) after the unfolding procedure of eigenvalues. The blue and red lines are the results for the classes A and  $AI^\dagger$ , respectively (for the class  $AI^\dagger$ , we show the same numerical data obtained in Fig. 6.3(B)). We obtain the results from averages over 10 samples with  $\gamma = 0.5$  and  $L = 7$ . We obtain the statistics from eigenvalues that are away from the edges of the spectrum. Taken from Fig. 3 in the fourth version of Ref. [112].

## 6.7 Discussions

We have studied the universality classes of the level-spacing distributions of non-Hermitian random matrices with symmetry. We numerically found that the symmetry classes  $AI^\dagger$  and  $AII^\dagger$  lead to new universality classes that are distinct from the GinUE. Thus, the three classes A,  $AI^\dagger$  and  $AII^\dagger$  defined by transposition symmetry ( $TRS^\dagger$ ) are considered as a natural non-Hermitian extension of Dyson's threefold way for Hermitian matrices.

As we have seen in Section 6.3, there are 38 symmetry classes in non-Hermitian matrices. On the other hand, it is expected that there are only three universality classes for  $p(s)$ , determined by the transposition symmetry ( $TRS^\dagger$ ). This is because the other fundamental symmetries (such as TRS and PHS) do not alter the interactions between neighboring eigenvalues. One of the examples is our study of the level-spacing distributions in the Lindblad spectrum, where the TRS (swap operator) is irrelevant for  $p(s)$ .

Our results will be the basis for probing nonintegrability and chaos in dissipative quantum systems with symmetry. As we have seen in the previous chapter, in non-Hermitian disordered systems, level-spacing distributions change from the random-matrix distribution to the Poisson distribution. In particular,

for the delocalized phase,  $p(s)$  for the gain-loss model is distinct from that for the asymmetric-hopping model. Our results clearly show that this distinction results from the presence of the TRS<sup>†</sup>, and not owing to a finite-size effect or the presence of hidden integrability.

# Chapter 7

## Conclusions and Outlook

In this Thesis, we have discussed some problems on thermalization in closed and open quantum many-body systems. As discussed in Chapter 1, problems of thermalization are deeply related to the foundations of quantum statistical mechanics, and attract extensive attention motivated by experiments in artificial quantum many-body systems represented by ultracold atoms.

In Chapter 2, we have reviewed basic properties on thermalization in closed quantum many-body systems. We have first shown that a quantum state after a sufficiently long time is locally described by a thermal ensemble under the assumption of the eigenstate thermalization hypothesis (ETH). The ETH is expected in many nonintegrable systems, which is also related to random matrix theory. On the other hand, the ETH and thermalization does not hold true for several classes of systems, such as the many-body localized (MBL) systems. We have also briefly mentioned recent study of dynamics in closed quantum systems before complete thermalization.

In Chapter 3, revisiting von Neumann's work, we have discussed the validity of the typicality argument, which relies on the Haar measure, for the physically relevant setting, *i.e.*, few-body (or local) setting. We rigorously show that diagonal matrix elements of most few-body observables behave atypically when the energy width decreases at most algebraically with increasing the system size. This result indicates that we need a scenario which does not rely on the typicality argument in order to explain the ETH.

One interesting future question is to investigate the relaxation dynamics before complete thermalization in few-body or local settings. Recently, it has been proposed that relaxation dynamics of quantum many-body systems may be understood by the typicality argument without few-body (local) structures [328].

Such a treatment predicts extremely fast decay of observables whose timescale does not depend on the system size, which is inconsistent with usual thermalization [329] but may explain local thermalization of the system [328].

On the other hand, since the information of the entire system cannot be perceived during the fast timescale owing to the Lieb-Robinson bound (for a local setting), invoking the typicality argument, which relies on the unitary Haar measure of the entire Hilbert space within the energy shell, may be inappropriate. It remains to be a challenge to rigorously investigate an atypical structure that is distinct from the prediction of the typicality argument for the relaxation dynamics in few-body or local settings. For that purpose, the random few-body and local operator measures that we have introduced in Chapter 3 (see Eqs. (3.29) and (3.49)) can be helpful.

In Chapter 4, we have reviewed theory of open quantum systems. We have first explained repeatedly or continuously measured quantum systems, which are now being realized using state-of-the-art experiments, such as those of ultracold atoms. As an interesting ingredient for such continuously measured quantum systems, properties of non-Hermitian Hamiltonians have been discussed in detail. We have also discussed previous studies on thermalization of open quantum many-body systems, which are nontrivially driven by external dissipation and cannot be understood by conventional theories.

In Chapter 5, we have discussed how the MBL can change the spectral and dynamical properties of open quantum many-body systems described by non-Hermitian Hamiltonians. We have shown that the imaginary part of many-body energy eigenvalues is suppressed owing to the MBL if the system respects time-reversal symmetry (TRS). In particular, we have found that non-Hermitian MBL in an interacting model with asymmetric hopping and disorder leads to a novel real-complex transition of eigenvalues, which affects dynamical stability of the system. We have also argued that the non-Hermitian MBL still occurs but the real-complex transition is absent in a system without TRS, such as a system with gain and loss.

One of the most important future research arenas is to study how we can extend the fundamental notions of thermalization in closed systems to open quantum systems. For example, the presence of the recurrence depends on whether the system is non-Hermitian MBL or not, in a manner similar to the Hermitian case. On the other hand, there have been yet no well-defined definitions for some concepts, *e.g.*, ergodicity, since stationary states are not thermal. Note, however,

that some features of non-Hermitian MBL remind us of non-ergodicity. For instance, while the initial information of the state is eventually lost for the complex-eigenenergy phase, it is not in the real-eigenenergy phase, the latter of which is reminiscent of the non-ergodicity in the Hermitian MBL. It is an open question to unambiguously formulate the ergodicity in dissipative quantum systems. We also note that it is also an important future problem to take quantum jumps into account, which may affect the purely non-Hermitian description of the dynamics.

In Chapter 6, we have studied fundamental universality classes of non-Hermitian random matrices and its application to open quantum many-body systems, encouraged by the relation between thermalization and random matrix theory in Hermitian systems. We have numerically shown that two new universality classes of level-spacing distributions, which are distinct from Ginibre's universality classes, appear if we consider transposition symmetry. We have argued that our results will be a probe for the nonintegrability, delocalization and chaos in open quantum systems with symmetry, such as the dissipative many-body spin systems described by the Lindblad equation and the non-Hermitian Hamiltonian.

One of the fundamental issues to be solved is joint probability distributions of eigenvalues for these classes for an arbitrary matrix size. It is also important to study if a new universality appears for other statistics, such as distributions of the edges of the spectrum. As applications, it is interesting to test our universalities for various systems, such as classical stochastic systems and open mesoscopic systems as well as dissipative quantum many-body systems. A related challenging problem is to find an experimentally observable quantity that reflects the three universality classes. From the viewpoint of thermalization, it merits further study to elucidate how the random-matrix-type level-spacing distribution is related to the dynamics in open quantum many-body systems, just as it is related to the relaxation to the thermal state (owing to the ETH) in the Hermitian case.

To summarize, this Thesis is devoted to some of the problems of thermalization in quantum many-body systems: the atypicality of few-body observables, which requires a new scenario to explain the ETH, the occurrence of many-body localization in non-Hermitian systems, and the universality of non-Hermitian matrices relevant for open quantum systems. We hope that our work will motivate further researches to study foundations of nonequilibrium statistical mechanics.

# Appendix A

## Details of Chapter 5

In this appendix, we explain details of Chapter 5, in particular the results for different parameters, models, and probes for the transition and the discussions on the similarity transformation.

### A.1 Results for other models and parameters

Here, we discuss real-complex phase transitions and MBL for different values of the parameters and models from those introduced in Chapter 5.

#### A.1.1 Real-complex transition for stronger non-Hermiticity $g$

We find the real-complex transition even in systems with non-Hermiticity stronger than that discussed previously, *e.g.*,  $g = 1$ , in Eq. (5.6). We show in Fig. A.1 how  $f_{\text{Im}}$  depends on  $h$  for different sizes of the system with  $g = 1$ . As  $L$  is increased,  $f_{\text{Im}}$  increases for  $h \lesssim h_c^{\text{R}} \simeq 16$  and decreases for  $h \gtrsim h_c^{\text{R}}$ . Moreover, we observe the scaling collapse around the critical point with a critical exponent  $\nu = 0.7$ . This transition point is different from that of the Hermitian counterpart ( $g = 0$ ) and is dependent on the non-Hermiticity  $g$ .

The non-Hermitian MBL transition occurs for  $g = 1$ , too. We show in Fig. A.1(b) the level-spacing distribution of energy eigenvalues, which are unfolded on the complex plane ( $h = 8$ ), and that of energy eigenvalues on the real axis ( $h = 20$ ) with  $L = 16$ . When  $h = 8$ ,  $P(s)$  obeys a Ginibre statistics  $P_{\text{Gin}}^{\text{C}}(s)$ , not a Poisson statistics  $P_{\text{Po}}^{\text{C}}(s) = \pi s e^{-\pi s^2/4}/2$  on the complex plane. When  $h = 20$ ,  $P(s)$  obeys a Poisson statistics on the real axis  $P_{\text{Po}}^{\text{R}}(s) = e^{-s}$ , rather than the Wigner-Dyson statistics  $P_{\text{WD}}^{\text{R}}(s) = \pi s e^{-\pi s^2/4}/2$ . This behavior is analogous to the case for

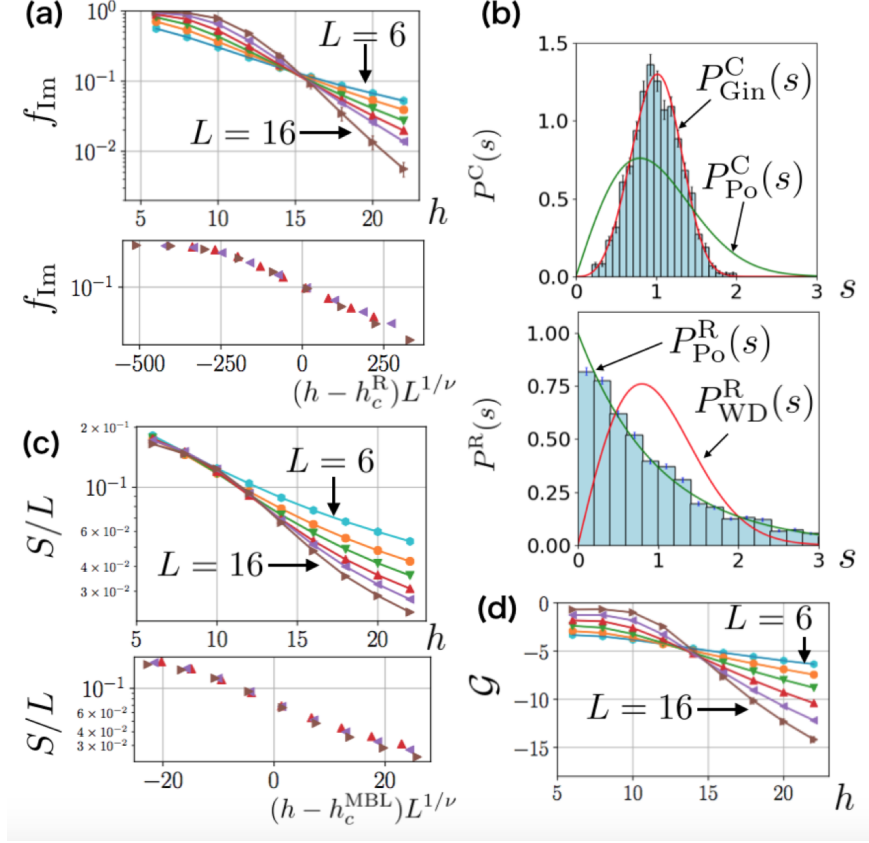


Figure A.1: Indicators of the real-complex transition and the MBL transition in the model with asymmetric hopping for  $g = 1$ . (a) Dependence of the fraction  $f_{\text{Im}}$  on the disorder strength  $h$  for  $L = 6, 8, 10, 12, 14$ , and  $16$ . (b) Level-spacing distribution of unfolded energy eigenvalues on the complex plane ( $h = 8$ ) and that of energy eigenvalues on the real axis ( $h = 20$ ) with  $L = 16$ . We take statistics from energy eigenvalues that lie within  $\pm 10\%$  in the middle of the spectrum with respect to real and imaginary parts. (c) Half-chain entanglement entropy  $S/L$  calculated from the average of  $S_\alpha/L$  over disorder and eigenstates whose energy eigenvalues are within  $\pm 2\%$  in the middle of the spectrum with respect to the real parts. We also find the scaling collapse around the critical point, where  $h_c^{\text{MBL}} = 13.5$  and  $\nu = 2.5$ . (d) Eigenstate stability  $\mathcal{G}$  for different sizes of the system, where  $\hat{V}_{\text{NH}} = \hat{b}_i^\dagger \hat{b}_{i+1}$ . For (a), (c), and (d), we have used  $N_{\text{sam}} = 10000$  for  $L = 6, 8, 10, 12$ ,  $N_{\text{sam}} = 1000$  for  $L = 14$ , and  $N_{\text{sam}} = 100$  for  $L = 16$ . Reproduced from Fig. A-1 of Ref. [111]. ©2019 American Physical Society.

the weak non-Hermitian case, *i.e.*,  $g = 0.1$ .

We can also discuss the entanglement entropy  $S$  for the right eigenstates. In Fig. A.1(c), we show how  $S_\alpha/L$  averaged over the eigenstates in the middle of the spectrum depends on  $L$ . We can confirm a crossover of  $S$  from the volume law to the area law for  $h \simeq h_c^{\text{MBL}}$  for  $g = 1$  as well. We also observe the scaling collapse around the critical point by rewriting the entropy as a function of  $(h - h_c^{\text{MBL}})L^{1/\nu}$ , where  $h_c^{\text{MBL}} = 13.5$  and  $\nu = 2.5$ .

Figure A.1(d) shows how  $\mathcal{G}$  depends on  $h$ . We find that  $\mathcal{G} \sim \alpha L$  ( $\alpha > 0$ ) and  $\mathcal{G} \sim -\beta L$  ( $\beta > 0$ ) for the delocalized and localized phases, respectively. The non-Hermitian MBL transition point is determined as  $h_c^{\text{MBL}} \simeq 14$  from the point at which  $\mathcal{G}$  becomes independent of  $L$ . This point is close to  $h_c^{\text{R}} \simeq 16$  for  $g = 1$ , where the small deviation is expected to arise because of a finite-size effect.

## A.1.2 Real-complex transition as a function of non-Hermiticity

$g$

Next, we consider varying  $g$  instead of  $h$  for the Hamiltonian in Eq. (5.6) and investigate the real-complex transition point  $g_c^{\text{R}}$ . In Fig. A.2(a), we show how  $f_{\text{Im}}$  and  $\Delta_{\text{Im}}$  depend on  $g$  for  $h = 2 < h_{0c}^{\text{MBL}}$ , where  $\Delta_{\text{Im}}$  is the maximum imaginary values of energy eigenvalues defined by Eq. (A.2) (explained later in this Appendix). Both  $f_{\text{Im}}$  and  $\Delta_{\text{Im}}$  increase with  $L$  increased for all  $g$ . In addition, the figure indicates that this behavior holds for infinitesimally small  $g$ , meaning that  $g_c^{\text{R}} = 0$  for  $h = 2$ .

In Fig. A.2(b), we also show how  $f_{\text{Im}}$  and  $\Delta_{\text{Im}}$  depend on  $g$  for  $h = 18 > h_{0c}^{\text{MBL}}$ . Both  $f_{\text{Im}}$  and  $\Delta_{\text{Im}}$  increase for  $g \gtrsim 2$  and decrease for  $g \lesssim 2$  with  $L$  increased. This implies that the real-complex transition occurs at  $g_c^{\text{R}} \simeq 2$  for  $h = 18$  in the thermodynamic limit. We have in general  $g_c^{\text{R}} > 0$  only for  $h > h_{0c}^{\text{MBL}}$  in this system.

## A.1.3 Case with quarter-filling

Here, we show that the model with the quarter-filling, *i.e.*,  $L = 4M$  shows the MBL and the real-complex transitions as well. Figure A.3 illustrates that both the real-complex phase transition (with respect to  $f_{\text{Im}}$ ) and the MBL transition (with respect to  $\mathcal{G}$ ) occur. These two transition points are close to each other (near  $h \simeq 6$ ), where a small deviation is presumably due to a finite-size effect.

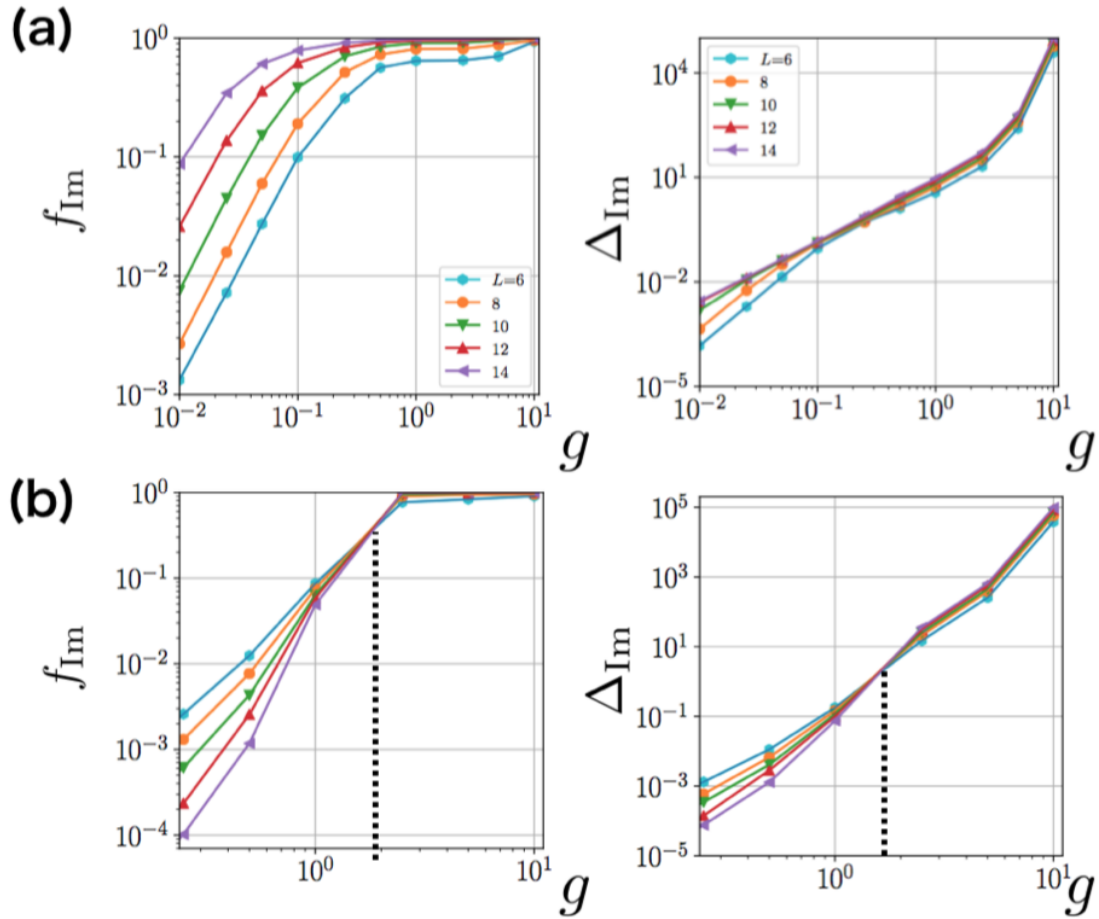


Figure A.2: Dependences of  $f_{\text{Im}}$  and  $\Delta_{\text{Im}}$  on the non-Hermiticity  $g$  for the Hamiltonian in Eq. (5.6) (a) in the weak-disorder case ( $h = 2 < h_{0c}^{\text{MBL}}$ ) and (b) in the strong-disorder case ( $h = 18 > h_{0c}^{\text{MBL}}$ ). Reproduced from Fig. A-2 of Ref. [111]. ©2019 American Physical Society.

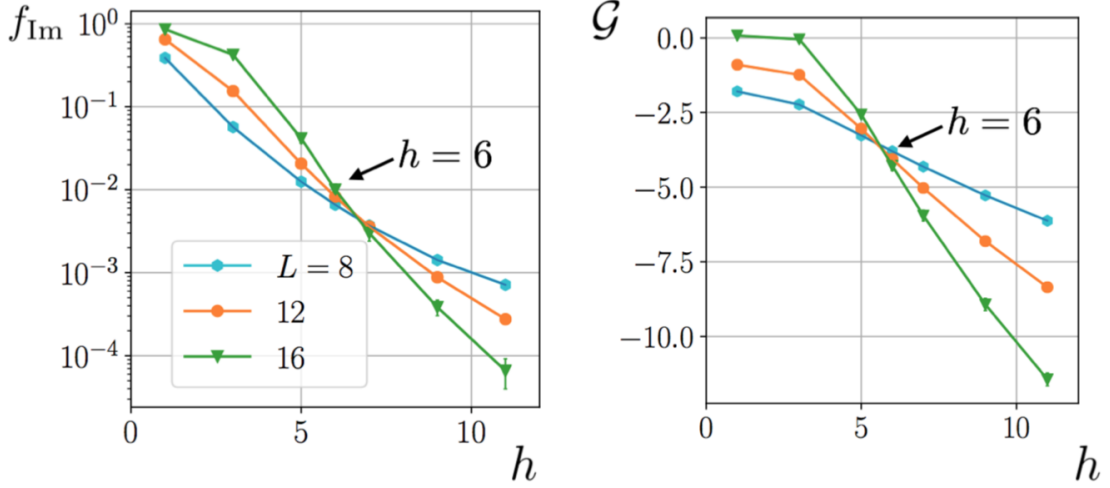


Figure A.3: Dependences of  $f_{\text{Im}}$  and  $\mathcal{G}$  on disorder strength in the case of the quarter filling, *i.e.*,  $L = 4M$ . We use  $N_{\text{sam}} = 10000$  for  $L = 8, 12$ , and  $N_{\text{sam}} = 100$  for  $L = 16$ . Reproduced from Fig. A-3 of Ref. [111]. ©2019 American Physical Society.

#### A.1.4 Real-complex transition for the Bose-Hubbard model with asymmetric hopping

Here, we consider the real-complex transition of many-body energy eigenvalues for the Bose-Hubbard model with disorder and asymmetric hopping [330], instead of hard-core bosons. The Hamiltonian reads

$$\hat{H}_{\text{BH}} = -J \sum_{i=1}^L (e^{-g} \hat{a}_{i+1}^\dagger \hat{a}_i + e^g \hat{a}_i^\dagger \hat{a}_{i+1}) + \frac{U}{2} \sum_{i=1}^L \hat{n}'_i (\hat{n}'_i - 1) + \sum_{i=1}^L h_i \hat{n}'_i, \quad (\text{A.1})$$

where  $\hat{n}'_i = \hat{a}_i^\dagger \hat{a}_i$  is the number operator at site  $i$  and  $\hat{a}_i$  is the bosonic annihilation operator at site  $i$ . Again, we consider  $J = 1$ ,  $U = 2$ , and  $M = L/2$  with the periodic boundary condition.

Figure A.4 illustrates the  $h$ -dependence of the fraction  $f_{\text{Im}}$  of complex energy eigenvalues. We find the occurrence of the real-complex transition at a disorder strength  $h_c^{\text{R}}$ , just as the case for hard-core bosons. In fact, as we increase the size of the system  $L$ , the fraction  $f_{\text{Im}}$  of complex energy eigenvalues increases for  $h \lesssim h_c^{\text{R}}$  and decreases for  $h \gtrsim h_c^{\text{R}}$ , where the critical point is  $h_c^{\text{R}} \simeq 10$  for  $g = 0.1$  and  $h_c^{\text{R}} \simeq 17$  for  $g = 1$ . We note that the size of the system in numerical simulations that is achievable is smaller for the Bose-Hubbard model than the case for hard-core bosons, since there can be arbitrary numbers of bosons in each site.

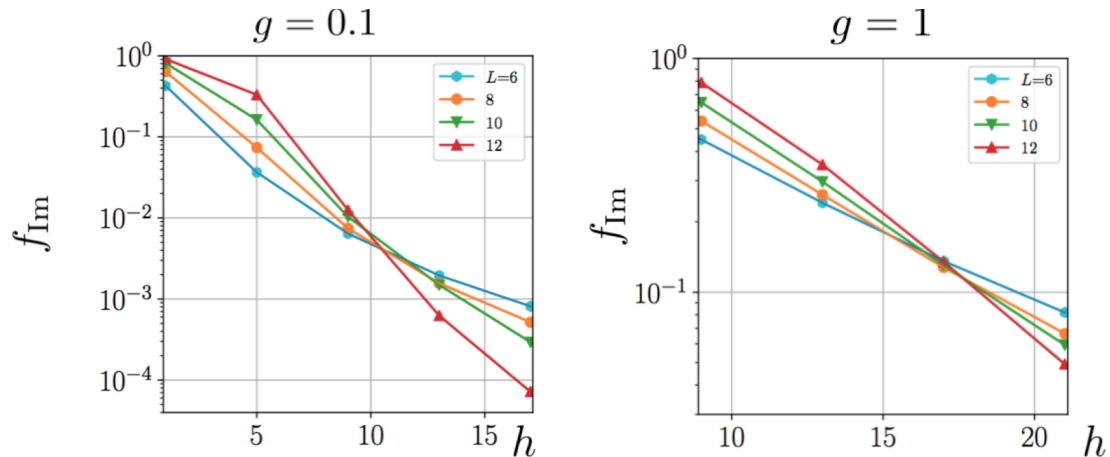


Figure A.4: Real-complex phase transition of the Bose-Hubbard system in Eq. (A.1) with respect to the disorder strength  $h$  for  $g = 0.1$  (left) and  $1$  (right). We show the data for  $f_{\text{Im}}$  averaged over  $N_{\text{sam}}$  samples, where  $N_{\text{sam}} = 10000$  for  $L = 6, 8$ ,  $N_{\text{sam}} = 1000$  for  $L = 10$ , and  $N_{\text{sam}} = 100$  for  $L = 12$ . Reproduced from Fig. A-4 of Ref. [111]. ©2019 American Physical Society.

## A.2 Other probes to characterize the transitions

Here we investigate other probes to determine the real-complex or MBL transitions.

### A.2.1 Maximum imaginary values

We have discussed the fraction  $f_{\text{Im}}$  of complex energy eigenvalues. On the other hand, we can instead define the maximum imaginary part  $\Delta_{\text{Im}}$  among energy eigenvalues as another measure of the real-complex transition. This is defined as

$$\Delta_{\text{Im}} = \overline{\max_{\alpha} |\text{Im}[E_{\alpha}]|}, \quad (\text{A.2})$$

where  $E_{\alpha}$  is an energy eigenvalue of  $\hat{H}$ .

The quantity  $\max_{\alpha} |\text{Im}[E_{\alpha}]|$  is relevant for the dynamical stability of non-Hermitian Hamiltonians; as the imaginary part of energy eigenvalues corresponds to the rate of amplification or decay of that mode, the system is stable for  $t \lesssim [\max_{\alpha} |\text{Im}[E_{\alpha}]|]^{-1}$ . We note that the transition point for  $\Delta_{\text{Im}}$  can be different from that for  $f_{\text{Im}}$  and the non-Hermitian MBL in general.

Figure A.5 shows how  $\Delta_{\text{Im}}$  depends on  $h$  for different sizes  $L$  with asymmetric hopping (Eq. (5.6)) or with gain and loss (Eq. (5.29)). For the former model,  $\Delta_{\text{Im}}$  increases slowly and exhibits saturation with increasing  $L$  for  $h \lesssim 8$  ( $g = 0.1$ ) or

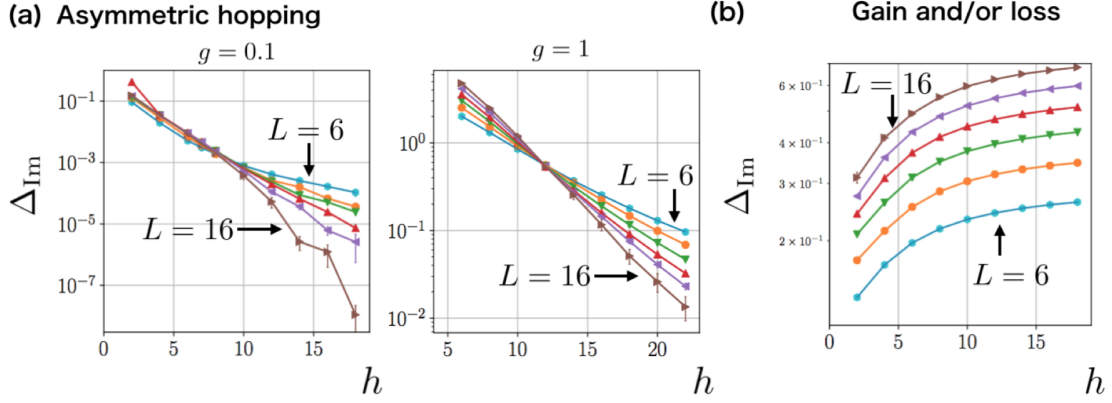


Figure A.5: Maximum imaginary part of energy eigenvalues. (a) The model with asymmetric hopping for two values of  $g$  in Eq. (5.6). (b) The model with gain and loss ( $\gamma = 0.1$ ) in Eq. (5.29). For both (a) and (b) we have used  $N_{\text{sam}} = 10000$  for  $L = 6, 8, 10, 12$ ,  $N_{\text{sam}} = 1000$  for  $L = 14$ , and  $N_{\text{sam}} = 100$  for  $L = 16$ . Reproduced from Fig. A-5 of Ref. [111]. ©2019 American Physical Society.

$h \lesssim 12$  ( $g = 1$ ), while it decreases rapidly for  $h \gtrsim 8$  ( $g = 0.1$ ) or  $h \gtrsim 12$  ( $g = 1$ ). This implies that a real-complex transition is present even for the measure of  $\Delta_{\text{Im}}$ . On the other hand, for the latter model,  $\Delta_{\text{Im}}$  decreases monotonically for all  $h$  as we increase  $L$ , which implies that the real-complex transition is absent. We note that the critical value of  $\Delta_{\text{Im}}$  for the asymmetric-hopping model differs from  $h_c^{\text{R}}$  and  $h_c^{\text{MBL}}$  for this finite size of the system, in particular for  $g = 1$ . The precise determination of the transition points for large  $L$  is left as a future challenge.

## A.2.2 Entanglement and eigenstate stability as functions of the size of the system

In Chapter 5, the results of the entanglement entropy  $S/L$  and the eigenstate stability  $\mathcal{G}$  have been shown as functions of  $h$  for different sizes of the system. In Fig. A.6, we instead illustrate  $S/L$  and  $\mathcal{G}$  as functions of  $L$  for different  $h$ . We can read out the MBL transition point ( $h_c^{\text{MBL}} \simeq 7$ ) from the change from the volume ( $S/L \sim \text{const}$ ) to the area laws ( $S/L \propto 1/L$ ) for the entanglement and from  $\mathcal{G} \sim \alpha L$  to  $\sim -\beta L$  ( $\alpha, \beta > 0$ ) for the eigenstate stability.

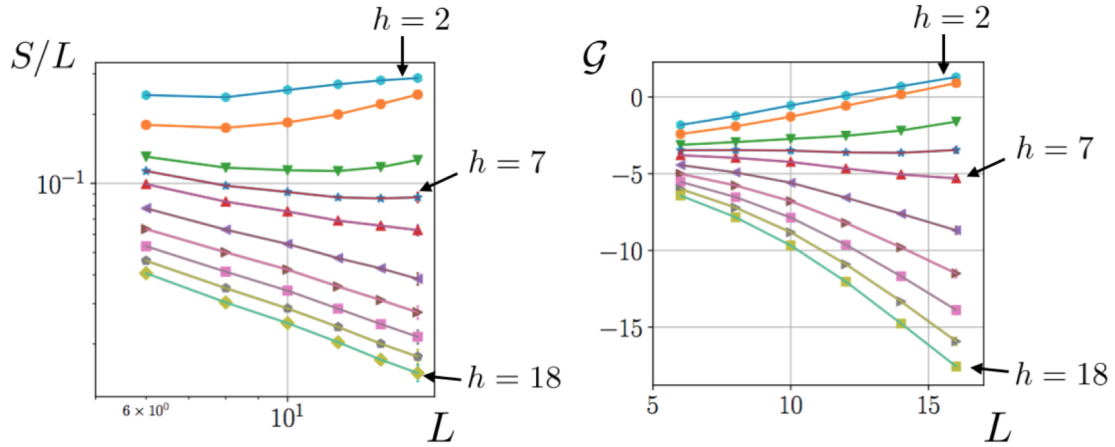


Figure A.6: Half-chain entanglement entropy  $S/L$  and eigenstate stability  $\mathcal{G}$  for different values of  $h$  as functions of  $L$ . Note that we use the same data in Figs. 5.5(b) and (c) in Chapter 5. Reproduced from Fig. A-6 of Ref. [111]. ©2019 American Physical Society.

### A.2.3 Standard deviation of entanglement

Here, we discuss the standard deviation  $\sigma$  of the (normalized) half-chain entanglement entropy  $S/L$  averaged over samples. This quantity is expected to exhibit a peak around the critical point for the Hermitian MBL ( $g = 0$ ) [170]. We show in Fig. A.7 that there appears a peak at a disorder strength ( $h \simeq 6$ ) which is not far from the MBL transition point if we consider the case for the weak non-Hermiticity ( $g = 0.1$ ). However, no peak appears for the stronger non-Hermiticity ( $g = 1$ ), in contrast with the Hermitian case [170] or the weak non-Hermitian case. The result indicates that the standard deviation of the entanglement should not be used as a measure of the MBL transition, in particular in the presence of large non-Hermiticity. We leave it as a future work to investigate the origin of this unconventional behavior for the large non-Hermiticity.

## A.3 Similarity transformation of the Hamiltonian with interaction and asymmetric hopping

The fact that the coalescence between neighboring eigenstates is absent owing to the non-Hermitian MBL is not a sufficient condition for a complete suppression of complex energy eigenvalues. Indeed, some (but rare) spatial regions can be reso-

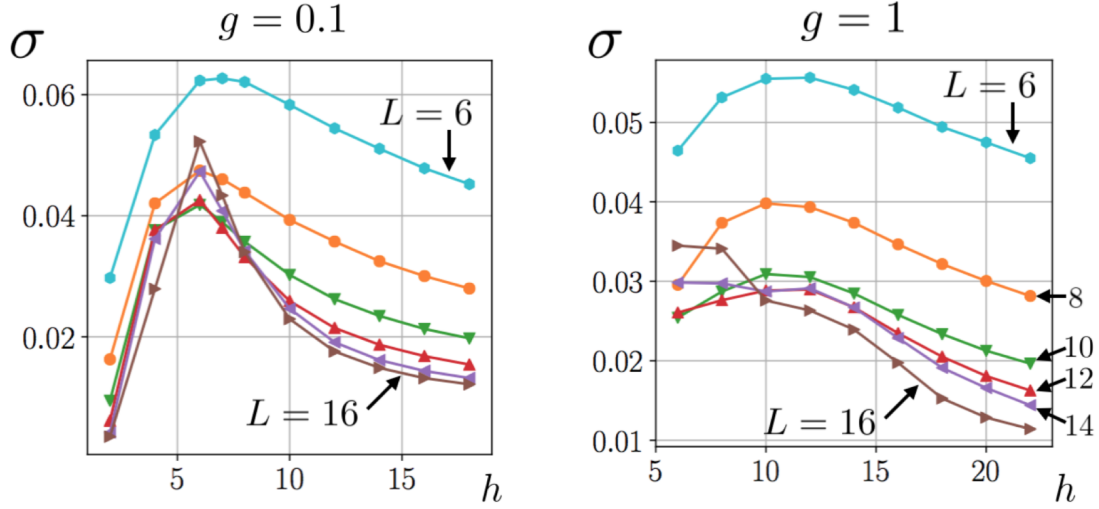


Figure A.7: Standard deviation  $\sigma$  of the normalized half-chain entanglement entropy for different system sizes  $L$  ( $= 6, 8, 10, 12, 14, 16$ ) over samples as a function of disorder strength  $h$ . We have used  $N_{\text{sam}} = 10000$  for  $L = 6, 8$ ,  $N_{\text{sam}} = 1000$  for  $L = 10$ , and  $N_{\text{sam}} = 100$  for  $L = 12$ . Reproduced from Fig. A-7 of Ref. [111]. ©2019 American Physical Society.

nant and susceptible to local perturbations [186, 187, 179, 180] because of statistical fluctuations of disorder, which leads to the possibility that non-adjacent eigenstates mix and form complex-conjugate pairs. In such regions, we should treat effects of non-Hermiticity non-perturbatively in general because the perturbation resonantly couples two different eigenstates.

On the other hand, for the asymmetric-hopping model in Eq. (5.6), we can consider a similarity transformation [235, 236, 237, 298, 299] such that the non-Hermitian perturbation is only supported on non-resonant regions. From an analysis of this transformed Hamiltonian, we find that the eigenstate-mixing is suppressed even for non-adjacent eigenstates, which leads to the emergence of the entirely real spectrum as explained in the following

To simplify the discussion, we consider the hard-core Boson Hamiltonian  $\hat{H}$  in Eq. (5.6) for sufficiently small  $g$ . We consider the decomposition of the Hamiltonian, *i.e.*,  $\hat{H} = \hat{H}_0 + \hat{V}_{\text{NH}}$ , where

$$\hat{H}_0 = \sum_{i=1}^L \left[ -J(\hat{b}_{i+1}^\dagger \hat{b}_i + \text{h.c.}) + U \hat{n}_i \hat{n}_{i+1} + h_i \hat{n}_i \right] \quad (\text{A.3})$$

is a Hermitian Hamiltonian and

$$\hat{V}_{\text{NH}} = -J \sum_{i=1}^L [(e^{-g} - 1)\hat{b}_{i+1}^\dagger \hat{b}_i + (e^g - 1)\hat{b}_i^\dagger \hat{b}_{i+1}] = \sum_{i=1}^L \hat{v}_{i,i+1} \quad (\text{A.4})$$

is a non-Hermitian Hamiltonian for  $g \neq 0$ . When  $\hat{H}_0$  is localized with large  $h$ , the local tunneling amplitude  $|\langle \mathcal{E}_b | \hat{v}_{i,i+1} | \mathcal{E}_a \rangle|$  by the perturbation  $\hat{v}_{i,i+1}$  is smaller than  $|\mathcal{E}_a - \mathcal{E}_b|$  for most  $i$ , where the two eigenstates  $|\mathcal{E}_a\rangle$  and  $|\mathcal{E}_b\rangle$  are assumed to be approximately written as product states and connected by terms  $\hat{b}_{i+1}^\dagger \hat{b}_i$  and  $\hat{b}_i^\dagger \hat{b}_{i+1}$ , which describe the hopping of the particles. This is due to the fact that moving particles within the localized regions costs large energy (*i.e.*,  $|\mathcal{E}_a - \mathcal{E}_b| \sim |h_{i+1} - h_i|$  is large enough). Therefore, we can deal with the effect of  $\hat{v}_{i,i+1}$  perturbatively. However, for some (but rare)  $i$ , localization can be very weak because of the statistical fluctuation of  $h_i$  and particles are relatively easy to move. This leads to  $|\langle \mathcal{E}_b | \hat{v}_{i,i+1} | \mathcal{E}_a \rangle| \simeq |\mathcal{E}_a - \mathcal{E}_b|$ . Thus, the perturbation owing to such resonant  $i$ , cannot be controlled for the original model.

Fortunately, we can show that the Hamiltonian in Eq. (5.6) is transformed into a Hamiltonian whose non-Hermitian perturbation is only supported on the regions that are not resonant. To see this, we consider

$$\hat{\mathcal{V}}_i = e^{g\theta_i \hat{n}_i} = 1 + (e^{g\theta_i} - 1)\hat{n}_i. \quad (\text{A.5})$$

We have

$$\begin{aligned} \hat{\mathcal{V}}_i \hat{b}_i \hat{\mathcal{V}}_i^{-1} &= \hat{b}_i [1 + (e^{-g\theta_i} - 1)\hat{n}_i] \\ &= \hat{b}_i + (e^{-g\theta_i} - 1)(1 - 2\hat{n}_i)\hat{b}_i \\ &= e^{-g\theta_i} \hat{b}_i, \end{aligned} \quad (\text{A.6})$$

where the relations  $\{\hat{b}_i, \hat{b}_i^\dagger\} = 1$  and  $\hat{b}_i^2 = 0$  for hard-core bosons have been used. Similarly, we have

$$\begin{aligned} \hat{\mathcal{V}}_i \hat{b}_i^\dagger \hat{\mathcal{V}}_i^{-1} &= [1 + (e^{g\theta_i} - 1)\hat{n}_i] \hat{b}_i^\dagger \\ &= \hat{b}_i^\dagger + (e^{g\theta_i} - 1)\hat{b}_i^\dagger (1 - 2\hat{n}_i) \\ &= e^{g\theta_i} \hat{b}_i^\dagger. \end{aligned} \quad (\text{A.7})$$

We then obtain

$$\hat{\mathcal{V}}_{i+1} \hat{\mathcal{V}}_i \hat{b}_{i+1}^\dagger \hat{b}_i \hat{\mathcal{V}}_i^{-1} \hat{\mathcal{V}}_{i+1}^{-1} = e^{g(\theta_{i+1}-\theta_i)} \hat{b}_{i+1}^\dagger \hat{b}_i, \quad (\text{A.8})$$

$$\hat{\mathcal{V}}_{i+1} \hat{\mathcal{V}}_i \hat{b}_i^\dagger \hat{b}_{i+1} \hat{\mathcal{V}}_i^{-1} \hat{\mathcal{V}}_{i+1}^{-1} = e^{-g(\theta_{i+1}-\theta_i)} \hat{b}_i^\dagger \hat{b}_{i+1}, \quad (\text{A.9})$$

$$\hat{\mathcal{V}}_i \hat{n}_i \hat{\mathcal{V}}_i^{-1} = \hat{n}_i, \quad (\text{A.10})$$

$$\hat{\mathcal{V}}_{i+1} \hat{\mathcal{V}}_i \hat{n}_{i+1} \hat{n}_i \hat{\mathcal{V}}_i^{-1} \hat{\mathcal{V}}_{i+1}^{-1} = \hat{n}_{i+1} \hat{n}_i. \quad (\text{A.11})$$

We now consider a similarity transformation

$$\hat{H}' = \hat{\mathcal{V}} \hat{H} \hat{\mathcal{V}}^{-1}, \quad (\text{A.12})$$

where

$$\hat{\mathcal{V}} = \bigotimes_{i=1}^L \hat{\mathcal{V}}_i. \quad (\text{A.13})$$

This is regarded as a second-quantized version of the imaginary gauge transformation [235, 236, 237] reviewed in Chapter 5. The similarity transformation cannot change the eigenvalues of  $\hat{H}$ . In fact, the eigenstate  $|E_\alpha^R\rangle$  of  $\hat{H}$  with the energy eigenvalue  $E_\alpha$  is obtained from  $|E_\alpha^R\rangle'$  of  $\hat{H}'$  with the same eigenvalue as  $|E_\alpha^R\rangle = \hat{\mathcal{V}}^{-1} |E_\alpha^R\rangle'$  because

$$\hat{H} |E_\alpha^R\rangle = \hat{H} \hat{\mathcal{V}}^{-1} |E_\alpha^R\rangle' = \hat{\mathcal{V}}^{-1} \hat{H}' |E_\alpha^R\rangle' = E_\alpha \hat{\mathcal{V}}^{-1} |E_\alpha^R\rangle' = E_\alpha |E_\alpha^R\rangle. \quad (\text{A.14})$$

Thus, we can investigate the energy eigenvalues of  $\hat{H}'$  instead of  $\hat{H}$ .

We obtain the transformed Hamiltonian  $\hat{H}'$  for which the non-Hermitian perturbations are only supported in non-resonant regions with an appropriate choice of  $\{\theta_i\}$ . To explain this, we investigate a simpler case, for which sites from 1 to  $y$  may have resonant regions and the other sites are non-resonant. We can suppose that  $y$  is much smaller than the size of the system  $L$ , since in the MBL phase resonant regions are rare [331]. By choosing

$$\begin{aligned} \theta_i &= i \quad (1 \leq i \leq y+1), \\ \theta_i &= -i + 2y + 2 \quad (y+2 \leq i \leq 2y+2), \\ \theta_i &= 0 \quad (2y+3 \leq i \leq L), \end{aligned} \quad (\text{A.15})$$

we have

$$\begin{aligned}
\hat{H}' &= \hat{\mathcal{V}}\hat{H}\hat{\mathcal{V}}^{-1} \\
&= -J \sum_{i=1}^L (e^{-gz_i} \hat{b}_{i+1}^\dagger \hat{b}_i + e^{gz_i} \hat{b}_i^\dagger \hat{b}_{i+1}) + \sum_{i=1}^L U \hat{n}_i \hat{n}_{i+1} + \sum_{i=1}^L h_i \hat{n}_i \\
&= \hat{H}_0 + \hat{V}'_{\text{NH}},
\end{aligned} \tag{A.16}$$

where

$$\begin{aligned}
z_i &= 0 \quad (1 \leq i \leq y, i = L), \\
z_i &= 2 \quad (y + 2 \leq i \leq 2y + 1), \\
z_i &= 1 \quad (2y + 2 \leq i \leq L - 1).
\end{aligned} \tag{A.17}$$

As  $\hat{V}'_{\text{NH}}$  is only supported on the non-resonant regions, it will not mix the eigenstates, which leads to further suppression of complex energy eigenvalues that are generally non-adjacent.

# Appendix B

## Details of the level-spacing distributions for small matrices in Chapter 6

In this appendix, we show the details of the level-spacing distributions for small matrices in Chapter 6, in particular the derivation of Eq. (6.76):

$$p_{\text{small}}(s) = \frac{(C_f s)^3}{\mathcal{N}_f} K_{\frac{f-2}{2}} \left( (C_f s)^2 \right), \quad (\text{B.1})$$

where

$$K_\alpha(x) = \int_0^\infty e^{-x \cosh z} \cosh(\alpha z) \quad (\text{B.2})$$

is the modified Bessel function, and  $C_f$  and  $\mathcal{N}_f$  are normalization constants.

### B.1 Probability distribution of $|X_f|^2$

[*Note: the derivation in this section is due to Mr. Naoto Kura.*]

As discussed in Chapter 6, we can calculate the level-spacing distribution  $p_{\text{small}}(s)$  from the distribution of  $X_f = z_1^2 + \cdots + z_f^2$ , where  $s \propto |X_f|^{1/2}$  and  $\{z_f\}$ 's are complex Gaussian random variables. Note that the proportionality constant is not important because we will normalize the non-normalized level-spacing distribution  $p(s)$  such that

$$\int_0^\infty ds p_{\text{small}}(s) = \int_0^\infty ds s p_{\text{small}}(s) = 1 \quad (\text{B.3})$$

at the last stage of our discussion.

We first consider the distribution of  $|X_f|^2$ . This is obtained as

$$P(|X_f|^2 = \kappa) \propto \int \delta\left(\kappa - \left|z_1^2 + \dots + z_f^2\right|^2\right) e^{-\|\vec{z}\|^2} d^{2f}\vec{z}, \quad (\text{B.4})$$

where  $\vec{z} = (z_1, \dots, z_f)$ . Let us decompose  $\vec{z}$  as real and imaginary vectors as  $\vec{z} = \vec{u} + i\vec{v}$ . Letting  $\theta$  denote the angle between  $\vec{u}$  and  $\vec{v}$ , we have

$$X_f = \|\vec{u}\|^2 - \|\vec{v}\|^2 + 2i\vec{u} \cdot \vec{v} = u^2 - v^2 + 2iuv \cos \theta, \quad (\text{B.5})$$

where  $u = \|\vec{u}\|$  and  $v = \|\vec{v}\|$ . Then we have

$$|X_f|^2 = u^4 + v^4 + 2u^2v^2(2\cos^2\theta - 1). \quad (\text{B.6})$$

By transforming variables from  $(u, v, \theta)$  to  $(U, V, c) = (u^2, v^2, \cos \theta)$ , we have

$$|X_f|^2 = U^2 + V^2 + 2UV(2c^2 - 1). \quad (\text{B.7})$$

In addition, the measure  $d^{2f}\vec{z}$  is also transformed as

$$\begin{aligned} d^{2f}\vec{z} &= d^f\vec{u}d^f\vec{v} = \frac{2\pi^{f/2}}{\Gamma(f/2)} \frac{2\pi^{(f-1)/2}}{\Gamma((f-1)/2)} u^{f-1} du v^{f-1} dv \sin^{f-2}\theta d\theta \\ &\propto u^{f-1} du v^{f-1} dv \sin^{f-2}\theta d\theta \\ &\propto (UV)^{(f-2)/2} dU dV (1-c^2)^{(f-3)/2} dc. \end{aligned} \quad (\text{B.8})$$

We thus obtain

$$P(|X_f|^2 = \kappa) \propto \int_0^\infty \int_0^\infty dU dV (UV)^{(f-2)/2} e^{-(U+V)} \quad (\text{B.9})$$

$$\times \int_{-1}^1 (1-c^2)^{(f-3)/2} dc \delta(\kappa - [U^2 + V^2 + 2UV(2c^2 - 1)]). \quad (\text{B.10})$$

The integration of the delta function can be carried out as follows. We first introduce

$$c_\kappa = \left( \frac{\kappa - (U - V)^2}{4UV} \right)^{1/2}, \quad (\text{B.11})$$

where  $0 \leq c_\kappa \leq 1$  is satisfied if and only if  $|U - V| \leq \sqrt{\kappa} \leq U + V$ . Then, we have

$$\delta(\kappa - [U^2 + V^2 + 2UV(2c^2 - 1)]) = \frac{1}{8UVc_\kappa} [\delta(c - c_\kappa) + \delta(c + c_\kappa)] \quad (\text{B.12})$$

and thus

$$\begin{aligned}
P\left(|X_f|^2 = \kappa\right) &\propto \int_{|U-V| \leq \sqrt{\kappa} \leq U+V} dU dV (4UV)^{(f-2)/2} e^{-(U+V)} \frac{(1 - c_\kappa^2)^{(f-3)/2}}{4UV c_\kappa} \\
&= \int_{|U-V| \leq \sqrt{\kappa} \leq U+V} dU dV e^{-(U+V)} \frac{[(U+V)^2 - \kappa]^{(f-3)/2}}{[\kappa - (U-V)^2]^{1/2}}. \quad (\text{B.13})
\end{aligned}$$

Finally, the transformation of the variables from  $(U, V)$  to  $(x, y) = (U + V, U - V)$  leads to

$$\begin{aligned}
P\left(|X_f|^2 = \kappa\right) &\propto \int_{\sqrt{\kappa}}^{\infty} dx \int_{-\sqrt{\kappa}}^{\sqrt{\kappa}} dy e^{-x} \frac{(x^2 - \kappa)^{(f-3)/2}}{(\kappa - y^2)^{1/2}} \\
&\propto \int_{\sqrt{\kappa}}^{\infty} dx e^{-x} (x^2 - \kappa)^{(f-3)/2}. \quad (\text{B.14})
\end{aligned}$$

To evaluate this, we use the following integral:

$$\int_r^{\infty} dx e^{-x} (x^2 - r^2)^{\alpha-1/2} = \frac{\Gamma(2\alpha)}{2^{\alpha-1}\Gamma(\alpha)} r^\alpha K_\alpha(r). \quad (\text{B.15})$$

Substitution of  $\alpha = f/2 - 1$  and  $r = \sqrt{\kappa}$  in Eq. (B.15) leads to the following probability distribution of  $|X_f|^2$ :

$$P\left(|X_f|^2 = \kappa\right) \propto \kappa^{f/4-1/2} K_{f/2-1}(\sqrt{\kappa}). \quad (\text{B.16})$$

### B.1.1 Level-spacing distribution for $H_{\text{small}}$

To obtain the level-spacing distribution, we consider the probability distribution  $p(s)ds$  from  $P(|X_f|^2 = \kappa)d\kappa$  obtained above. Using  $s = |X_f|^{1/2} = \kappa^{1/4}$ , we have

$$p(s) \propto s^3 P(|X_f|^2 = \kappa)|_{\kappa=s^4} \propto s^{f+1} K_{f/2-1}(s^2). \quad (\text{B.17})$$

From this, we see that the level repulsion is  $O(s^3)$  for  $f > 2$  and  $O(s^3 \log(1/s))$  at  $f = 2$ .

Finally, we rescale the probability distribution by considering  $p_{\text{small}}(s) = ap(bs)$  for appropriate constants  $a$  and  $b$ . Revoking Eq. (B.3), we obtain

$$p(s) = \frac{1}{\mathcal{N}_f} (C_f s)^{f+1} K_{f/2-1}((C_f s)^2), \quad (\text{B.18})$$

with

$$C_f = \frac{\Gamma(1/4)\Gamma(f/2 + 1/4)}{2\sqrt{2}\Gamma(f/2)} \quad (\text{B.19})$$

and

$$\mathcal{N}_f = 2^{f/2-2} \Gamma\left(\frac{f}{2}\right) C_f^{-1}. \quad (\text{B.20})$$

## B.2 Simpler forms

The obtained level-spacing distributions can be simplified by using

$$K_{1/2}(x) = \sqrt{\frac{\pi}{2x}} e^{-x}, \quad (\text{B.21})$$

$$K_{3/2}(x) = \sqrt{\frac{\pi}{2x}} \left(1 + \frac{1}{x}\right) e^{-x}. \quad (\text{B.22})$$

Simpler forms of  $p_{\text{small}}(s)$  for  $f = 2, 3$ , and  $5$  are

$$\begin{aligned} p_{\text{small,A}}(s) &= 2C_3^4 s^3 e^{-C_3^2 s^2}, \\ p_{\text{small,AI}^\dagger}(s) &= 2C_2^4 s^3 K_0(C_2^2 s^2), \\ p_{\text{small,AII}^\dagger}(s) &= \frac{2C_5^4 s^3}{3} (1 + C_5^2 s^2) e^{-C_5^2 s^2}, \end{aligned} \quad (\text{B.23})$$

where  $C_2 = \frac{1}{8\sqrt{2}} \Gamma\left(\frac{1}{4}\right)^2 = 1.16187\dots$ ,  $C_3 = \frac{3}{4}\sqrt{\pi} = 1.32934\dots$  and  $C_5 = \frac{7}{8}\sqrt{\pi} \simeq 1.5509\dots$ . Here we have used the formula

$$\Gamma(x)\Gamma(1-x) = \frac{\pi}{\sin \pi x} \quad (\text{B.24})$$

to obtain  $C_3$  and  $C_5$ .

# Acknowledgements

This thesis would not have been completed without the support of many people. I would like to express my deep sense of gratitude to them.

First and foremost, I would like to thank my supervisor, Professor Masahito Ueda. He always encourages me to advance my research with his exceptional skills as a physicist and a teacher. The discussions with him were full of inspiring advice, with which I was able to accomplish my research projects with joy. I am also grateful to him for reading this PhD thesis and giving me a lot of helpful comments.

I am also grateful to Prof. Masaki Sano and Prof. Hidetoshi Katori, who are the subadvisor of "Advanced Leading Graduate Course for Photon Science (ALPS)." In particular, Prof. Sano gave me many exciting comments on my work from an expert's standpoint of nonequilibrium statistical mechanics.

I would also like to thank all members of the thesis committee, Prof. Hatano, Prof. Kaneko, Prof. Sagawa, Prof. Shimizu, and Prof. Takeuchi for the careful review and numerous important comments of this PhD thesis. Moreover, they willingly accepted the change of the date of my defense after I became ill before the original schedule. I would like to express my apology for this trouble and appreciation for the kind concern and support.

Concerning my illness, I deeply thank doctors in the Disease Control & Prevention Center and nurses in the Center Hospital of the National Center for Global Health and Medicine. They not only treated me for my acute hepatitis promptly but also understood my situation and ease me of my worries.

I sincerely appreciate continuous discussions and help from my collaborators. I would like to thank Mr. Kohei Kawabata, without whom our works on non-Hermitian systems in Chapters 5 and 6 would never be completed. I am also thankful to Mr. Naoto Kura, who always gave me insightful comments on my work, one of which resulted in the collaboration in Chapter 6. In addition, it has been very fortunate for me to discuss with Prof. Ehud Altman, Dr. Marin

Bukov, Prof. Kazuya Fujimoto, Prof. Snir Gazit, Mr. Zongping Gong, Prof. Tatsuhiko Ikeda, Mr. Naoyuki Shibata, and Mr. Nobuyuki Yoshioka, who taught me a lot of aspects of nonequilibrium statistical mechanics, quantum many-body systems, isolated and dissipative systems, and numerical simulations through fruitful collaborations.

I would appreciate assistance of many great physicists trying to uncover the mystery of quantum many-body systems, especially Prof. Yuto Ashida, Prof. Shunsuke Furukawa, Dr. Taiki Haga, Dr. Sho Higashikawa, Mr. Kazuya Kaneko, Dr. Takashi Mori, Prof. Masaya Nakagawa, Prof. Keiji Saito, Prof. Naoto Shiraishi, and Dr. Naoto Tsuji. It has always been stimulating to discuss with these researchers. Needless to say, I am also indebted to all of the present and former members in Masahito Ueda's Group for providing me an enjoyable, relaxing, and encouraging environment for doing my research.

I wish to thank my family, Noriko, Takanobu, Manatsu, and Kosuke, for their understanding, encouragement and supports. Last but not least, I thank Ms. Mamiko Tatsuta, my fiancée, for enjoyable discussions on foundation of quantum mechanics and for her warm love.

Finally, I would like to acknowledge the financial support from the Japan Society for the Promotion of Science (JSPS) through the Program for Leading Graduate Schools (ALPS) and Grant-in-Aid for JSPS Research Fellow (JPSJ KAKENHI Grant No. JP17J03189).

# Bibliography

- [1] Lev Davidovich Landau and EM Lifshitz. Statistical physics, part i, 1980.
- [2] J v Neumann. Beweis des Ergodensatzes und des H-Theorems in der Neuen Mechanik. *Zeitschrift für Physik*, 57(1-2):30–70, 1929.
- [3] Sheldon Goldstein, Joel L Lebowitz, Roderich Tumulka, and Nino Zanghi. Long-time behavior of macroscopic quantum systems. *The European Physical Journal H*, 35(2):173–200, 2010.
- [4] M Fierz. Ergodensatz in der Quantenmechanik. *Helvetica Phys. Acta*, 28:705–715, 1955.
- [5] IE Farquhar and PT Landsberg. On the quantum-statistical ergodic and H-theorems. In *Proceedings of the Royal Society of London A: Mathematical, Physical and Engineering Sciences*, volume 239, pages 134–144. The Royal Society, 1957.
- [6] P Bocchieri and A Loinger. Ergodic theorem in quantum mechanics. *Phys. Rev.*, 111(3):668, 1958.
- [7] Sandu Popescu, Anthony J Short, and Andreas Winter. Entanglement and the foundations of statistical mechanics. *Nature Physics*, 2(11):754–758, 2006.
- [8] Sheldon Goldstein, Joel L. Lebowitz, Roderich Tumulka, and Nino Zanghi. Canonical typicality. *Phys. Rev. Lett.*, 96:050403, Feb 2006.
- [9] Sheldon Goldstein, David A. Huse, Joel L. Lebowitz, and Roderich Tumulka. Thermal equilibrium of a macroscopic quantum system in a pure state. *Phys. Rev. Lett.*, 115:100402, Sep 2015.
- [10] Sheldon Goldstein, David A Huse, Joel L Lebowitz, and Roderich Tumulka. Macroscopic and microscopic thermal equilibrium. *Annalen der Physik*, 2017.

- [11] Sheldon Goldstein, Joel L. Lebowitz, Christian Mastrodonato, Roderich Tumulka, and Nino Zanghi. Approach to thermal equilibrium of macroscopic quantum systems. *Phys. Rev. E*, 81:011109, Jan 2010.
- [12] Hal Tasaki. Typicality of thermal equilibrium and thermalization in isolated macroscopic quantum systems. *Journal of Statistical Physics*, 163(5):937–997, 2016.
- [13] Ayumu Sugita. On the basis of quantum statistical mechanics. *arXiv preprint cond-mat/0602625*, 2006.
- [14] Asher Peres. Ergodicity and mixing in quantum theory. I. *Phys. Rev. A*, 30:504–508, Jul 1984.
- [15] R. V. Jensen and R. Shankar. Statistical behavior in deterministic quantum systems with few degrees of freedom. *Phys. Rev. Lett.*, 54:1879–1882, Apr 1985.
- [16] Mark Srednicki. Chaos and quantum thermalization. *Phys. Rev. E*, 50:888–901, Aug 1994.
- [17] J. M. Deutsch. Quantum statistical mechanics in a closed system. *Phys. Rev. A*, 43:2046–2049, Feb 1991.
- [18] Marcos Rigol, Vanja Dunjko, and Maxim Olshanii. Thermalization and its mechanism for generic isolated quantum systems. *Nature*, 452(7189):854–858, 2008.
- [19] Marcos Rigol. Quantum quenches and thermalization in one-dimensional fermionic systems. *Phys. Rev. A*, 80:053607, Nov 2009.
- [20] Giulio Biroli, Corinna Kollath, and Andreas M. Läuchli. Effect of rare fluctuations on the thermalization of isolated quantum systems. *Phys. Rev. Lett.*, 105:250401, Dec 2010.
- [21] S. Genway, A. F. Ho, and D. K. K. Lee. Thermalization of local observables in small Hubbard lattices. *Phys. Rev. A*, 86:023609, Aug 2012.
- [22] Ehsan Khatami, Guido Pupillo, Mark Srednicki, and Marcos Rigol. Fluctuation-dissipation theorem in an isolated system of quantum dipolar Bosons after a quench. *Phys. Rev. Lett.*, 111:050403, Jul 2013.

- [23] R. Steinigeweg, J. Herbrych, and P. Prelovšek. Eigenstate thermalization within isolated spin-chain systems. *Phys. Rev. E*, 87:012118, Jan 2013.
- [24] W. Beugeling, R. Moessner, and Masudul Haque. Finite-size scaling of eigenstate thermalization. *Phys. Rev. E*, 89:042112, Apr 2014.
- [25] Hyungwon Kim, Tatsuhiko N. Ikeda, and David A. Huse. Testing whether all eigenstates obey the eigenstate thermalization hypothesis. *Phys. Rev. E*, 90:052105, Nov 2014.
- [26] Wouter Beugeling, Roderich Moessner, and Masudul Haque. Off-diagonal matrix elements of local operators in many-body quantum systems. *Phys. Rev. E*, 91:012144, Jan 2015.
- [27] David J. Luitz and Yevgeny Bar Lev. Anomalous thermalization in ergodic systems. *Phys. Rev. Lett.*, 117:170404, Oct 2016.
- [28] Ivan M. Khaymovich, Masudul Haque, and Paul A. McClarty. Eigenstate thermalization, random matrix theory, and behemoths. *Phys. Rev. Lett.*, 122:070601, Feb 2019.
- [29] Ryusuke Hamazaki and Masahito Ueda. Random-matrix behavior of quantum nonintegrable many-body systems with Dyson’s three symmetries. *Phys. Rev. E*, 99:042116, Apr 2019.
- [30] Peter Reimann. Generalization of von Neumann’s approach to thermalization. *Phys. Rev. Lett.*, 115:010403, Jul 2015.
- [31] Ryusuke Hamazaki and Masahito Ueda. Atypicality of most few-body observables. *Phys. Rev. Lett.*, 120:080603, Feb 2018.
- [32] Heinz-Peter Breuer, Francesco Petruccione, et al. *The theory of open quantum systems*. Oxford University Press on Demand, 2002.
- [33] J. C. Bergquist, Randall G. Hulet, Wayne M. Itano, and D. J. Wineland. Observation of quantum jumps in a single atom. *Phys. Rev. Lett.*, 57:1699–1702, Oct 1986.
- [34] Warren Nagourney, Jon Sandberg, and Hans Dehmelt. Shelved optical electron amplifier: Observation of quantum jumps. *Phys. Rev. Lett.*, 56:2797–2799, Jun 1986.

- [35] Th. Sauter, W. Neuhauser, R. Blatt, and P. E. Toschek. Observation of quantum jumps. *Phys. Rev. Lett.*, 57:1696–1698, Oct 1986.
- [36] Sebastien Gleyzes, Stefan Kuhr, Christine Guerlin, Julien Bernu, Samuel Deleglise, Ulrich Busk Hoff, Michel Brune, Jean-Michel Raimond, and Serge Haroche. Quantum jumps of light recording the birth and death of a photon in a cavity. *Nature*, 446(7133):297, 2007.
- [37] ZK Mineev, SO Mundhada, Shyam Shankar, Philip Reinhold, Ricardo Gutiérrez-Jáuregui, RJ Schoelkopf, Mazyar Mirrahimi, HJ Carmichael, and MH Devoret. To catch and reverse a quantum jump mid-flight. *Nature*, page 1, 2019.
- [38] Carl M. Bender and Stefan Boettcher. Real spectra in non-Hermitian Hamiltonians having  $\mathcal{PT}$  symmetry. *Phys. Rev. Lett.*, 80:5243–5246, Jun 1998.
- [39] Ramy El-Ganainy, Konstantinos G Makris, Mercedeh Khajavikhan, Ziad H Musslimani, Stefan Rotter, and Demetrios N Christodoulides. Non-Hermitian physics and PT symmetry. *Nature Physics*, 14(1):11, 2018.
- [40] Richard P Feynman. Simulating physics with computers. *International journal of theoretical physics*, 21(6):467–488, 1982.
- [41] Iulia Buluta and Franco Nori. Quantum simulators. *Science*, 326(5949):108–111, 2009.
- [42] I. M. Georgescu, S. Ashhab, and Franco Nori. Quantum simulation. *Rev. Mod. Phys.*, 86:153–185, Mar 2014.
- [43] Soonwon Choi, Joonhee Choi, Renate Landig, Georg Kucsko, Hengyun Zhou, Junichi Isoya, Fedor Jelezko, Shinobu Onoda, Hitoshi Sumiya, Vedika Khemani, et al. Observation of discrete time-crystalline order in a disordered dipolar many-body system. *Nature*, 543(7644):221, 2017.
- [44] J Zhang, PW Hess, A Kyprianidis, P Becker, A Lee, J Smith, G Pagano, I-D Potirniche, Andrew C Potter, A Vishwanath, et al. Observation of a discrete time crystal. *Nature*, 543(7644):217, 2017.
- [45] Stefan Trotzky, Yu-Ao Chen, Andreas Flesch, Ian P McCulloch, Ulrich Schollwöck, Jens Eisert, and Immanuel Bloch. Probing the relaxation towards equilibrium in an isolated strongly correlated one-dimensional Bose gas. *Nature Physics*, 8(4):325–330, 2012.

- [46] Adam M. Kaufman, M. Eric Tai, Alexander Lukin, Matthew Rispoli, Robert Schittko, Philipp M. Preiss, and Markus Greiner. Quantum thermalization through entanglement in an isolated many-body system. *Science*, 353(6301):794–800, 2016.
- [47] Govinda Clos, Diego Porras, Ulrich Warring, and Tobias Schaetz. Time-resolved observation of thermalization in an isolated quantum system. *Phys. Rev. Lett.*, 117:170401, Oct 2016.
- [48] Immanuel Bloch, Jean Dalibard, and Wilhelm Zwerger. Many-body physics with ultracold gases. *Rev. Mod. Phys.*, 80:885–964, Jul 2008.
- [49] Immanuel Bloch, Jean Dalibard, and Sylvain Nascimbene. Quantum simulations with ultracold quantum gases. *Nature Physics*, 8(4):267–276, 2012.
- [50] Christian Gross and Immanuel Bloch. Quantum simulations with ultracold atoms in optical lattices. *Science*, 357(6355):995–1001, 2017.
- [51] Immanuel Bloch. Ultracold quantum gases in optical lattices. *Nature Physics*, 1(1):23–30, 2005.
- [52] Rainer Blatt and CF Roos. Quantum simulations with trapped ions. *Nature Physics*, 8(4):277–284, 2012.
- [53] Philip Richerme, Zhe-Xuan Gong, Aaron Lee, Crystal Senko, Jacob Smith, Michael Foss-Feig, Spyridon Michalakis, Alexey V Gorshkov, and Christopher Monroe. Non-local propagation of correlations in quantum systems with long-range interactions. *Nature*, 511(7508):198–201, 2014.
- [54] Rajibul Islam, Ruichao Ma, Philipp M Preiss, M Eric Tai, Alexander Lukin, Matthew Rispoli, and Markus Greiner. Measuring entanglement entropy in a quantum many-body system. *Nature*, 528(7580):77–83, 2015.
- [55] A. Piñeiro Orioli, A. Signoles, H. Wildhagen, G. Günter, J. Berges, S. Whitlock, and M. Weidemüller. Relaxation of an isolated dipolar-interacting Rydberg quantum spin system. *Phys. Rev. Lett.*, 120:063601, Feb 2018.
- [56] C. Neill, P. Roushan, M. Fang, Y. Chen, M. Kolodrubetz, Z. Chen, A. Megrant, R. Barends, B. Campbell, B. Chiaro, A. Dunsworth, E. Jeffrey, J. Kelly, J. Mutus, P. J. J. O’Malley, C. Quintana, D. Sank, A. Vainsencher, J. Wenner, T. C. White, A. Polkovnikov, and J. M. Martinis. Ergodic dynamics and thermalization in an isolated quantum system. *Nature Physics*, 2016.

- [57] Arijeet Pal and David A. Huse. Many-body localization phase transition. *Phys. Rev. B*, 82:174411, Nov 2010.
- [58] Rahul Nandkishore and David A. Huse. Many-body localization and thermalization in quantum statistical mechanics. *Annual Review of Condensed Matter Physics*, 6(1):15–38, 2015.
- [59] Michael Schreiber, Sean S. Hodgman, Pranjal Bordia, Henrik P. Lüschen, Mark H. Fischer, Ronen Vosk, Ehud Altman, Ulrich Schneider, and Immanuel Bloch. Observation of many-body localization of interacting fermions in a quasirandom optical lattice. *Science*, 349(6250):842–845, 2015.
- [60] Pranjal Bordia, Henrik P. Lüschen, Sean S. Hodgman, Michael Schreiber, Immanuel Bloch, and Ulrich Schneider. Coupling identical one-dimensional many-body localized systems. *Phys. Rev. Lett.*, 116:140401, Apr 2016.
- [61] Jae-yoon Choi, Sebastian Hild, Johannes Zeiher, Peter Schauß, Antonio Rubio-Abadal, Tarik Yefsah, Vedika Khemani, David A. Huse, Immanuel Bloch, and Christian Gross. Exploring the many-body localization transition in two dimensions. *Science*, 352(6293):1547–1552, 2016.
- [62] Pranjal Bordia, Henrik Lüschen, Sebastian Scherg, Sarang Gopalakrishnan, Michael Knap, Ulrich Schneider, and Immanuel Bloch. Probing slow relaxation and many-body localization in two-dimensional quasiperiodic systems. *Phys. Rev. X*, 7:041047, Nov 2017.
- [63] Pranjal Bordia, Henrik Lüschen, Ulrich Schneider, Michael Knap, and Immanuel Bloch. Periodically driving a many-body localized quantum system. *Nature Physics*, 13(5):460, 2017.
- [64] Alexander Lukin, Matthew Rispoli, Robert Schittko, M Eric Tai, Adam M Kaufman, Soonwon Choi, Vedika Khemani, Julian Léonard, and Markus Greiner. Probing entanglement in a many-body-localized system. *Science*, 364(6437):256–260, 2019.
- [65] Jacob Smith, Aaron Lee, Philip Richerme, Brian Neyenhuis, Paul W Hess, Philipp Hauke, Markus Heyl, David A Huse, and Christopher Monroe. Many-body localization in a quantum simulator with programmable random disorder. *Nature Physics*, 12(10):907–911, 2016.

- [66] Ken Xuan Wei, Chandrasekhar Ramanathan, and Paola Cappellaro. Exploring localization in nuclear spin chains. *Phys. Rev. Lett.*, 120:070501, Feb 2018.
- [67] P Roushan, C Neill, J Tangpanitanon, VM Bastidas, A Megrant, R Barends, Y Chen, Z Chen, B Chiaro, A Dunsworth, et al. Spectroscopic signatures of localization with interacting photons in superconducting qubits. *Science*, 358(6367):1175–1179, 2017.
- [68] Kai Xu, Jin-Jun Chen, Yu Zeng, Yu-Ran Zhang, Chao Song, Wuxin Liu, Qiujiang Guo, Pengfei Zhang, Da Xu, Hui Deng, Keqiang Huang, H. Wang, Xiaobo Zhu, Dongning Zheng, and Heng Fan. Emulating many-body localization with a superconducting quantum processor. *Phys. Rev. Lett.*, 120:050507, Feb 2018.
- [69] Georg Kucsko, Soonwon Choi, Joonhee Choi, Peter C Maurer, Hitoshi Sumiya, Shinobu Onoda, Junich Isoya, Fedor Jelezko, Eugene Demler, Norman Y Yao, et al. Critical thermalization of a disordered dipolar spin system in diamond. *arXiv preprint arXiv:1609.08216*, 2016.
- [70] Marcos Rigol. Breakdown of thermalization in finite one-dimensional systems. *Phys. Rev. Lett.*, 103:100403, Sep 2009.
- [71] Toshiya Kinoshita, Trevor Wenger, and David S Weiss. A quantum Newton’s cradle. *Nature*, 440(7086):900–903, 2006.
- [72] Michael Gring, Maximilian Kuhnert, Tim Langen, Takuya Kitagawa, Bernhard Rauer, Matthias Schreitl, Igor Mazets, D Adu Smith, Eugene Demler, and Jörg Schmiedmayer. Relaxation and prethermalization in an isolated quantum system. *Science*, 337(6100):1318–1322, 2012.
- [73] Tim Langen, Remi Geiger, Maximilian Kuhnert, Bernhard Rauer, and Joerg Schmiedmayer. Local emergence of thermal correlations in an isolated quantum many-body system. *Nature Physics*, 9(10):640–643, 2013.
- [74] Tim Langen, Sebastian Erne, Remi Geiger, Bernhard Rauer, Thomas Schweigler, Maximilian Kuhnert, Wolfgang Rohringer, Igor E Mazets, Thomas Gasenzer, and Jörg Schmiedmayer. Experimental observation of a generalized Gibbs ensemble. *Science*, 348(6231):207–211, 2015.

- [75] Hannes Bernien, Sylvain Schwartz, Alexander Keesling, Harry Levine, Ahmed Omran, Hannes Pichler, Soonwon Choi, Alexander S Zibrov, Manuel Endres, Markus Greiner, et al. Probing many-body dynamics on a 51-atom quantum simulator. *Nature*, 551(7682):579, 2017.
- [76] Christopher J Turner, Alexios A Michailidis, Dmitry A Abanin, Maksym Serbyn, and Z Papić. Weak ergodicity breaking from quantum many-body scars. *Nature Physics*, 14(7):745, 2018.
- [77] B Neyenhuis, J Smith, AC Lee, J Zhang, P Richerme, PW Hess, Z-X Gong, AV Gorshkov, and C Monroe. Observation of prethermalization in long-range interacting spin chains. *arXiv preprint arXiv:1608.00681*, 2016.
- [78] J. Berges, Sz. Borsányi, and C. Wetterich. Prethermalization. *Phys. Rev. Lett.*, 93:142002, Sep 2004.
- [79] Martin Eckstein, Marcus Kollar, and Philipp Werner. Thermalization after an interaction quench in the Hubbard model. *Phys. Rev. Lett.*, 103:056403, Jul 2009.
- [80] Marcus Kollar, F. Alexander Wolf, and Martin Eckstein. Generalized Gibbs ensemble prediction of prethermalization plateaus and their relation to nonthermal steady states in integrable systems. *Phys. Rev. B*, 84:054304, Aug 2011.
- [81] Hyosub Kim, YeJe Park, Kyungtae Kim, H.-S. Sim, and Jaewook Ahn. Detailed balance of thermalization dynamics in Rydberg-atom quantum simulators. *Phys. Rev. Lett.*, 120:180502, May 2018.
- [82] Marc Cheneau, Peter Barmettler, Dario Poletti, Manuel Endres, Peter Schauß, Takeshi Fukuhara, Christian Gross, Immanuel Bloch, Corinna Kollath, and Stefan Kuhr. Light-cone-like spreading of correlations in a quantum many-body system. *Nature*, 481(7382):484–487, 2012.
- [83] P. Jurcevic, B. P. Lanyon, P. Hauke, C. Hempel, P. Zoller, R. Blatt, and C. F. Roos. Quasiparticle engineering and entanglement propagation in a quantum many-body system. *Nature*, 511(7508):202–205, 2014.
- [84] Jiehang Zhang, Guido Pagano, Paul W Hess, Antonis Kyprianidis, Patrick Becker, Harvey Kaplan, Alexey V Gorshkov, Z-X Gong, and Christopher

- Monroe. Observation of a many-body dynamical phase transition with a 53-qubit quantum simulator. *Nature*, 551(7682):601, 2017.
- [85] Thomas WB Kibble. Topology of cosmic domains and strings. *Journal of Physics A: Mathematical and General*, 9(8):1387, 1976.
- [86] Wojciech H Zurek. Cosmological experiments in superfluid helium? *Nature*, 317(6037):505, 1985.
- [87] Giacomo Lamporesi, Simone Donadello, Simone Serafini, Franco Dalfovo, and Gabriele Ferrari. Spontaneous creation of Kibble–Zurek solitons in a Bose–Einstein condensate. *Nature Physics*, 9(10):656, 2013.
- [88] S Ulm, J Roßnagel, G Jacob, C Degünther, ST Dawkins, UG Poschinger, R Nigmatullin, A Retzker, MB Plenio, F Schmidt-Kaler, et al. Observation of the Kibble–Zurek scaling law for defect formation in ion crystals. *Nature communications*, 4:2290, 2013.
- [89] Alexander Keesling, Ahmed Omran, Harry Levine, Hannes Bernien, Hannes Pichler, Soonwon Choi, Rhine Samajdar, Sylvain Schwartz, Pietro Silvi, Subir Sachdev, et al. Quantum Kibble–Zurek mechanism and critical dynamics on a programmable Rydberg simulator. *Nature*, 568(7751):207, 2019.
- [90] Maximilian Prüfer, Philipp Kunkel, Helmut Strobel, Stefan Lannig, Daniel Linnemann, Christian-Marcel Schmied, Jürgen Berges, Thomas Gasenzer, and Markus K Oberthaler. Observation of universal dynamics in a spinor Bose gas far from equilibrium. *Nature*, 563(7730):217, 2018.
- [91] Sebastian Erne, Robert Bücke, Thomas Gasenzer, Jürgen Berges, and Jörg Schmiedmayer. Universal dynamics in an isolated one-dimensional Bose gas far from equilibrium. *Nature*, 563(7730):225, 2018.
- [92] Ulrich Schneider, Lucia Hackermüller, Jens Philipp Ronzheimer, Sebastian Will, Simon Braun, Thorsten Best, Immanuel Bloch, Eugene Demler, Stephan Mandt, David Rasch, et al. Fermionic transport and out-of-equilibrium dynamics in a homogeneous Hubbard model with ultracold atoms. *Nature Physics*, 8(3):213–218, 2012.
- [93] J. P. Ronzheimer, M. Schreiber, S. Braun, S. S. Hodgman, S. Langer, I. P. McCulloch, F. Heidrich-Meisner, I. Bloch, and U. Schneider. Expansion

- dynamics of interacting Bosons in homogeneous lattices in one and two dimensions. *Phys. Rev. Lett.*, 110:205301, May 2013.
- [94] Jun Li, Ruihua Fan, Hengyan Wang, Bingtian Ye, Bei Zeng, Hui Zhai, Xinhua Peng, and Jiangfeng Du. Measuring out-of-time-order correlators on a nuclear magnetic resonance quantum simulator. *Phys. Rev. X*, 7(3):031011, 2017.
- [95] Martin Gärttner, Justin G Bohnet, Arghavan Safavi-Naini, Michael L Wall, John J Bollinger, and Ana Maria Rey. Measuring out-of-time-order correlations and multiple quantum spectra in a trapped-ion quantum magnet. *Nature Physics*, 2017.
- [96] G. Barontini, R. Labouvie, F. Stubenrauch, A. Vogler, V. Guarrera, and H. Ott. Controlling the dynamics of an open many-body quantum system with localized dissipation. *Phys. Rev. Lett.*, 110:035302, Jan 2013.
- [97] Ralf Labouvie, Bodhaditya Santra, Simon Heun, and Herwig Ott. Bistability in a driven-dissipative superfluid. *Phys. Rev. Lett.*, 116:235302, Jun 2016.
- [98] Samantha Lapp, Jackson Ang'ong'a, Fangzhao Alex An, and Bryce Gadway. Engineering tunable local loss in a synthetic lattice of momentum states. *New Journal of Physics*, 21(4):045006, apr 2019.
- [99] Takafumi Tomita, Shuta Nakajima, Ippei Danshita, Yosuke Takasu, and Yoshiro Takahashi. Observation of the Mott insulator to superfluid crossover of a driven-dissipative Bose-Hubbard system. *Science advances*, 3(12):e1701513, 2017.
- [100] Niels Syassen, Dominik M Bauer, Matthias Lettner, Thomas Volz, Daniel Dietze, Juan J Garcia-Ripoll, J Ignacio Cirac, Gerhard Rempe, and Stephan Dürr. Strong dissipation inhibits losses and induces correlations in cold molecular gases. *Science*, 320(5881):1329–1331, 2008.
- [101] Bo Yan, Steven A Moses, Bryce Gadway, Jacob P Covey, Kaden RA Hazard, Ana Maria Rey, Deborah S Jin, and Jun Ye. Observation of dipolar spin-exchange interactions with lattice-confined polar molecules. *Nature*, 501(7468):521, 2013.

- [102] Ralf Labouvie, Bodhaditya Santra, Simon Heun, Sandro Wimberger, and Herwig Ott. Negative differential conductivity in an interacting quantum gas. *Phys. Rev. Lett.*, 115:050601, Jul 2015.
- [103] Y. S. Patil, S. Chakram, and M. Vengalattore. Measurement-induced localization of an ultracold lattice gas. *Phys. Rev. Lett.*, 115:140402, Oct 2015.
- [104] Henrik P. Lüschen, Pranjal Bordia, Sean S. Hodgman, Michael Schreiber, Saubhik Sarkar, Andrew J. Daley, Mark H. Fischer, Ehud Altman, Immanuel Bloch, and Ulrich Schneider. Signatures of many-body localization in a controlled open quantum system. *Phys. Rev. X*, 7:011034, Mar 2017.
- [105] Manuel Endres, Hannes Bernien, Alexander Keesling, Harry Levine, Eric R Anschuetz, Alexandre Krajenbrink, Crystal Senko, Vladan Vuletic, Markus Greiner, and Mikhail D Lukin. Atom-by-atom assembly of defect-free one-dimensional cold atom arrays. *Science*, 354(6315):1024–1027, 2016.
- [106] Daniel Barredo, Sylvain De Léséleuc, Vincent Lienhard, Thierry Lahaye, and Antoine Browaeys. An atom-by-atom assembler of defect-free arbitrary two-dimensional atomic arrays. *Science*, 354(6315):1021–1023, 2016.
- [107] Daniel Barredo, Vincent Lienhard, Sylvain De Leseleuc, Thierry Lahaye, and Antoine Browaeys. Synthetic three-dimensional atomic structures assembled atom by atom. *Nature*, 561(7721):79, 2018.
- [108] Julio T Barreiro, Markus Müller, Philipp Schindler, Daniel Nigg, Thomas Monz, Michael Chwalla, Markus Hennrich, Christian F Roos, Peter Zoller, and Rainer Blatt. An open-system quantum simulator with trapped ions. *Nature*, 470(7335):486, 2011.
- [109] Tiejun Gao, E Estrecho, KY Bliokh, TCH Liew, MD Fraser, Sebastian Brodbeck, Martin Kamp, Christian Schneider, Sven Höfling, Y Yamamoto, F Nori, YS Kivshar, AG Truscott, RG Dall, and EA Ostrovskaya. Observation of non-Hermitian degeneracies in a chaotic exciton-polariton billiard. *Nature*, 526(7574):554, 2015.
- [110] J. Raftery, D. Sadri, S. Schmidt, H. E. Türeci, and A. A. Houck. Observation of a dissipation-induced classical to quantum transition. *Phys. Rev. X*, 4:031043, Sep 2014.

- [111] Ryusuke Hamazaki, Kohei Kawabata, and Masahito Ueda. Non-Hermitian many-body localization. *Phys. Rev. Lett.*, 123:090603, Aug 2019.
- [112] Ryusuke Hamazaki, Kohei Kawabata, Naoto Kura, and Masahito Ueda. The threefold way in non-Hermitian random matrices. *arXiv preprint arXiv:1904.13082*, 2019.
- [113] P. Bocchieri and A. Loinger. Quantum recurrence theorem. *Phys. Rev.*, 107:337–338, Jul 1957.
- [114] L. S. Schulman. Note on the quantum recurrence theorem. *Phys. Rev. A*, 18:2379–2380, Nov 1978.
- [115] Peter Reimann. Foundation of statistical mechanics under experimentally realistic conditions. *Phys. Rev. Lett.*, 101:190403, Nov 2008.
- [116] Mark Srednicki. The approach to thermal equilibrium in quantized chaotic systems. *Journal of Physics A: Mathematical and General*, 32(7):1163, 1999.
- [117] Tatsuhiko N. Ikeda and Masahito Ueda. How accurately can the micro-canonical ensemble describe small isolated quantum systems? *Phys. Rev. E*, 92:020102, Aug 2015.
- [118] Eiki Iyoda, Kazuya Kaneko, and Takahiro Sagawa. Fluctuation theorem for many-body pure quantum states. *Phys. Rev. Lett.*, 119:100601, Sep 2017.
- [119] O. Bohigas, M. J. Giannoni, and C. Schmit. Characterization of chaotic quantum spectra and universality of level fluctuation laws. *Phys. Rev. Lett.*, 52:1–4, Jan 1984.
- [120] Michael V Berry and Michael Tabor. Level clustering in the regular spectrum. In *Proceedings of the Royal Society of London A: Mathematical, Physical and Engineering Sciences*, volume 356, pages 375–394. The Royal Society, 1977.
- [121] Michael V Berry. Regular and irregular semiclassical wavefunctions. *Journal of Physics A: Mathematical and General*, 10(12):2083, 1977.
- [122] Naoto Shiraishi and Takashi Mori. Systematic construction of counterexamples to the eigenstate thermalization hypothesis. *Phys. Rev. Lett.*, 119:030601, Jul 2017.

- [123] Jean-Sébastien Caux and Jorn Mossel. Remarks on the notion of quantum integrability. *Journal of Statistical Mechanics: Theory and Experiment*, 2011(02):P02023, 2011.
- [124] Marcos Rigol, Vanja Dunjko, Vladimir Yurovsky, and Maxim Olshanii. Relaxation in a completely integrable many-body quantum system: An *Ab Initio* study of the dynamics of the highly excited states of 1d lattice hardcore Bosons. *Phys. Rev. Lett.*, 98:050405, Feb 2007.
- [125] Marcus Kollar and Martin Eckstein. Relaxation of a one-dimensional Mott insulator after an interaction quench. *Phys. Rev. A*, 78:013626, Jul 2008.
- [126] Amy C. Cassidy, Charles W. Clark, and Marcos Rigol. Generalized thermalization in an integrable lattice system. *Phys. Rev. Lett.*, 106:140405, Apr 2011.
- [127] Pasquale Calabrese, Fabian H. L. Essler, and Maurizio Fagotti. Quantum quench in the transverse-field Ising chain. *Phys. Rev. Lett.*, 106:227203, Jun 2011.
- [128] Miguel A. Cazalilla, Anibal Iucci, and Ming-Chiang Chung. Thermalization and quantum correlations in exactly solvable models. *Phys. Rev. E*, 85:011133, Jan 2012.
- [129] Maurizio Fagotti and Fabian H. L. Essler. Reduced density matrix after a quantum quench. *Phys. Rev. B*, 87:245107, Jun 2013.
- [130] Jorn Mossel and Jean-Sébastien Caux. Generalized TBA and generalized Gibbs. *Journal of Physics A: Mathematical and Theoretical*, 45(25):255001, 2012.
- [131] Jean-Sébastien Caux and Robert M. Konik. Constructing the generalized Gibbs ensemble after a quantum quench. *Phys. Rev. Lett.*, 109:175301, Oct 2012.
- [132] Tatsuhiko N. Ikeda, Yu Watanabe, and Masahito Ueda. Finite-size scaling analysis of the eigenstate thermalization hypothesis in a one-dimensional interacting Bose gas. *Phys. Rev. E*, 87:012125, Jan 2013.
- [133] Márton Kormos, Aditya Shashi, Yang-Zhi Chou, Jean-Sébastien Caux, and Adilet Imambekov. Interaction quenches in the one-dimensional Bose gas. *Phys. Rev. B*, 88:205131, Nov 2013.

- [134] G. Mussardo. Infinite-time average of local fields in an integrable quantum field theory after a quantum quench. *Phys. Rev. Lett.*, 111:100401, Sep 2013.
- [135] B. Wouters, J. De Nardis, M. Brockmann, D. Fioretto, M. Rigol, and J.-S. Caux. Quenching the anisotropic Heisenberg chain: Exact solution and generalized Gibbs ensemble predictions. *Phys. Rev. Lett.*, 113:117202, Sep 2014.
- [136] F. H. L. Essler, G. Mussardo, and M. Panfil. Generalized Gibbs ensembles for quantum field theories. *Phys. Rev. A*, 91:051602, May 2015.
- [137] Vincenzo Alba. Eigenstate thermalization hypothesis and integrability in quantum spin chains. *Phys. Rev. B*, 91:155123, Apr 2015.
- [138] E. Ilievski, J. De Nardis, B. Wouters, J.-S. Caux, F. H. L. Essler, and T. Prosen. Complete generalized Gibbs ensembles in an interacting theory. *Phys. Rev. Lett.*, 115:157201, Oct 2015.
- [139] David A. Huse, Rahul Nandkishore, and Vadim Oganesyan. Phenomenology of fully many-body-localized systems. *Phys. Rev. B*, 90:174202, Nov 2014.
- [140] Ryusuke Hamazaki. Theoretical study on thermalization in isolated quantum systems, 2017. Master’s thesis, arXiv:1901.01481.
- [141] Luca D’Alessio, Yariv Kafri, Anatoli Polkovnikov, and Marcos Rigol. From quantum chaos and eigenstate thermalization to statistical mechanics and thermodynamics. *Advances in Physics*, 65(3):239–362, 2016.
- [142] Rubem Mondaini and Marcos Rigol. Eigenstate thermalization in the two-dimensional transverse field Ising model. II. off-diagonal matrix elements of observables. *Phys. Rev. E*, 96:012157, Jul 2017.
- [143] Mario Feingold and Asher Peres. Distribution of matrix elements of chaotic systems. *Phys. Rev. A*, 34:591–595, Jul 1986.
- [144] Freeman J Dyson. The threefold way. Algebraic structure of symmetry groups and ensembles in quantum mechanics. *Journal of Mathematical Physics*, 3(6):1199–1215, 1962.
- [145] Fritz Haake. *Quantum signatures of chaos*, volume 54. Springer Science & Business Media, 2010.

- [146] Michael Berry. Quantum chaology, not quantum chaos. *Physica Scripta*, 40(3):335, 1989.
- [147] Sebastian Müller, Stefan Heusler, Petr Braun, Fritz Haake, and Alexander Altland. Semiclassical foundation of universality in quantum chaos. *Phys. Rev. Lett.*, 93:014103, Jul 2004.
- [148] Sebastian Müller, Stefan Heusler, Petr Braun, Fritz Haake, and Alexander Altland. Periodic-orbit theory of universality in quantum chaos. *Phys. Rev. E*, 72:046207, Oct 2005.
- [149] Pavel Kos, Marko Ljubotina, and Tomaž Prosen. Many-body quantum chaos: Analytic connection to random matrix theory. *Phys. Rev. X*, 8:021062, Jun 2018.
- [150] Bruno Bertini, Pavel Kos, and Tomaž Prosen. Exact spectral form factor in a minimal model of many-body quantum chaos. *Phys. Rev. Lett.*, 121:264101, Dec 2018.
- [151] Petr Braun, Daniel Waltner, Maram Akila, Boris Gutkin, and Thomas Guhr. Transition from quantum chaos to localization in spin chains. *arXiv preprint arXiv:1902.06265*, 2019.
- [152] Adam Nahum, Jonathan Ruhman, Sagar Vijay, and Jeongwan Haah. Quantum entanglement growth under random unitary dynamics. *Phys. Rev. X*, 7:031016, Jul 2017.
- [153] Adam Nahum, Sagar Vijay, and Jeongwan Haah. Operator spreading in random unitary circuits. *Phys. Rev. X*, 8:021014, Apr 2018.
- [154] C. W. von Keyserlingk, Tibor Rakovszky, Frank Pollmann, and S. L. Sondhi. Operator hydrodynamics, OTOCs, and entanglement growth in systems without conservation laws. *Phys. Rev. X*, 8:021013, Apr 2018.
- [155] Amos Chan, Andrea De Luca, and J. T. Chalker. Spectral statistics in spatially extended chaotic quantum many-body systems. *Phys. Rev. Lett.*, 121:060601, Aug 2018.
- [156] Aaron J Friedman, Amos Chan, Andrea De Luca, and JT Chalker. Spectral statistics and many-body quantum chaos with conserved charge. *arXiv preprint arXiv:1906.07736*, 2019.

- [157] Bruno Bertini, Pavel Kos, and Tomaž Prosen. Entanglement spreading in a minimal model of maximal many-body quantum chaos. *Phys. Rev. X*, 9:021033, May 2019.
- [158] Amos Chan, Andrea De Luca, and J. T. Chalker. Solution of a minimal model for many-body quantum chaos. *Phys. Rev. X*, 8:041019, Nov 2018.
- [159] Bela Bauer and Chetan Nayak. Area laws in a many-body localized state and its implications for topological order. *Journal of Statistical Mechanics: Theory and Experiment*, 2013(09):P09005, 2013.
- [160] Kartiek Agarwal, Sarang Gopalakrishnan, Michael Knap, Markus Müller, and Eugene Demler. Anomalous diffusion and Griffiths effects near the many-body localization transition. *Phys. Rev. Lett.*, 114:160401, Apr 2015.
- [161] Hyungwon Kim and David A. Huse. Ballistic spreading of entanglement in a diffusive nonintegrable system. *Phys. Rev. Lett.*, 111:127205, Sep 2013.
- [162] Jens H. Bardarson, Frank Pollmann, and Joel E. Moore. Unbounded growth of entanglement in models of many-body localization. *Phys. Rev. Lett.*, 109:017202, Jul 2012.
- [163] AI Larkin and Yu N Ovchinnikov. Quasiclassical method in the theory of superconductivity. *Sov Phys JETP*, 28(6):1200–1205, 1969.
- [164] A Kitaev. A simple model of quantum holography. In *KITP strings seminar and Entanglement*, 2015.
- [165] Alexei Kitaev. Hidden correlations in the Hawking radiation and thermal noise. In *talk given at Fundamental Physics Prize Symposium*, 2014.
- [166] Juan Maldacena, Stephen H. Shenker, and Douglas Stanford. A bound on chaos. *Journal of High Energy Physics*, 2016(8):106, 2016.
- [167] Yichen Huang, Yong-Liang Zhang, and Xie Chen. Out-of-time-ordered correlators in many-body localized systems. *Annalen der Physik*, 529(7), 2017.
- [168] Ruihua Fan, Pengfei Zhang, Huitao Shen, and Hui Zhai. Out-of-time-order correlation for many-body localization. *Science Bulletin*, 2017.

- [169] Brian Swingle and Debanjan Chowdhury. Slow scrambling in disordered quantum systems. *Phys. Rev. B*, 95:060201, Feb 2017.
- [170] Jonas A. Kjäll, Jens H. Bardarson, and Frank Pollmann. Many-body localization in a disordered quantum Ising chain. *Phys. Rev. Lett.*, 113:107204, Sep 2014.
- [171] Roderich Moessner and Shivaji Lal Sondhi. Equilibration and order in quantum Floquet matter. *Nature Physics*, 13(5):424, 2017.
- [172] Maksym Serbyn, Z. Papić, and Dmitry A. Abanin. Local conservation laws and the structure of the many-body localized states. *Phys. Rev. Lett.*, 111:127201, Sep 2013.
- [173] David J. Luitz, Nicolas Laflorencie, and Fabien Alet. Many-body localization edge in the random-field Heisenberg chain. *Physical Review B*, 91:081103(R), Feb 2015.
- [174] M. Friesdorf, A. H. Werner, W. Brown, V. B. Scholz, and J. Eisert. Many-body localization implies that eigenvectors are matrix-product states. *Phys. Rev. Lett.*, 114:170505, May 2015.
- [175] Xiongjie Yu, David Pekker, and Bryan K. Clark. Finding matrix product state representations of highly excited eigenstates of many-body localized Hamiltonians. *Phys. Rev. Lett.*, 118:017201, Jan 2017.
- [176] Frank Schindler, Nicolas Regnault, and Titus Neupert. Probing many-body localization with neural networks. *Phys. Rev. B*, 95:245134, Jun 2017.
- [177] Yi-Ting Hsu, Xiao Li, Dong-Ling Deng, and S. Das Sarma. Machine learning many-body localization: Search for the elusive nonergodic metal. *Phys. Rev. Lett.*, 121:245701, Dec 2018.
- [178] Jan Šuntajs, J Bonča, Tomaz Prosen, and Lev Vidmar. Quantum chaos challenges many-body localization. *arXiv preprint arXiv:1905.06345*, 2019.
- [179] John Z. Imbrie. Diagonalization and many-body localization for a disordered quantum spin chain. *Phys. Rev. Lett.*, 117:027201, Jul 2016.
- [180] John Z Imbrie. On many-body localization for quantum spin chains. *Journal of Statistical Physics*, 163(5):998–1048, 2016.

- [181] Wojciech De Roeck and François Huveneers. Stability and instability towards delocalization in many-body localization systems. *Phys. Rev. B*, 95:155129, Apr 2017.
- [182] Thorsten B Wahl, Arijeet Pal, and Steven H Simon. Signatures of the many-body localized regime in two dimensions. *Nature Physics*, 15(2):164, 2019.
- [183] Andrew C. Potter and Romain Vasseur. Symmetry constraints on many-body localization. *Phys. Rev. B*, 94:224206, Dec 2016.
- [184] Vedika Khemani, D. N. Sheng, and David A. Huse. Two universality classes for the many-body localization transition. *Phys. Rev. Lett.*, 119:075702, Aug 2017.
- [185] Maksym Serbyn, Z. Papić, and Dmitry A. Abanin. Criterion for many-body localization-delocalization phase transition. *Phys. Rev. X*, 5:041047, Dec 2015.
- [186] Ronen Vosk, David A. Huse, and Ehud Altman. Theory of the many-body localization transition in one-dimensional systems. *Phys. Rev. X*, 5:031032, Sep 2015.
- [187] Andrew C. Potter, Romain Vasseur, and S. A. Parameswaran. Universal properties of many-body delocalization transitions. *Phys. Rev. X*, 5:031033, Sep 2015.
- [188] Vedika Khemani, S. P. Lim, D. N. Sheng, and David A. Huse. Critical properties of the many-body localization transition. *Phys. Rev. X*, 7:021013, Apr 2017.
- [189] Samy Mailoud, Fausto Borgonovi, and Felix Izrailev. Can quantum many-body systems behave as strongly chaotic, being completely integrable? *arXiv preprint arXiv:1907.01893*, 2019.
- [190] E. T. Jaynes. Information theory and statistical mechanics. *Phys. Rev.*, 106:620–630, May 1957.
- [191] E. T. Jaynes. Information theory and statistical mechanics. II. *Phys. Rev.*, 108:171–190, Oct 1957.

- [192] Ryusuke Hamazaki, Tatsuhiko N. Ikeda, and Masahito Ueda. Generalized Gibbs ensemble in a nonintegrable system with an extensive number of local symmetries. *Phys. Rev. E*, 93:032116, Mar 2016.
- [193] Eric J. Heller. Bound-state eigenfunctions of classically chaotic Hamiltonian systems: Scars of periodic orbits. *Phys. Rev. Lett.*, 53:1515–1518, Oct 1984.
- [194] C. J. Turner, A. A. Michailidis, D. A. Abanin, M. Serbyn, and Z. Papić. Quantum scarred eigenstates in a Rydberg atom chain: Entanglement, breakdown of thermalization, and stability to perturbations. *Phys. Rev. B*, 98:155134, Oct 2018.
- [195] Zongping Gong, Nobuyuki Yoshioka, Naoyuki Shibata, and Ryusuke Hamazaki. Universal error bound for constrained quantum dynamics. *arXiv preprint arXiv:2001.03419*, 2020.
- [196] Zongping Gong, Nobuyuki Yoshioka, Naoyuki Shibata, and Ryusuke Hamazaki. Error bounds for constrained dynamics in gapped quantum systems: Rigorous results and generalizations. *arXiv preprint arXiv:2001.03421*, 2020.
- [197] Vedika Khemani, Chris R. Laumann, and Anushya Chandran. Signatures of integrability in the dynamics of Rydberg-blockaded chains. *Phys. Rev. B*, 99:161101, Apr 2019.
- [198] Wen Wei Ho, Soonwon Choi, Hannes Pichler, and Mikhail D. Lukin. Periodic orbits, entanglement, and quantum many-body scars in constrained models: Matrix product state approach. *Phys. Rev. Lett.*, 122:040603, Jan 2019.
- [199] Cheng-Ju Lin and Olexei I. Motrunich. Exact quantum many-body scar states in the Rydberg-blockaded atom chain. *Phys. Rev. Lett.*, 122:173401, Apr 2019.
- [200] Sanjay Moudgalya, Stephan Rachel, B. Andrei Bernevig, and Nicolas Regnault. Exact excited states of nonintegrable models. *Phys. Rev. B*, 98:235155, Dec 2018.
- [201] Sanjay Moudgalya, Nicolas Regnault, and B. Andrei Bernevig. Entanglement of exact excited states of affleck-kennedy-lieb-tasaki models: Exact results, many-body scars, and violation of the strong eigenstate thermalization hypothesis. *Phys. Rev. B*, 98:235156, Dec 2018.

- [202] Andrew J. A. James, Robert M. Konik, and Neil J. Robinson. Nonthermal states arising from confinement in one and two dimensions. *Phys. Rev. Lett.*, 122:130603, Apr 2019.
- [203] Thomas Iadecola and Marko Žnidarič. Exact localized and ballistic eigenstates in disordered chaotic spin ladders and the Fermi-Hubbard model. *Phys. Rev. Lett.*, 123:036403, Jul 2019.
- [204] Michael Schecter and Thomas Iadecola. Weak ergodicity breaking and quantum many-body scars in spin-1  $XY$  magnets. *Phys. Rev. Lett.*, 123:147201, Oct 2019.
- [205] Shriya Pai, Michael Pretko, and Rahul M. Nandkishore. Localization in fractonic random circuits. *Phys. Rev. X*, 9:021003, Apr 2019.
- [206] Takashi Mori and Naoto Shiraishi. Thermalization without eigenstate thermalization hypothesis after a quantum quench. *Phys. Rev. E*, 96:022153, Aug 2017.
- [207] Subir Sachdev. Bekenstein-Hawking entropy and strange metals. *Phys. Rev. X*, 5:041025, Nov 2015.
- [208] Juan Maldacena and Douglas Stanford. Remarks on the Sachdev-Ye-Kitaev model. *Phys. Rev. D*, 94(10):106002, 2016.
- [209] Pavan Hosur, Xiao-Liang Qi, Daniel A Roberts, and Beni Yoshida. Chaos in quantum channels. *Journal of High Energy Physics*, 2016(2):4, 2016.
- [210] Ryusuke Hamazaki, Kazuya Fujimoto, and Masahito Ueda. Operator noncommutativity and irreversibility in quantum chaos. *arXiv preprint arXiv:1807.02360*, 2018.
- [211] Mehran Kardar, Giorgio Parisi, and Yi-Cheng Zhang. Dynamic scaling of growing interfaces. *Phys. Rev. Lett.*, 56:889–892, Mar 1986.
- [212] Samuel Frederick Edwards and DR Wilkinson. The surface statistics of a granular aggregate. *Proceedings of the Royal Society of London. A. Mathematical and Physical Sciences*, 381(1780):17–31, 1982.
- [213] Manas Kulkarni, David A. Huse, and Herbert Spohn. Fluctuating hydrodynamics for a discrete Gross-Pitaevskii equation: Mapping onto the Kardar-Parisi-Zhang universality class. *Phys. Rev. A*, 92:043612, Oct 2015.

- [214] Marko Ljubotina, Marko Žnidarič, and Tomaž Prosen. Kardar-Parisi-Zhang physics in the quantum Heisenberg magnet. *Phys. Rev. Lett.*, 122:210602, May 2019.
- [215] Maxime Dupont and Joel E Moore. Universal spin dynamics in infinite-temperature one-dimensional quantum magnets. *arXiv preprint arXiv:1907.12115*, 2019.
- [216] Kazuya Fujimoto, Ryusuke Hamazaki, and Yuki Kawaguchi. Family-Vicsek scaling of roughness growth in a strongly interacting Bose gas. *arXiv preprint arXiv:1911.10707*, 2019.
- [217] Felix Weiner, Peter Schmitteckert, Soumya Bera, and Ferdinand Evers. High-temperature spin dynamics in the Heisenberg chain: Magnon propagation and emerging Kardar-Parisi-Zhang scaling in the zero-magnetization limit. *Phys. Rev. B*, 101:045115, Jan 2020.
- [218] Henk van Beijeren. Exact results for anomalous transport in one-dimensional Hamiltonian systems. *Phys. Rev. Lett.*, 108:180601, Apr 2012.
- [219] Herbert Spohn. Nonlinear fluctuating hydrodynamics for anharmonic chains. *Journal of Statistical Physics*, 154(5):1191–1227, 2014.
- [220] A-L Barabási and Harry Eugene Stanley. *Fractal concepts in surface growth*. Cambridge university press, 1995.
- [221] Alan J Bray. Theory of phase-ordering kinetics. *Advances in Physics*, 51(2):481–587, 2002.
- [222] Johannes Hofmann, Stefan S. Natu, and S. Das Sarma. Coarsening dynamics of binary Bose condensates. *Phys. Rev. Lett.*, 113:095702, Aug 2014.
- [223] Kazue Kudo and Yuki Kawaguchi. Coarsening dynamics driven by vortex-antivortex annihilation in ferromagnetic Bose-Einstein condensates. *Phys. Rev. A*, 91:053609, May 2015.
- [224] Lewis A. Williamson and P. B. Blakie. Universal coarsening dynamics of a quenched ferromagnetic spin-1 condensate. *Phys. Rev. Lett.*, 116:025301, Jan 2016.

- [225] Kazuya Fujimoto, Ryusuke Hamazaki, and Masahito Ueda. Unconventional universality class of one-dimensional isolated coarsening dynamics in a spinor Bose gas. *Phys. Rev. Lett.*, 120:073002, Feb 2018.
- [226] Jürgen Berges, Alexander Rothkopf, and Jonas Schmidt. Nonthermal fixed points: Effective weak coupling for strongly correlated systems far from equilibrium. *Phys. Rev. Lett.*, 101:041603, Jul 2008.
- [227] Sandu Popescu, Anthony J Short, and Andreas Winter. The foundations of statistical mechanics from entanglement: Individual states vs. averages. *arXiv preprint quant-ph/0511225*, 2005.
- [228] Marcos Rigol and Mark Srednicki. Alternatives to eigenstate thermalization. *Phys. Rev. Lett.*, 108:110601, Mar 2012.
- [229] E. J. Torres-Herrera and Lea F. Santos. Local quenches with global effects in interacting quantum systems. *Phys. Rev. E*, 89:062110, Jun 2014.
- [230] Marcin Mierzejewski and Lev Vidmar. Eigenstate thermalization hypothesis and integrals of motion. *arXiv preprint arXiv:1908.08569*, 2019.
- [231] Luca D'Alessio and Marcos Rigol. Long-time behavior of isolated periodically driven interacting lattice systems. *Phys. Rev. X*, 4(4):041048, 2014.
- [232] Achilleas Lazarides, Arnab Das, and Roderich Moessner. Equilibrium states of generic quantum systems subject to periodic driving. *Phys. Rev. E*, 90(1):012110, 2014.
- [233] Andrew J Daley. Quantum trajectories and open many-body quantum systems. *Advances in Physics*, 63(2):77–149, 2014.
- [234] Ali Mostafazadeh. Pseudo-Hermiticity versus PT symmetry: the necessary condition for the reality of the spectrum of a non-Hermitian Hamiltonian. *Journal of Mathematical Physics*, 43(1):205–214, 2002.
- [235] Naomichi Hatano and David R. Nelson. Localization transitions in non-Hermitian quantum mechanics. *Phys. Rev. Lett.*, 77:570–573, Jul 1996.
- [236] Naomichi Hatano and David R. Nelson. Vortex pinning and non-Hermitian quantum mechanics. *Phys. Rev. B*, 56:8651–8673, Oct 1997.

- [237] Naomichi Hatano and David R. Nelson. Non-Hermitian delocalization and eigenfunctions. *Phys. Rev. B*, 58:8384–8390, Oct 1998.
- [238] K. G. Makris, R. El-Ganainy, D. N. Christodoulides, and Z. H. Musslimani. Beam dynamics in  $\mathcal{PT}$  symmetric optical lattices. *Phys. Rev. Lett.*, 100:103904, Mar 2008.
- [239] Z. H. Musslimani, K. G. Makris, R. El-Ganainy, and D. N. Christodoulides. Optical solitons in  $\mathcal{PT}$  periodic potentials. *Phys. Rev. Lett.*, 100:030402, Jan 2008.
- [240] S. Longhi. Bloch oscillations in complex crystals with  $\mathcal{PT}$  symmetry. *Phys. Rev. Lett.*, 103:123601, Sep 2009.
- [241] A. Guo, G. J. Salamo, D. Duchesne, R. Morandotti, M. Volatier-Ravat, V. Aimez, G. A. Siviloglou, and D. N. Christodoulides. Observation of  $\mathcal{PT}$ -symmetry breaking in complex optical potentials. *Phys. Rev. Lett.*, 103:093902, Aug 2009.
- [242] Christian E Rüter, Konstantinos G Makris, Ramy El-Ganainy, Demetrios N Christodoulides, Mordechai Segev, and Detlef Kip. Observation of parity–time symmetry in optics. *Nature Physics*, 6(3):192, 2010.
- [243] Vladimir V. Konotop, Jianke Yang, and Dmitry A. Zezyulin. Nonlinear waves in  $\mathcal{PT}$ -symmetric systems. *Rev. Mod. Phys.*, 88:035002, Jul 2016.
- [244] Zongping Gong, Yuto Ashida, Kohei Kawabata, Kazuaki Takasan, Sho Higashikawa, and Masahito Ueda. Topological phases of non-Hermitian systems. *Phys. Rev. X*, 8:031079, Sep 2018.
- [245] Kohei Kawabata, Sho Higashikawa, Zongping Gong, Yuto Ashida, and Masahito Ueda. Topological unification of time-reversal and particle-hole symmetries in non-Hermitian physics. *Nature Communications*, 10(1):297, 2019.
- [246] Kohei Kawabata, Ken Shiozaki, Masahito Ueda, and Masatoshi Sato. Symmetry and topology in non-Hermitian physics. *Phys. Rev. X*, 9:041015, Oct 2019.
- [247] Rainer Grobe, Fritz Haake, and Hans-Jürgen Sommers. Quantum distinction of regular and chaotic dissipative motion. *Phys. Rev. Lett.*, 61:1899–1902, Oct 1988.

- [248] Rainer Grobe and Fritz Haake. Universality of cubic-level repulsion for dissipative quantum chaos. *Phys. Rev. Lett.*, 62:2893–2896, Jun 1989.
- [249] J. T. Chalker and Z. Jane Wang. Diffusion in a random velocity field: Spectral properties of a non-Hermitian Fokker-Planck operator. *Phys. Rev. Lett.*, 79:1797–1800, Sep 1997.
- [250] David R. Nelson and Nadav M. Shnerb. Non-Hermitian localization and population biology. *Phys. Rev. E*, 58:1383–1403, Aug 1998.
- [251] H. J. Sommers, A. Crisanti, H. Sompolinsky, and Y. Stein. Spectrum of large random asymmetric matrices. *Phys. Rev. Lett.*, 60:1895–1898, May 1988.
- [252] Herbert Spohn and Joel L Lebowitz. Irreversible thermodynamics for quantum systems weakly coupled to thermal reservoirs. *Adv. Chem. Phys.*, 38:109–142, 1978.
- [253] Tatsuhiko Shirai and Takashi Mori. Thermalization in open many-body systems based on eigenstate thermalization hypothesis. *arXiv preprint arXiv:1812.09713*, 2018.
- [254] Sebastian Diehl, A Micheli, A Kantian, B Kraus, HP Büchler, and P Zoller. Quantum states and phases in driven open quantum systems with cold atoms. *Nature Physics*, 4(11):878, 2008.
- [255] Frank Verstraete, Michael M Wolf, and J Ignacio Cirac. Quantum computation and quantum-state engineering driven by dissipation. *Nature physics*, 5(9):633, 2009.
- [256] Sebastian Diehl, Enrique Rico, Mikhail A Baranov, and Peter Zoller. Topology by dissipation in atomic quantum wires. *Nature Physics*, 7(12):971, 2011.
- [257] Jiasen Jin, Alberto Biella, Oscar Viyuela, Leonardo Mazza, Jonathan Keeling, Rosario Fazio, and Davide Rossini. Cluster mean-field approach to the steady-state phase diagram of dissipative spin systems. *Phys. Rev. X*, 6:031011, Jul 2016.
- [258] Jiasen Jin, Alberto Biella, Oscar Viyuela, Cristiano Ciuti, Rosario Fazio, and Davide Rossini. Phase diagram of the dissipative quantum Ising model on a square lattice. *Phys. Rev. B*, 98:241108, Dec 2018.

- [259] Tomaž Prosen and Marko Žnidarič. Matrix product simulations of non-equilibrium steady states of quantum spin chains. *Journal of Statistical Mechanics: Theory and Experiment*, 2009(02):P02035, 2009.
- [260] Tomaž Prosen and Enej Ilievski. Families of quasilocal conservation laws and quantum spin transport. *Phys. Rev. Lett.*, 111:057203, Aug 2013.
- [261] Zongping Gong, Ryusuke Hamazaki, and Masahito Ueda. Discrete time-crystalline order in cavity and circuit QED systems. *Phys. Rev. Lett.*, 120:040404, Jan 2018.
- [262] F. Iemini, A. Russomanno, J. Keeling, M. Schirò, M. Dalmonte, and R. Fazio. Boundary time crystals. *Phys. Rev. Lett.*, 121:035301, Jul 2018.
- [263] Tomaž Prosen. Third quantization: a general method to solve master equations for quadratic open Fermi systems. *New Journal of Physics*, 10(4):043026, 2008.
- [264] Mariya V. Medvedyeva, Fabian H. L. Essler, and Tomaz Prosen. Exact Bethe Ansatz spectrum of a tight-binding chain with dephasing noise. *Phys. Rev. Lett.*, 117:137202, Sep 2016.
- [265] Zi Cai and Thomas Barthel. Algebraic versus exponential decoherence in dissipative many-particle systems. *Phys. Rev. Lett.*, 111:150403, Oct 2013.
- [266] Jian Cui, J. Ignacio Cirac, and Mari Carmen Bañuls. Variational matrix product operators for the steady state of dissipative quantum systems. *Phys. Rev. Lett.*, 114(22):220601, jan 2015.
- [267] Hendrik Weimer. Variational principle for steady states of dissipative quantum many-body systems. *Phys. Rev. Lett.*, 114:040402, Jan 2015.
- [268] A. H. Werner, D. Jaschke, P. Silvi, M. Kliesch, T. Calarco, J. Eisert, and S. Montangero. Positive tensor network approach for simulating open quantum many-body systems. *Phys. Rev. Lett.*, 116:237201, Jun 2016.
- [269] Jiasen Jin, Alberto Biella, Oscar Viyuela, Leonardo Mazza, Jonathan Keeling, Rosario Fazio, and Davide Rossini. Cluster mean-field approach to the steady-state phase diagram of dissipative spin systems. *Phys. Rev. X*, 6:031011, Jul 2016.

- [270] Adil A. Gangat, Te I, and Ying-Jer Kao. Steady states of infinite-size dissipative quantum chains via imaginary time evolution. *Phys. Rev. Lett.*, 119:010501, Jul 2017.
- [271] Augustine Kshetrimayum, Hendrik Weimer, and Román Orús. A simple tensor network algorithm for two-dimensional steady states. *Nature communications*, 8(1):1291, 2017.
- [272] Nobuyuki Yoshioka and Ryusuke Hamazaki. Constructing neural stationary states for open quantum many-body systems. *Phys. Rev. B*, 99:214306, Jun 2019.
- [273] Michael J. Hartmann and Giuseppe Carleo. Neural-network approach to dissipative quantum many-body dynamics. *arXiv:1902.05131*, 2019.
- [274] Alexandra Nagy and Vincenzo Savona. Variational quantum Monte Carlo with neural network ansatz for open quantum systems. *arXiv preprint arXiv:1902.09483*, 2019.
- [275] Filippo Vicentini, Alberto Biella, Nicolas Regnault, and Cristiano Ciuti. Variational neural network ansatz for steady states in open quantum systems. *arXiv preprint arXiv:1902.10104*, 2019.
- [276] Emanuele Levi, Markus Heyl, Igor Lesanovsky, and Juan P. Garrahan. Robustness of many-body localization in the presence of dissipation. *Phys. Rev. Lett.*, 116:237203, Jun 2016.
- [277] Mariya V. Medvedyeva, Tomaz Prosen, and Marko Znidaric. Influence of dephasing on many-body localization. *Phys. Rev. B*, 93:094205, Mar 2016.
- [278] Mark H Fischer, Mykola Maksymenko, and Ehud Altman. Dynamics of a many-body-localized system coupled to a bath. *Phys. Rev. Lett.*, 116:160401, Apr 2016.
- [279] I. Yusipov, T. Lapyteva, S. Denisov, and M. Ivanchenko. Localization in open quantum systems. *Phys. Rev. Lett.*, 118:070402, Feb 2017.
- [280] I. Vakulchyk, I. Yusipov, M. Ivanchenko, S. Flach, and S. Denisov. Signatures of many-body localization in steady states of open quantum systems. *Phys. Rev. B*, 98:020202, Jul 2018.

- [281] Yuto Ashida, Keiji Saito, and Masahito Ueda. Thermalization and heating dynamics in open generic many-body systems. *Phys. Rev. Lett.*, 121:170402, Oct 2018.
- [282] Yaodong Li, Xiao Chen, and Matthew P. A. Fisher. Quantum Zeno effect and the many-body entanglement transition. *Phys. Rev. B*, 98:205136, Nov 2018.
- [283] Brian Skinner, Jonathan Ruhman, and Adam Nahum. Measurement-induced phase transitions in the dynamics of entanglement. *Phys. Rev. X*, 9:031009, Jul 2019.
- [284] Amos Chan, Rahul M. Nandkishore, Michael Pretko, and Graeme Smith. Unitary-projective entanglement dynamics. *Phys. Rev. B*, 99:224307, Jun 2019.
- [285] M. Szyniszewski, A. Romito, and H. Schomerus. Entanglement transition from variable-strength weak measurements. *Phys. Rev. B*, 100:064204, Aug 2019.
- [286] Qicheng Tang and W Zhu. Measurement-induced phase transition: A case study in the non-integrable model by density-matrix renormalization group calculations. *arXiv preprint arXiv:1908.11253*, 2019.
- [287] Soonwon Choi, Yimu Bao, Xiao-Liang Qi, and Ehud Altman. Quantum error correction and entanglement phase transition in random unitary circuits with projective measurements. *arXiv preprint arXiv:1903.05124*, 2019.
- [288] Yimu Bao, Soonwon Choi, and Ehud Altman. Theory of the phase transition in random unitary circuits with measurements. *arXiv preprint arXiv:1908.04305*, 2019.
- [289] Michael J Gullans and David A Huse. Scalable probes of measurement-induced criticality. *arXiv preprint arXiv:1910.00020*, 2019.
- [290] Michael J Gullans and David A Huse. Dynamical purification phase transition induced by quantum measurements. *arXiv preprint arXiv:1905.05195*, 2019.
- [291] Yuto Ashida and Masahito Ueda. Full-counting many-particle dynamics: Nonlocal and chiral propagation of correlations. *Phys. Rev. Lett.*, 120:185301, May 2018.

- [292] Masaya Nakagawa, Naoto Tsuji, Norio Kawakami, and Masahito Ueda. Negative-temperature quantum magnetism in open dissipative systems. *arXiv preprint arXiv:1904.00154*, 2019.
- [293] K. B. Efetov. Directed quantum chaos. *Phys. Rev. Lett.*, 79:491–494, Jul 1997.
- [294] Joshua Feinberg and A Zee. Non-Gaussian non-Hermitian random matrix theory: phase transition and addition formalism. *Nuclear Physics B*, 501(3):643–669, 1997.
- [295] Ilya Ya. Goldsheid and Boris A. Khoruzhenko. Distribution of eigenvalues in non-Hermitian Anderson models. *Phys. Rev. Lett.*, 80:2897–2900, Mar 1998.
- [296] H. Markum, R. Pullirsch, and T. Wettig. Non-Hermitian random matrix theory and lattice QCD with chemical potential. *Phys. Rev. Lett.*, 83:484–487, Jul 1999.
- [297] Joshua Feinberg and A. Zee. Non-Hermitian localization and delocalization. *Phys. Rev. E*, 59:6433–6443, Jun 1999.
- [298] Stefano Longhi, Davide Gatti, and Giuseppe Della Valle. Non-Hermitian transparency and one-way transport in low-dimensional lattices by an imaginary gauge field. *Phys. Rev. B*, 92:094204, Sep 2015.
- [299] Stefano Longhi, Davide Gatti, and Giuseppe Della Valle. Robust light transport in non-Hermitian photonic lattices. *Scientific Reports*, 5:13376, 2015.
- [300] Evert PL van Nieuwenburg, J Yago Malo, Andrew J Daley, and Mark Hannes Fischer. Dynamics of many-body localization in the presence of particle loss. *Quantum Science and Technology*, 3(1):01LT02, 2017.
- [301] Doochul Kim. Bethe Ansatz solution for crossover scaling functions of the asymmetric XXZ chain and the Kardar-Parisi-Zhang-type growth model. *Phys. Rev. E*, 52:3512–3524, Oct 1995.
- [302] Marko Žnidarič, Tomaž Prosen, and Peter Prelovšek. Many-body localization in the Heisenberg XXZ magnet in a random field. *Phys. Rev. B*, 77:064426, Feb 2008.

- [303] Henning Schomerus. Random matrix approaches to open quantum systems. *Stochastic Processes and Random Matrices: Lecture Notes of the Les Houches Summer School: Volume 104, July 2015*, 104:409, 2017.
- [304] Madan Lal Mehta. *Random matrices*, volume 142. Academic press, 2004.
- [305] Dorje C Brody. Biorthogonal quantum mechanics. *Journal of Physics A: Mathematical and Theoretical*, 47(3):035305, 2013.
- [306] Tomaž Prosen.  $\mathbb{PT}$ -symmetric quantum Liouvillean dynamics. *Phys. Rev. Lett.*, 109:090404, Aug 2012.
- [307] Moos van Caspel and Vladimir Gritsev. Symmetry-protected coherent relaxation of open quantum systems. *Phys. Rev. A*, 97:052106, May 2018.
- [308] Tony E. Lee and Ching-Kit Chan. Heralded magnetism in non-Hermitian atomic systems. *Phys. Rev. X*, 4:041001, Oct 2014.
- [309] Jean Ginibre. Statistical ensembles of complex, quaternion, and real matrices. *Journal of Mathematical Physics*, 6(3):440–449, 1965.
- [310] Alexander Altland and Martin R. Zirnbauer. Nonstandard symmetry classes in mesoscopic normal-superconducting hybrid structures. *Phys. Rev. B*, 55:1142–1161, Jan 1997.
- [311] Nils Lehmann and Hans-Jürgen Sommers. Eigenvalue statistics of random real matrices. *Phys. Rev. Lett.*, 67:941–944, Aug 1991.
- [312] Alan Edelman and Eric Kostlan. How many zeros of a random polynomial are real? *Bulletin of the American Mathematical Society*, 32(1):1–37, 1995.
- [313] J. T. Chalker and B. Mehlige. Eigenvector statistics in non-Hermitian random matrix ensembles. *Phys. Rev. Lett.*, 81:3367–3370, Oct 1998.
- [314] Eugene Kanzieper and Gernot Akemann. Statistics of real eigenvalues in ginibre’s ensemble of random real matrices. *Phys. Rev. Lett.*, 95:230201, Nov 2005.
- [315] Peter J. Forrester and Taro Nagao. Eigenvalue statistics of the real Ginibre ensemble. *Phys. Rev. Lett.*, 99:050603, Aug 2007.

- [316] Zdzislaw Burda, Jacek Grela, Maciej A. Nowak, Wojciech Tarnowski, and Piotr Warchoł. Dysonian dynamics of the Ginibre ensemble. *Phys. Rev. Lett.*, 113:104102, Sep 2014.
- [317] Denis Bernard and André LeClair. A classification of non-Hermitian random matrices. In *Statistical Field Theories*, pages 207–214. Springer, 02.
- [318] Ulrika Magnea. Random matrices beyond the cartan classification. *Journal of Physics A: Mathematical and Theoretical*, 41(4):045203, 2008.
- [319] Kenta Esaki, Masatoshi Sato, Kazuki Hasebe, and Mahito Kohmoto. Edge states and topological phases in non-Hermitian systems. *Phys. Rev. B*, 84:205128, Nov 2011.
- [320] Masatoshi Sato, Kazuki Hasebe, Kenta Esaki, and Mahito Kohmoto. Time-reversal symmetry in non-Hermitian systems. *Progress of Theoretical Physics*, 127(6):937–974, 2012.
- [321] Cumulants that are higher than the second are not necessarily captured by small matrices, since we neglect the influence of close eigenvalues other than two closest ones when we compute  $p_{\text{small}}(s)$ .
- [322] Jun John Sakurai. *Advanced quantum mechanics*. Pearson Education India, 1967.
- [323] Mario Feingold, Nimrod Moiseyev, and Asher Peres. Ergodicity and mixing in quantum theory. II. *Phys. Rev. A*, 30:509–511, Jul 1984.
- [324] Lea F. Santos and Marcos Rigol. Onset of quantum chaos in one-dimensional bosonic and fermionic systems and its relation to thermalization. *Phys. Rev. E*, 81:036206, Mar 2010.
- [325] Rubem Mondaini, Keith R. Fratus, Mark Srednicki, and Marcos Rigol. Eigenstate thermalization in the two-dimensional transverse field Ising model. *Phys. Rev. E*, 93:032104, Mar 2016.
- [326] Here, a superoperator is a linear operator that acts on a vector space of linear operators. We also call the solution of eigen-equation about superoperators as supereigenvalues and supereigenstates.
- [327] Tony E. Lee, H. Häffner, and M. C. Cross. Collective quantum jumps of Rydberg atoms. *Phys. Rev. Lett.*, 108:023602, Jan 2012.

- [328] Peter Reimann. Typical fast thermalization processes in closed many-body systems. *Nature Communications*, 7, 2016.
- [329] Sheldon Goldstein, Takashi Hara, and Hal Tasaki. Extremely quick thermalization in a macroscopic quantum system for a typical nonequilibrium subspace. *New Journal of Physics*, 17(4):045002, 2015.
- [330] Kihong Kim and David R. Nelson. Interaction effects in non-Hermitian models of vortex physics. *Phys. Rev. B*, 64:054508, Jul 2001.
- [331] Several work [187, 188] suggested that the resonant regions are distributed over the whole sites, even when they are rare. We expect that our discussion is qualitatively true for that situation as well.